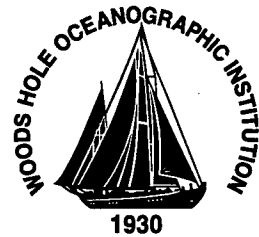


MIT/WHOI 98-07

**Massachusetts Institute of Technology
Woods Hole Oceanographic Institution**



**Joint Program
in Oceanography/
Applied Ocean Science
and Engineering**



DOCTORAL DISSERTATION

Deep-Sea Corals: A New Oceanic Archive

by

Jess F. Adkins

February 1998

19990526 072

DTIC QUALITY INSPECTED 1

MIT/WHOI

98-07

Deep-Sea Corals: A New Oceanic Archive

by

Jess F. Adkins

Massachusetts Institute of Technology
Cambridge, Massachusetts 02139

and

Woods Hole Oceanographic Institution
Woods Hole, Massachusetts 02543

February 1998

DOCTORAL DISSERTATION

Funding was provided by a NASA Global Change Fellowship, the Tokyo Electric Power Company, the MIT Student Research Fund and grants from NOAA and NSF.

Reproduction in whole or in part is permitted for any purpose of the United States Government. This thesis should be cited as: Jess F. Adkins, 1998. Deep-Sea Corals: A New Oceanic Archive. Ph.D. Thesis. MIT/WHOI, 98-07.

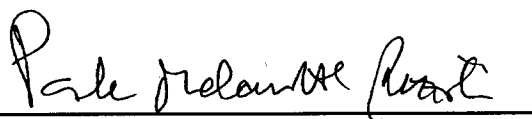
Approved for publication; distribution unlimited.

Approved for Distribution:

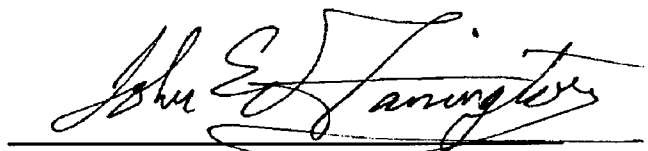


Michael P. Bacon, Chair

Department of Marine Chemistry and Geochemistry



Paola Malanotte-Rizzoli
MIT Director of Joint Program



John W. Farrington
WHOI Dean of Graduate Studies

Deep-Sea Corals: A New Oceanic Archive

by

Jess F. Adkins

B.S., Chemistry
Haverford College, 1990

SUBMITTED IN PARTIAL FULFILLMENT OF THE REQUIREMENTS FOR THE
DEGREE OF

DOCTOR OF PHILOSOPHY

at the

MASSACHUSETTS INSTITUTE OF TECHNOLOGY

and the

WOODS HOLE OCEANOGRAPHIC INSTITUTION

February, 1998

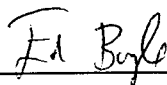
© 1998 Massachusetts Institute of Technology. All rights reserved.

Signature of Author



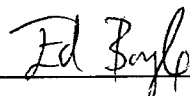
Joint Program in Oceanography/Applied Ocean Science and Engineering
Massachusetts Institute of Technology and Woods Hole Oceanographic Institution
January 7, 1998

Certified by



Edward A. Boyle
Professor of Oceanography
Thesis Supervisor

Accepted by



Edward A. Boyle
Professor of Oceanography
Chair, Joint Committee for Chemical Oceanography

Deep-Sea Corals: A New Oceanic Archive

by

Jess F. Adkins

Submitted to the Massachusetts Institute of Technology/Woods Hole Oceanographic Institution Joint Program in Oceanography/Applied Ocean Science and Engineering on January 7, 1998, in partial fulfillment of the requirements for the degree of Doctor of Philosophy

Abstract

Deep-sea corals are an extraordinary new archive of deep ocean behavior. Through their relatively slow growth rates and intermediate to abyssal depth habitats, these species can record deep ocean changes in chemistry and circulation at sub-decadal timescales. The species *Desmophyllum cristagalli* is a solitary coral composed of uranium rich, density banded aragonite. Modern specimens from dredge collections can be used to calibrate paleoceanographic tracers and study this species' growth rates and patterns. Using a newly developed ICP-MS age screening method, large numbers of samples can be processed relatively quickly and inexpensively to uncover interesting corals for further analysis. Fossil specimens can constrain two important problems in current paleoclimate research: the deep ocean's behavior during rapid climate changes in the past glacial cycle and the rate of deep ocean circulation in the past.

Calibration of *D. cristagalli* using modern samples shows that the stable isotope tracers $\delta^{18}\text{O}$ and $\delta^{13}\text{C}$ are severely affected by the coral's biologically mediated calcification. The magnitude of this "vital effect" is directly related to the banding pattern within a single septum. Optically dense bands are the furthest out of isotopic equilibrium. Less dense bands from the thin portion of a coral's septa are at equilibrium for $\delta^{18}\text{O}$ but are still slightly depleted in $\delta^{13}\text{C}$. Cd/Ca ratios from the skeleton of *D. cristagalli* covary with water [Cd]. The Cd partition coefficient between coral and seawater is estimated to be 1.6 or greater. Cd/Ca ratios in fossil corals are a robust indicator of past water mass conditions over and above a slight "vital effect".

Deep-Sea corals can also be used to calculate the past $\Delta^{14}\text{C}$ of a water mass. Combining uranium series and radiocarbon decay schemes allows for the direct measurement of initial $\Delta^{14}\text{C}$ in the coral. Combined with Cd/Ca data from the same sample, in order to account for water mass mixing, this $\Delta^{14}\text{C}$ value is a direct measurement of the past ventilation age. Samples from 1800 meters depth in the North Atlantic at 15.4 ka show a large deep water circulation switch that occurs in under 160 years. This deep event is coincident with the first sea surface warming of the deglaciation in the North Atlantic. This data shows that deep circulation can change on comparable timescales to the rapid events previously observed for the atmosphere and the surface ocean. In addition, the combined ^{14}C and Cd/Ca data show that the deepest waters in the North Atlantic prior to 15.4 ka were about 500 years old, significantly older than the modern ventilation age.

Thesis advisor: Dr. Edward Boyle, Professor of Oceanography

Acknowledgments

While it seems that every graduate student completing a thesis acknowledges that it is impossible to thank and recognize all of the people who contributed to the work, we all try. I am no different in my aims and apologize ahead of time to the reader for the length of this section.

Completing a Ph.D. with Ed Boyle is an amazing experience. Ed's incredible breadth of knowledge in all areas of Oceanography is truly awe inspiring. It is because of Ed's high expectations and patient teachings that I am any semblance of a scientist today. For all of your guidance, time, insights and good humor all I can say Ed is, "Thank you". Ed is the standard by which all advisors should be measured.

My committee members - Mike Bacon, Michael Bender and Bill Curry - have all contributed to this thesis and my general scientific education. Mike Bacon introduced me to the world of Uranium series disequilibria during an early summer in the Joint Program. Michael Bender not only provided new ideas for uses of deep-sea corals but was also an excellent filter of my 'mushy thinking'. Bill Curry poured over the early stable isotope results with me and offered suggestions for the next step at each stage of our discovery. I am indebted to them all for their encouragement and wisdom.

I have also had the benefit of working closely with several other scientists. Ellen Druffel's unflagging enthusiasm is known to all who have worked with her. She has helped me to unveil the mysteries of radiocarbon calculations and opened her lab to my novice abilities. Larry Edwards and Hai Cheng have made the precision TIMS dates in this thesis and offered many insights to the data interpretation. I look forward to working with them both in the future. While the specific results of his efforts do not appear in this thesis, Lloyd Keigwin has been, and continues to be, an amazing source of scientific ideas and samples. Conversations with Lloyd have helped guide my thoughts on the interplay between core and coral data. Greg Ravizza has been a sounding board for many of my newest data and ideas. He is also one of the few people I know who remembers more Bill Murray quotes than I do.

Without the knowledge and generosity of Dr. Steve Carins at the Smithsonian Institution, this thesis would not have come to fruition. Dr. Cairns allowed me access to and guided me through the extensive deep-sea coral collection at the National Museum of Natural History. He has made the collection into a true scientific archive and introduced me to the biology of deep-sea corals, such as it is known. In addition, Dr. Cairns introduced me to Dr. Helmut Zibrowius in Marseilles, France. The French collection of screened corals in Chapter 3 comes from his lab. Dr. Zibrowius was also an excellent host during my all to brief stay in the south of France.

Three people have been especially helpful with my laboratory work. Barry Grant is one of the chief reasons that students can complete their theses in E34. His insights from a classical chemist point of view and his knowledge of the newest developments in mass spectrometry made for many long and fruitful conversations. No radiocarbon data would appear in this thesis without the efforts of Sheila Griffin. She guided me in the use of gas lines while I was in Irvine, and on several occasions made the measurements herself when we needed the data quickly. Rick, Roseanne, Lisa, Maria, Anna and Lila were part of a key group of technicians and students that helped keep the lab running at MIT.

David Lea gave me my first job in Oceanography and encouraged me to go work for Ed. For at least these two reasons, I will always be indebted to him. John Edmond has been a font of knowledge and a constant source of anecdotes during my tenure in E34. Rob Sherrell, Lex van Geen, Scott Lehman, Delia Oppo, Ed Sholkovitz, Jim Broda, Eben Franks, Dan Repeta, Jim Moffet, Stan Hart, Roger Francois and Dan Schrag are part of the many other scientists and staff members who helped me along the way.

I have had the good fortune to meet many friends over the past few years. Yair, Hedy, Danny, Karen, Chris, Natalie, Cathy, Liz, Rebecca, Youngsook, Bill W., Nick, Bill S.,

Lahini, Susie, Jeff, Michael, Payal, Matt and Yu Harn have all lightened the load of five years in the confines of E34. My introduction to life the Boyle lab was from a screaming Israeli named Yair Rosenthal who turned out to be one of the smartest and kindest people with whom I could ever hope to work. Danny Sigman shares my passion for paleoceanography and can hit the outside jumpers, but his rebounding still needs work. Together, Danny, Bill and Lahini have always provided me with a place to stay and a good party in Wood Hole. Jeff Berry has been a supportive office mate and has survived the 'Adkins curse'. Susie Carter is a funny, intelligent, Guinness swilling friend who is leading the next wave of the 'E34 revival' begun by Hedy Edmonds.

Finally, Gilly and my family have provided support and encouragement through all parts of this work. From points as far flung as Indonesia, Africa and Cambridge, MA they offered their hearts, I hope I can repay the debt.

This research was supported by a NASA Global Change Fellowship, the Tokyo Electric Power Company, the MIT Student Research Fund and grants from NOAA and NSF.

Table of Contents

Title Page	1
Abstract	3
Acknowledgments	5
Table of Contents	7
Chapter 1: Introduction	9
I. Rapid Climate Change and Deep Ventilation	10
II. Deep-Sea Corals	14
III. Thesis Structure	27
IV. References	30
Chapter 2: Calculation of Paleo-Ventilation Ages from Coupled Radiocarbon and Calendar Ages	33
I. Introduction	34
II. Effect of Changing Atmospheric $\Delta^{14}\text{C}$ on Ventilation Ages	34
III. Recalculation Method	36
IV. Implications of New Method	38
V. Conclusions	40
VI. References	41
Chapter 3: Uranium Series Dating of Deep-Sea Corals	42
I. Introduction	42
II. Coral Cleaning Techniques	44
III. Uranium Series Age Screening	51
IV. Precise Uranium Series Dating	68
Abstract	68
Samples and Methods	69
Results and Discussion	76
V. Conclusions	95
VI. References	97
VII. Appendix	101
Chapter 4: Radiocarbon Methods and Calibration	108
I. Introduction	108
II. Methods	109
III. Modern Ocean Calibration and Holocene Data	121
IV. References	131
V. Appendix	133
Chapter 5: Stable Isotopes in Deep-Sea Corals	138
I. Introduction	138
II. Methods Tests	141
III. Septal vs. Innerseptal Studies	149
IV. Mapping Out the Vital Effect	162
V. Conclusions	177
VI. References	178
VII. Appendix	181

Chapter 6: Deglacial Deep-Sea Corals and Cd/Ca Data.....	193
I. Deep-Sea Coral Evidence for Rapid Climate Change in Ventilation of the Deep North Atlantic at 15.4 ka	193
II. Cd/Ca Analytical Methods.....	211
III. Cd Vital Effects and Modern Calibration	217
IV. Conclusions.....	228
V. References.....	229
VI. Appendix.....	230
Biographical Note	234

Chapter 1: Introduction

Bereft of instrumental records of such important climate parameters as past ocean temperatures, atmospheric composition and dynamic circulation patterns, paleoceanographers have had to develop tracers for these variables. Several archives of tracer history have been used in this effort. Deep-sea sediment cores were the original source of information [Emiliani, 1955], and continue today to be the key reservoir of paleoclimatic data. Ice cores from polar [Barnola et al., 1987; GRIP, 1993] and tropical [Thompson et al., 1997] environments provide atmospheric information at extremely high temporal resolution. Massive, reef building surface corals are used to generate high resolution records of sea surface temperature [Fairbanks and Dodge, 1979; Beck et al., 1992] and precipitation [Cole et al., 1993]. This thesis attempts to elucidate a new ocean archive; deep-sea corals.

With their density banded, uranium rich, aragonitic skeletons, these animals can address two key problems in paleoceanography that have limited the understanding of the mechanisms of rapid climate change. Solitary individuals have a regular density banding pattern and grow at rates between 0.2-1.0 mm/yr. Samples can be several dozen to a few hundred years old. Deep-sea corals, therefore, offer the potential of high temporal resolution, as achieved in ice cores and surface corals, in the deep ocean realm of the sediment cores. Because they are uranium rich, deep-sea corals also are a deep ocean archive that can be directly dated beyond the radiocarbon age window. Further, the combination of uranium series and radiocarbon dates within the same sample make deep-sea corals a unique archive of past ocean ^{14}C concentration. Using these coupled radioactive decay schemes, deep-sea corals can constrain the rate of past circulation as well as the volumes and distributions of water masses. By monitoring the deep ocean behavior at decadal time scales, and by providing constraints on the rate of past ocean circulation, this new archive has a vast potential to constrain the mechanisms of rapid climate changes.

This section introduces the two scientific problems that are most suited to deep-sea coral work. The background to rapid climate changes and deep ocean ventilation ages is then followed by a brief introduction to deep-sea corals themselves. Morphology and growth patterns of one species, *Desmophyllum cristagalli*, are briefly outlined. The last section describes the order and content of the following thesis chapters.

I. Rapid Climate Change and Deep Ventilation

Figure 1.1 shows data from rapidly accumulating archives representative of three important climate reservoirs; the atmosphere, the surface ocean and the deep ocean. The $\delta^{18}\text{O}$ of ice at the Greenland summit is a proxy for local atmospheric temperature [Grootes et al., 1993]. The most recent climate epoch, the Holocene, which has lasted for about the last 9,000 years, is characterized by very stable atmospheric temperatures over Greenland. In contrast, the last glacial period and the last deglaciation show very rapid, large amplitude temperature shifts (Figure 1.1). These rapid returns to near interglacial temperatures are called interstadials, twenty-one of which are identified for the last 80,000 years. Transitions into and out of interstadials occur over several decades or less. A strikingly similar pattern has been found for the sea surface temperature (SST) record of the high latitude North Atlantic. Relative abundances of the cold dwelling planktonic foraminifera *N. pachyderma* reflect sea surface temperature oscillations between about 5°C (100% pachy) and 10°C (0% pachy) [Bond et al., 1993]. Every interstadial in the ice core record corresponds to a *N. pachyderma* decrease. Several other studies have shown that this pattern of rapid returns to more mild climates is global in nature. Gray scale reflectance data from the laminated sediments of the Cariaco Basin show the same pattern of oscillations as the ice core $\delta^{18}\text{O}$ throughout the deglaciation [Hughen et al., 1996]. A bioturbation index from the Santa Barbara Basin on the California borderland also captures all of the ice core interstadials [Behl and Kennett, 1996]. Benthic $\delta^{13}\text{C}$ from the Atlantic sector of the Southern Ocean also seems to vary in concert with the $\delta^{18}\text{O}$ of ice

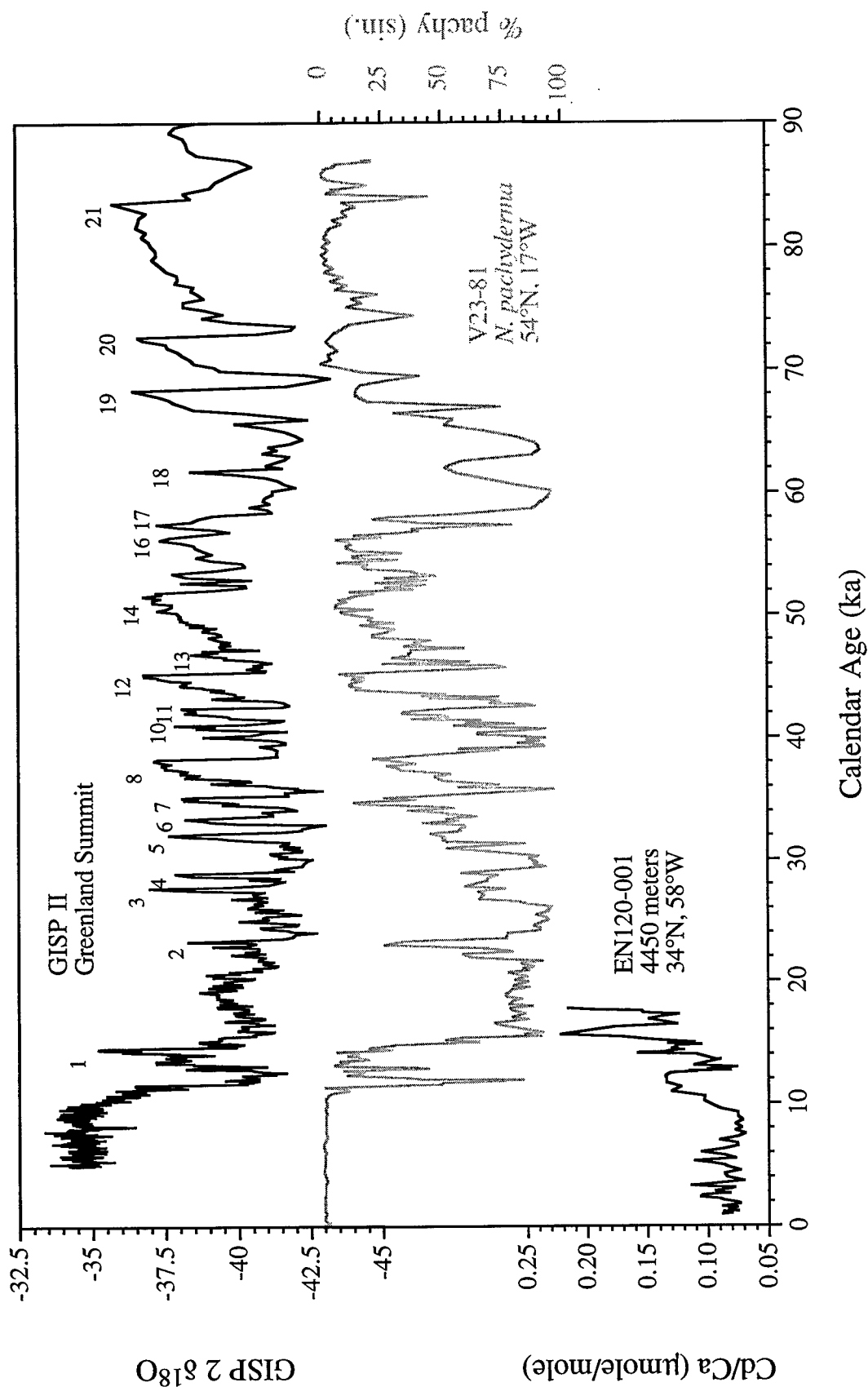


Figure 1.1. Records of climate variability over the past 90,000 years. The age model for the V23-81 % *N. pachyderma* record (-) is based on a correlation with the $\delta^{18}\text{O}$ of ice in GISP 2 (-). The age model for the EN120-001 Cd/Ca record (-) is based on radiocarbon measurements of planktonic foraminifera. Numbers above the warm events in the GISP 2 record correspond to the standard interstadial nomenclature.

[Charles et al., 1996]. Clearly, the pattern seen in the first two records of Figure 1.1 is not a local North Atlantic phenomenon, but is global in its scope.

Currently the understanding of the deep ocean's behavior during these rapid climate switches is not nearly as well constrained. One of the best data sets for this purpose, from a rapidly accumulating sediment core at 4400 meters depth on the Bermuda Rise, is the third data set in Figure 1.1 [Boyle and Keigwin, 1987]. Cd/Ca ratios in benthic foraminifera reflect the concentration of nutrients in the bottom water at a core site through time [Hester and Boyle, 1982; Boyle, 1988]. Because deep waters of a southern origin and deep waters of a northern origin have very different nutrient contents, Cd/Ca can be used as a quasi-conservative tracer of deep water mass mixing between these two sources [Boyle and Keigwin, 1982]. High Cd/Ca values correspond to a larger proportion of southern source waters at this site, and low Cd/Ca values correspond to a larger North Atlantic Deep Water (NADW) influence. The records indicate that a dramatic decrease in the nutrient content of the deep North Atlantic and a rapid increase in high latitude SST occurred at about 15,600 years ago. The inverse pattern holds for the Younger Dryas period, about 11,500-13,000 years ago. This data clearly shows that the deep Atlantic's balance of northern and southern source waters is related to some of the rapid oscillations in surface and atmospheric properties. However, due to bioturbation in the sediments, we need a new archive, like deep-sea corals, to be able to monitor the full amplitude of the deep ocean's behavior at time scales comparable to the surface ocean and atmospheric records. But what, then, is the mechanism that could link the surface and deep reservoirs on these short time scales in the first place?

Massive reorganizations of the ocean-atmosphere circulation system are a leading hypothesis to explain both the rate of climate change seen in Figure 1.1 and possibly its surface to deep link [Broecker and Denton, 1989]. In this scenario, deep ocean circulation is delicately poised between different modes of operation. Studies with a variety of ocean models have found multiple stable deep circulation states that include the

modern 20 Sverdrups of NADW formation and several other modes with reduced or non-existent NADW circulation [Stommel, 1961; Manabe and Stouffer, 1988; Marotzke and Willebrand, 1991; Rahmstorf, 1995]. An essential forcing factor in all of this work is the fresh water balance of the Atlantic basin. The relative rates of salt transfer out of the Atlantic by thermohaline circulation, NADW export around the tip of Africa, and fresh water flux across the Isthmus of Panama, or from the Atlantic to the Indo-Pacific in general, is known as the salt oscillator [Birchfield and Broecker, 1990; Broecker et al., 1990]. In this hypothesis, it is the fluxes of heat and salt in the Atlantic that are crucial for understanding how the climate system can shift rapidly between stable states.

However, to calculate these fluxes in the past we need data on the temperature and salinity of a water mass, its total volume, and the rate at which that volume moves. One of the hardest of these properties to measure precisely has been the paleo ventilation rate. In the modern deep ocean, ventilation rates are based on radiocarbon measurements. The radiocarbon clock is reset at the surface by air/sea CO_2 exchange. Once a water mass leaves the surface, it begins to lose ^{14}C at its known decay rate. Downstream measurements of the ^{14}C content, denoted $\Delta^{14}\text{C}$, reflect the age of the water since leaving the surface [Broecker et al., 1960; Broecker and Peng, 1982; Broecker et al., 1991]. Previously, studies of the radiocarbon difference between contemporaneous benthic and planktonic foraminifera have been our only measure these ventilation rates in the past ocean [Broecker et al., 1988; Shackleton et al., 1988; Duplessy et al., 1989; Broecker et al., 1990]. The combination of uranium series and radiocarbon decay series within deep-sea corals frees ^{14}C from being a chronometer and allows us to measure past water $\Delta^{14}\text{C}$ values at higher precision and with better calendar age control than the benthic-planktonic data. With enough constraints on the spatial distribution of ^{14}C in the past and an understanding of the amount of water mass mixing, it is possible to calculate paleotransports as we do for the modern ocean. Deep-sea corals therefore have the

potential to constrain one of the key variables in the current understanding of how deep circulation may affect climate changes.

Many studies have shown the glacial Atlantic had very different patterns and volumes of deep water masses. These studies imply that there are large circulation signals to be found in deep-sea coral studies. One widely accepted result is that modern NADW shoaled at the Last Glacial Maximum (LGM) to become Glacial North Atlantic Intermediate/Deep Water (GNAI/DW) [Boyle and Keigwin, 1987; Duplessy et al., 1988]. A recent study [Oppo and Lehman, 1993] used a depth transect of cores from the sub-polar North Atlantic to extend this work and constrain the glacial boundary between the northern and the southern source deep waters to be between 1500 and 2000 meters in the high latitude North Atlantic. This result will be a crucial piece of background information in the study described in Chapter Six. Besides examining glacial to interglacial differences, other studies have used the nutrient tracer $\delta^{13}\text{C}$ in benthic foraminifera to monitor rapid changes in deep circulation. By identifying two light $\delta^{13}\text{C}$ values from *P. wuellerstorfi*, Keigwin and Lehman showed early evidence for a deep water signal during Heinrich Event 1 [Keigwin and Lehman, 1994]. Data from the Equatorial Atlantic show synchronous changes in sea surface temperature and NADW production which also correlate with the longer duration interstadials found in the polar ice cores [Curry and Oppo, 1997]. Records from the eastern basin of the North Atlantic and the Southern Ocean also show rapid fluctuations in the $\delta^{13}\text{C}$ of benthic foraminifera [Sarthein et al., 1994; Charles et al., 1996]. These studies show that there is the potential to find deep circulation switches associated with rapid climate events using deep-sea corals.

II. Deep-Sea Corals

Probably the major deterrents to date for studying deep sea corals have been their perceived scarcity, their inaccessibility and a supposed inability to collect fossil specimens. While it is true most of these species are solitary, some do form elevated

carbonate mounds, or bioherms, and are therefore classified as constructional rather than ahermatypic [Schuhmacher and Zibrowius, 1985]. These bioherms represent localized areas of high species density over long time periods [Tiechert, 1958]. By dating both modern and 28,000 year old corals from a single mound, Neumann et al. [Neumann et al., 1977] showed that these deep-sea features may represent continuous calcification over tens of thousands of years. Certain species of the solitary corals, while not as long lived as the mounds, are found throughout the major ocean basins. There are several species of scleractinia and at least one gorgonian that are cosmopolitan in the modern ocean. These species; *Desmophyllum cristagalli*, *Lophelia pertusa*, *Enallopsamia sp.*, *Solenosmilia variabilis* and the gorgonian *Coralium sp.*; offer the best chance of using deep sea corals for high resolution paleoceanographic time series. Deep-sea corals in general are widely distributed in the modern ocean; they have a temperature range of 4°-20°C and a depth range of 60-6000 meters [Cairns and Stanley, 1981]. However, highest population densities are found between about 500 and 2000 meters depth. While an individual species may be more limited than this overall range, most of the above coral types have been found in at least three of the major ocean basins. Pictures of *D. cristagalli* and *Lophelia* are shown in Figures 1.2 and 1.3.

For the solitary and pseudo-colonial corals, there are several features of their distribution that can aid in their collection. These animals are believed to be filter feeders. They derive their food source from organic detritus in the deep water column. Communities growing on the sides and summits of seamounts concentrate in areas of high current flow to maximize their exposure to these suspended nutrients [Genin et al., 1986]. In addition, a deep-sea coral's life cycle can include the production of planulae. These planktonic juveniles must find a hard substrate on which to recruit [Cairns, 1988]. Often this substrate is one of the previous generation of corals. This recruitment strategy leads to "patch" development with many generations in the same spot [Wilson, 1979] and offers the possibility of linking several individuals together in longer time series. In our



Figure 1.2: Drawing of the solitary deep-sea coral *D. cristagalli*. This sample grew from the fragments of previous individuals (see bottom). A single polyp lived in the central cavity formed by the radially symmetric septa. Drawing by Karen Coluzzi of the Woods Hole Oceanographic Institution.



Figure 1.3: Drawing of the constructional deep-sea coral *Lophelia prolifera*. Polyps grow from the "buds" of radially symmetric septa. Taken from Cairns (1981).

sample collection there are two dredges from the New England Seamounts that sampled such a patch of *D. cristagalli*. The need for high currents and hard substrates limits deep-sea corals to certain areas of the deep where they may be easier to find. The spatial distribution and density banded uranium rich skeletons of deep-sea corals make them ideal for some problems but less suited to others in paleoceanography. Table 1.1 summarizes some of the relative benefits and drawbacks in four different paleoclimate archives.

Largely because we have an extensive fossil collection of *D. cristagalli*, I have chosen to concentrate on this species. Both modern and fossil skeletons are 100% aragonite (Figure 1.4). *D. cristagalli* is a solitary deep-sea scleractinian that can sometimes be found with several individuals linked together in a pseudo-colonial morphology. Because individual corals are not new buds from the polyp below, this arrangement does not guarantee continuous growth between the individuals [Smith et al., 1997]. Viewed from above, this species is radially symmetric with five or more cycles of septa (Figure 1.5). A single animal, the polyp, lives in the center of the circle and secretes the regular septal pattern. The largest septa (S1) can be sampled from the rest of the skeleton with a small cutting tool along the sampling lines that are shown in Figure 1.5. While septa are thinnest at the polyp center, at the edge they are connected by innerseptal aragonite which makes the skeleton much thicker. Overall an individual *D. cristagalli* resembles a hollow cone, with the walls thickened, that has thin flanges protruding radially towards the center axis from the conical wall.

Using the single septum as a negative, alternating light and dark density bands can be imaged with a photographic enlarger. Figure 1.6 is a transmitted light image of the "side view" of a septum. The banding pattern has the same morphology as that found in surface, reef building corals. Images of the interior structure of a single septum can be generated by slicing down a septal axis, mounting this surface to a glass slide and milling down to an appropriate thickness. A "front view" of this interior banding comes from

Archive	Pros	Cons
Deep-Sea Sediments	<ol style="list-style-type: none"> 1. Long continuous time series 2. Large data and sample base exists 	<ol style="list-style-type: none"> 1. Bioturbation leads to lower time resolution 2. No direct dating beyond ^{14}C timescale
Surface Corals	<ol style="list-style-type: none"> 1. Annual banding 2. U/Th and ^{14}C dating possible 	<ol style="list-style-type: none"> 1. Short records 2. Few fossil samples recovered
Deep-Sea Corals	<ol style="list-style-type: none"> 1. Density bands 2. U/Th and ^{14}C dating possible 3. Intermediate to upper deep water 	<ol style="list-style-type: none"> 1. Short records 2. Utility only beginning to be explored
Ice Cores	<ol style="list-style-type: none"> 1. Annual bands 2. Long continuous time series 	<ol style="list-style-type: none"> 1. Limited geographic distribution

Table 1.1 Relative merits of several paleoclimate archives.

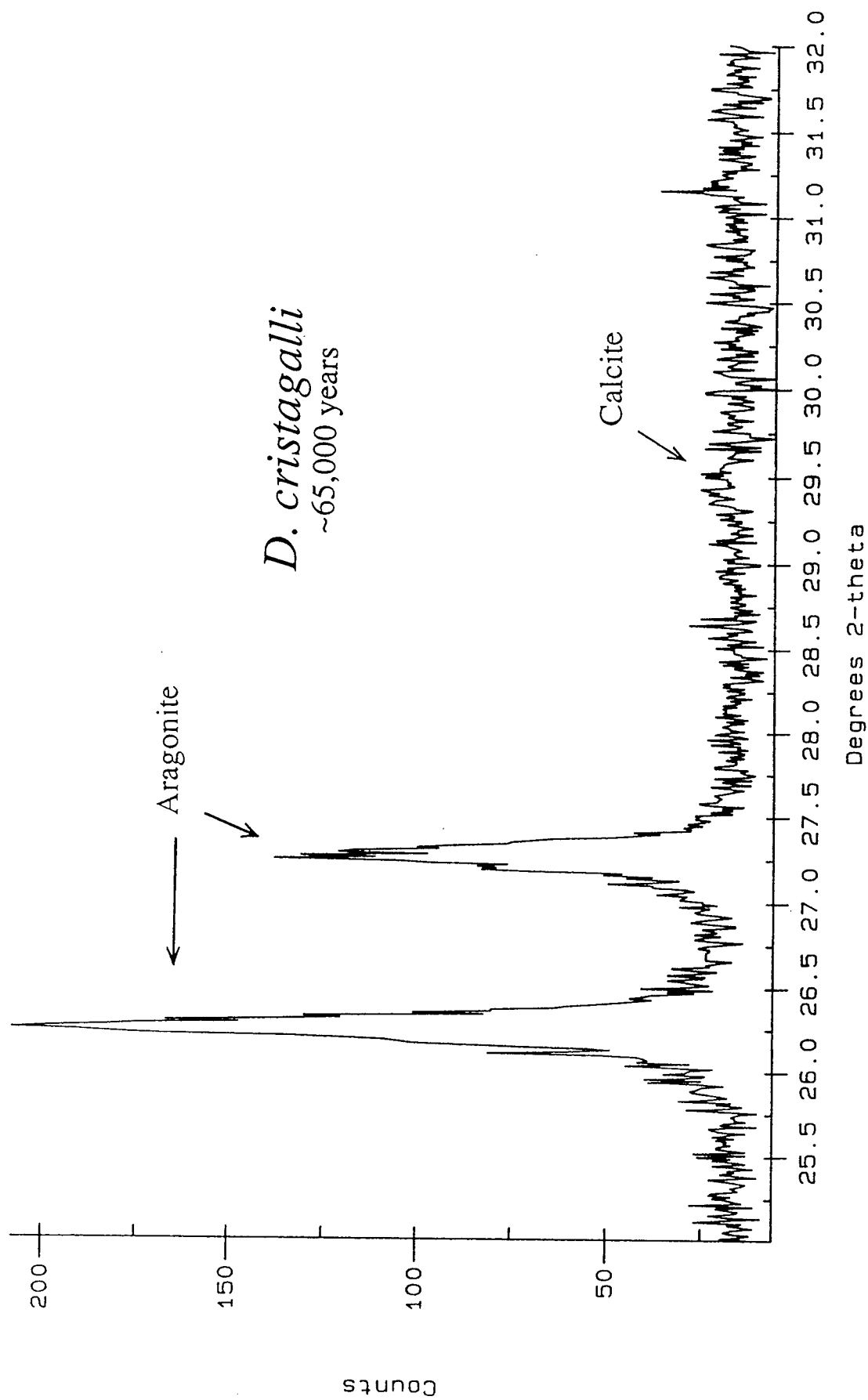


Figure 1.4: XRD spectrum of a 65,000 year old *D. cristagalli*. This sample shows no evidence of diagenetic alteration from aragonite to calcite.

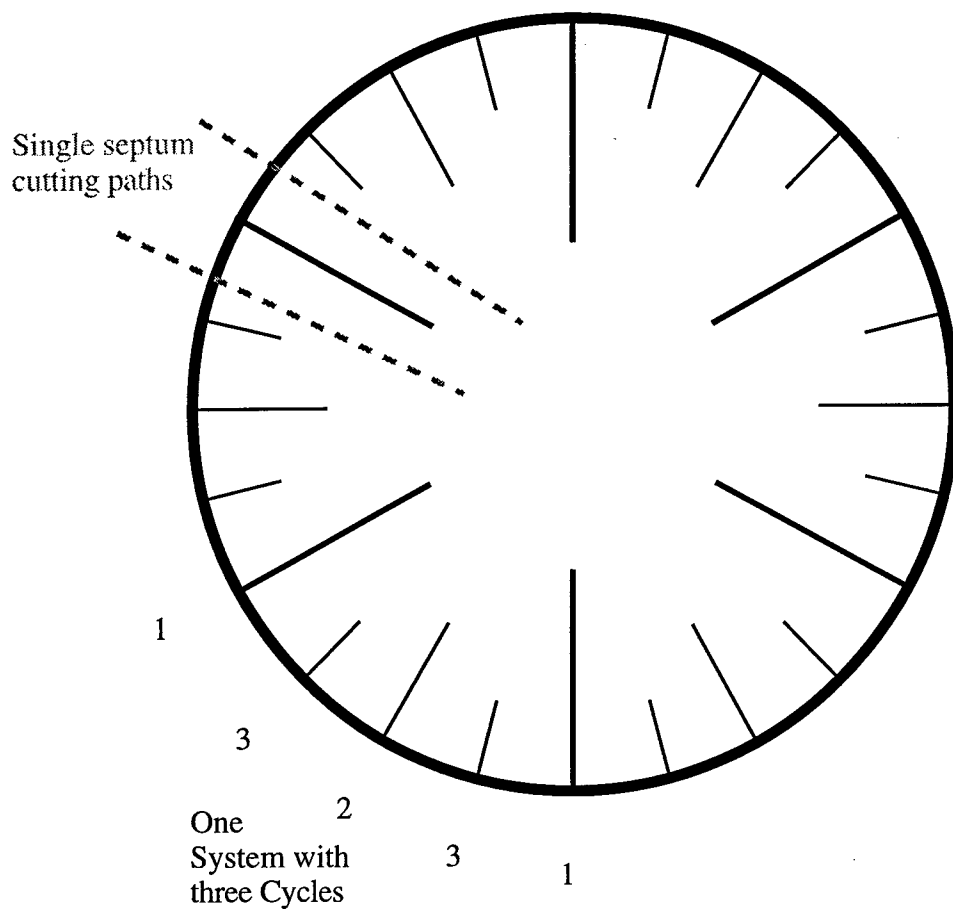


Figure 1.5: Schematic top view of a deep-sea coral with radially symmetric septa. *D. cristagalli* has at least five cycles of septa within one system. Sampling strategy for cutting out a single S1 septum is shown with gray dashed lines.

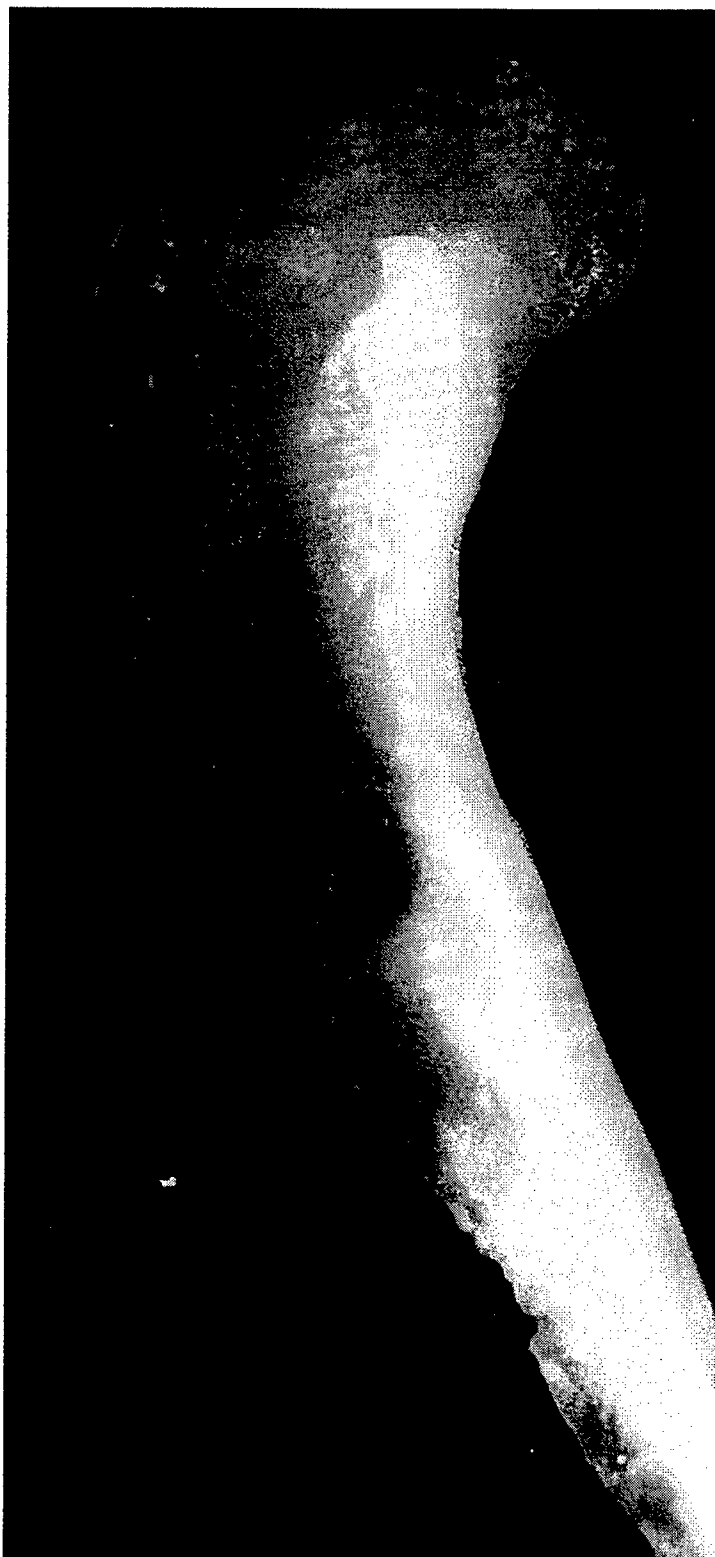


Figure 1.6. Side view of a single septum of *D. cristagalli*. The thinnest septal material shows a regular banding pattern. This pattern is exactly analogous to the banding seen in surface corals. Opaque thick aragonite is seen as white on the right side of this negative image.

cutting down from top to bottom roughly parallel to the septal edge. This exposed surface is epoxied to a glass slide and the excess coral is cut off. Grinding down the sample to a thickness where the banding shows through usually requires a 600 grit polishing wheel. The final sample thickness is variable between individuals but is generally between 200 and 250 μm . The resulting "front view" is shown in Figure 1.7. On the S1 septum, there is a distinct white band that runs the length of the sample. This band is optically dense and "outcrops" at the growing tip of the septum. Assuming that this is the first aragonite precipitated for each phase of new growth, subsequent sheets are added to the sides of the white band as the septum thickens. These sheets show the alternating light and dark density bands. A "top view" of the interior septal and innerseptal surfaces is shown in Figure 1.8. This image was prepared in the same manner as above except that initially the top of a single septum was sliced off and mounted to a glass slide. In Figure 1.8 the center white band can be seen clearly running the length of the septum. White bands for the two smaller side septa can also be seen. The overall banding structure between the two types of septa is clearly different. Side septa have much broader density bands, while the S1 septum seems to be mostly constructed of optically less dense aragonite.

The information from these images can be combined to construct an idealized banding pattern in *D. cristagalli* (Figure 1.9). When viewed from the front, a single septum resembles a series of stacked chevrons. The white, optically dense band seen in Figure 1.7 runs up the apex of these chevrons always finishing at the site of most recent extension. Alternating light and dark density bands are added to the sides of this band as the entire septum thickens. It is the relative concentration of dark versus white bands that gives the side view pattern in Figure 1.6. Slicing off the top of these stacked chevrons reveals an image that resembles mid-ocean ridge magnetics. The white band bisects the image while strips of light and dark bands alternate out to the sides. This view is also very similar to that presented by slicing off the top of an anticline and looking down from



Figure 1.7. Front view of *D. cristagalli* sample number 47407-2A. White band down center of S1 septum is optically dense and assumed to be the first aragonite precipitated.

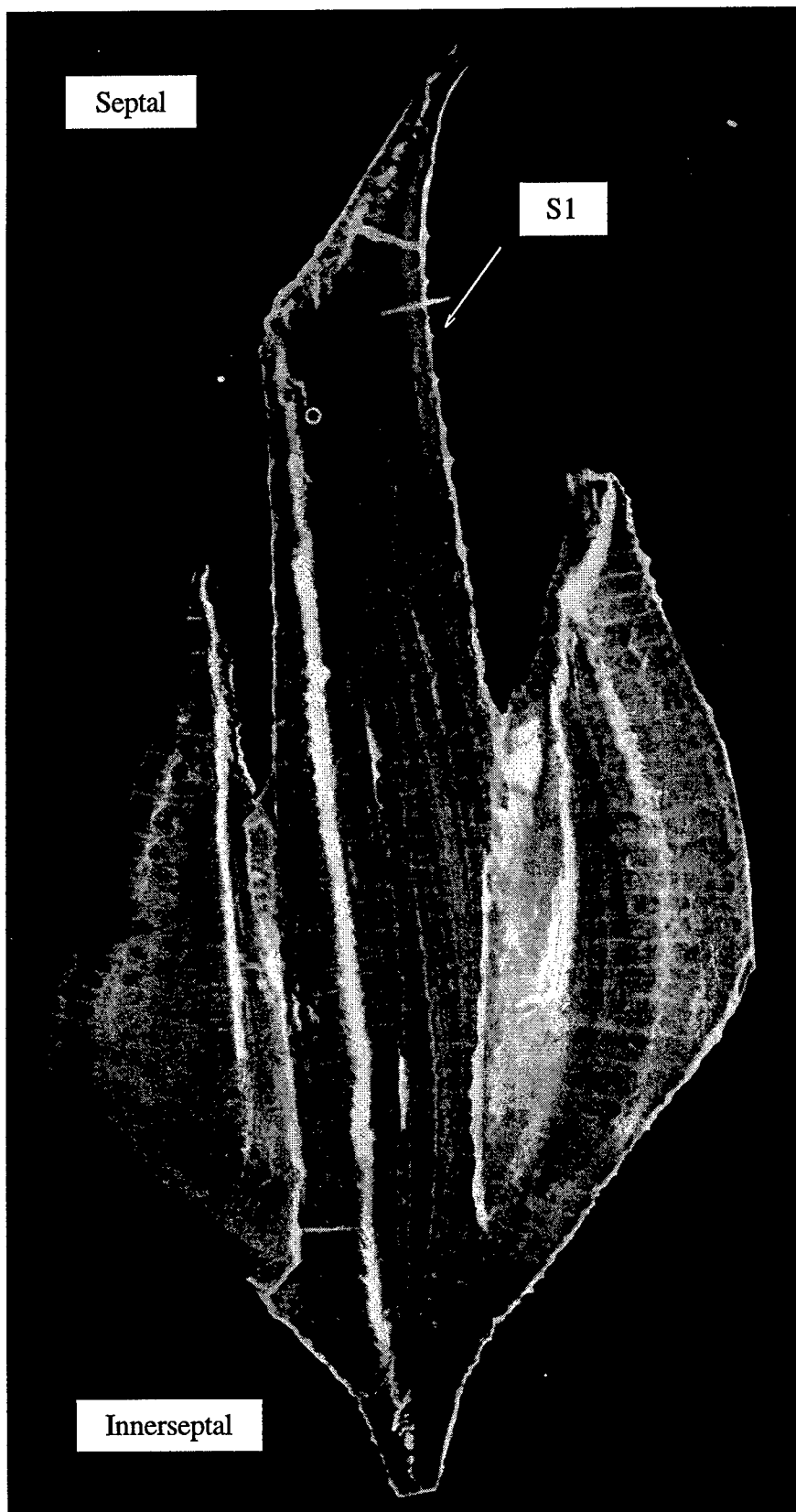


Figure 1.8. Top view of sample number 47407.

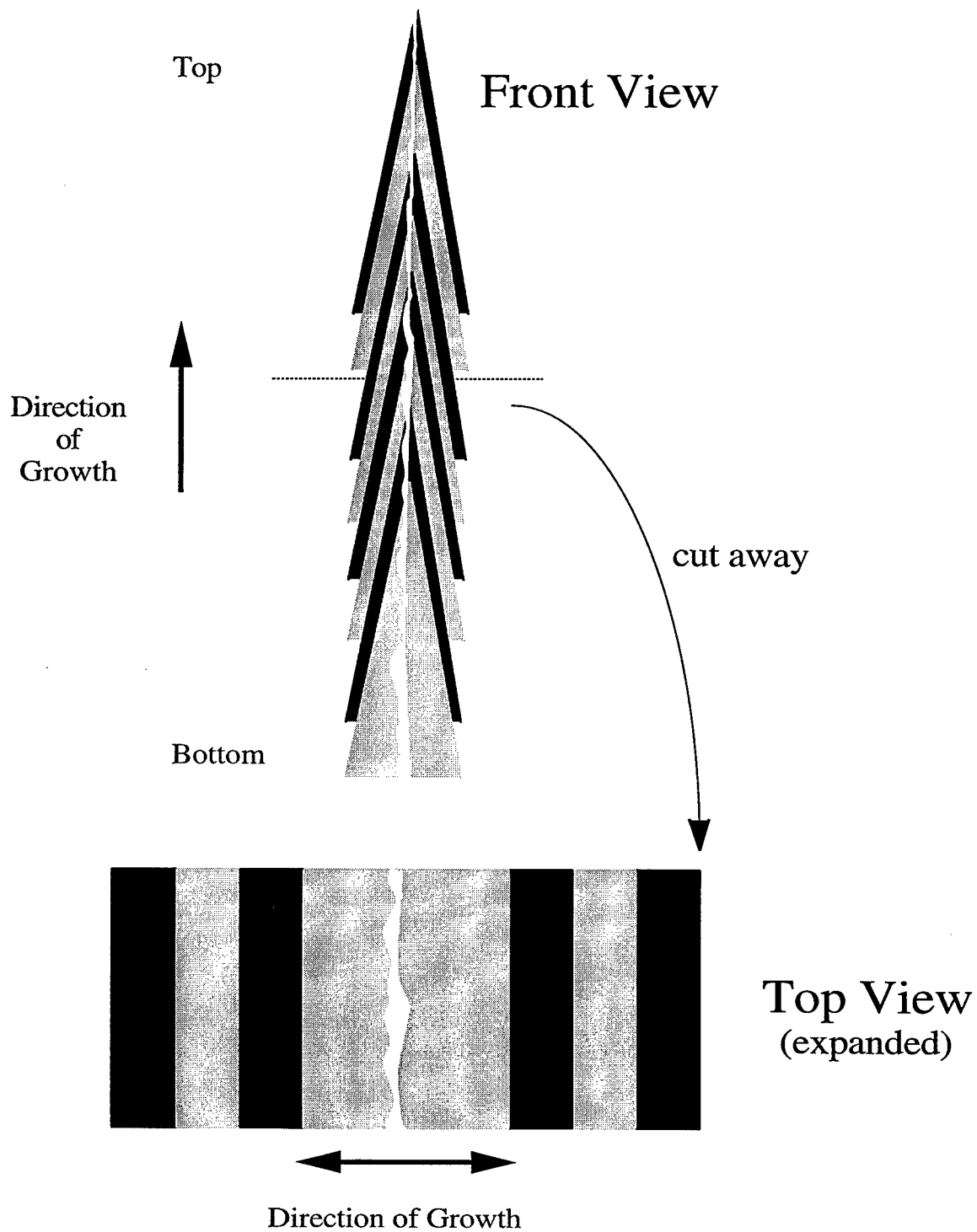


Figure 1.9. Idealized banding pattern in *D. cristagalli*. The front view is pictured as if you are looking directly at the thin edge of a single septum. The top view is looking down on a single septum that has had its top cut off.

above. While Figure 1.9 is an idealized version of *D. cristagalli's* banding, actual samples can emphasize one half of the banding symmetry over the other. In addition, the difference between major (S1) and minor septa is clear in the photos but is not part of the idealized model.

III. Thesis Structure

The combination of density banding and a uranium rich skeleton in *Desmophyllum cristagalli* offers a potentially powerful new archive in deep water paleoceanography. My goal in this thesis is to actualize that potential. Chapter 2 is the theoretical basis of using deep-sea corals for paleo-ventilation rate measurements and has already appeared in the literature [Adkins and Boyle, 1997]. While this section is chiefly about reinterpreting benthic-planktonic foraminiferal radiocarbon data, the basic idea is applicable to the deep-sea corals. Coral measurements provide a water $\Delta^{14}\text{C}$ value at a precise moment in time. Converting this $\Delta^{14}\text{C}$ value into a ventilation age requires some assumptions about the atmospheric $\Delta^{14}\text{C}$ history and the composition of the paleo water mass. This chapter reviews the assumptions and establishes a new type of calculation to convert the $\Delta^{14}\text{C}$ data into water mass age information.

Chapters 3 and 4 describe the laboratory methods and necessary assumptions to generate paleo $\Delta^{14}\text{C}$ data and high precision calendar ages from deep-sea corals. Most of the uranium series dating work described in this thesis is contained in Chapter 3. Data was collected at both MIT and the University of Minnesota in the laboratory of Prof. Larry Edwards and Dr. Hai Cheng. An Inductively Coupled Plasma-Mass Spectrometry method to rapidly and inexpensively screen corals for their ages was developed at MIT. This work places over 300 corals in 5,000 year wide age "bins" that enables efficient identification of the most interesting samples to pursue. The necessary cleaning methods for uranium series dating were also developed at MIT. Both modern and fossil samples deemed important for more precise uranium series dating were sent to Minnesota. There

Dr. Hai Cheng made the high precision Thermal Ionization Mass Spectrometry measurements. This data set includes dates of several fossil samples and constraints on the growth rates of some modern *D. cristagalli* specimens.

Chapter 4 is another collaborative effort, this time with Dr. Ellen Druffel and Sheila Griffin at the University of California at Irvine. Radiocarbon ages of both modern and fossil corals were measured in their lab. Graphite prepared at UCI was analyzed by the Lawrence Livermore National Laboratory Center for Accelerator Mass Spectrometry (CAMS). The main result of this chapter establishes the 1:1 relationship between seawater dissolved inorganic carbon $\Delta^{14}\text{C}$ and deep-sea coral $\Delta^{14}\text{C}$. This modern calibration also constrains the amount of isotopically light CO_2 that is incorporated into a coral's skeleton. In addition, several methods tests were performed to test the veracity of the coral data. Finally, several fossil measurements were made to constrain the ^{14}C history of past water masses in both the Holocene and the last deglaciation.

The stable isotope composition of deep-sea corals is investigated in Chapter 5. Through a collaboration with Dr. Bill Curry, this work was done at the Woods Hole Oceanographic Institution. The previously established linear trend between $\delta^{13}\text{C}$ and $\delta^{18}\text{O}$ in deep-sea corals is confirmed for *D. cristagalli*. There is a slight difference between the stable isotope value of septal and innerseptal aragonite. There is also the possibility that a small amount of light carbon is incorporated into the aragonite skeleton. However, the exact amount is difficult to judge because of uncertainties in calculating the isotopic equilibrium value. The relation between banding pattern and stable isotope composition is investigated using the slides pictured above. The strong correlation between the two implies a sampling strategy that can retrieve time series of $\delta^{18}\text{O}$ of aragonite formed at equilibrium with past seawater.

Finally, in Chapter 6, the information from the previous chapters is used to investigate the circulation behavior of the waters at 1800 meters depth in the North Atlantic at 15.4 ka. In three separate corals from the same dredge that all have the same uranium series

age, there is a large difference in their ^{14}C age. All three samples have younger radiocarbon ages at the bottom than they do at the top. The largest difference implies a 670 year age change in the water at this site in under 160 years. Cd/Ca data from this sample confirms the large water mass transition implied by the ^{14}C data. A preliminary modern calibration, similar to a foraminiferal core top calibration, of Cd/Ca in *D. cristagalli* is also presented. While this is still preliminary work, the data show a partition coefficient of around 1.6 or larger. The combination of the radioactive tracer ^{14}C and the mixing tracer Cd/Ca shows that the radiocarbon age of southern source deep waters in the North Atlantic prior to 15.4 ka was about 500 years.

References

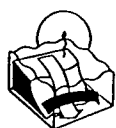
- Adkins, J. F. and E. A. Boyle, Changing atmospheric $\delta^{14}\text{C}$ and the record of deep water paleoventilation ages, *Paleoceanography*, 12, 337-344, 1997.
- Barnola, J. M., D. Raynaud, Y. S. Korotkevitch and C. Lorius, Vostok ice core: a 160,000-year record of atmospheric CO_2 , *Nature*, 329, 408-414, 1987.
- Beck, W. J., L. R. Edwards, E. Ito, F. W. Taylor, J. Recy, F. Rougerie, P. Joannot, et al., Sea-Surface temperature from coral skeletal strontium/calcium ratios, *Science*, 257, 644-647, 1992.
- Behl, R. J. and J. P. Kennett, Brief interstadial events in the Santa Barbara basin, NE Pacific, during the past 60 kyr, *Nature*, 379, 243-246, 1996.
- Birchfield, G. E. and W. S. Broecker, A salt oscillator in the glacial Atlantic? 2. A "scale analysis" model, *Paleoceanography*, 5, 835-843, 1990.
- Bond, G., W. C. Broecker, S. Johnsen, J. McManus, L. Labeyrie, J. Jouzel and G. Bonani, Correlations between climate records from North Atlantic sediments and Greenland ice, *Nature*, 365, 143-147, 1993.
- Boyle, E. A., Cadmium: chemical tracer of deepwater paleoceanography, *Paleoceanography*, 3, 471-489, 1988.
- Boyle, E. A. and L. D. Keigwin, Deep circulation of the North Atlantic over the last 200,000 years: Geochemical evidence, *Science*, 218, 784-787, 1982.
- Boyle, E. A. and L. D. Keigwin, North Atlantic thermohaline circulation during the last 20,000 years linked to high latitude surface temperature, *Nature*, 330, 35-40, 1987.
- Broecker, W. S., G. Bond, M. Klas, G. Bonani and W. Wolfli, A salt oscillator in the glacial northern Atlantic? 1. The concept, *Paleoceanography*, 5, 469-477, 1990.
- Broecker, W. S. and G. H. Denton, The role of ocean-atmosphere reorganizations in glacial cycles, *Geochim. et Cosmochim. Acta*, 53, 2465-2501, 1989.
- Broecker, W. S., R. Gerard, M. Ewing and B. C. Heezen, Natural radiocarbon in the Atlantic Ocean, *Journal of Geophysical Research*, 65, 2903-2931, 1960.
- Broecker, W. S., M. Klas, N. Ragano-Beavan, G. Mathieu, A. Mix, M. Andree, H. Oeschger, et al., Accelerator mass spectrometry radiocarbon measurements on marine carbonate samples from deep-sea cores and sediment traps, *Radiocarbon*, 30, 261-295, 1988.
- Broecker, W. S. and T.-H. Peng, *Tracers in the Sea*, Eldigio Press, Eldigio Press, 690, 1982.
- Broecker, W. S., T. H. Peng, S. Trumbore, G. Bonani and W. Wolfli, The distribution of radiocarbon in the glacial ocean, *Global Biogeochemical Cycles*, 4, 103-117, 1990.
- Broecker, W. S., A. Virgilio and T.-H. Peng, Radiocarbon age of waters in the deep Atlantic revisited, *Geophysical Research Letters*, 18, 1-3, 1991.

- Cairns, S. D., A sexual reproduction in solitary scleractinia, *Proceedings of the 6th International Coral Reef Symposium, Australia.*, Vol. 2, 641-646, 1988.
- Cairns, S. D. and G. D. Stanley Jr., Ahermatypic coral banks: living and fossil counterparts, *Proceedings of the Fourth International Coral Reef Symposium, Manila, I*, 611-618, 1981.
- Charles, C. D., J. Lynch-Stieglitz, U. S. Ninnemann and R. G. Fairbanks, Climate connections between the hemisphere revealed by deep sea sediment core/ice core correlations, *Earth and Planetary Science Letters*, 142, 19-27, 1996.
- Cole, J., E., R. Fairbanks G. and G. Shen T., Recent variability in the Southern Oscillation: isotopic records from a Tarawa Atoll coral, *Science*, 260, 1790-1793, 1993.
- Curry, W., B. and D. Oppo W., Synchronous, high-frequency oscillations in tropical sea surface temperatures and North Atlantic Deep Water production during the last glacial cycle., *Paleoceanography*, 12, 1-14, 1997.
- Duplessy, J.-C., M. Arnold, E. Bard, A. Juillet-Leclerc, N. Kallel and L. Labeyrie, AMS ^{14}C study of transient events and of the ventilation rate of the Pacific intermediate water during the last deglaciation, *Radiocarbon*, 31, 493-502, 1989.
- Duplessy, J. C., N. J. Shackleton, R. G. Fairbanks, L. Labeyrie, D. Oppo and N. Kallel, Deep water source variations during the last climatic cycle and their impact on the global deep water circulation, *Paleoceanography*, 3, 343-360, 1988.
- Emiliani, C., Pleistocene temperatures, *Journal of Geology*, 63, 538-578, 1955.
- Fairbanks, R. G. and R. E. Dodge, Annual periodicity of the $^{18}\text{O}/^{16}\text{O}$ and $^{13}\text{C}/^{12}\text{C}$ ratios in the coral *Montastrea annularis*., *Geochimica et Cosmochimica Acta*, 43, 1009-1020, 1979.
- Genin, A., P. K. Dayton, P. F. Lonsdale and F. N. Spiess, Corals on seamount peaks provide evidence of current acceleration over deep-sea topography, *Nature*, 322, 59-61, 1986.
- GRIP, Climate instability during the last interglacial period recorded in the GRIP ice core, *Nature*, 364, 203-207, 1993.
- Grootes, P. M., M. Stuiver, J. W. C. White, S. Johnsen and J. Jouzel, Comparison of oxygen isotope records from GISP2 and GRIP Greenland ice cores, *Nature*, 366, 552-554, 1993.
- Hester, K. and E. A. Boyle, Water chemistry control of cadmium in recent benthic foraminifera., *Nature*, 298, 260-262, 1982.
- Hughen, K. A., J. T. Overpeck, L. C. Peterson and S. Trumbore, Rapid climate changes in the tropical Atlantic region during the last deglaciation, *Nature*, 380, 51-54, 1996.
- Keigwin, L. D. and S. J. Lehman, Deep circulation change linked to Heinrich event 1 and Younger Dryas in a middepth North Atlantic core., *Paleoceanography*, 9, 185-194, 1994.

- Manabe, S. and R. J. Stouffer, Two stable equilibria of a coupled ocean-atmosphere model, *Journal of Climate*, 1, 841-866, 1988.
- Marotzke, J. and J. Willebrand, Multiple equilibria of the global thermohaline circulation., *Journal of Physical Oceanography*, 21, 1372-1385, 1991.
- Neumann, A. C., J. W. Kofoed and G. H. Keller, Lithohierms in the Straits of Florida, *Geology*, 5, 4-10, 1977.
- Oppo, D. W. and S. J. Lehman, Mid-depth circulation of the subpolar North Atlantic during the last glacial maximum, *Science*, 259, 1148-1152, 1993.
- Rahmstorf, S., Bifurcations of the Atlantic thermohaline circulation in response to changes in the hydrological cycle., *Nature*, 378, 145-149, 1995.
- Sarnthein, M., K. Winn, S. J. A. Jung, J.-C. Duplessy, L. Labeyrie, Erlenkeuser and G. Ganssen, Changes in east Atlantic deepwater circulation over the last 30,000 years: Eight time slice reconstructions, *Paleoceanography*, 9, 209-268, 1994.
- Schuhmacher, H. and H. Zibrowius, What is hermatypic? A redefinition of ecological groups in corals and other organisms, *Coral Reefs*, 4, 1-9, 1985.
- Shackleton, N. J., J.-C. Duplessy, M. Arnold, P. Maurice, M. A. Hall and J. Cartlidge, Radiocarbon age of the last glacial Pacific deep water, *Nature*, 335, 708-711, 1988.
- Smith, J., E., M. Risk J., H. P. Schwarcz and T. A. McConnaughey, Rapid climate change in the North Atlantic during the Younger Dryas recorded by deep-sea corals, *Nature*, 386, 818-820, 1997.
- Stommel, H., Thermohaline convection with two stable regimes of flow, *Tellus*, 13, 224-230, 1961.
- Thompson, L. G., T. Yao, M. E. Davis, K. A. Henderson, E. Mosley-Thompson, P.-N. Lin, J. Beer, et al., Tropical climate instability: the last glacial cycle from a Qinghai-Tibetan ice core, *Science*, 276, 1821-1825, 1997.
- Tiechert, C., Cold and deep-water coral banks, *Bulletin of the American Association of Petroleum Geologists*, 42, 1064-1082, 1958.
- Wilson, J. B., 'Patch' development of the deep-water coral *lophelia pertusa* (L.) on Rockall Bank., *J. Mar. Biol. Ass. U.K.*, 59, 165-177, 1979.

Chapter 2: Calculation of Paleo-Ventilation ages from Coupled Radiocarbon and Calendar Ages

This chapter has already appeared in print, *Paleoceanography*, **12** 337-344 (1997).
Copyright by the American Geophysical Union.



Changing atmospheric $\Delta^{14}\text{C}$ and the record of deep water paleoventilation ages

Jess F. Adkins¹ and Edward A. Boyle

Department of Earth, Atmosphere and Planetary Sciences, Massachusetts Institute of Technology, Cambridge

Abstract. We propose a new calculation method to better estimate the deep water ventilation age from benthic-planktonic foraminifera ^{14}C ages. Our study is motivated by the fact that changes in atmospheric $\Delta^{14}\text{C}$ through time can cause contemporary benthic and planktonic foraminifera to have different initial $\Delta^{14}\text{C}$ values. This effect can cause spurious ventilation age changes to be interpreted from the geologic data. Using a new calculation method, ^{14}C projection ages, we recalculate the data from the Pacific Ocean. Contrary to previous results, we find that the Pacific intermediate and deep waters were about 600 years older than today at the last glacial maximum. In addition, there are possible signals of ventilation age change prior to ice sheet melting and at the Younger Dryas. However, the data are still too sparse to constrain these ventilation transients.

Introduction

Studies of the past oceanic nutrient distributions have provided insight into changing patterns of paleo-ocean circulation [Boyle and Keigwin, 1982; Oppo and Fairbanks, 1987; Duplessy *et al.*, 1988; Boyle, 1992; Sarnthein *et al.*, 1995]. However, these data do not provide direct information on the rate of circulation. As the ocean is presumed to play a large part in the Earth's heat transport, circulation rate information is of prime importance for the study of past climates. Accelerator mass spectrometry (AMS) studies of the radiocarbon content of contemporary benthic and planktonic foraminifera have provided our only direct information on these rates [Broecker *et al.*, 1988; Shackleton *et al.*, 1988; Duplessy *et al.*, 1989; Broecker *et al.*, 1990a, b; Duplessy *et al.*, 1991; Kennett and Ingram, 1995]. In these studies, it is assumed that the age difference between benthic foraminifera and planktonic foraminifera from the same depth in a sediment core is equal to the radiocarbon age difference between the waters in which they grew. By comparing benthic and planktonic pairs from different depths in the core, the radiocarbon age history of deep water at one site is then reconstructed.

The most comprehensive of these studies [Broecker *et al.*, 1990b] compared glacial time slices from several cores to their corresponding core top and modern water ventilation ages. These authors found that the glacial Pacific was slightly older than today and that the glacial intermediate Atlantic was about half as old as it is today. The Atlantic results are consistent with the nutrient tracer data that show, relative to today, an invasion of nutrient-rich southern-source bottom waters farther north in the glacial deep Atlantic. Other studies have attempted to measure benthic-planktonic ventilation ages (B-P ages) through time at a

single site [Andree *et al.*, 1986; Duplessy *et al.*, 1989]. In this paper, we examine how B-P ages can be biased by changes in the atmospheric radiocarbon inventory since the last glacial maximum. We propose a new scheme for calculating past ventilation ages in a changing atmospheric environment called ^{14}C projection ages. By using the B-P data and the record of atmospheric $\Delta^{14}\text{C}$ variations, we compare the B-P ages with our new ^{14}C age projections. After developing the recalculation scheme, we summarize the ^{14}C projection ages of the deglacial Pacific.

Effect of Changing Atmospheric $\Delta^{14}\text{C}$ on Ventilation Ages

There are at least two processes that can alter benthic-planktonic ages from the true deep water ventilation age. B-P ages assume that the initial $^{14}\text{C}/^{12}\text{C}$ ratio of the planktonic foraminifera represents the $^{14}\text{C}/^{12}\text{C}$ ratio that a water mass had when it left the surface. However, it has been shown that surface waters in high-latitude deep water formation sites have ^{14}C ages up to 900 years older than tropical and subtropical surface waters [Broecker, 1963; Bard, 1988; Berkman and Forman, 1996]. This age difference between surface water at a core site and surface water in deep water formation sites means that true water ventilation ages are not identical to deep-surface ages. Second, the atmospheric $\Delta^{14}\text{C}$, and therefore the surface (^{14}C), has been shown to change over the past 20,000 years [Bard *et al.*, 1990; Bard *et al.*, 1993; Edwards *et al.*, 1993; Kromer and Becker, 1993; Pearson *et al.*, 1993; Stuiver and Becker, 1993]. Water masses that left deep water recharge zones at some point before the benthic foraminifera grew did not necessarily equilibrate with the same atmospheric $\Delta^{14}\text{C}$ as their coexisting planktonic counterparts. This latter process is the starting point for this study.

In order to illustrate how benthic-planktonic ages can be biased by changing atmospheric $\Delta^{14}\text{C}$, we have modeled three simple atmospheric $\Delta^{14}\text{C}$ scenarios. In Figures 1a-1c, the atmospheric $\Delta^{14}\text{C}$ time histories (solid gray lines) are prescribed for (a) a constant value of $\Delta^{14}\text{C}$, (b) a sloping value of $\Delta^{14}\text{C}$, and

¹ Also at Massachusetts Institute of Technology/Woods Hole Oceanographic Institution Joint Program in Oceanography, Woods Hole, Massachusetts.

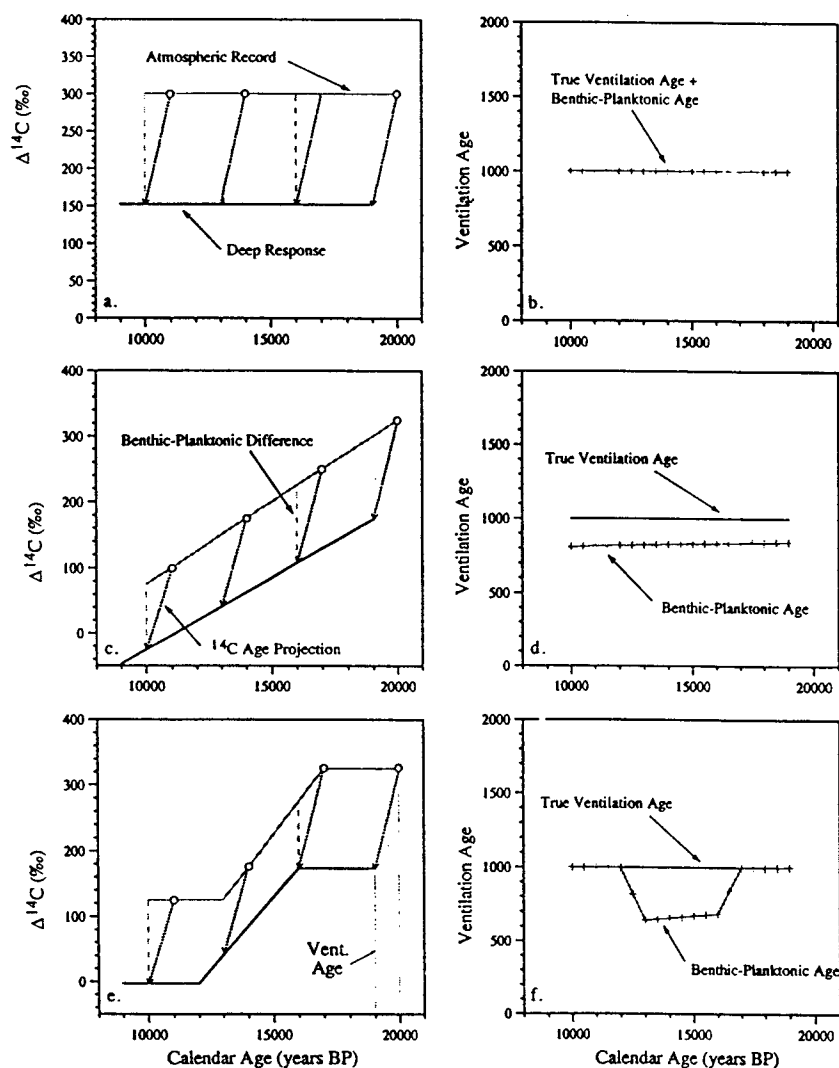


Figure 1. Three theoretical atmospheric $\Delta^{14}\text{C}$ scenarios with their deep water responses. Figures 1a, 1c and 1e prescribe an atmospheric $\Delta^{14}\text{C}$ (gray lines) and then calculate the deep response for a 1000-year ventilation age. Benthic-planktonic ages (B-P ages) are calculated by subtracting the deep $\Delta^{14}\text{C}$ from the contemporary surface value, while the true ventilation age is prescribed to be 1000 years in all cases. Figures 1b, 1d and 1f compare the B-P ages with the true ventilation age for the three corresponding atmospheric $\Delta^{14}\text{C}$ histories. Changes in atmospheric $\Delta^{14}\text{C}$ are recorded in the deep as phase lags that can lead to spurious B-P ventilation ages.

(c) a changing value of $\Delta^{14}\text{C}$. Deep water responses (solid black lines) to these atmospheric scenarios are then generated from a given atmospheric value by calculating the $\Delta^{14}\text{C}$ after 1000 years of decay. For example, in Figure 1a the atmosphere has a $\Delta^{14}\text{C}$ of 300‰ at 20 ka. After 1000 years of decay the $\Delta^{14}\text{C}$ is 152‰. This value is then assigned to the deep waters at 19 ka. In order to generate the deep response line, this process is repeated for the entire atmospheric record. Because the ventilation age is held constant for all scenarios, the deep response is just a phase-lagged version of the atmosphere. This procedure simulates a deep water mass that has (a) a single source region at the surface

(i.e., no mixing between deep waters of different ages), (b) a 1000-year ventilation age and (c) no reservoir age for the surface waters in the source region.

The three idealized atmospheric $\Delta^{14}\text{C}$ records of Figures 1a, 1c and 1e are used to generate B-P ventilation ages. These ages are calculated from the $\Delta^{14}\text{C}$ difference between the surface and deep records at a given time in the past (dashed gray lines in Figures 1a-1c). This $\Delta^{14}\text{C}$ is then converted into time using the true radiocarbon mean life. The deep response, however, follows different trajectories than the dotted gray lines indicating B-P ages. In this model, once the surface water leaves contact with

the atmosphere, it follows a closed system ^{14}C decay path (dotted black lines). This 1000-year decay time causes the deep response to mimic the shape of the atmospheric curve but with a 1000 year time lag. Because the ventilation age was prescribed to be 1000 years, all dotted black lines have nearly the same length.

Figures 1b, 1d and 1f compare the B-P age calculation method to the prescribed ages for the three separate scenarios. When the atmosphere has a constant $\Delta^{14}\text{C}$ (Figure 1a), there is no difference between the B-P age and the true age (Figure 1b). An atmosphere with a constant but nonzero slope in $\Delta^{14}\text{C}$ (Figure 1c) generates a constant offset between the B-P age and the prescribed 1000 years (Figure 1d). The B-P ages are always too low because they assume a smaller initial $^{14}\text{C}/^{12}\text{C}$ ratio for the deep water than was actually the case. For example, the deep water in Figure 1b at 16 ka left the surface with a $\Delta^{14}\text{C}$ value of 250‰. However, the B-P age calculation only "sees" a value of 225‰ and therefore underestimates the ventilation age. Finally, when the atmospheric $\Delta^{14}\text{C}$ record changes slope, the phase-lagged nature of the deep response produces false ventilation age changes (Figure 1f). Whenever the surface and deep records parallel one another, the B-P ventilation age offset will be constant. However, there can be situations (Figure 1e) where the deep $\Delta^{14}\text{C}$ record is constant while the surface record is changing (16-15 ka) or vice versa (13-12 ka). This type of situation creates false ventilation age changes in B-P data and can lead to misinterpretation of past climate systems.

Recalculation Method

We propose a new calculation scheme, the ^{14}C projection method, that is essentially the inverse of the deep response calculation described above. Instead of starting from the atmosphere and decaying for a known time, we use the measured deep water $\Delta^{14}\text{C}$ and project backward in time to its intersection with the surface. We use the atmosphere as the reference point for this calculation and then correct for surface reservoir ages afterward. Therefore the ^{14}C projection method requires a calendar age estimate for the sediment sample, a deep $\Delta^{14}\text{C}$, and a record of atmospheric $\Delta^{14}\text{C}$ in order to calculate a ventilation age. Calendar ages for a benthic and planktonic foraminiferal pair can be calculated from the planktonic radiocarbon age and the tree ring/coral calibration curves. This calculation requires knowing the reservoir age of the planktonic foraminifera's growth environment and may introduce a small source of error into the ventilation age. Given the calendar (cal) age, the deep $\Delta^{14}\text{C}$ value can be calculated in the following manner. First, the benthic foraminifera's ^{14}C age is converted to a measured (meas) $^{14}\text{C}/^{12}\text{C}$ ratio:

$$\left(\frac{^{14}\text{C}}{^{12}\text{C}}\right)_{\text{meas}} = \left(\frac{^{14}\text{C}}{^{12}\text{C}}\right)_{\text{PIPN}} e^{-^{14}\text{C age}/8033}$$

PIPN is the preindustrial pre-nuclear atmosphere [Stuiver and Polach, 1977], and 8033 is the Libby mean life for radiocarbon. The measured isotopic ratio is a function of the $^{14}\text{C}/^{12}\text{C}$ of the deep water mass in which the foraminifera grew and the time since the foraminifera died:

$$\left(\frac{^{14}\text{C}}{^{12}\text{C}}\right)_{\text{meas}} = \left(\frac{^{14}\text{C}}{^{12}\text{C}}\right)_{\text{deep water}} e^{-\text{cal age}/8266}$$

Here 8266 is the true ^{14}C mean life in years. So, equating the two expressions for $(^{14}\text{C}/^{12}\text{C})_{\text{meas}}$

$$\left(\frac{^{14}\text{C}}{^{12}\text{C}}\right)_{\text{deep water}} = \frac{\left(\frac{^{14}\text{C}}{^{12}\text{C}}\right)_{\text{PIPN}} e^{-^{14}\text{C age}/8033}}{e^{-\text{cal age}/8266}}$$

and using the definition of $\Delta^{14}\text{C}$:

$$\Delta^{14}\text{C}_{\text{deep water}} = \left[\frac{\left(\frac{^{14}\text{C}}{^{12}\text{C}}\right)_{\text{deep water}} - \left(\frac{^{14}\text{C}}{^{12}\text{C}}\right)_{\text{PIPN}}}{\left(\frac{^{14}\text{C}}{^{12}\text{C}}\right)_{\text{PIPN}}} \right] \times 1000$$

The expression for the deep water isotope ratio can be substituted into the above expression to generate the deep water $\Delta^{14}\text{C}$ value:

$$\Delta^{14}\text{C}_{\text{deep water}} = \left(\frac{e^{-^{14}\text{C age}/8033}}{e^{-\text{cal age}/8266}} - 1 \right) \times 1000$$

This expression does not depend on knowing the PIPN atomic ratio, the measured fraction modern [Donahue et al., 1990], or the $\delta^{13}\text{C}$ of the samples [Stuiver and Polach, 1977]. These values are already incorporated into the reported ^{14}C ages.

Using the equation above, previously published benthic/planktonic pairs can be converted to deep water $\Delta^{14}\text{C}$ values. The problem is how to relate this deep $\Delta^{14}\text{C}$ to a true water ventilation age. The deep water $\Delta^{14}\text{C}$ is a function of the source zone's reservoir age, the ventilation age, and the atmospheric $\Delta^{14}\text{C}$. Deciding which past atmospheric $\Delta^{14}\text{C}$ value to correct to is, in turn, dependent on the ventilation age itself. By back calculating the ^{14}C history the deep water parcel would have had if it followed closed system decay, we propose to account for the effect of changing atmospheric $\Delta^{14}\text{C}$ on the deep $\Delta^{14}\text{C}$ concentration. Though there are several assumptions involved with the new method (discussed below), the ^{14}C projection calculation provides a consistent and independent way to choose the best initial atmospheric $\Delta^{14}\text{C}$ value for the deep water mass.

An example of this calculation is shown in Figure 2 using the intermediate western North Pacific data of Duplessy et al. [1989] (CH 84-14, 41°44'N, 142°33'E, 978 m depth). The atmospheric $\Delta^{14}\text{C}$ record from tree rings and corals is shown in gray, and the converted benthic foraminifera values are shown in black. Error bars for the benthic data are large because of uncertainties in the radiocarbon to calendar age conversion and plateaus in the radiocarbon timescale. Black lines that begin at the benthic data and extend back toward the atmospheric record are the ^{14}C age projections. This is the path, in $\Delta^{14}\text{C}$ space, that deep water with the measured calendar age and $\Delta^{14}\text{C}$ would have followed if it behaved as a closed system for radiocarbon decay. If there was no mixing between deep waters of different source regions, then the intersection of these projections with the atmospheric record is the estimated time the deep water parcels left the surface. Therefore the calendar age difference between the intersection point and the benthic data point is the ventilation age relative to the atmosphere (see the area labeled vent. age in Figure 2 for the graphical calculation).

However, this ventilation age still needs to be corrected for two factors: the reservoir age of the deep water source region

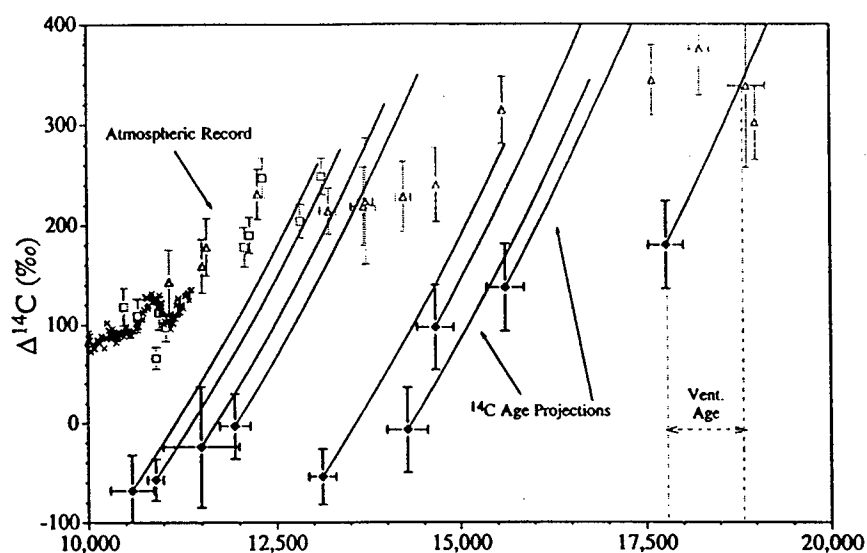


Figure 2. Data from Duplessy *et al.* [1989] transformed into deep $\Delta^{14}\text{C}$ values (solid diamonds). The atmospheric records of $\Delta^{14}\text{C}$ from tree rings and corals are in gray: German oak and pine record (crosses), Bard *et al.* [1993] data (open triangles) and Edwards *et al.* [1993] data (open squares). Error bars are 2σ . The ^{14}C age projections are the $\Delta^{14}\text{C}$ values the Duplessy *et al.* data would have had if they followed closed system radiocarbon decay. The intersection of the age projections and the atmospheric record indicate the time in the past the deep water left the surface. The difference between the deep age and the intersection age is the ventilation age relative to the atmosphere.

and, as mentioned above, mixing between waters of two source regions. If the deep water is from a single source region that has a constant offset from the atmosphere, the region's reservoir age can be subtracted and the calculation is straightforward. Exactly how constant the reservoir ages of deep water source regions are through time is the subject of current research [Bard *et al.*, 1994; Austin *et al.*, 1995; Goslar *et al.*, 1995]. From the comparison between the tree ring and coral records over the past 11.5 kyr, we know that the tropical reservoir age in both the Atlantic and Pacific has remained roughly 400 years [Bard *et al.*, 1990; Bard *et al.*, 1993; Edwards *et al.*, 1993]. When this reservoir age is subtracted from the coral record, it agrees precisely with the record of atmospheric $\Delta^{14}\text{C}$ as measured in tree rings. Only three of the nineteen coral points that overlap with the tree ring record lie outside 2σ errors. On the other hand, recent work on terrestrial and marine carbon that is coeval with the Vedde Ash has shown that the high-latitude surface North Atlantic may have been 300 years older than today during the Younger Dryas [Bard *et al.*, 1994; Austin *et al.*, 1995; Gronvold *et al.*, 1995; Birks *et al.*, 1996]. In any event, the B-P and the ^{14}C projection calculations both will contain the same errors due to possible reservoir age differences at the deep water source zones.

If the deep water is a mixture of southern and northern source waters, calculating the exact reservoir age is more complicated [Broecker, 1979; Broecker *et al.*, 1991]. In certain "two source" deep waters, like the modern deep Atlantic, the ^{14}C projection ages can overstate the ventilation age. The error arises from

choosing the incorrect reservoir age to subtract from the ^{14}C projection ages. When waters with old reservoir ages from the Southern Ocean mix with northern source waters with younger reservoir ages, the resulting "initial" value for the deep water mass is older than the usual planktonic correction of 400 years. This means that the ^{14}C projection age will not fully account for the reservoir age and will predict a ventilation age that is too high. We have examined this effect in some detail and concluded that it is a secondary effect that requires more detailed treatment elsewhere.

There is another possible complication to the ^{14}C projection method based on how the atmospheric $\Delta^{14}\text{C}$ changes are caused in the first place: through production rate variations or changes in the carbon pool exchange rates. While it is possible that changes in ocean circulation themselves can cause changes in atmospheric $\Delta^{14}\text{C}$, analysis of the paleogeomagnetic field [Tric *et al.*, 1992] and the radiocarbon timescale [Mazaud *et al.*, 1991] have shown that nearly all of the long-term radiocarbon inventory changes can be explained by production rate variations. However, several recent studies [Goslar *et al.*, 1995; Björk *et al.*, 1996; Stocker and Wright, 1996] have argued that there was an increase in atmospheric $\Delta^{14}\text{C}$ at the beginning of the Younger Dryas that could be caused by a decrease in North Atlantic Deep Water (NADW) formation. This circulation change causes the atmosphere $\Delta^{14}\text{C}$ to rise sharply, thus making ^{14}C projection ages and B-P ages look older than reality. Though there are situations where the ventilation age can be overstated by systematically and

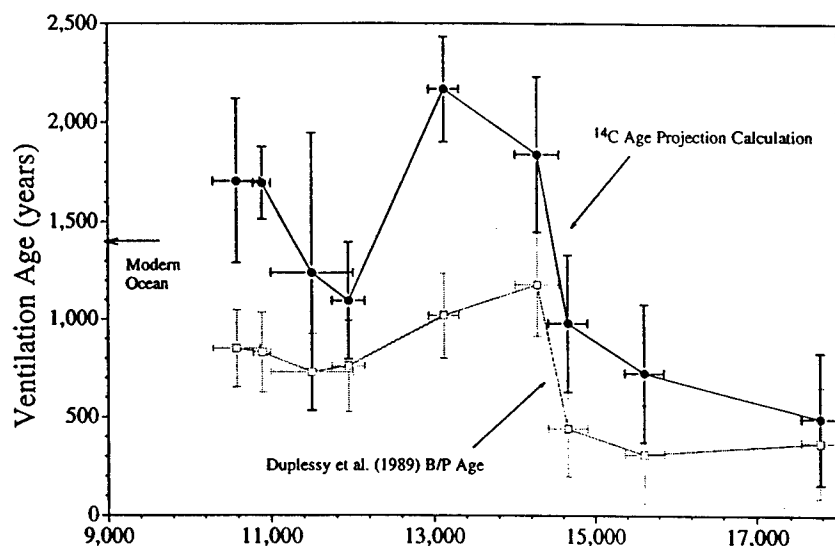


Figure 3. Ventilation ages predicted by the data in Figure 2 compared with the B-P ages reported by Duplessy *et al.* [1989]. The black arrow labeled modern ocean indicates the age of modern bottom waters at this site. A 560-year reservoir age has been subtracted from the ^{14}C projection ages.

independently removing the effect of atmospheric $\Delta^{14}\text{C}$ variations, the ^{14}C projection ages can provide a better estimate of circulation rate.

Implications of New Method

The Duplessy *et al.* [1989] data in Figure 2 are from the western North Pacific core CH 84-14 (41°44'N, 142°33'E, 978 m depth). This area probably fits the criterion of a single source for the deep waters. We therefore disregard the secondary effects on ventilation ages due to mixing. Once the Duplessy *et al.* benthic results are converted to deep water $\Delta^{14}\text{C}$ values, we can use Figure 2 to graphically calculate the ^{14}C projection ages for this data set and compare them with the B-P ages (Figure 3, Table 1). We have subtracted a 560-year reservoir age from all ^{14}C projection ages in order to be consistent with Duplessy *et al.*'s age calculations. As shown in Figure 3, all of the ^{14}C projection ages are higher than the B-P ages. This result is due to the fact that the long-term trend in atmospheric $\Delta^{14}\text{C}$ from 20 to 10 ka is a decrease from about 300‰ to 100‰. As was shown in the model calculations (Figures 1c and 1d), this trend will lead to B-P ages that underestimate the true ventilation age. In addition, the point where the two methods are in the best agreement (17.7 ka) occurs where the atmospheric record is relatively constant.

The biggest difference in the structure of the two curves is seen for the four most recent points. Here the B-P ages predict, within error, a constant ventilation age. The ^{14}C projection ages, on the other hand, rise toward the modern value. Examination of the atmospheric record shows that the planktonic foraminifera record a $\Delta^{14}\text{C}$ decrease in surface waters, yet the deep waters left the surface when the $\Delta^{14}\text{C}$ was nearly flat. In this case, planktonic foraminifera were recording a changing atmosphere

that the benthic water masses never "saw." This type of artifact in B-P ages occurs at ^{14}C age plateaus. Because they are caused by the rate of atmospheric ^{14}C decrease being equal to the natural rate of ^{14}C decay, plateaus are times when the ^{14}C projections will parallel the atmospheric record. Carbon 14 projections will therefore predict a much different starting atmospheric value of $\Delta^{14}\text{C}$ for the benthic foraminifera than recorded by the planktonic foraminifera. In such situations, the atmospheric correction to ventilation ages is very important.

Recent work, as was discussed above, has argued for a rapid rise in atmospheric $\Delta^{14}\text{C}$, due to a reduction in NADW formation, during the period spanned by these last four points in Figure 3. Because the ^{14}C projection method is sensitive to atmospheric $\Delta^{14}\text{C}$ changes, the corrected data in Figure 3 may be overstated. However, during this period, the atmosphere clearly changes from an average value of about 200‰ to about 100‰ (Figure 2). So while the situation is more complicated than a passive ocean responding to an atmospheric $\Delta^{14}\text{C}$ change, there is some component of changing $\Delta^{14}\text{C}$ missing in the B-P ages during the ^{14}C age plateau. The effect of the most recent ^{14}C age plateau on modern ventilation age estimates has been previously addressed [Broecker *et al.*, 1991]. These authors found that the plateau from 1600 to 1950 A.D., shown to be due to production rate changes modulated by the Sun, had at most a 10-15% effect on the modern Atlantic ventilation ages. However, as pointed out by the authors, the full effect of the plateau has not been seen because the Atlantic contains southern component waters which are buffered against the atmospheric changes of the last millennium.

In an effort to synthesize the Pacific ventilation age results, we have reanalyzed the available data. We concentrate here on three cores: CH 84-14 from the northwestern intermediate Pacific

ADKINS AND BOYLE: ATMOSPHERIC $\Delta^{14}\text{C}$ AND PALEOVENTILATION AGES

Table 1. Recalculated Foraminiferal Ventilation Ages from the Pacific

Depth cm	Calendar Age		Benthic ^{14}C		$[\text{C}^{14}]$		Intersection		Ventilation Age	
	Years	Error	Years	Error	‰	Error	Age, years	Error	Years	Error
<i>Core CH 84-14 (41°44'N 142°33'E, 978 m)^a</i>										
230	10,585	285	10,850	140	-68	36	12,850	300	1,705	414
280	10,895	105	11,060	150	-57	21	13,150	150	1,695	183
310	11,500	500	11,370	130	-24	61	13,300	500	1,240	707
340	11,944	200	11,630	180	-3	33	13,600	225	1,096	301
400	13,122	186	13,200	150	-54	28	15,850	190	2,168	266
430	14,362	211	13,010	170	125	37	age reversal in core			
480	14,276	273	13,930	220	-7	43	16,675	280	1,839	391
510	14,660	248	13,500	200	97	43	16,200	250	980	352
550	15,615	248	14,140	200	137	44	16,900	250	725	352
690	17,772	236	15,940	190	180	44	18,825	240	493	337
<i>Core Sonne 50-37KL (18°54'N 115°46'E, 2695 m)^b</i>										
60-65	9,070	110	10,030	120	-140	17	11,550	250	2,080	273
80-85	11,500	500	11,890	110	-85	57	13,900	500	2,400	707
160-165	17,537	132	17,100	220	-7	31	20,350	150	2,400	200
175-180	18,380	101	17,430	140	55	22	20,850	125	2,070	161
195-200	20,197	136	18,940	160	89	28	22,500	140	1,903	195
205-210	20,311	162	19,445	190	37	32	23,100	170	2,390	235
<i>Core TR 163-31B (3°37'S 83°58'W, 3210 m)^c</i>										
85	16,755	248	15,660	270	81	49	18,600	250	1,270	350
103	18,286	285	16,850	230	121	50	20,100	285	1,245	403
114	19,149	322	19,510	330	-106	51	age reversal in benthics ^d			
121	19,796	298	17,400	240	257	59	20,850	330	475	445
153	23,174	322	22,140	310	49	58	26,100	350	2,345	475
166	25,795 ^d	347	23,420	310	228	70	27,640	350	1,280	493
176	25,758	310	24,530	470	64	74	28,700	320	2,380	445

^aFrom Duplessy et al. [1989]. 560-year reservoir age correction.

^bFrom Broecker et al. [1990a]. 400-year reservoir age correction. Only used data with replicated planktonic ages.

^cFrom Shackleton et al. [1988]. 580-year reservoir age correction. All data from depths with benthics.

^dThe Shackleton et al. data have two points where ^{14}C ages show reversals, one planktonic and one benthic. Following their ideas, we interpret the benthic record as less susceptible to atmospheric fluctuations in ^{14}C inventory and throw out the benthic age reversal. The planktonic reversal leads to the two different ventilation ages at 26 ka in Figure 4. This discrepancy may be due to rapid variations in the atmospheric $\Delta^{14}\text{C}$ that do not propagate down to the depth of the core location. See the text. The data table shows all the data used to compile the Pacific ventilation age history in Figure 4. The depths and benthic ^{14}C ages are taken directly from the data tables in the original papers. Calendar ages are calculated from the reported planktonic ^{14}C ages and the tree ring/coral calibration data. Benthic $\Delta^{14}\text{C}$ was calculated from the calendar age, and the ^{14}C age for the benthic foraminifera was calculated according to the equations in the Recalculation Method section of the present paper. Intersection and ventilation ages were calculated graphically as described in the text and Figure 2.

(41°44'N, 142°33'E, 978 m) [Duplessy et al., 1989]; Sonne 50-37KL from the South China Sea with a sill depth of about 2500 m (18°54'N, 115°46'E, 2695 m) [Broecker et al., 1990a, b] and TR 163-31B from the eastern Pacific in the Panama Basin (3°37.2'S, 83°58'W, 3210 m) [Shackleton et al., 1988]. The results are shown in Figure 4 and listed in Table 1. When available, we only used points where all planktonic species from the same depth had the same radiocarbon age within 2 σ errors. Modern ventilation ages for the three sites, calculated from the Geochemical Ocean Sections Study (GEOSECS) data, are also pictured. Errors from the calendar ages are propagated in the deep $\Delta^{14}\text{C}$ calculations and can lead to large uncertainties. The points at 11.5 ka are particularly affected by the calendar age errors because they derive from a ^{14}C age plateau and therefore provide little constraint on the ventilation age. A reinterpreted record of the meltwater record in corals is also pictured in Figure 4. We have fitted a polynomial through the combined sea level data of Bard et al. [1993] and Edwards et al. [1993] and

calculated the fit's first derivative. No corrections were made for possible variations in a particular coral species depth of growth.

Ventilation ages of both the intermediate and deep Pacific waters were about 600 years older than today's values during the last glacial. This is older than Broecker et al.'s [1990b] previous result but is in rough agreement with the analysis of Shackleton et al. [1988]. Broecker et al. attribute this difference to upwelling at the site of TR 163-31B. However, this analysis shows that different atmospheric histories of $\Delta^{14}\text{C}$ for the Sonne data, 20-15 ka, as opposed to the Trident data, before 20 ka, can also contribute to the different results. Though poorly constrained by the coral data, there is more of a decrease in atmospheric $\Delta^{14}\text{C}$ during 20-15 ka than before 20 ka. This difference in atmospheric $\Delta^{14}\text{C}$ slope can lead to offsets between B-P ages from the two different times.

The data also show a decrease in ventilation age before the onset of rapid melting in the North Atlantic. However, this result requires patching together cores. No one record preserves the

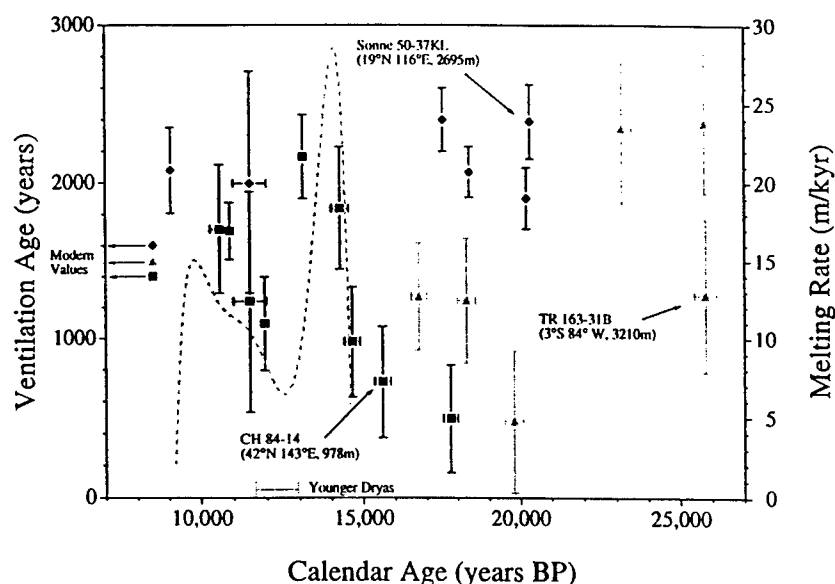


Figure 4. Summary of Pacific deep ventilation age data. The data from three cores CH 84-14 (solid squares) from the South China Sea (41°44'N, 142°33'E, 978 m depth), Sonne 50-37KL (solid diamonds) from the western tropical Pacific (18°54'N, 115°46'E, 2695 m) and TR163-31B (gray triangles) from the eastern Pacific (3°37.2'S, 83°58'W, 3210 m) in the Panama Basin have been recalculated using ^{14}C age projections. The meltwater history predicted by the sea level data of *Bard et al.* [1993] and *Edwards et al.* [1993] is plotted as a dashed line. Modern values for the bottom waters at the three core sites are shown at the left. The age of the Younger Dryas cold interval as found in the GISP2 ice core [Alley et al., 1993] is shown at the bottom.

entire transition, and the best constrained record, Sonne 50-37KL, alone shows no transient in ventilation age. While this result is intriguing, we require further data before the exact timing of ventilation age changes and ice sheet decay can be established. In the data of *Duplessy et al.* [1989], there is also an indication of a speedup of intermediate circulation during the Younger Dryas that is partially supported by the South China Sea core. Recalculated data from the Santa Barbara basin also indicate a decrease in Pacific intermediate ventilation age at the beginning of the Younger Dryas [Ingram and Kennett, 1995; Kennett and Ingram, 1995]. Pacific deep water values are still several hundred years older than modern values at the beginning of the Holocene. This feature was seen in earlier data from the South China Sea [Andree et al., 1986], but different species of planktonic foraminifera from the same depths rarely gave the same radiocarbon age in these cores and so were determined to be biased by dissolution artifacts. Until better dated records of ventilation age changes are obtained, the conclusion that ocean circulation changes preceded ice sheet decay is preliminary at best.

Conclusions

The traditional calculation method for benthic-planktonic ventilation ages can be biased by changes in the atmosphere's radiocarbon inventory. These biases have different effects depending on the temporal history of the atmospheric record, but under plausible circumstances this effect can show false ventilation age changes when ocean circulation was in an

unchanging state. Using the new calculation scheme of ^{14}C projection ages, the primary effect of the changing atmospheric record can be removed. A key assumption of this new method is that atmospheric $\delta^{14}\text{C}$ is driven chiefly by production rate effects and not by exchanges between carbon reservoirs. However, both the B-P ages and the ^{14}C projection ages are affected by changes in surface reservoir ages, so both calculation schemes are estimates rather than true values. In addition, the ^{14}C projection method can underestimate the ventilation ages for deep waters that are a mixture of waters from two different source regions.

Our reanalysis of the existing data shows that Pacific intermediate and deep waters were both about 600 years older than their modern values at the last glacial maximum. At the beginning of the Holocene, the deep waters were still several hundred years older than core top and modern water data, indicating that there have been circulation changes during the past 10,000 years. In addition to the steady circulations, two transients in ventilation age are also apparent in the recalculated data. The first is a minimum in ventilation age at the time of glacial melting. The circulation change appears to precede the meltwater pulse, but the exact date of the ventilation age switch is not well constrained. There is also the hint of better ventilated intermediate waters during the Younger Dryas on both sides of the Pacific basin, but the data are too sparse to draw firm conclusions. A faster ocean circulation prior to ice sheet melting may indicate that increased ocean heat transports initiated glacial decay. This ventilation signal could be better constrained by records from deep-sea corals and more B-P data from high sedimentation rate cores.

Acknowledgments. We would like to thank Delia Oppo, Nick Shackleton and Daniel Sigman for helpful discussions. Edouard Bard, J. R. Toggweiler and M. L. Delaney provided constructive reviews of the manuscript. J. F. A. was supported by a NASA Global Change Fellowship and a grant from the Tokyo Electric and Power Company. We gratefully acknowledge the support of NSF grant # OCE-94-02198 and NOAA grant # NA46GP0282.

References

- Alley, R. B., et al., Abrupt increase in Greenland snow accumulation at the end of the Younger Dryas event, *Nature*, 362, 527-529, 1993.
- Andree, M., et al., Limits on the ventilation rate for the deep ocean over the last 12,000 years, *Clim. Dyn.*, 1, 53-62, 1986.
- Austin, W. E. N., E. Bard, J. B. Hunt, D. Kroon, and J. D. Peacock, The ^{14}C age of the Icelandic Vedde Ash: Implications for Younger Dryas marine reservoir age corrections, *Radiocarbon*, 37, 53-62, 1995.
- Bard, E., Correction of accelerator mass spectrometry ^{14}C ages measured in planktonic foraminifera: Paleoceanographic implications, *Paleoceanography*, 3, 635-645, 1988.
- Bard, E., B. Hamelin, R. G. Fairbanks and, A. Zindler, Calibration of the ^{14}C timescale over 30,000 years using mass spectrometric U-Th ages from Barbados corals, *Nature*, 345, 405-410, 1990.
- Bard, E., M. Arnold, R. Fairbanks, and B. Hamelin, ^{230}Th - ^{234}U and ^{14}C ages obtained by mass spectrometry on corals, *Radiocarbon*, 35, 191-199, 1993.
- Bard, E., M. Arnold, J. Mangerud, M. Paterne, L. Labeyrie, J. Duprat, M.-A. Melieres, E. Sonstegaard, and J. C. Duplessy, The North Atlantic atmosphere-sea surface ^{14}C gradient during the Younger Dryas climatic event, *Earth Planet. Sci. Lett.*, 126, 275-287, 1994.
- Berkman, P. A., and S. L. Forman, Prebomb radiocarbon and the reservoir correction for calcareous marine species in the Southern Ocean, *Geophys. Res. Lett.*, 23, 363-366, 1996.
- Birks, H. H., S. Gulliksen, H. Hafliðason, J. Mangerud, and G. Possnert, New radiocarbon dates for the Vedde Ash and the Saksunarvatn Ash from western Norway, *Quat. Res.*, 45, 119-127, 1996.
- Björk, S., et al., Synchronized terrestrial-atmosphere deglacial records around the North Atlantic, *Science*, 274, 1155-1160, 1996.
- Boyle, E. A., Cadmium and $\delta^{13}\text{C}$ paleochemical ocean distributions during the stage 2 glacial maximum, *Ann. Rev. of Earth Planet. Sci.*, 20, 245-287, 1992.
- Boyle, E. A., and L. D. Keigwin, Deep circulation of the North Atlantic over the last 200,000 years: Geochemical evidence, *Science*, 218, 784-787, 1982.
- Broecker, W. S., $^{14}\text{C}/^{12}\text{C}$ ratios in surface ocean water, *Nuc. Geophys., Nucl. Sci. Ser., Rep. 38*, Natl. Acad. of Sci.-Natl. Res. Council., Washington, D. C., 1963.
- Broecker, W. S., A revised estimate for the radiocarbon age of North Atlantic Deep Water, *J. Geophys. Res.*, 84, 3218-3226, 1979.
- Broecker, W. S., et al., Accelerator mass spectrometry radiocarbon measurements on marine carbonate samples from deep-sea cores and sediment traps, *Radiocarbon*, 30, 261-295, 1988.
- Broecker, W. S., M. Klas, E. Clark, S. Trumbore, G. Bonani, W. Wolfli, and S. Ivy, Accelerator mass spectrometric measurements on foraminifera shells from deep sea cores, *Radiocarbon*, 32, 119-133, 1990a.
- Broecker, W. S., T. H. Peng, S. Trumbore, G. Bonani, and W. Wolfli, The distribution of radiocarbon in the glacial ocean, *Global Biogeochem. Cycles*, 4, 103-117, 1990b.
- Broecker, W. S., A. Virgilio, and T.-H. Peng, Radiocarbon age of waters in the deep Atlantic revisited, *Geophys. Res. Lett.*, 18, 1-3, 1991.
- Donahue, D. J., T. W. Linick, and A. J. T. Jull, Isotope ratio and background corrections for accelerator mass spectrometry radio carbon measurements, *Radiocarbon*, 32, 135-142, 1990.
- Duplessy, J. C., N. J. Shackleton, R. G. Fairbanks, L. Labeyrie, D. Oppo, and N. Kallel, Deep water source variations during the last climatic cycle and their impact on the global deep water circulation, *Paleoceanography*, 3, 343-360, 1988.
- Duplessy, J.-C., M. Arnold, E. Bard, A. Juillet-Leclerc, N. Kallel, and L. Labeyrie, AMS ^{14}C study of transient events and of the ventilation rate of the Pacific intermediate water during the last deglaciation, *Radiocarbon*, 31, 493-502, 1989.
- Duplessy, J.-C., E. Bard, M. Arnold, N. J. Shackleton, J. Duprat, and L. Labeyrie, How fast did the ocean-atmosphere system run during the last deglaciation?, *Earth Planet. Sci. Lett.*, 103, 27-40, 1991.
- Edwards, L. R., W. J. Beck, G. S. Burr, D. J. Donahue, J. M. A. Chappell, A. L. Bloom, E. R. M. Druffel, and F. W. Taylor, A large drop in atmospheric $^{14}\text{C}/^{12}\text{C}$ and reduced melting in the Younger Dryas, documented with ^{230}Th ages of corals, *Science*, 260, 962-967, 1993.
- Goslar, T., et al., High concentration of atmospheric ^{14}C during the Younger Dryas cold episode, *Nature*, 377, 414-417, 1995.
- Gronvold, K., N. Oskarsson, S. J. Johnsen, H. B. Clausen, C. U. Hammer, G. Bond, and E. Bard, Ash layers from Iceland in the Greenland GRIP ice core correlated with oceanic and land sediments, *Earth Planet. Sci. Lett.*, 135, 149-155, 1995.
- Ingram, B. L., and J. P. Kennett, Radiocarbon chronology and planktonic-benthic foraminiferal ^{14}C age differences in Santa Barbara basin sediments, Hole 893A, *Proc. Ocean Drill. Program Sci. Results*, 146 (part 2), 19-27, 1995.
- Kennett, J. P. and, B. L. Ingram, A 20,000-year record of ocean circulation and climate change from the Santa Barbara basin, *Nature*, 377, 510-514, 1995.
- Kromer, B. and, B. Becker, German oak and pine ^{14}C Calibration, 7200-9439 BC, *Radiocarbon*, 35, 125-135, 1993.
- Mazaud, A., C. Laj, E. Bard, M. Arnold and, E. Tric, Geomagnetic field control of ^{14}C production over the last 80 kyr: Implications for the radiocarbon timescale, *Geophys. Res. Lett.*, 18, 1885-1888, 1991.
- Oppo, D. and, R. G. Fairbanks, Variability in the deep and intermediate water circulation of the Atlantic Ocean during the past 25,000 years: Northern hemisphere modulation of the Southern Ocean, *Earth Planet. Sci. Lett.*, 86, 1-15, 1987.
- Pearson, G. W., B. Becker, and F. Qua, High-precision ^{14}C measurement of German and Irish oaks to show the natural ^{14}C variations from 7890 to 5000 BC, *Radiocarbon*, 35, 93-104, 1993.
- Sarnthein, M., et al., Variations in Atlantic surface ocean paleoceanography, 50°-80°N: A time slice record of the last 30,000 years, *Paleoceanography*, 10, 1063-1094, 1995.
- Shackleton, N. J., J.-C. Duplessy, M. Arnold, P. Maurice, M. A. Hall, and J. Cartlidge, Radiocarbon age of the last glacial Pacific deep water, *Nature*, 335, 708-711, 1988.
- Stocker, T. F. and, D. G. Wright, Rapid changes in ocean circulation and atmospheric radiocarbon, *Paleoceanography*, 11, 773-796, 1996.
- Stuiver, M. and, B. Becker, High precision decadal calibration of the radiocarbon time scale, AD 1950-6000 BC, *Radiocarbon*, 35, 35-65, 1993.
- Stuiver, M. and, H. A. Polach, Reporting of ^{14}C data, *Radiocarbon*, 19, 355-363, 1977.
- Tric, E., J.-P. Valet, P. Tucholka, M. Paterne, L. Labeyrie, F. Guichard, L. Tauxe, and M. Fontugne, Paleointensity of the geomagnetic field during the last 80,000 years, *J. Geophys. Res.*, 97, 9337-9351, 1992.

J. F. Adkins and E. A. Boyle, Department of Earth, Atmosphere and Planetary Sciences, Mail Stop E34-209, Massachusetts Institute of Technology, Cambridge, MA 02139. (e-mail: adkins@mit.edu; eaboyle@mit.edu)

(Received September 19, 1996; revised January 22, 1997; accepted January 26, 1997.)

Chapter 3: Uranium series dating of deep-sea corals

I. Introduction

Uranium series dates from surface corals provide constraints on several late Quaternary climate processes. Past sea level estimates from α -counted ^{230}Th dates on raised coral terraces from Barbados confirmed the Milankovitch hypothesis on the relation between glacier ice volume and insolation [Broecker et al., 1968]. Later Thermal Ionization Mass Spectrometry (TIMS) work confirmed the early α -counting data in a variety of locations [Edwards et al., 1986/87; Edwards et al., 1987; Stein et al., 1993; Gallup et al., 1994; Muhs et al., 1994; Szabo et al., 1994; Stirling et al., 1995]. Drill cores of submerged corals that have been precisely dated by ^{230}Th methods contain our most detailed and continuous record of sea-level since the last glacial maximum [Bard et al., 1990; Bard et al., 1993; Edwards et al., 1993]. Coupled high precision radiocarbon and uranium series dates from surface corals constrain the history of atmospheric $\Delta^{14}\text{C}$ beyond the tree ring calibration [Bard et al., 1993; Edwards et al., 1993]. Finally, TIMS dates provide precise ages for coral tracer based studies of past oceanographic conditions.

Precise U-series dates of deep-sea corals can address the timing of deep-ocean changes and, with radiocarbon dates, the rate of past ocean circulation. The theoretical basis for using coupled uranium series and radiocarbon dates to measure ocean ventilation rates is described in Chapter 2. In order to also use time series of tracers measured in the corals as constraints on deep circulation history, we need to understand the growth rates of this new archive. Several studies using a variety of methods have examined this aspect of deep-sea coral behavior. Duncan [1877] and Pratje [1924] reported growth rates of 6.8-7.5 mm/year in specimens of the genus *Lophelia* attached to underwater transatlantic cables. In a separate study, Teichert [Teichert, 1958] estimated a growth rate of 7.5-15 mm/year for *Lophelia*. However, all of these studies have been criticized for incorrect identification the coral species. Grigg [Grigg, 1974] determined a value of about 20 mm/year vertically and 3 mm/year horizontally for two gorgonians by

tagging colonies of *Muricea californica* and *Muricea furticosa* from a relatively shallow depth of 14-20 m. He suggested that the periodicity of growth ring formation was annual based on comparing the estimated ages to observed growth rates and numbers of growth rings. Druffel et al. [Druffel et al., 1990] calculated a mean value of 0.11 ± 0.02 mm/year horizontally using α -counting of ^{210}Pb in a calcitic deep-sea gorgonian, *Corallium niobe*, from 600 m depth in the Florida Straights. The banding in this sample was not annual. Stein et al. [Stein et al., 1991] determined TIMS ^{230}Th ages from the solitary coral *Balanophyllia elegans* that lives in the intertidal zone. However, the only modern sample was heavily contaminated and gave no information about its age and growth rate. Older samples from their study show relatively high ^{232}Th contamination and elevated $\delta^{234}\text{U}$ values over those for modern seawater and surface corals. In sum, there is still very little information on the growth rate of solitary deep-sea corals, their $\delta^{234}\text{U}$ values, their ^{232}Th concentration and the initial $^{230}\text{Th}/^{232}\text{Th}$ ratios in pristine samples [Cheng et al., 1995; Goldstein et al., 1996].

At the end of this chapter, ^{230}Th TIMS dating techniques for both modern and fossil deep-sea corals from various localities are presented. As *D. cristagalli* is the most abundant coral in our collection of fossil specimens, this species was the focus of our work. The magnitude of the uncertainty in dating caused by ^{230}Th contamination associated with ^{232}Th is discussed. Based on the Th and the U isotopic composition and the size of a single septum, the ranges in mean ages and growth rates are calculated for some modern corals. Comparison between the number of growth bands and the calculated mean ages provides an estimate the periodicity of band formation. In addition, the data show a constant $\delta^{234}\text{U}$ value for modern samples and a relatively large variation of uranium contents for both old and modern samples. The first part of this chapter is a detailed discussion of the cleaning methods used to remove contaminating crusts from the coral samples. This section is followed by the description and results of a new coral age

screening technique that is used to evaluate individual coral samples for their paleoceanographic utility.

II. Coral Cleaning Techniques

Cleaning methods for uranium series dating were developed from the trace metal methods previously described for surface corals [Shen and Boyle, 1988] and foraminifera [Boyle, 1981]. As the fossil deep-sea corals are covered in a black crust and the modern samples often have organic material remaining in septal interstices, we developed an extensive pre-cleaning routine to remove the bulk of these contaminants before samples were treated to the more rigorous full cleaning. This expansion of the pre-cleaning step is the main deviation from the methods of Shen and Boyle (1988). Because we could not identify the contaminating phase, we felt a cleaning step was warranted before measurement by mass spectrometry. Previous studies have chosen not to chemically clean samples as there is some concern that uranium and thorium will be fractionated during the wet leaches. It is possible that our method slightly alters the true $^{230}\text{Th}/^{238}\text{U}$ ratio, but contamination by external crusts is so large that cleaning is necessary to make any measurements at all. While the trace metal methods clearly removed contaminating uranium and thorium, some ^{232}Th was also being left behind. At the end of this section we describe some preliminary results on ligand complexation steps that can be added to the normal cleaning procedure to further purify samples for uranium series dating. Errors due to contamination not cleaned from samples are fully discussed in the TIMS dating section and included in all the reported.

Pre-cleaning steps were developed to remove black crusts from the exterior of fossil samples. An electron probe of the black crust on fossil corals (Figure 3.1) reveals that it is a manganese and iron oxide that traps significant amounts of detrital aluminosilicates. Mn and Fe peaks are not large in Figure 3.1 because this sample had already been pre-treated before being run on the electron probe. Interestingly, the crusts are most easily

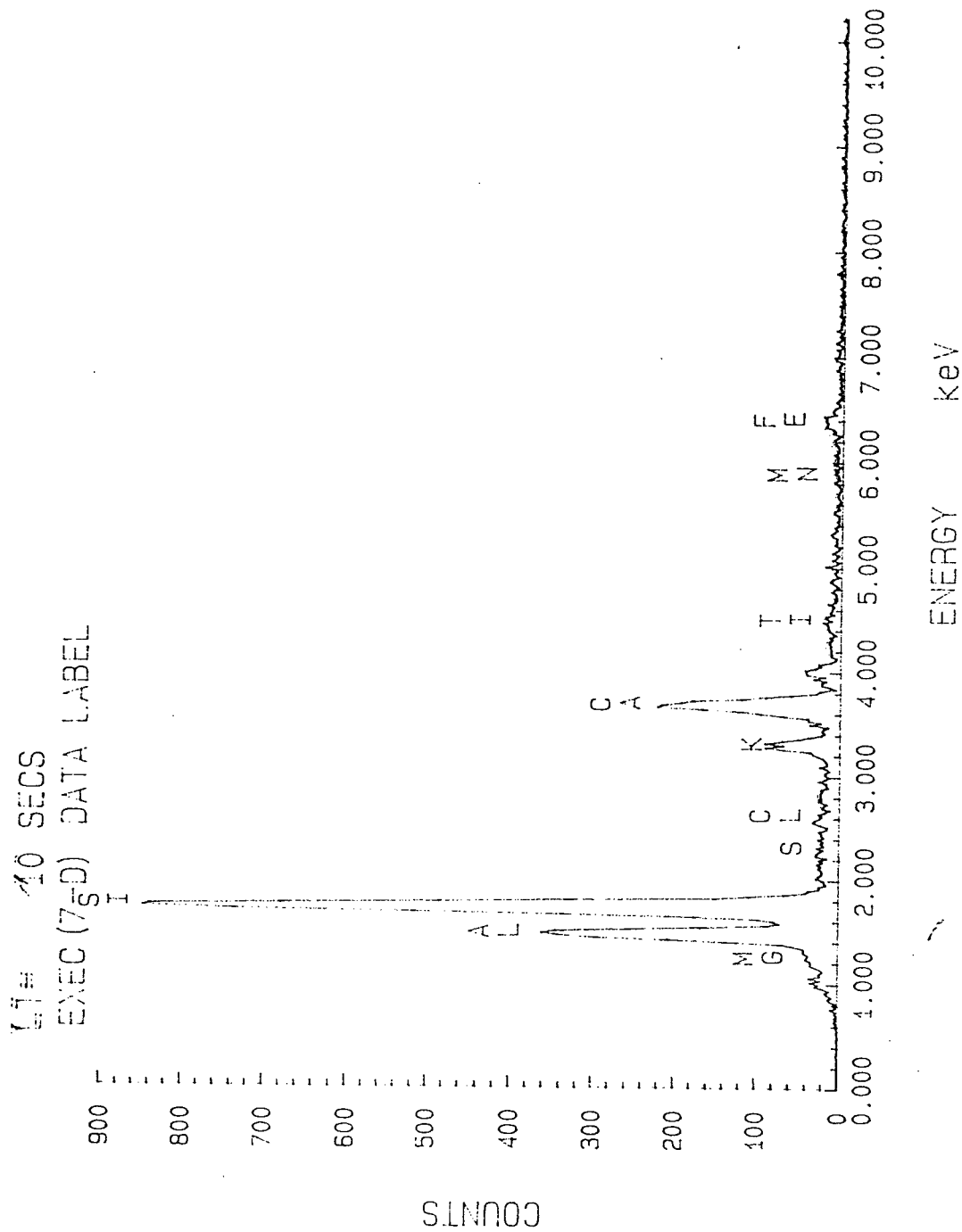


Figure 3.1. Electron probe of the black crust covering fossil deep-sea corals. There is a clear detrital signature. Mn and Fe peaks are reduced because this sample had been precleaned before loading particles to be analyzed.

removed with an oxidizing step, after which they flake off in small sheets. This is evidence that the crust is bound by an organic "glue", possibly composed of remnant polyp organic matter. The mechanical and chemical pre-cleaning steps are designed to remove this organic coating between the coral and the crust. Cleaning begins with water rinses and scrubbing with a brush to remove sediment from inside the coral and between the septa. Samples are then immersed in a 50/50 mixture of 30% H_2O_2 and 1N NaOH and ultrasonicated for 15 minutes. This oxidizing solution step is repeated several times. Occasionally between oxidizing steps samples are again scrubbed with a brush. Oxidizing solution steps are repeated until there is very little black crust left on a sample. However, this process often leaves a brownish/orange organic stain on the CaCO_3 . Quick dips (30 seconds to 2 minutes) in a 50/50 mixture of 30% H_2O_2 and 1% HClO_4 efficiently remove this stain. However, the perchloric acid also dissolves about 5-10% of the sample. It is important to note that the pH of this solution is always less than 2 during this step so thorium released during cleaning most likely remains in solution. Small siphons for spent cleaning solutions and plastic racks to hold samples aid in the mechanics of the cleaning process. After the dilute perchloric step, samples are rinsed thoroughly with clean distilled water.

The above pre-cleaning technique is followed by a more rigorous trace metal cleaning process. Samples are broken up with an agate mortar and pestle and then sieved for the 250-710 μm size fraction. These pieces are placed in an acid cleaned 2.0 ml polyethylene centrifuge tube, which is positioned in a hand made acrylic rack. Samples are rinsed several times with clean distilled water ($\text{d-H}_2\text{O}$) and ultrasonicated for 5 minutes during each rinse. Every ultrasonication step is followed by resuspension of the sample in $\text{d-H}_2\text{O}$ and immediate siphoning to remove the water and unwanted fine particles. 30 seconds of ultrasonication in 500 μL of 2% HNO_3 is followed by 2 minutes of ultrasonication in 500 μL CH_3OH with resuspension after both steps. One other $\text{d-H}_2\text{O}$ rinse with 5 minutes of ultrasonication precedes the first oxidative step. Oxidizing

solution, identical to the one described above except that 0.1N NaOH is used instead of 1N, is added to each of the samples. Vials are covered with a screw tightened plastic lid and heated for 20 minutes in a boiling water bath. During the heating the sample rack is removed every 2 minutes for 10 seconds of ultrasonication. After 20 minutes, the samples are rinsed with two 5 minute d-H₂O ultrasonication steps.

Oxidized contaminants are removed with a reducing solution that contains citric acid to complex any released metals. The citric acid solution is prepared beforehand by dissolving 30 grams of citric acid monohydrate in 250 ml of d-H₂O and 250μL of concentrated NH₄OH. To remove metal contaminants, 100μL of a wet Chelex resin slurry in 6N HCl is added, and the whole solution is shaken overnight. Resin beads are removed by filtration and the solution is stored in the hood. At the time of sample cleaning a working solution is prepared by mixing 10 ml of the citric acid solution, 10 ml of concentrated NH₄OH and 750μL of hydrazine in a small beaker. 1500μL of this solution is added to each sample vial, the samples are covered with a screw tightened lid and the whole rack is heated in a boiling water bath for 30 minutes. At 2 minute intervals the samples are ultrasonicated for 10 seconds and then placed back in the hot water bath. After 30 minutes the whole rack is rinsed thoroughly in the hood with d-H₂O and the samples are then rinsed several times with d-H₂O. A single d-H₂O rinse with 5 minutes of ultrasonication follows the reducing step. Samples are then subjected to a repeat of the heated oxidative step described above. Finally the corals are rinsed with d-H₂O with 5 minutes of ultrasonication and then transferred to new clean vials. The last step is to ultrasonicate for 30 seconds with 1000μL of 2% HNO₃ to remove any adsorbed contaminants and then rinse thoroughly with d-H₂O. The acid rinse step is not long enough to allow the pH to rise above two.

In the TIMS dating section that follows, it will be shown that our cleaning technique adopted from the trace metal methods works, but it is also clear that it is not cleaning all the adsorbed thorium. As thorium has a much lower solubility than many of the

transition metals, we believe that it is being cleaned from the coral surfaces but then re-adsorbed before the cleaning solution can be siphoned away. To eliminate this problem we tried to use several different thorium complexing ligands to hold thorium in solution once all contaminating phases had been removed. The experiment was designed to mimic the end of the trace metal cleaning method where a clean coral is surrounded by some amount of contaminating thorium. We soaked crushed and sieved coral pieces (250-710 μ m) that had already been pre-cleaned in a ^{232}Th standard overnight. These doped corals are 70-180 times enriched in ^{232}Th over their background level after pre-cleaning (Figure 3.2a). Doped samples were then exposed to either DTPA, Oxalic Acid, HCl or d-H₂O to examine how much thorium each of these solutions could remove. The experiment was divided into three steps as depicted in Table 3.1. Each ultrasonication step lasted for 15 minutes, and the solutions were siphoned off between steps. After all three steps the remaining sample was dissolved in HNO₃ and measured by ICP-MS for [^{232}Th] and by FAA for [Ca]. Half of the DTPA and oxalic acid samples were treated twice with ligand, but this seems to make very little difference (Figure 3.2). The most dramatic effect is with DTPA. This complexing agent is able to remove nearly all of the added ^{232}Th . Other solutions removed variable amounts of thorium, with HCl being the next best cleaning agent. The drawback to DTPA is that it also has a high affinity for calcium. Percent recoveries were the lowest for DTPA indicating significant sample loss. Some mechanical loss must have occurred, because the d-H₂O control samples show some loss of calcium as well. While none of the samples in this thesis were actually treated with a new complexing agent, a DTPA step seems to be a good candidate to add to the method. In future work, one thing that would need to be determined is whether the large sample loss associated with DTPA leads to a change in the absolute age.

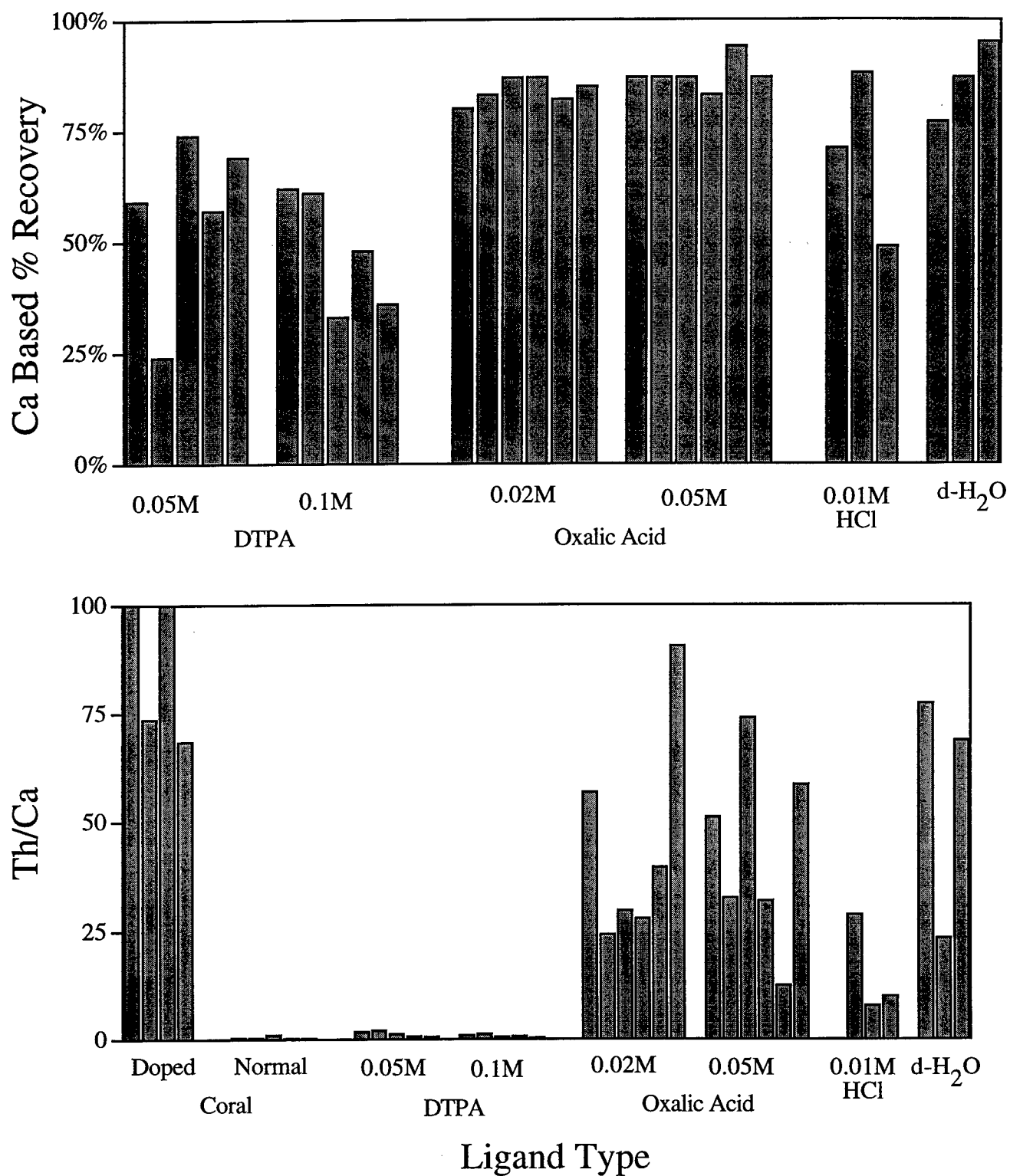


Figure 3.2. Results of ligand ^{232}Th cleaning test. Th/Ca ratios are reduced to near background levels with DTPA but % recoveries can be poor. There is some mechanical loss as the d-H₂O samples do not show 100% recovery.

Ligand:	DTPA	Oxalic Acid	HCl	d-H ₂ O
Step 1	HCl	Oxalic	HCl	d-H ₂ O
Step 2	DTPA	NaOH	-----	-----
Step 3	half the samples get more DTPA	half the samples get more Oxalic	Liquid siphoned off	Liquid siphoned off

Table 3.1: Thorium complexing experimental procedure. There was no difference between samples exposed 1x and 2x to the same ligand.

III. Uranium Series Age Screening

While TIMS uranium series dating and Accelerator Mass Spectrometry (AMS) radiocarbon dating of carbonates are widely used, these techniques are both time consuming and expensive. With over 300 samples collected from dredge collections and the Smithsonian, we needed a method to rapidly and inexpensively date deep-sea corals. Previous work on excess ^{230}Th in marine sediments [Shaw and Francois, 1991] demonstrated that Inductively Coupled Plasma-Mass Spectrometry (ICP-MS) is faster than and equally as precise as α -counting methods. Based on this study, we developed an ICP-MS method to screen deep-sea corals for their ages. Though not as precise as TIMS or AMS dating, this screening method allows us to decide which specimens are suitable for further study by placing them in 5,000 year wide age "bins". This method is especially useful for deciding which corals grew in the 5-35,000 year age window that is appropriate for paleo-ventilation rate studies of the ocean.

Approximately 1g of sample was subjected to the pre-cleaning steps described in the previous section. As this is a screening technique and not designed for the most precise dating, we eliminated the full cleaning treatment to save time. The sample was crushed into several smaller pieces with an agate mortar and pestle to facilitate dissolution. A flow diagram of the age screening process is shown in Figure 3.3. Five milliliters of concentrated (16N) HNO_3 were added to the reservoir of a capillary, slow, gravity drip coral dissolver ("Mr. Coral") and the sample was placed underneath in a clean pre-weighed 16 ml polyethylene tube. Samples were left in "Mr. Coral" to dissolve overnight. Because the coral samples react vigorously with the addition of concentrated nitric acid, "Mr. Coral" was developed to allow for unattended spill-free dissolution. After dissolution, 20 μl of ^{229}Th spike (~ 10 nM) was added to the sample, the total weight was measured and the sample was vortex mixed. A 25 μL aliquot was removed from the solution spiked with 250 μL ^{235}U standard and diluted with 1.5 ml of 0.1N HNO_3 . This solution was run directly on the ICP-MS (see below). The total weight of the uranium

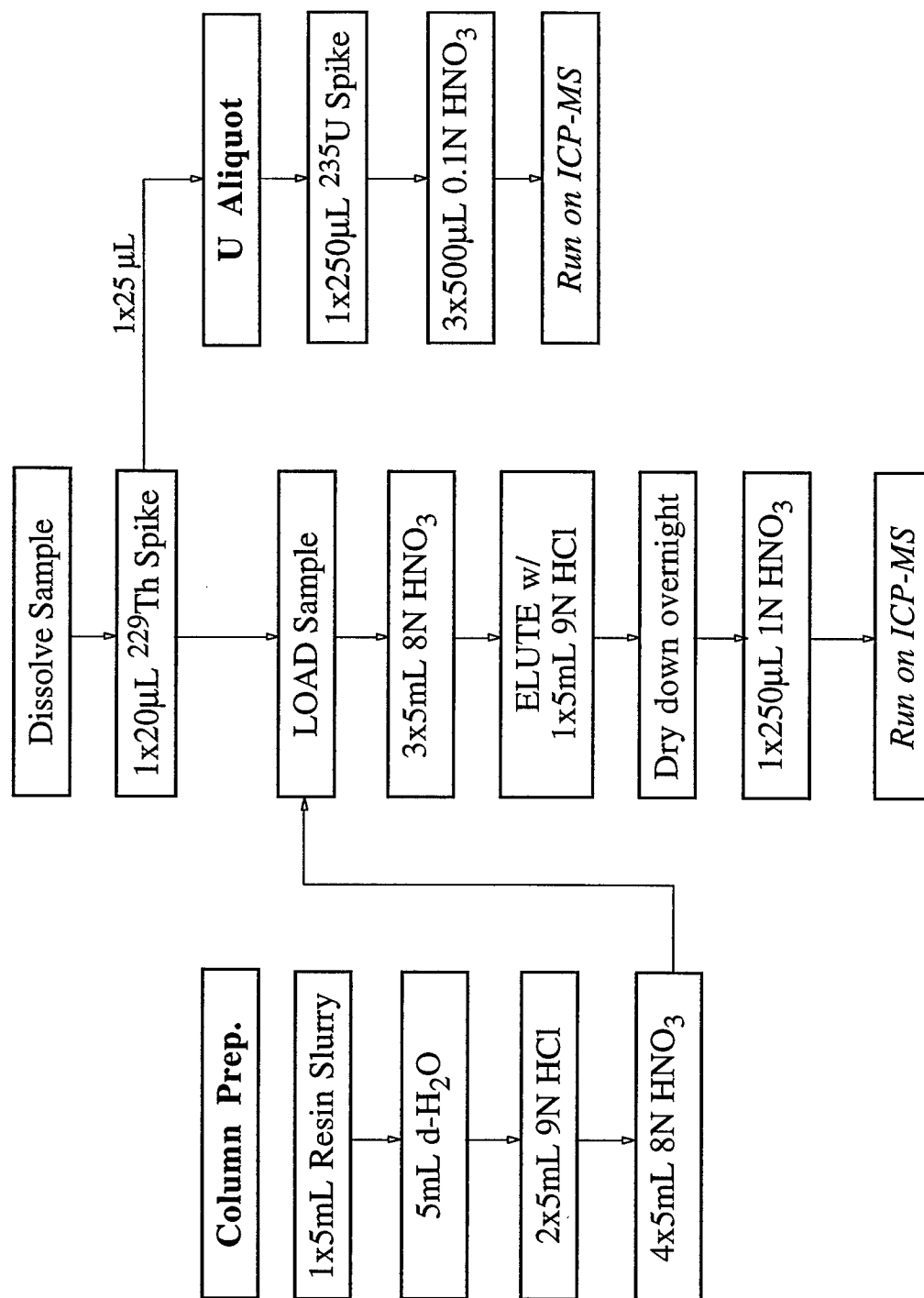


Figure 3.3. Age screening flow chart.

aliquot was compared to the total weight of the dissolved sample for the $^{230}\text{Th}/^{238}\text{U}$ ratio calculation.

Thorium was purified and concentrated with an anion exchange column. Five milliliters of a 50/50 mixture of wet Dowex AG1-X8, 100-200 mesh, resin and 8N HNO_3 was added to cleaned Kontes polyethylene columns. Distilled water was used to wash the resin into position. Approximately four column volumes of 9N HCl , the eluant for thorium, was added to eliminate any blank. Columns were pre-conditioned with 20 ml of 8N HNO_3 , and the dissolved sample was then loaded directly onto the resin (Figure 3.3). Normally the next step would be to elute the sample; however, we found that large amounts of Ca clogged the sample aperture of the mass spectrometer and quickly decreased instrument sensitivity. Calcium was rinsed from the column with 20 ml of 8N HNO_3 . We determined the amount of rinse solution needed by loading a synthetic sample (10g of CaCO_3 dissolved in 50 ml of 8N HNO_3) on the columns. 20 ml of clean distilled water was added to the top and collected in 1 ml fractions dripping from the bottom. 500 μL of each of these fractions was diluted with 5 ml of a La/ HCl matrix solution and measured for [Ca] by flame atomic adsorption spectrometry (FAA). The results of two replicate tests are pictured in Figure 3.4. Below 10 ml the [Ca] was off scale on the FAA. After 15 ml the [Ca] was back to near baseline levels. The gain in ICP-MS sensitivity outweighs the small Th loss from the 20 ml of rinse solution.

Column concentration and purification was completed by eluting the sample with 5 ml of 9N HCl into a conical bottom acid-leached Teflon vial and drying down overnight. The residue was taken up in 250 μl of 0.1N HNO_3 and run on the ICP-MS. By adding ^{232}Th to a synthetic coral solution, and spiking with ^{229}Th after elution, we determined the column efficiency to be between 40-50% (Table 3.2). Without Ca flushing rinses, column recoveries were generally higher. However, a combination of using 8N HNO_3 , rather than water, and 15 ml, instead of 20 ml, of rinse allowed us to elute a reasonable amount of thorium. Additional rinses with 9N HCl , after the 5 ml elution step, removed

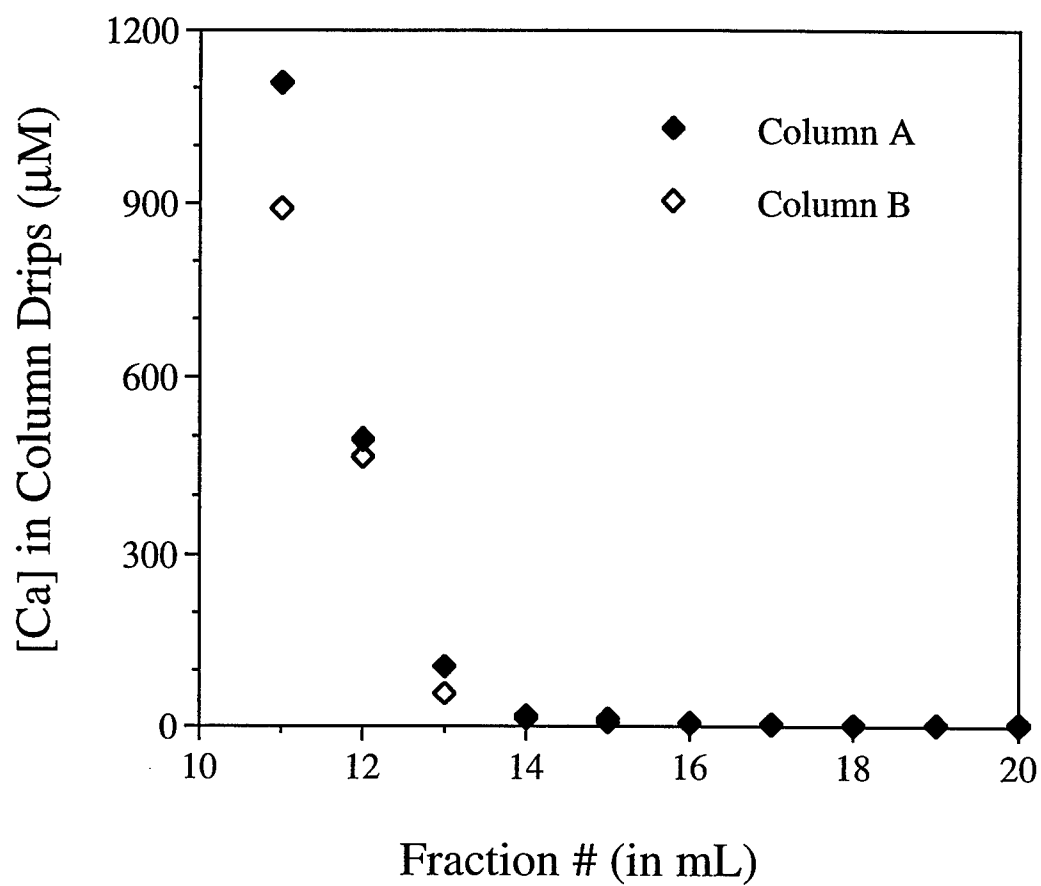


Figure 3.4. Calcium rinse out test. Samples before 10 mL were off scale on the FAA

Date	% Rec.	Comments
2/17/94	71%	No rinse step.
	51%	
	73%	
2/21/94	40%	20 mL H ₂ O rinse
	42%	
	47%	
	19%	
	37%	
2/23/94	59%	15 mL H ₂ O rinse
	36%	
2/28/94	53%	15 mL H ₂ O rinse
	42%	
4/14/94	37%	15 mL H ₂ O rinse
	42%	
	41%	
	39%	
7/27/94	35%	15 mL H ₂ O rinse
	31%	
9/27/94	54%	20 mL 8N HNO ₃
	41%	

Table 3.2: Column % recovery test results

less than 10% more thorium. Replicate column blanks measured with each set of ten samples rarely showed ^{230}Th amounts above background on the ICP-MS.

Because a new ICP-MS was purchased during the course of this work, measurements of uranium and thorium were made on two different instruments. Basic operating parameters were about the same on both machines and are listed in Table 3.3. Mass 229/230 ratios are adjusted for instrumental bias by running a spiked gravimetric standard (SGS) of known ratio several times during a run. Long term stability of the SGS ratio was quite good (Table 3.4). Two separate solutions were run from 7/95 to 4/97 with the older solution spanning the switch from one ICP-MS to the other. As can be seen from Table 3.4, the precision is very close to that predicted by counting statistics. I used a VG Plasma Quad for the first 100 age screening measurements. Later we obtained a VG PQ2+ that is 10-20x more sensitive at the high masses than the earlier instrument. This upgrade allowed for two important changes. I was able to switch from scanning the 228-231 mass range to peak hopping on the 229 and 230 peaks, and I was able to shrink the sample size to 0.5 grams. Figure 3.5 shows the difference in peak shapes and sensitivity for the old SGS run on both instruments. Sensitivity is over 10x higher and the peak shapes are much smoother on the newer instrument. A representative sample from the earlier instrument is also pictured to show the irregularity of the peak tops. This irregularity coupled with an occasionally unstable quadrupole required the use of peak scanning at these low levels of thorium concentration. However, the new instrument could be run in peak hopping mode and therefore increase the total number of counts and decrease the counting statistics error bars. This added sensitivity also reduced the sample size requirements by a factor of two. Switching to peak hopping allowed me to also measure ^{232}Th , in order to better constrain the extent of cleaning of individual samples. ^{232}Th , as will be examined later in this chapter, comes from contaminating sources that can also be elevated in ^{230}Th . This excess ^{230}Th is not due to closed system decay within

<u>Gas Flows</u>	<u>(ml/min)</u>
Nebulizer	0.85
Auxiliary	0.87
Cool	14

<u>Front End</u>	
RF Power	1350 watts
Nebulizer	Mienhard
Flow Rate	750-1000 μ l/min

<u>Vacuum Pressure</u>	<u>(mbar)</u>
Expansion	2.2E+00
Intermediate	2.0E-04
Analyzer	1.7E-06

<u>High Tension</u>	
volts	1750-2500

-This value is highly dependent on the age of the multiplier

<u>Peak Jumping</u>	
DAC Steps	5
Points/peak	3
Aquire Time	~16 sec

<u>Scanning</u>	
Sweeps	190
Dwell Time	160 μ sec
Channels	512

Table 3.3: ICP-MS running parameters. Values are similar for old and new instruments.

Table 3.4: A: Daily Th SGS statistics on the old ICP-MS

Date	229 Total Counts	230	Ratio	Counting err	Daily Statistics	
7/25/95	4860	3352	1.457	0.033	Average	1.466
	4984	3452	1.450	0.032	StDev	0.051
	4993	3405	1.473	0.033	RSD	3.51%
	3305	2174	1.533	0.042		
	4023	2760	1.466	0.036		
	4076	2876	1.424	0.035		
	3136	2057	1.538	0.044		
	3733	2597	1.446	0.037		
	3997	2874	1.397	0.034		
	2856	1974	1.458	0.043		
	4007	2596	1.554	0.039		
	3908	2806	1.399	0.035		
	4899	3286	1.503	0.034	Average	1.477
7/26/95	4832	3200	1.523	0.035	StDev	0.041
	4690	3272	1.444	0.033	RSD	2.78%
	3129	2135	1.483	0.042		
	3950	2716	1.468	0.037		
	3879	2793	1.400	0.035		
	3197	2120	1.527	0.043		
	3901	2631	1.497	0.038		
7/31/95	4074	2834	1.450	0.035		
	3681	2688	1.498	0.038	Average	1.476
	3800	2642	1.446	0.037	StDev	0.041
	3984	2813	1.423	0.035	RSD	2.81%
	2415	1635	1.492	0.048		
	2699	1782	1.529	0.047		
	2776	1847	1.517	0.046		
	2351	1637	1.454	0.047		
	2581	1731	1.509	0.047		
	2605	1854	1.420	0.043		
11/8/95	5646	3746	1.506	0.032	Average	1.453
	5374	3582	1.499	0.032	StDev	0.060
	5117	3523	1.450	0.032	RSD	4.12%
	2754	1955	1.403	0.042		
	3300	2181	1.511	0.042		
	3296	2289	1.436	0.039		
	1966	1295	1.515	0.054		
	2522	1784	1.408	0.044		
	2878	2129	1.345	0.038		
11/26/95	3329	2318	1.449	0.039	Average	1.479
	3546	2442	1.465	0.039	StDev	0.034
	3536	2368	1.508	0.040	RSD	2.31%
	3437	2274	1.527	0.041		
	3634	2543	1.440	0.037		
	3578	2429	1.486	0.039		

Table 3.4: A: (Con't)

12/6/95	4295	2918	1.485	0.036	Average	1.475
	4446	2972	1.509	0.036	StDev	0.026
	4581	3166	1.458	0.034	RSD	1.76%
	4463	3023	1.489	0.035		
	4662	3117	1.508	0.035		
	4518	3096	1.471	0.034		
	4429	3122	1.429	0.033		
	4865	3368	1.455	0.033		
	4792	3277	1.474	0.033		

SGS Totals				
Average	3820	2620	1.470	0.038
Stdev	870	592	0.044	
RSD	23%	23%	2.96%	

Table 3.4: B: Th SGS statistics on the new ICP-MS

Date Run	229	230	Ratio	Counting err	Daily Statistics		
Total counts							
Old SGS							
2/18/96	182285	123493	1.476	0.005	Ave.	1.467	
	190034	129974	1.462	0.005	Stdev	0.006	
	194667	132599	1.468	0.005	RSD	0.39%	
	178614	121362	1.472	0.005			
	192407	131565	1.463	0.005			
3/11/96	200541	137002	1.464	0.005			
	191474	129887	1.474	0.005	Ave.	1.479	
	201664	136902	1.473	0.005	Stdev	0.006	
	205749	138819	1.482	0.005	RSD	0.41%	
	186256	126389	1.473	0.005			
	195562	132629	1.474	0.005			
	199530	134610	1.482	0.005			
	198013	133159	1.487	0.005			
	198127	133872	1.479	0.005			
	200503	134626	1.489	0.005			
4/6/96	70853	47188	1.505	0.009	Ave.	1.479	
	70991	48254	1.474	0.009	Stdev	0.015	
	72414	49113	1.477	0.009	RSD	1.03%	
	48258	33102	1.462	0.010			
	35128	24000	1.469	0.012			
4/7/96	32494	21935	1.488	0.013			
	68064	46701	1.461	0.009	Ave.	1.481	
	70767	47754	1.485	0.009	Stdev	0.018	
	70457	48010	1.471	0.009	RSD	1.19%	
	87522	59131	1.483	0.008			
6/1/96	85749	58196	1.476	0.008			
	86677	57414	1.513	0.008			
	102115	68941	1.483	0.007	Ave.	1.484	
	109335	73390	1.492	0.007	Stdev	0.010	
	113533	77220	1.472	0.007	RSD	0.70%	
	97984	66064	1.485	0.007			
	108026	72697	1.488	0.007			
7/7/96	112055	74957	1.497	0.007			
	70496	47276	1.494	0.009			
	74342	50838	1.465	0.008			
	79644	53839	1.482	0.008			
	72321	48866	1.481	0.009	Ave.	1.478	
	71904	49511	1.453	0.008	Stdev	0.012	
	74463	50418	1.478	0.009	RSD	0.81%	
	75591	50538	1.497	0.009			
	73968	50012	1.480	0.009			
	75856	50936	1.490	0.009			
New SGS Solution	74477	50453	1.477	0.009			
	74539	50496	1.477	0.009			
	74394	50521	1.474	0.008			
	7/7/96	79187	52553	1.508	0.008	Ave.	1.500
	78158	52219	1.498	0.008	Stdev	0.013	
78467	52525	1.495	0.008	RSD	0.86%		
77189	50750	1.522	0.009				
75363	50059	1.506	0.009				
74835	50207	1.491	0.009				
81208	53654	1.514	0.008				
80606	54298	1.485	0.008				
81411	54846	1.485	0.008				

Table 3.4: B: (Con't)

7/30/96	165681	111980	1.480	0.006	Ave.	1.498
	166947	112271	1.487	0.006	Stdev	0.016
	168906	112148	1.507	0.006	RSD	1.06%
	93862	62179	1.506	0.008		
	97554	65223	1.492	0.008		
	92450	61313	1.504	0.008		
	102249	67186	1.520	0.008		
	103612	68876	1.503	0.007		
	103559	69385	1.491	0.007		
	91684	60182	1.518	0.008		
	94210	61472	1.527	0.008		
	93602	62629	1.489	0.008		
	72244	48277	1.485	0.009		
	67970	45230	1.490	0.009		
	64814	43671	1.471	0.009		
4/8/97	82772	54910	1.512	0.008	Ave.	1.518
	82892	54905	1.515	0.008	Stdev	0.008
	83696	55529	1.512	0.008	RSD	0.54%
	69378	45625	1.528	0.009		
	70494	46305	1.530	0.009		
	70850	47031	1.513	0.009		

Totals Old SGS

Average	116663	78992	1.479
Stdev	57899	39289	0.012
RSD	50%	50%	0.81%

Totals New SGS

Average	91528	60915	1.503
Stdev	27807	18752	0.016
RSD	30%	31%	1.04%

1.4757 is the ratio for the old SGS as measured by Larry Edwards' Lab

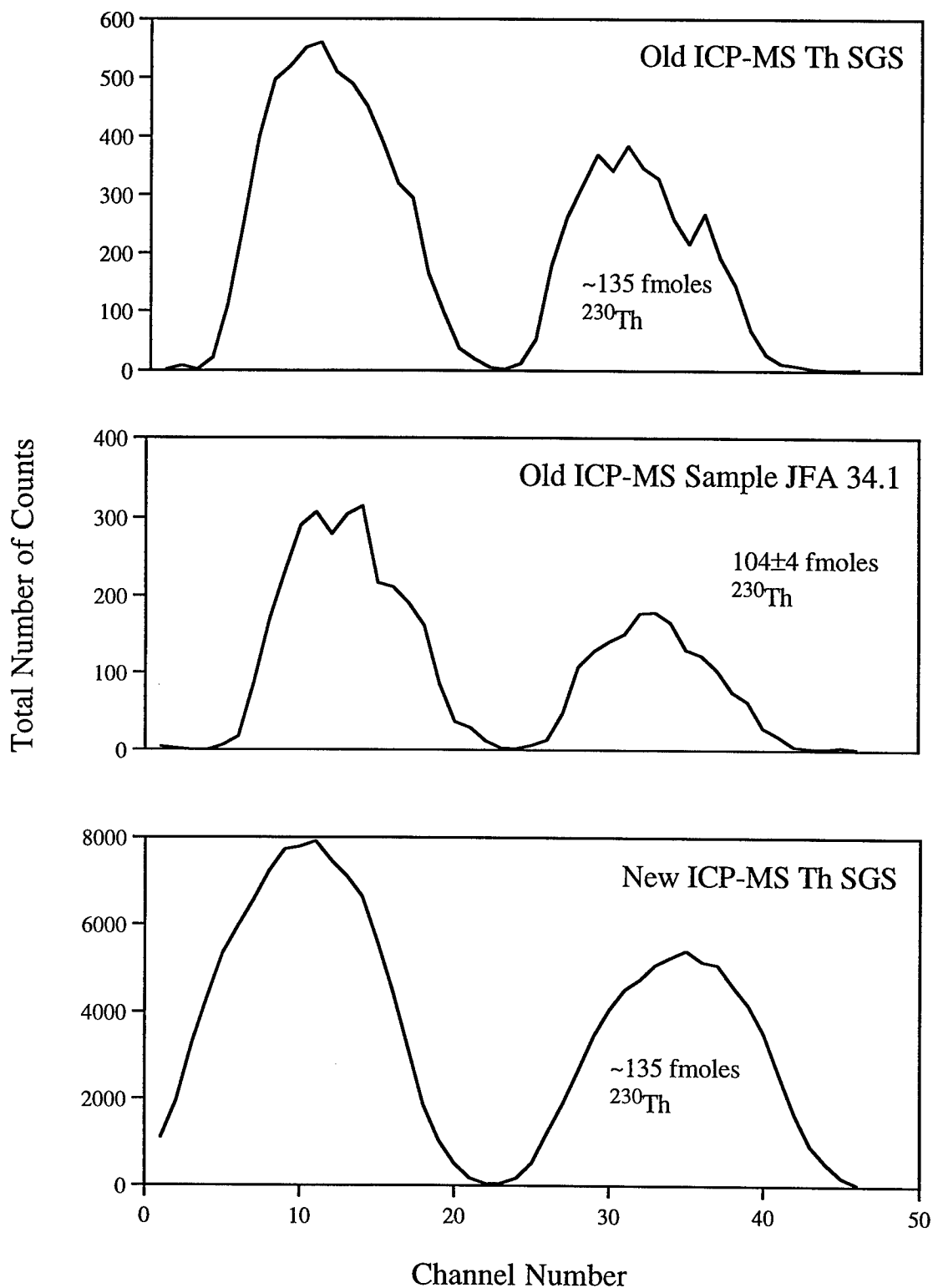


Figure 3.5. ICP-MS ^{229}Th and ^{230}Th peak shapes. Top two pannels are from the older, less sensitive machine. There is about a factor of 10 increase in total counts on the new machine.

the coral's lattice and can cause ages to appear too old. Measurements of ^{232}Th and an assumed $^{230}\text{Th}/^{232}\text{Th}$ ratio can be used to correct for this age bias (see next section).

During the methods development stage on the old ICP-MS, we checked the reproducibility of our age screening by measuring six samples on two separate occasions. Figure 3.6 shows that within the age errors of the old instrument method the two runs agree. There is a slight systematic bias to older ages for the first run over the second run that may be due to different cleaning intensities. In addition, ICP-MS ages from the new instrument method were compared to TIMS ages (see next section) for several samples. Figure 3.7 shows that the ICP-MS and TIMS ages agree and that the screening technique is accurate as well as precise. There is a tendency for older samples to fall off the 1:1 line in Figure 3.7. However, there is good agreement in the crucial range of the radiocarbon age window, 5-35,000 years. All of our age screened samples are shown in a histogram in Figure 3.8 and in Table 1 of the Appendix. As is expected, most of our samples fall in the modern, 0-5,000 year, age window. There are over 50 samples from the early Holocene and the deglaciation as well as several from glacial stage 2. All of these are interesting for paleo-ventilation age work, and some of them will be discussed in later chapters. Nearly all of the samples are from the Atlantic Ocean with the majority of those coming from the subtropics and the northern sub-polar regions. While there are considerable numbers of deep-sea corals from isotopic stages 3-5 in Figure 3.8, some of these may be biased by the old method that does not include ^{232}Th corrections. Figure 3.9 is a histogram of the sub set of samples from Figure 3.8 that were run on the new ICP-MS with the ^{232}Th age corrections included (see Appendix). There are no samples older than about 75,000 years in this data. None of the oldest samples in Figure 3.8 were run again with the new method, but some may be compromised by unsupported ^{230}Th . Overall this new ICP-MS age screening method offers a rapid and inexpensive alternative to AMS or TIMS dating for large numbers of samples.

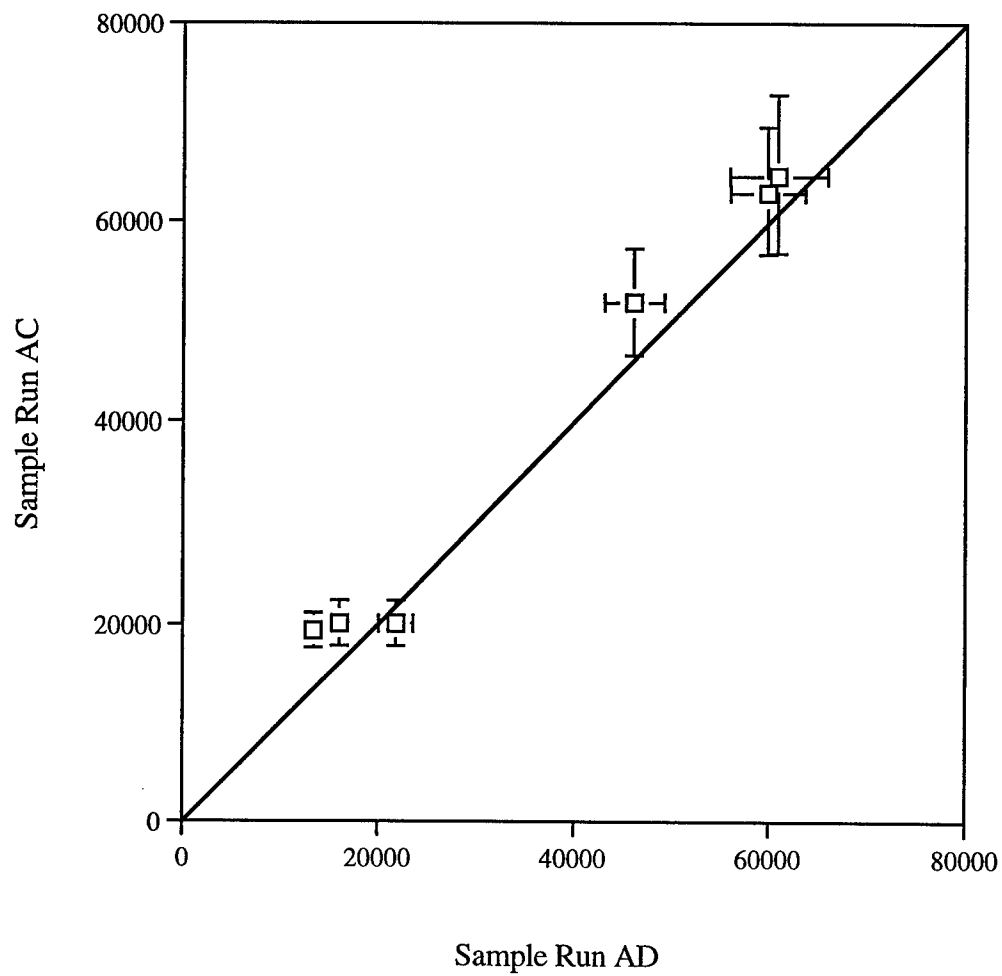


Figure 3.6. Replicate analyses of screened coral. Separate runs of the same individuals show a 1:1 correspondence in age.

Age Screening Method Test

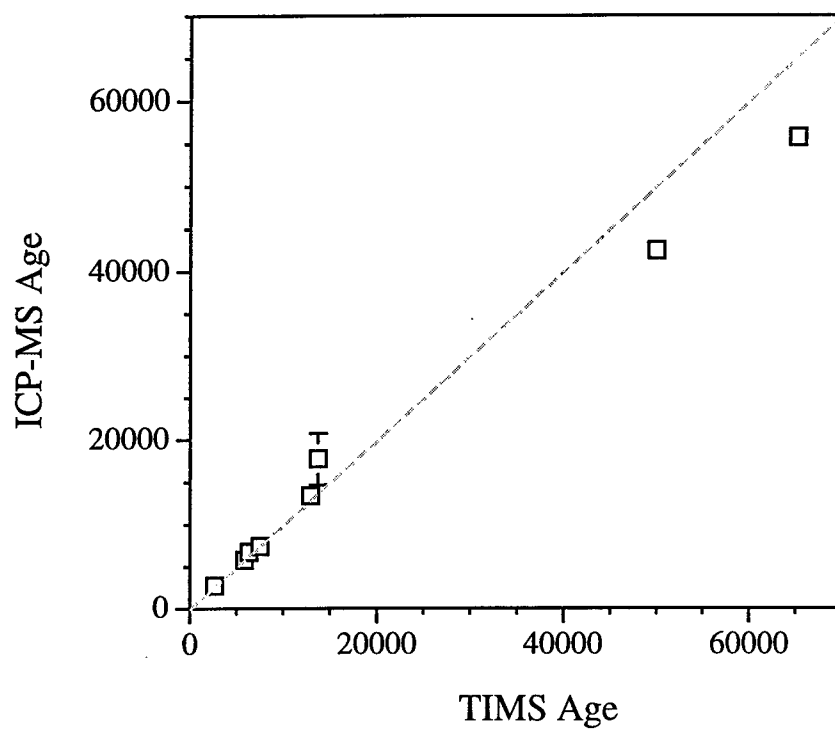


Figure 3.7. Comparison of TIMS and ICP-MS ages.

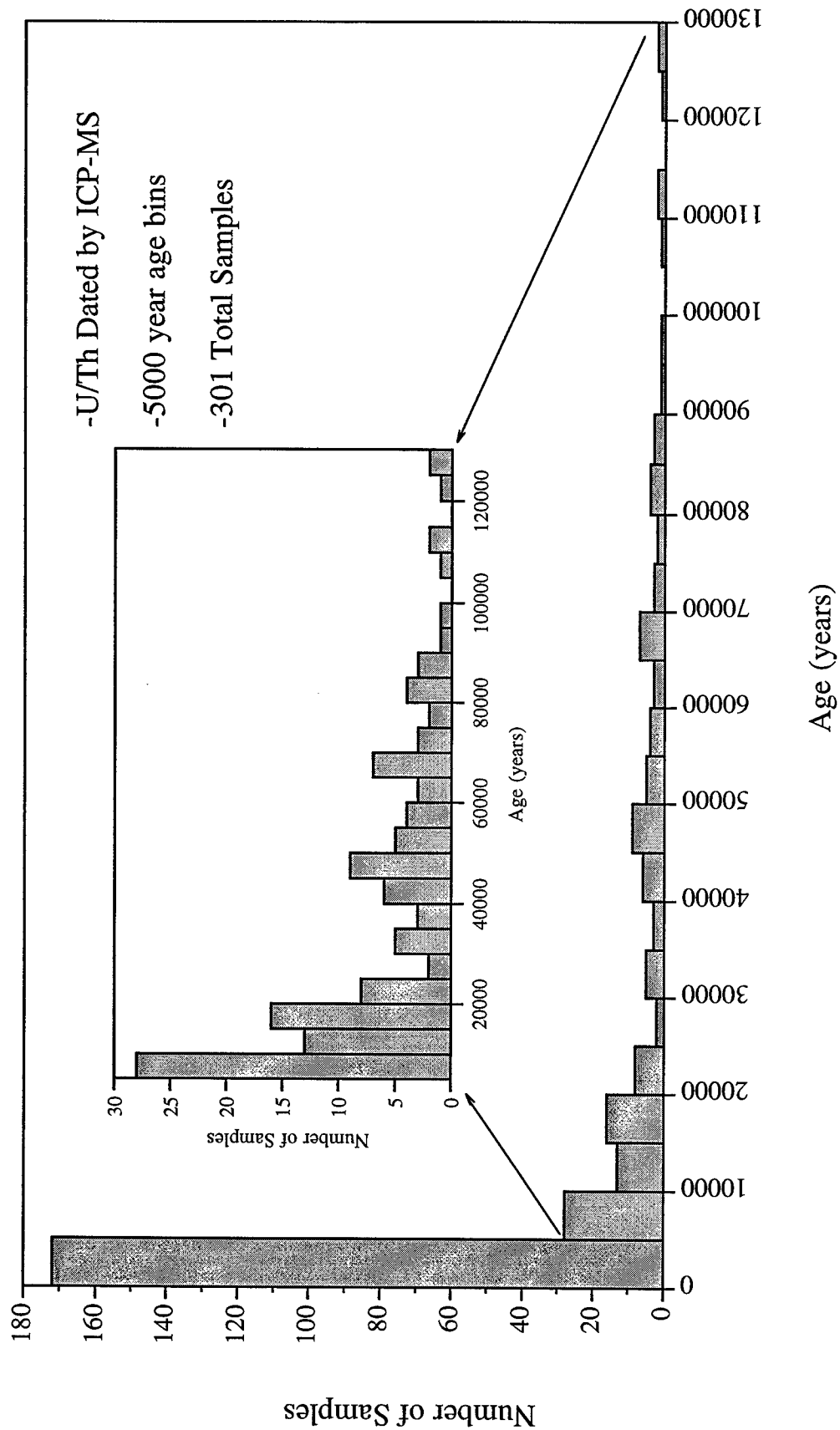


Figure 3.8. Histogram of deep-sea coral ages. Around 60% of the samples are "modern". There are several dozen in the radiocarbon age window.

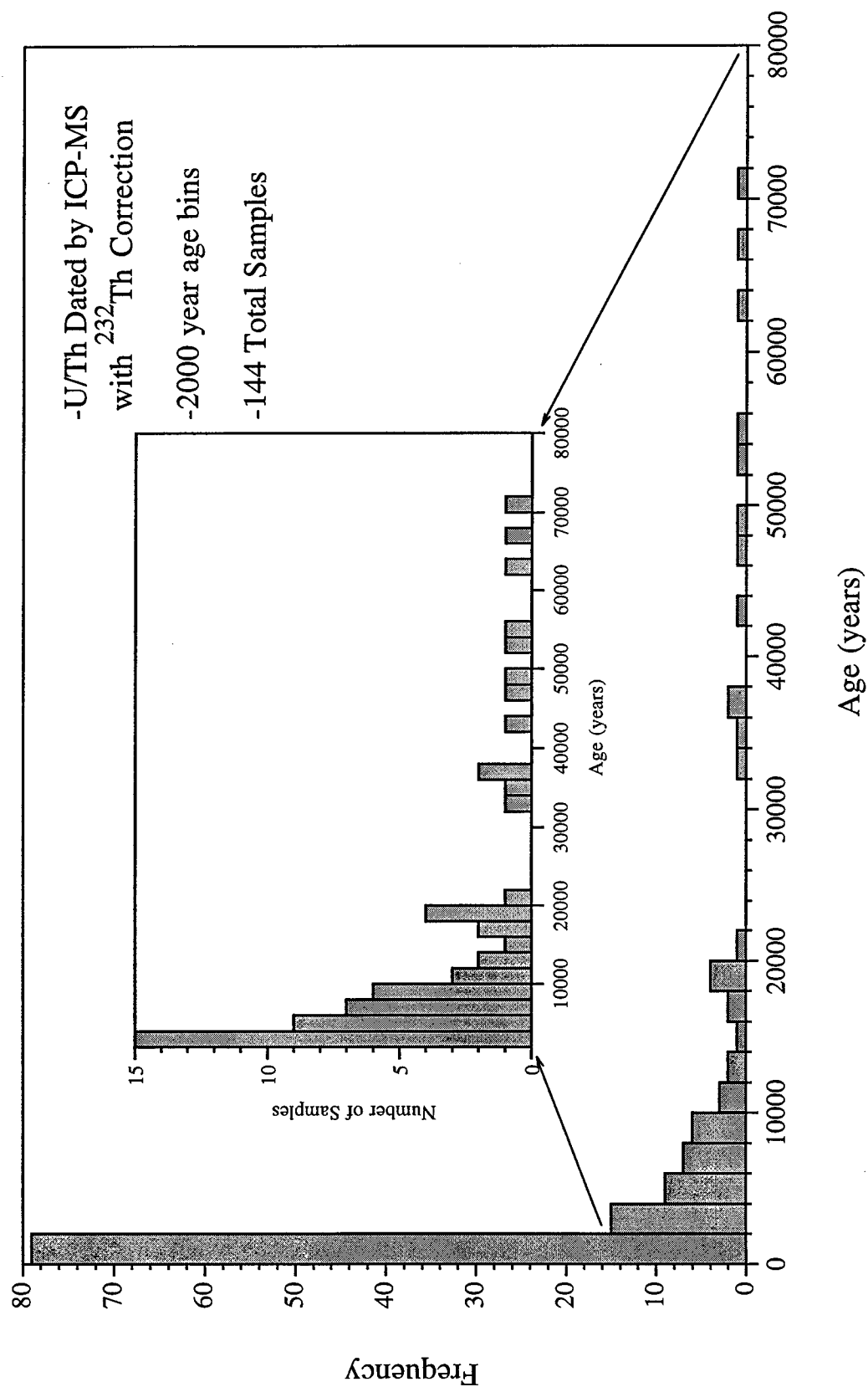


Figure 3.9. Age histogram of ^{232}Th corrected data. Accounting for cleaning shinks the "tail" to younger ages.

IV. Precise Uranium Series Dating

In addition to the ICP-MS age screening techniques described above, we developed a more precise mass spectrometric method to date deep-sea corals. The rest of this chapter is the bulk of a paper, for submission to *Geochimica et Cosmochimica Acta*, that describes the results of our collaboration with Drs Hai Cheng and Larry Edwards at the University of Minnesota. All of the rest of the data reported in this chapter was generated in their laboratory, while the interpretation and writing were done together.

Abstract

^{230}Th , ^{234}U and ^{238}U compositions of several deep-sea solitary corals, mainly the species *Desmophyllum cristagalli*, were determined by thermal ionization mass spectrometry (TIMS) techniques. It is possible to obtain pristine, low [^{232}Th] (5 to a few hundred ppt), modern samples and to get high-precision ages close to those obtained from surface corals. However, because the amount of initial unsupported ^{230}Th is not known *a priori*, older fossil corals can have an age uncertainty of around 3%. We determined an initial $^{230}\text{Th}/^{232}\text{Th}$ ratio from a suite of modern corals and used the measured ^{232}Th value of older samples to estimate this initial ^{230}Th contribution to the age. The essential problem for precise ^{230}Th dating is to get rid of contaminants, which contain elevated ^{232}Th and associated ^{230}Th , from around the coral lattice. A modification of the foraminiferal and surface coral trace metal cleaning methods can significantly reduce this contamination.

By counting the visible growth bands and measuring the mean age of a single septum, the growth rate in the vertical direction of *D. cristagalli* is estimated to be between 0.1 and 1 mm/year. Bands may be precipitated annually, but more work is needed to confirm this hypothesis. If appropriate tracer calibrations can be established, these corals are suitable recorders of decadal or sub-decadal oceanographic changes over their lifetimes. The $\delta^{234}\text{U}$ values of all modern samples from different localities and

depths are similar (mean $149.1 \pm 1.9\%$) and indistinguishable from the data obtained from surface corals. At a precision of about ± 2 per mil, we find no structure in the oceanic profile of $^{234}\text{U}/^{238}\text{U}$ ratios from the surface to about 2000m. The ranges of U concentrations of *D. cristagalli* are similar between the modern coral sample set (2963 ~ 5531 ppb) and the old coral sample set (3109 ~ 4935 ppt). As the sea water U concentration is conservative, this large variation of coral U content implies either a response to other variables in the different environments in which the deep-sea corals grew or a "vital effect" from the biologically driven calcification process.

Samples and Methods

Deep-sea coral samples were obtained from the Smithsonian Institution, the Woods Hole Oceanographic Institution dredge collection and Dr. Lauren Mullineaux (WHOI). Nine modern samples were collected by dredging and submersible in the Pacific, the Atlantic, the Indian and the Southern Oceans over the past 30 years (Table 3.5 and Fig. 3.10). Samples come from 420 to 2200 meters depth. Five of the modern samples are *D. cristagalli*; one is *Enallopsamia rostrata*; one is *Stephanocyathus nobilis*; one is *Stephanocyathus campaniformis*, and one is unidentified. They were judged to be modern either because of intact organic matter upon recovery or very fresh looking preservation in the dredge collections. There are six fossil samples that were dredged from the Atlantic from 1700–2000 meters depth (Table 3.5). Most of these specimens are also *D. cristagalli* except for one sample of *Solenosmilia sp.* and one unidentified sample. Fossil samples are almost always covered by a black aluminosilicate rich crust of iron and manganese oxides.

Cleaning Methods

Five modern *D. cristagalli* samples (DC 1-5 in Table 3.5) were cut into small

Sample Set	Sample Number	Analysis Number ¹	Collection Date	Depth (m)	Locality		Coral Species	Solitary or Colonial
Modern Samples								
	47413	DC-2 a, b	Jan. 21, 1964	421	50°38'S	167°38'E	D. cristagalli	Solitary
	84820	DC-4 a, b	Nov. 23, 1986	806	0°14'N	91°36'W	D. cristagalli	Solitary
	85080	DC-3 a, b	Feb. 25, 1990	990-1150	43°47S	150°29'E	D. cristagalli	Solitary
	48740	DC-5	Oct. 28, 1973	1420-1470	48°40'N	10°54'W	D. cristagalli	Solitary
	78459	DC-1	Apr. 16, 1987	2110-2180	38°45'N	72°39'W	D. cristagalli	Solitary
	86873.1	AO-5	Feb. 2, 1984	1112	25°53'S	5°44'E	St. campaniformis	Solitary
	BI-103-3	AO-16	Aug. 25, 1993	1355	Bishop Seamount		E. rostrata	Solitary
	91545.2	AO-4	Oct. 2, 1964	1510-1600	21°18'S	36°18'E	St. nobilis	Solitary
	JFA-47.1	AO-9	Feb. 23, 1967	1790-1803	48°10'S	148°16'E	?	?
Fossil Samples								
	JFA-2	2		1684-1829	42°N	29°W	?	?
	JFA-17	17		1684-1829	42°N	29°W	Solenosmillia sp.	Colonial
	JFA-24C	24		1784	38°N	60°W	D. cristagalli	Solitary
	JFA-20A	20A		1954	38°N	62°W	D. cristagalli	Solitary
	JFA-20B	20B		1954	38°N	62°W	D. cristagalli	Solitary
	JFA-20C	20C		1954	38°N	62°W	D. cristagalli	Solitary

¹ a and b are different septa of the same sample.

Table 3.5. Deep sea coral samples used in this Chapter.

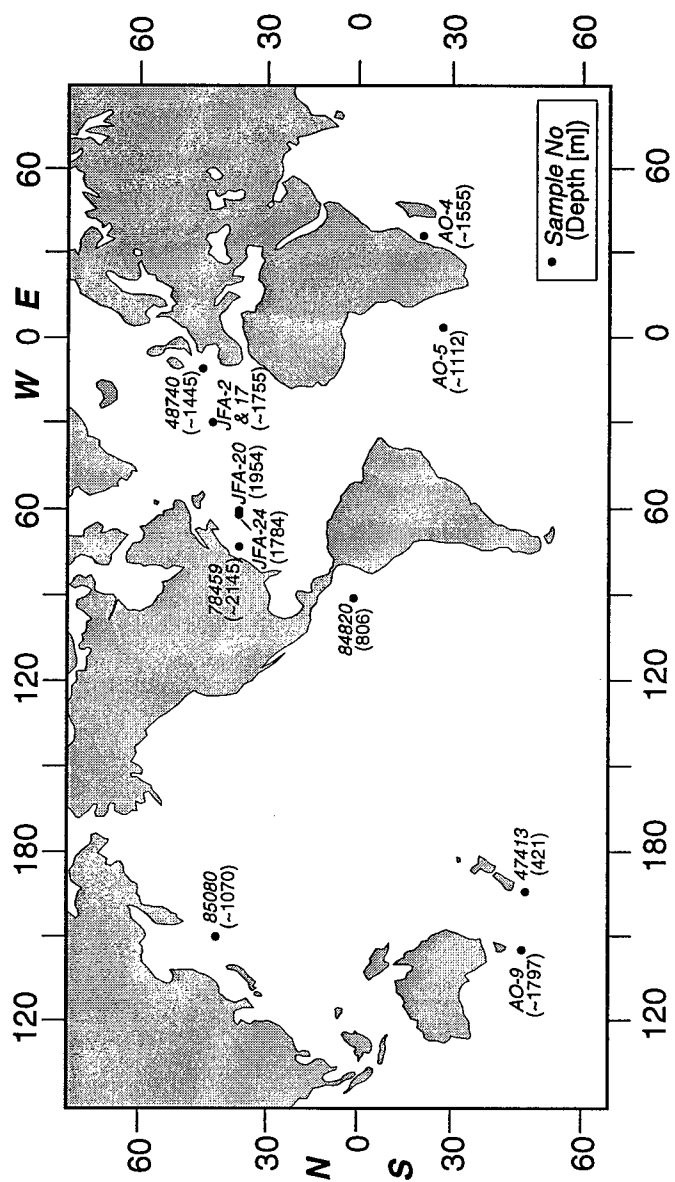


Figure 3.10. Locations for TIMS dated samples in this chapter.

slabs parallel to the radially symmetric septa. Each slab generally consists of one whole S1 septum associated with either one or two smaller septa (S2 or S3) on both sides of the S1 septum (refer to [Cairns and Stanley, 1981] and Chapter 1 for the definition of S1, S2 and S3) (Fig. 3.11). These septa are connected by the thick walled theca, which encircles the polyp. The overall sample size is different for separate septa. Sample length and width have a range about 2-4 cm and 0.5-1 cm, respectively. The thickness of an individual septum is about 0.1 to 0.7 mm, and generally $S1 > S2 > S3$. Each septum's thickness decreases vertically from a bulge near the top and increases from the interior towards the theca. Subsamples were cut roughly parallel to growth bands using a small blade (Fig. 3.11). Final weights were 28.9-143.3 mg. Under a binocular microscope, samples were checked for yellowish organic material, which was scrubbed off using small dental tools. Samples were put in a plastic bottle, ultrasonically cleaned in ultra pure water for 10 minutes and then completely rinsed. This process was repeated several times until the coral looked very clean under the microscope. The above procedure was repeated three times in a Teflon beaker with 5 minutes of ultrasonic cleaning each time. Finally, the sample was dried in an oven at about 70°C. Some yellowish materials scrubbed off from sample 85080 and 78459 were also analyzed (DC-1, D and DC-3a, D in Table 3.6).

Pieces of five of the fossil corals in Table 3.6 were also cleaned with only the above ultrasonic method. The black detrital coatings from JFA 2 and JFA 24C were also analyzed for uranium series isotopic content. Because we could identify one of the contaminating phases for TIMS dating, the aluminosilicate rich black iron and manganese oxide crusts, we utilized a series of chemical leaches to clean these samples. The modern samples with analysis numbers AO-4,5,9, and 16 (Table 3.6) and all of the fossil samples marked as "(CI)" in Table 3.7 were subjected to this rigorous chemical and physical cleaning technique described in the above "Coral Cleaning Techniques" section.

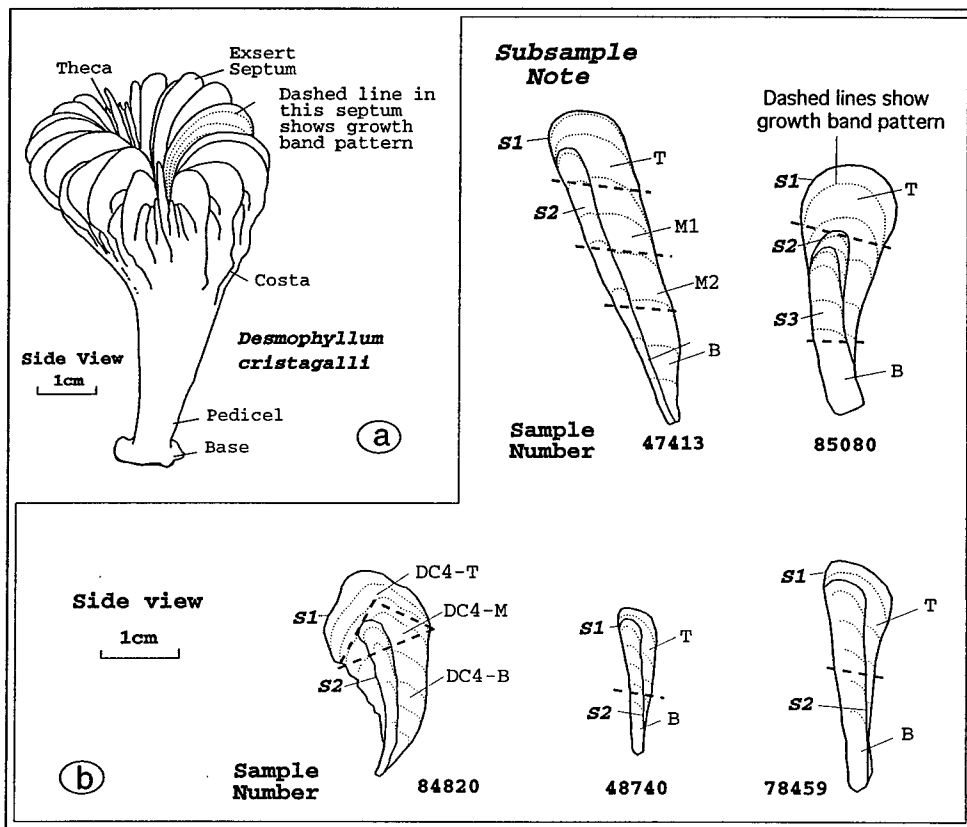


Figure 3.11. Sampling strategy for modern corals

Sample Number	Analysis Number	Weight (mg)	²³⁸ U (ppb)	²³² Th (ppt)	²³⁰ Th/ ²³² Th (atomic, ppm)	δ^{234} U (measured)	²³⁰ Th/ ²³⁸ U (activity)	Age (year [†])	δ^{234} U (initial)
47413	DC-2a								
	T	129.19	3305 ±2	5 ±18	4296 ±15050	148.6 ±1.5	0.000407 ±0.000047	7.7 ±4.5	148.6 ±1.5
	M1	114.24	2963 ±2	40 ±21	570 ±304	149.3 ±1.6	0.000463 ±0.000058	12.9 ±5.5	149.3 ±1.6
	M2	100.13	3088 ±2	52 ±24	501 ±242	150.7 ±1.1	0.000509 ±0.000058	17.2 ±5.5	150.7 ±1.1
	B	81.09	3257 ±2	153 ±31	221 ±56	148.9 ±2.9	0.000632 ±0.000069	28.9 ±6.5	148.9 ±2.9
	DC-2b								
	T	43.87	3003 ±2	63 ±41	344 ±244	148.1 ±1.9	0.000439 ±0.000124	10.7 ±11.8	148.1 ±1.9
	M	47.57	3024 ±15	69 ±49	386 ±292	147.3 ±5.2	0.000537 ±0.000138	22.3 ±12.7	147.3 ±5.2
84820	DC-4a								
	T	72.04	5232 ±2	139 ±35	1028 ±259	148.0 ±1.2	0.001661 ±0.000072	149.5 ±6.8	148.1 ±1.2
	M	66.05	5335 ±3	107 ±37	1138 ±397	148.6 ±1.7	0.001386 ±0.000063	123.3 ±6.0	148.6 ±1.7
	B	139.9	4898 ±2	76 ±27	1667 ±607	147.1 ±1.3	0.001564 ±0.000096	140.4 ±9.1	147.1 ±1.3
	DC-4b								
	T	41.3	5531 ±2	140 ±63	1134 ±512	149.0 ±1.3	0.001751 ±0.000097	157.8 ±9.2	149.0 ±1.3
	B	40.3	4893 ±3	109 ±58	1282 ±689	147.5 ±1.5	0.001731 ±0.000096	156.2 ±9.1	147.5 ±1.5
85080	DC-3a								
	T	135.71	3729 ±2	66 ±17	373 ±103	148.5 ±1.2	0.000400 ±0.000037	33.0 ±3.5	148.5 ±1.2
	B	58.6	3779 ±2	2293 ±42	154 ±5	148.9 ±1.4	0.005695 ±0.000150	535.5 ±14.3	149.2 ±1.4
	D	0.81	21104 ±36	1.38x10 ⁵ ±3x10 ³	90.3 ±21.1	111.6 ±36	0.035848 ±0.008356		
	DC-3b								
	T	78.06	3520 ±2	21 ±30	897 ±1303	149.5 ±2.2	0.000325 ±0.000068	25.8 ±6.5	149.5 ±2.2
	B	94.52	3208 ±2	159 ±26	316 ±63	150.1 ±1.4	0.000893 ±0.000114	79.5 ±10.8	150.1 ±1.4
48740	DC-5								
	T	95.62	3674 ±2	971 ±37	91 ±4	149.9 ±1.5	0.001462 ±0.000093	117.1 ±8.8	149.9 ±1.5
	B	28.89	3769 ±4	2196 ±102	69 ±5	146.3 ±3.2	0.002434 ±0.000183	210.0 ±17.0	146.4 ±3.2
78459	DC-1								
	T(I)	354.6	3711 ±2	1438 ±67	122 ±9	149.8 ±1.2	0.002883 ±0.000150	265.3 ±14.2	149.9 ±1.2
	T(II)		3710 ±2	1374 ±24	132 ±4	149.2 ±1.1	0.002979 ±0.000064	274.6 ±6.1	149.3 ±1.1
	B	143.3	3516 ±2	1112 ±35	128 ±5	150.2 ±1.2	0.002454 ±0.000048	224.6 ±4.7	150.3 ±1.2
	D	13	3815 ±221	4x10 ⁵ ±3x10 ³	12 ±1	146 ±126	0.07806 ±0.00701		
86973	AO-5	191	4191 ±11	1039 ±27	315 ±12	150.0 ±5.2	0.00475 ±0.00013	450 ±13	150.2 ±5.2
BI-103-3	AO-16	177.7	5553 ±4	154 ±27	4362 ±751	148.6 ±1.1	0.00736 ±0.00007	699 ±6	148.9 ±1.1
91545	AO-4	106.3	4952 ±4	371 ±44	1023 ±123	150.0 ±1.4	0.00466 ±0.00008	441 ±13	150.2 ±1.4
JFA-47.1	AO-9	98.6	4706 ±3	227 ±48	3126 ±656	149.4 ±1.2	0.00916 ±0.00010	870 ±10	149.7 ±1.2

(I) and (II) - different aliquots of the same sample. a and b - Different septa of the same sample. T, M and B - Top, Middle and Bottom fragments of a septum (see Fig. 3.11). D - Detrital material scrubbed off from the surface of the coral.

$\delta^{234}\text{U} = \left\{ \left[\left(\frac{{}^{234}\text{U}}{{}^{238}\text{U}} \right) / \left(\frac{{}^{234}\text{U}}{{}^{238}\text{U}} \right)_{\text{eq}} \right] - 1 \right\} \times 10^3$, where $\left(\frac{{}^{234}\text{U}}{{}^{238}\text{U}} \right)_{\text{eq}}$ is the atomic ratio at secular equilibrium and is equal to 5.472×10^{-5} . $\delta^{234}\text{U}(0)$ is the measured value. $\delta^{234}\text{U}(T)$ is the initial value and is equal to $\delta^{234}\text{U}(0)e^{\lambda^{234}T}$.

Activity ratio is calculated from the atomic ${}^{230}\text{Th}/{}^{238}\text{U}$ ratio by multiplying by $\lambda_{230}/\lambda_{238}$.

Ages are calculated using $[{}^{230}\text{Th}/{}^{238}\text{U}]_{\text{act}} - 1 = -e^{-\lambda^{230}T} + \{\delta^{234}\text{U}(0)/1000\} [(\lambda_{230}/(\lambda_{230} - \lambda_{234})) \times (1 - e^{-(\lambda_{230} - \lambda_{234})T})]$ where T is the age in years.

[†] Age before collection.

Table 3.6. U and Th isotopic composition and ${}^{230}\text{Th}$ ages of modern solitary deep sea corals. The uncertainty is 2σ error.

Sample Number	Analysis Number	^{238}U (ppb)	^{232}Th (ppt)	$^{230}\text{Th}/^{232}\text{Th}$ (atmic $\times 10^{-6}$)	$\delta^{234}\text{U}$ (measured)	$^{230}\text{Th}/^{238}\text{U}$ (activity)	Age (BP year [†])	$\delta^{234}\text{U}$ (initial)
JFA 2	2	3752 \pm 2	1723 \pm 26	4936 \pm 78	144.8 \pm 1.5	0.13787 \pm 0.00068	13874 \pm 75	150.6 \pm 1.6
	2 (N) (I)	4059 \pm 2	4217 \pm 49	2195 \pm 28	146.0 \pm 1.3	0.13870 \pm 0.00076	13948 \pm 83	151.9 \pm 1.3
	2 (N) (II)	4196 \pm 2	6749 \pm 43	1421 \pm 16	145.0 \pm 1.4	0.13898 \pm 0.00124	13991 \pm 135	150.9 \pm 1.5
	2 (N) (D)	4114 \pm 4	757300 \pm 9350	102 \pm 2	146.7 \pm 3.0	1.14028 \pm 0.01724		
JFA 17	17	3851 \pm 1	877 \pm 22	9372 \pm 232	147.1 \pm 1.3	0.12976 \pm 0.00057	12977 \pm 63	152.7 \pm 1.3
JFA 24C	24 (I)	3740 \pm 3	2901 \pm 26	3317 \pm 31	148.0 \pm 2.8	0.15644 \pm 0.00058	15838 \pm 73	154.8 \pm 2.9
	24 (II)	3858 \pm 1	3255 \pm 36	3020 \pm 35	144.8 \pm 1.3	0.15497 \pm 0.00059	15727 \pm 68	151.4 \pm 1.4
	24 (N) (I)	3293 \pm 2	7960 \pm 53	1084 \pm 9	148.3 \pm 2.1	0.15934 \pm 0.00064	16150 \pm 77	155.3 \pm 2.2
	24 (N) (II)	3521 \pm 5	19231 \pm 176	502 \pm 5	148.7 \pm 4.1	0.16680 \pm 0.00092	16961 \pm 121	156.1 \pm 4.4
	24 (N) (D)	2941 \pm 40	4511000 \pm 37800	48 \pm 1	210 \pm 79	4.43729 \pm 0.06871		
JFA 20A	20A	4524 \pm 2	1623 \pm 24	23470 \pm 343	120.0 \pm 1.2	0.51205 \pm 0.00133	65544 \pm 254	144.5 \pm 1.5
	20A (N)	4935 \pm 3	8472 \pm 48	4943 \pm 37	123.1 \pm 1.3	0.51596 \pm 0.00248	65957 \pm 445	148.4 \pm 1.6
JFA 20B	20B	4507 \pm 1	4809 \pm 43	6834 \pm 64	123.1 \pm 1.2	0.44339 \pm 0.00151	54000 \pm 248	143.5 \pm 1.4
	20B (N)	4473 \pm 2	6555 \pm 35	5045 \pm 29	124.4 \pm 1.3	0.44962 \pm 0.00135	54893 \pm 229	145.4 \pm 1.5
JFA 20C	20C	3114 \pm 2	856 \pm 17	30920 \pm 612	132.3 \pm 1.0	0.51694 \pm 0.00166	65340 \pm 296	159.3 \pm 1.3
	20C (N) (I)	3109 \pm 1	2108 \pm 36	12501 \pm 213	146.2 \pm 1.4	0.51542 \pm 0.00144	63942 \pm 266	175.3 \pm 1.7
	20C (N) (II)	3319 \pm 25	3043 \pm 69	9086 \pm 212	143.8 \pm 8.7	0.50666 \pm 0.00462	62676 \pm 1025	171.8 \pm 10.2

(I) and (II) - Different pieces of the same sample. (D) - Detrital material scrubbed off from the surface of the coral. (N) - Only cleaned with an ultrasonic bath, others were cleaned by the method described in the text.

[†] Age before 1950.

Table 3.7. U and Th isotopic composition and ^{230}Th ages of fossil deep sea corals. The uncertainty is the 2 σ error.

TIMS Methods

The development of high-precision thermal ionization mass spectrometric ^{238}U - ^{234}U - ^{230}Th dating [Chen, 1986; Edwards et al., 1986/87; Edwards et al., 1987] is our basis for coral age determinations. Chemistry and instrument analysis of uranium and thorium isotope compositions by TIMS techniques are modifications of those previously described for surface corals [Chen, 1986; Edwards et al., 1987; Edwards et al., 1988; Edwards et al., 1993]. Cleaned samples (weighing between 29 ~ 143 mg) were slowly dissolved in 7N HNO_3 (HF was used to dissolve detrital samples) and then spiked with ^{233}U - ^{236}U ($^{233}\text{U}/^{236}\text{U} = 1.010527$) and ^{229}Th solutions of known concentration. Following the chemical separations of Th and U, the Th fraction was loaded on a graphite-coated single Re filament that had been previously checked for its Th blank. The filament blank of ^{232}Th is relatively high, about 100-150 counts per second at around 1700 °C and becomes higher when the temperature is increased. Therefore we ran ^{232}Th at under 1700 °C and report errors based on counting statistics and the variability in the blank. The U fraction was loaded on a Re filament without graphite and run with the double-filament technique. U and Th were measured on the Minnesota Isotope Laboratory's Finnigan-MAT 262-RPQ mass spectrometer equipped with an electron multiplier.

Results and Discussion

Uranium and thorium isotope compositions of modern and fossil samples are presented in Tables 3.6 and 3.7 respectively. All replicates of ^{230}Th ages and $\delta^{234}\text{U}(\text{T})$ values ($\delta^{234}\text{U}(\text{T})$ is the initial $\delta^{234}\text{U}$ at the time of coral growth as defined in Table 3.6 and [Edwards et al., 1986/87]) from different aliquots of the same dissolved sample and from different septa of the same coral agree within 2σ errors.

3.1. U Concentration and Isotopic Composition

Ku et al. [Ku et al., 1977] and Chen et al. [Chen, 1986] demonstrated that uranium is conservative in seawater. Based on this water column behavior and the temperature dependent fractionation factor between aragonite and seawater, U concentrations of surface corals have been related to variations in seawater temperature through time [Min et al., 1995; Shen and Dunbar, 1995]. Our data show U concentrations of *D. cristagalli* that vary from 2963 to 5531 ppb for modern samples and from 3109 to 4935 ppb for fossil samples (Tables 3.6 and 3.7). These U concentrations are higher than most hermatypic corals (e.g., 2–4 ppm, [Burnett and Veeh, 1993]) and are similar to other ahermatypic corals [Thompson and Livingston, 1970; Stein, 1991]. The U concentration variations within a single species of deep-sea coral are large relative to the range found in surface corals. This big variation may be a combination of the different environmental conditions in which a coral grew, such as temperature, pH, carbonate ion concentration, or biologically induced fractionations. Smaller variations of U concentrations in different parts of a septum from the same sample (consider samples 84820 and 85080) may represent a spatially dependent "vital effect" [Gvirtzman et al., 1973].

$\delta^{234}\text{U(T)}$ values for modern deep-sea corals are between 146.4 and 150.7‰ with a mean and standard deviation of $149.0 \pm 2.3\%$ (for all 24 samples) or $149.1 \pm 1.9\%$ (for 20 samples, excluding the four samples with large errors). These modern samples were collected from nine different depths across the Pacific, the Atlantic, the Indian and the Southern Oceans and they all have $\delta^{234}\text{U(T)}$ values indistinguishable from those of modern surface corals (149.3 ± 1.9 , [Edwards et al., 1993] and our unpublished data) (Fig. 3.12). These data show for the upper 2000 meters that the $\delta^{234}\text{U}$ value is conservative in seawater at a precision of about $\pm 2\%$. Some fossil deep-sea corals in our study also have $\delta^{234}\text{U(T)}$ values similar to modern values. Surface coral data indicate that since the last glacial maximum [Bard et al., 1993; Edwards et al., 1993] and for sea

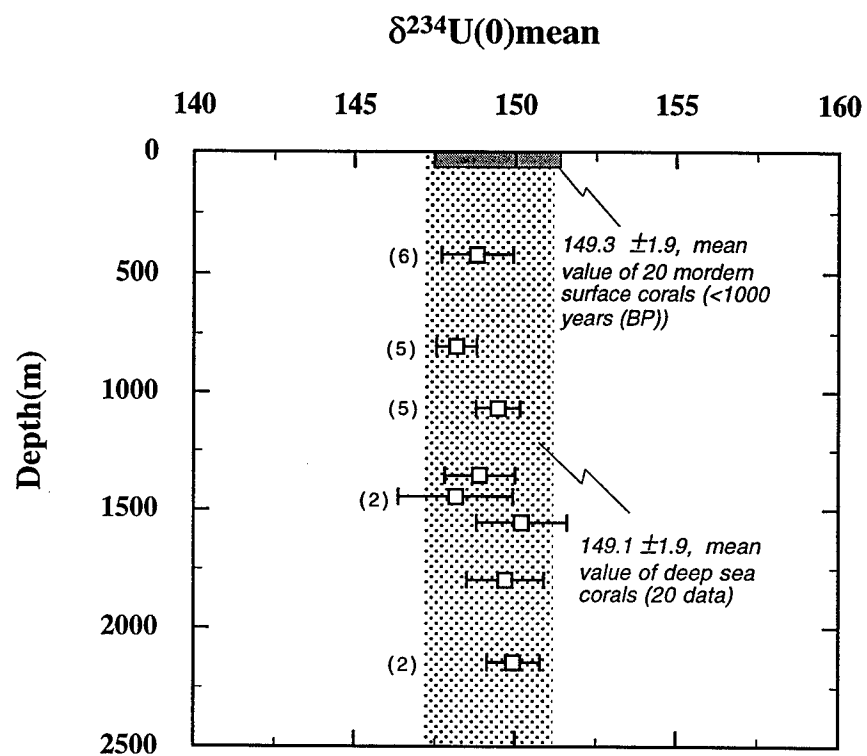


Figure 3.12. Modern deep-sea coral $\delta^{234}\text{U}$ data. Gray bar is range of modern surface coral data from the lab of Larry Edwards.

level high stands over the past 200,000 years [Gallup et al., 1994] the $\delta^{234}\text{U}$ of surface seawater was the same as the modern value.

These surface coral data, coupled with the conservative profile of $\delta^{234}\text{U}$, indicate that $\delta^{234}\text{U}$ values in fossil deep-sea corals are a check of diagenetic alteration. For example, the lower $\delta^{234}\text{U}(\text{T})$ value of sample JFA-20B may suggest uranium or thorium exchange since deposition. Besides using initial $\delta^{234}\text{U}$ as diagenetic check, the data in Table 3.7 can be used to calculate excess ^{234}U ages. Table 3.8 lists the results of this calculation for the fossil deep-sea coral data. Dating errors are quite large because of the relatively young ages of the samples relative to the ^{234}U half-life, and the errors on the $\delta^{234}\text{U}$ measurements. Comparison with the corrected ^{230}Th dates of Table 3.9 (see next section) shows that the two dating schemes agree. When the ^{234}U age is lower than the ^{230}Th age, the initial $\delta^{234}\text{U}$ is higher than the seawater value. Conversely, a higher ^{234}U age corresponds to a lower $\delta^{234}\text{U}$ than the presumably constant seawater value. The age errors in Table 3.8 show the same information as the initial $\delta^{234}\text{U}$ data in Table 3.9.

Initial ^{230}Th contamination and correction

The ^{230}Th dating method is based on ^{230}Th ingrowth from ^{234}U decay within a closed system and knowledge of the initial ^{230}Th concentration. We can write the ^{230}Th age equation without the common surface coral assumption that initial ^{230}Th is equal to zero:

$$\frac{A_{230}}{A_{238}} = 1 + \left(A_{232}^{\text{meas}} \left(\frac{A_{230}}{A_{232}} \right)^0 \frac{1}{A_{238}} - 1 \right) e^{-\lambda_{230}t} + \frac{\delta^{234}\text{U}(0)}{1000} \left(\frac{\lambda_{230}}{\lambda_{230} - \lambda_{234}} \right) (1 - e^{(\lambda_{234} - \lambda_{230})t})$$

where radioisotopes are represented as activities and the term $\delta^{234}\text{U}(0)$ is the measured $^{234}\text{U}/^{238}\text{U}$ ratio normalized to a per mil scale [Edwards et al., 1986/87]. Our strategy is to expand the initial ^{230}Th value into two values we can account for: the initial $^{230}\text{Th}/^{232}\text{Th}$ ratio and the measured $^{232}\text{Th}/^{238}\text{U}$ ratio. Generally, there are three ^{230}Th sources for

Sample Number	Analysis Number	$[^{238}\text{U}]$		Measured $\delta^{234}\text{U}$		Age		$\delta^{234}\text{U}$		^{234}U Ages	
		ppb	error	‰	error	years BP	error	initial	error	years	error
JFA 2	2	3752	2	144.8	1.5	13,870	80	150.6	1.6	10,800	29,900
JFA 17	17	3851	1	147.1	1.3	12,980	60	152.7	1.3	5,200	24,700
JFA 24C	24 (I)	3740	3	148.0	2.8	15,840	70	154.8	2.9	3,100	52,300
	24 (II)	3858	1	144.8	1.3	15,730	70	151.4	1.4	10,800	25,800
JFA 20A	20A	4524	2	120.0	1.2	65,540	250	144.5	1.5	76,900	41,000
JFA 20B	20B	4507	1	123.1	1.2	54,000	250	143.5	1.4	68,000	38,000
JFA 20C	20C	3114	2	132.3	1.0	65,340	300	159.3	1.3	42,600	26,000

Table 3.8: Excess ^{234}U dating of fossil corals.

Sample Number	^{232}Th		$\delta^{234}\text{U}$		Age (years BP)	Corrected Data		
	ppt	error	measured	error		error	initial	$\delta^{234}\text{U}$ error
JFA 2	1723	26	144.8	1.5	13,690	220	150.5	1.6
JFA 17	877	22	147.1	1.3	12,910	120	152.6	1.3
JFA 24C	2901	26	148	2.8	15,500	360	154.7	2.9
JFA 24C	3255	36	144.8	1.3	15,360	390	151.2	1.4
JFA 20A	1623	24	120	1.2	65,410	240	144.5	1.4
JFA 20B	4809	43	123.1	1.2	53,520	530	143.3	1.4
JFA 20C	856	17	132.3	1.0	65,250	240	159.2	1.2

Table 3.9: Fossil samples age corrections.

corals: (1) supported ^{230}Th from ^{234}U decay within the coral lattice; (2) unsupported ^{230}Th within the coral lattice and (3) ^{230}Th associated with coatings on the surface of the coral, such as the Fe-Mn oxide crusts we find on the deep-sea corals. The first category is the ^{230}Th we want to measure for dating. The second source is probably thorium adsorbed from seawater and therefore has a large, relative to crustal values, but depth and location dependent, initial $^{230}\text{Th}/^{232}\text{Th}$ ratio. The third source has a very large uncertainty in the $^{230}\text{Th}/^{232}\text{Th}$ ratio. Aluminosilicates associated with the crusts will have a relatively low $^{230}\text{Th}/^{232}\text{Th}$ ratio, similar to the bulk earth atomic value of about 10 ppm [Wedepohl, 1978], but there is probably also a component of adsorbed and organically associated thorium in this fraction, with a higher ratio, closer to that of seawater.

Because surface corals generally have low ^{232}Th contents and surface sea water has very low [^{230}Th], the ^{230}Th from sources 2 and 3 is usually ignored for surface coral ^{230}Th dating. However, both the [^{230}Th] and the $^{230}\text{Th}/^{232}\text{Th}$ ratio increase with depth in the ocean [Moore, 1981; Nozaki et al., 1981; Bacon and Anderson, 1982; Anderson et al., 1983; Cochran et al., 1987; Huh and Beasley, 1987; Nozaki et al., 1987; Guo et al., 1995; Moran et al., 1995; Roy-Barman et al., 1996; Moran et al., 1997]. This feature of the thorium profile leads to larger initial ^{230}Th in deep-sea corals (source number 2 mentioned above). We have attempted to account for initial ^{230}Th in fossil samples by multiplying the measured ^{232}Th with an estimate of the initial $^{230}\text{Th}/^{232}\text{Th}$ ratio from modern corals.

Modern deep-sea corals have large variations in their ^{232}Th concentration. Concentrations are quite different between samples and between fragments of the same sample. In general, modern samples (5 ~ 2293 ppt) are lower in ^{232}Th content than fossil samples (856 ~ 19231 ppt) including some samples (47413, 84820, 85080, BI-103-3, 91545.2 and JFA-47.1) which have ^{232}Th contents similar to pristine surface corals (several tens or a few hundreds ppt, [Edwards et al., 1988; Gallup et al., 1994]). This suggests that pristine deep-sea coral samples can have low ^{232}Th contents. However,

some fragments of our modern samples have high ^{232}Th contents, about 1120 ~ 2293 ppt, which are close to, or higher than, several of the well cleaned old samples. These high ^{232}Th fragments have varying amounts of yellowish material on the surface and between the septa. Based on direct measurements of this detrital/organic material (samples DC-1, D and DC-3a, D), the contaminant has a much higher ^{232}Th concentration than the pure corals. So, ^{232}Th contents of these samples seem to depend on the extent of contamination from sources 2 or 3 described above. High $[\text{}^{232}\text{Th}]$ generally will result in a larger uncertainty in the ^{230}Th age dates, because the large uncertainty in the initial $^{230}\text{Th}/^{232}\text{Th}$ ratio will dominate the age errors. Figure 3.13 shows that our cleaning technique removes substantial amounts of ^{232}Th from the fossil corals. All cleaned samples have lower $[\text{}^{232}\text{Th}]$, by about 30-80%, than their untreated counterparts. Several of the cleaned samples have ^{232}Th concentrations that are comparable to modern corals without black crusts. However, no cleaned fossil sample has a $[\text{}^{232}\text{Th}]$ that could be considered "pristine". Ages of cleaned corals are not substantially different than uncleaned parts from the same sample (Table 3.7). Based on this evidence, we believe the cleaning technique is removing a "detrital" thorium fraction with relatively low initial $^{230}\text{Th}/^{232}\text{Th}$.

No matter how clean the coral, there is, more or less, some ^{230}Th contamination. Thus, it is important to evaluate the effect of this contamination on the ^{230}Th dating results. From the modern data set (Table 3.6), the samples with the highest $[\text{}^{232}\text{Th}]$ have $^{230}\text{Th}/^{232}\text{Th}$ atomic ratios between 5-160 ppm. These values are intermediate between continental and seawater end members, about ten and a few hundred ppm respectively. Pristine modern samples, with very low $[\text{}^{232}\text{Th}]$, have higher $^{230}\text{Th}/^{232}\text{Th}$ ratios that are closer to a pure seawater influence. However, the ^{232}Th contents of these samples are low enough that, in fossil samples older than about 10,000 years, they would not impact the calculated age. Based on the $^{230}\text{Th}/^{232}\text{Th}$ ratios in the measured detritus and the

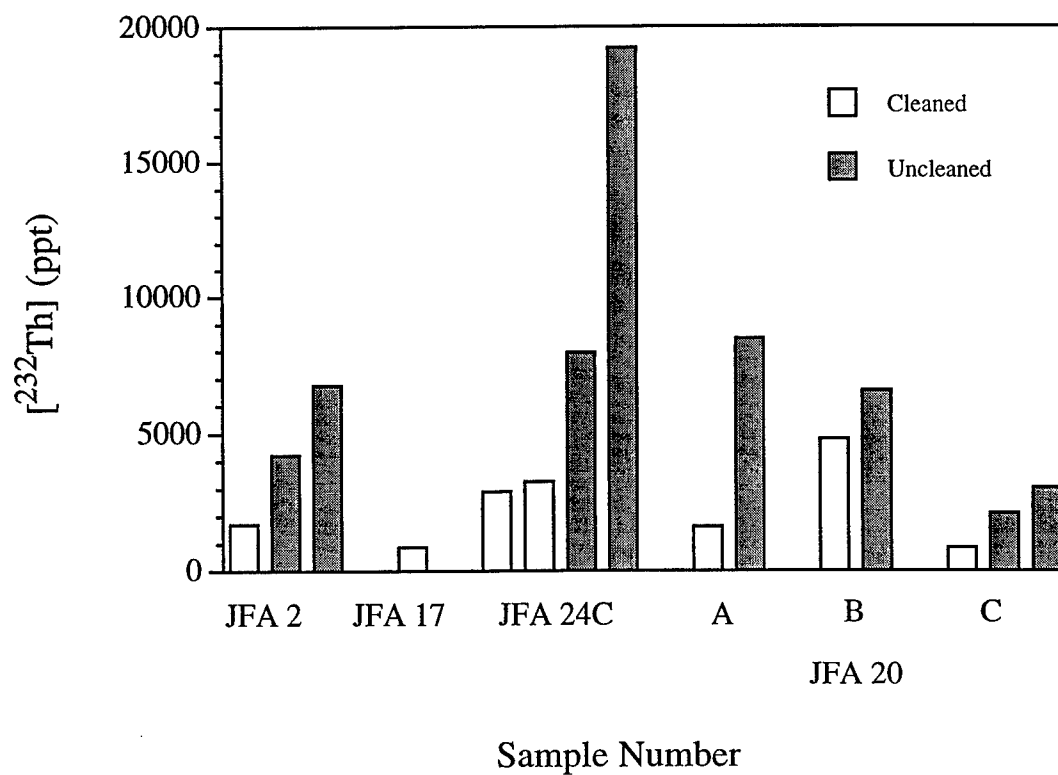


Figure 3.13. Cleaning treatment's effect on ^{232}Th content.

modern isochrons described in the next section, we choose a conservative estimate of 80 ± 80 ppm (2σ) for the initial $^{230}\text{Th}/^{232}\text{Th}$ ratio used in the ^{230}Th age equation.

Assuming that contamination occurs near time zero, Figure 3.14a is a plot of total error in age versus the absolute age, given the uncertainty in our initial ratio estimate. Here the effect of the large uncertainty in the initial $^{230}\text{Th}/^{232}\text{Th}$ ratio can be assessed. The thick black line represents typical analytical errors associated with the TIMS method. Age errors due to the 80 ± 80 value are dependent on the amount of ^{232}Th measured in a fossil specimen and are plotted as thin solid lines in Figure 3.14. The dashed lines in Figure 3.14 represent the boundary between overall errors that are dominated by the uncertainty in the initial $^{230}\text{Th}/^{232}\text{Th}$ ratio (to the left of the dashed lines in Fig. 5a and b) and errors that are a combination of analytical and initial ratio uncertainties (to the right of the dashed lines). Black dots are all data not corrected for initial ^{230}Th , and open circles are corrected values using the above age equation. Corrected data are shifted to younger and more uncertain values.

The effect of cleaning exterior ^{232}Th can be seen from these diagrams. A 10,000 year old coral with 500 ppt ^{232}Th has an overall age error of about 500 years, which is dominated by uncertainty in the initial $^{230}\text{Th}/^{232}\text{Th}$ ratio. However, if this same coral is cleaned to a level of 100 ppt, the overall error shrinks to about 150 years and is dominated by analytical uncertainties. Figure 3.14b shows how the error estimates would be affected if we could better constrain the initial ratio to $\pm 50\%$ rather than $\pm 100\%$. Table 3.9 is a list of the recalculated ages of our fossil samples using the full ^{230}Th age equation and an initial $^{230}\text{Th}/^{232}\text{Th}$ ratio of 80 ± 80 ppm. By making conservative assumptions about the nature of ^{230}Th contamination, which are based on measurements of modern samples, we can calculate the ^{230}Th age of fossil deep-sea coral samples. Better cleaning techniques to further remove exterior contamination will improve the error estimates described here.

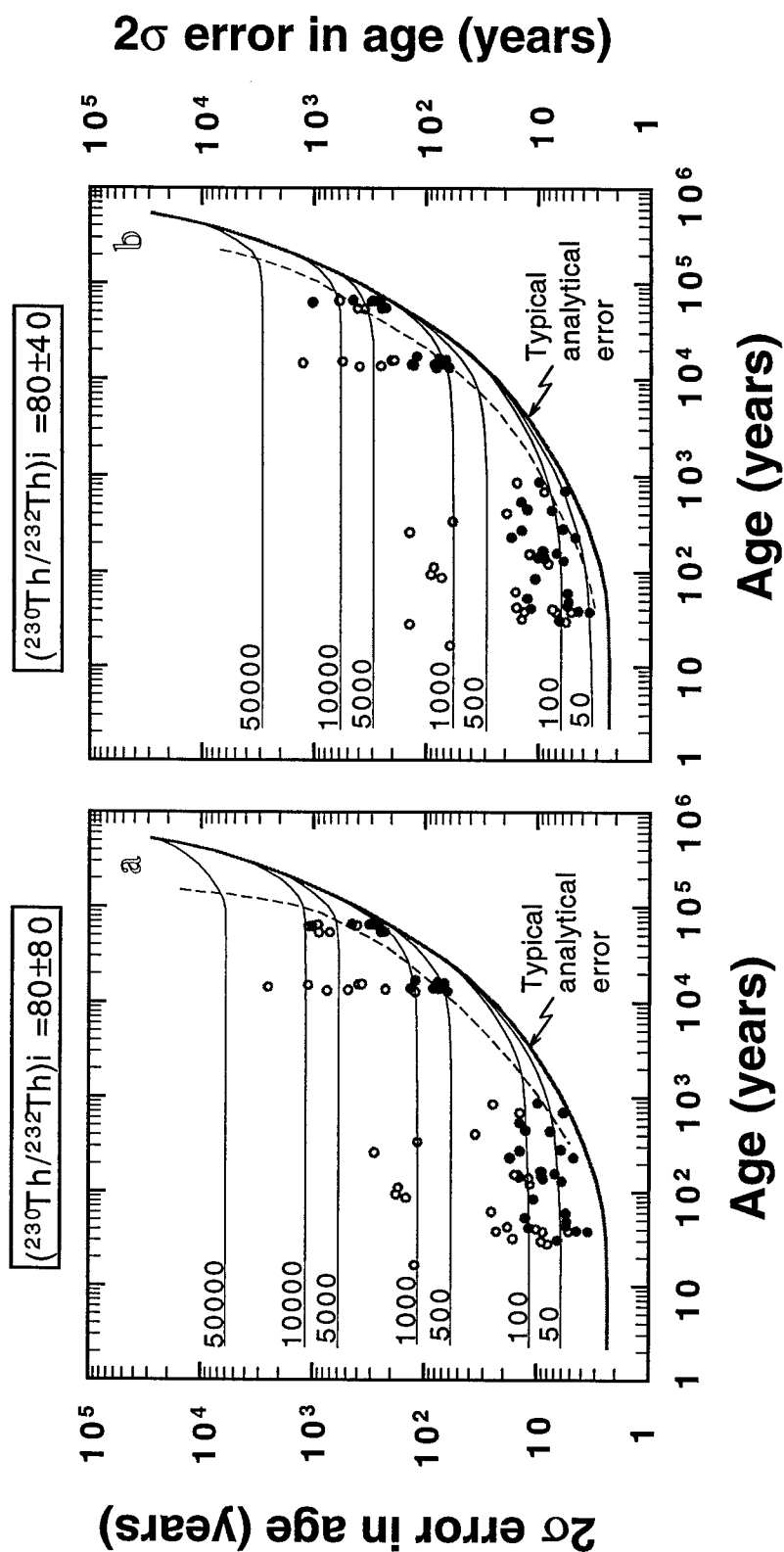


Figure 3.14. Effect of uncertainty in the $^{230}\text{Th}/^{232}\text{Th}$ initial ratio and cleaning intensity on TMS ages. The heavy black line is the typical analytical error from TMS measurements. Thin solid lines are age errors for a particular measured ^{232}Th content. To the left of the thin dashed line errors are dominated by uncertainty in the initial ratio. To the right of the dashed line errors are a combination of initial ratio uncertainty and analytical errors. Two different initial ratios are shown in the two panels.

Banding and Growth Rate

In order to use individual *D. cristagalli* specimens as archives of oceanographic time series, we need to constrain their growth rate and band periodicity. By calculating the mean age for an entire modern septum and measuring both the length and the number of band pairs for that septum, we can determine both quantities. However, as described above, we do not know the amount of unsupported closed system ^{230}Th in our samples, and therefore can not directly calculate the true ages from the uranium series data in Table 3.6. Using the samples for which we have multiple measurements from a single septum, we employ isotope development diagrams, which explicitly show how $^{230}\text{Th}/^{232}\text{Th}$ ratios change with time. These diagrams can constrain both the age and the initial $^{230}\text{Th}/^{232}\text{Th}$ ratios for our data set. The isochron diagrams are analogous to the Rb/Sr development diagrams for dating metamorphic rocks [Faure, 1986]. It is important to note that cleaning of these samples consisted only of the water rinses and ultrasonication described above.

The age equation for short lived modern corals can ignore decay of the long lived radioisotope ^{238}U (half life 4.47×10^9 years). The rate of ^{230}Th ingrowth is then the balance between production from ^{234}U and loss from ^{230}Th decay:

$$\frac{d^{230}\text{Th}}{dt} = \lambda_{234}^{234}\text{U} - \lambda_{230}^{230}\text{Th}$$

Here radioisotopes are written as atomic abundances, not activity values. If we assume that at time zero there was an initial amount of ^{230}Th , denoted $^{230}\text{Th}^0$, then the solution to this differential equation is:

$$^{230}\text{Th} = \frac{\lambda_{234}}{\lambda_{230} - \lambda_{234}} ^{234}\text{U} (e^{-\lambda_{234}t} - e^{-\lambda_{230}t}) + ^{230}\text{Th}^0 e^{-\lambda_{230}t}$$

Because we are concerned with time spans of 200 years or less, which are small relative to the 75,200 year half-life of ^{230}Th , we can linearize this equation with the first two terms of the power series expansion of $e^{\lambda t}$:

$$e^{\lambda t} = 1 + \lambda t + \frac{(\lambda t)^2}{2!} + \frac{(\lambda t)^3}{3!} + \frac{(\lambda t)^4}{4!} + \dots$$

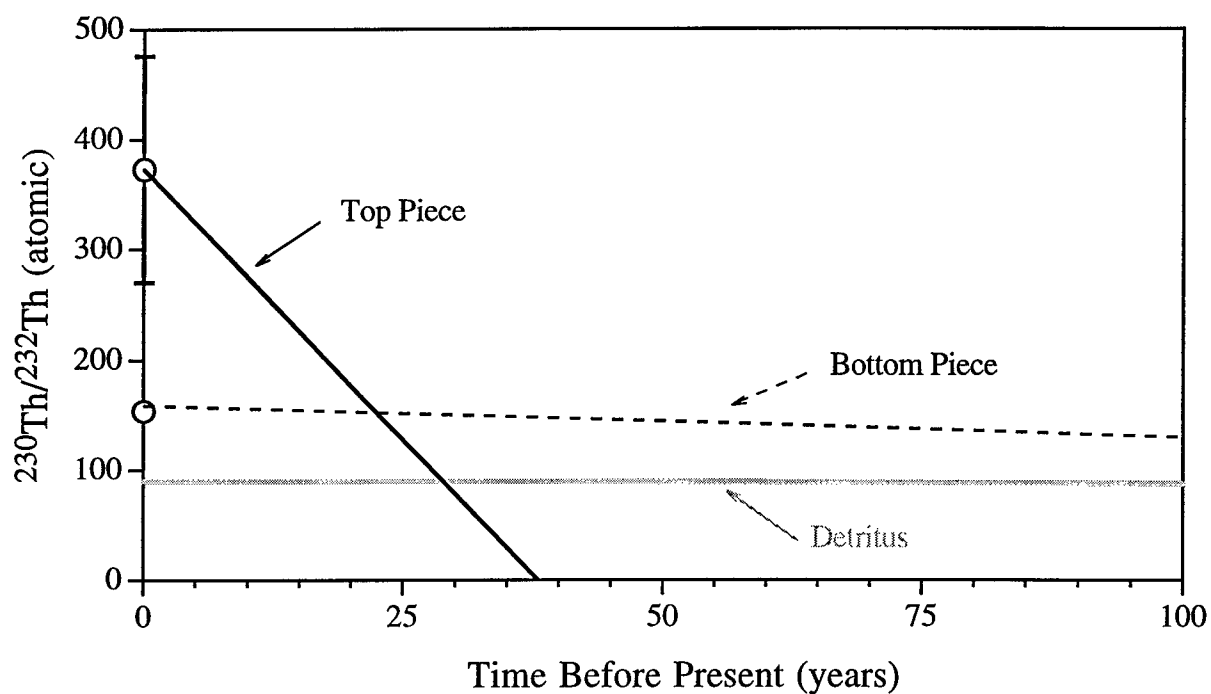
Multiplying the resulting equation by $^{234}\text{U}/^{232}\text{Th}$ on both sides to normalize for detrital Th and collecting terms gives:

$$\frac{^{230}\text{Th}}{^{232}\text{Th}} = \left(-\lambda_{234} \frac{^{234}\text{U}}{^{232}\text{Th}} + \lambda_{230} \frac{^{230}\text{Th}^{\circ}}{^{232}\text{Th}} \right) t + \frac{^{230}\text{Th}^{\circ}}{^{232}\text{Th}}$$

This is the equation of a straight line on a plot of time versus $^{230}\text{Th}/^{232}\text{Th}$. I have changed the sign of the slope term to reflect the fact that we consider the date of measurement as time zero and then extrapolate back in time. This assumption means that the initial thorium ratio, $^{230}\text{Th}^{\circ}/^{232}\text{Th}$, is not the value the coral started with, but the value at the time of measurement. Because the equation is linearized, switching time reference points does not alter the calculated ages. From the measurements in Table 3.6 we know the y-intercept, which is the measured $^{230}\text{Th}/^{232}\text{Th}$, and slope of this line. Every sample with ^{232}Th , ^{230}Th and ^{234}U data appears as an individual line on a plot of time versus $^{230}\text{Th}/^{232}\text{Th}$. The lines are the set of points that are solutions to the above equation, so that any age read from the plots implies a particular initial $^{230}\text{Th}/^{232}\text{Th}$ ratio at the time of coral growth. The older the coral the smaller the initial ratio. Ingrowth from ^{234}U is more important than decay of initial ^{230}Th so that all of our calculated slopes are negative.

Plots of the modern coral data are shown in Figures 3.15-3.17. No sample can have a negative $^{230}\text{Th}/^{232}\text{Th}$ ratio (negative age), and the top piece of a septum must be the same age or younger than the bottom piece. These two constraints, along with the assumption that each piece from a single coral had the same initial $^{230}\text{Th}/^{232}\text{Th}$ ratio when formed, allow us to assign ages to the samples in isochron diagrams. For sample number 85080 from south of Tasmania in 990-1150 meters of water, we measured two septa and an organic piece of detritus which are shown in Figure 3.15. Both the detrital sample and the bottom of septum A are ^{232}Th rich and provide a range of possible initial $^{230}\text{Th}/^{232}\text{Th}$ values. While the bottom of septum A does not constrain the age, the initial $^{230}\text{Th}/^{232}\text{Th}$ ratio can not be larger than the measured bottom value without implying a negative age. The detrital sample is so elevated in ^{232}Th that it provides a minimum value for the initial

Sample 85080, Septum A



Sample 85080, Septum B

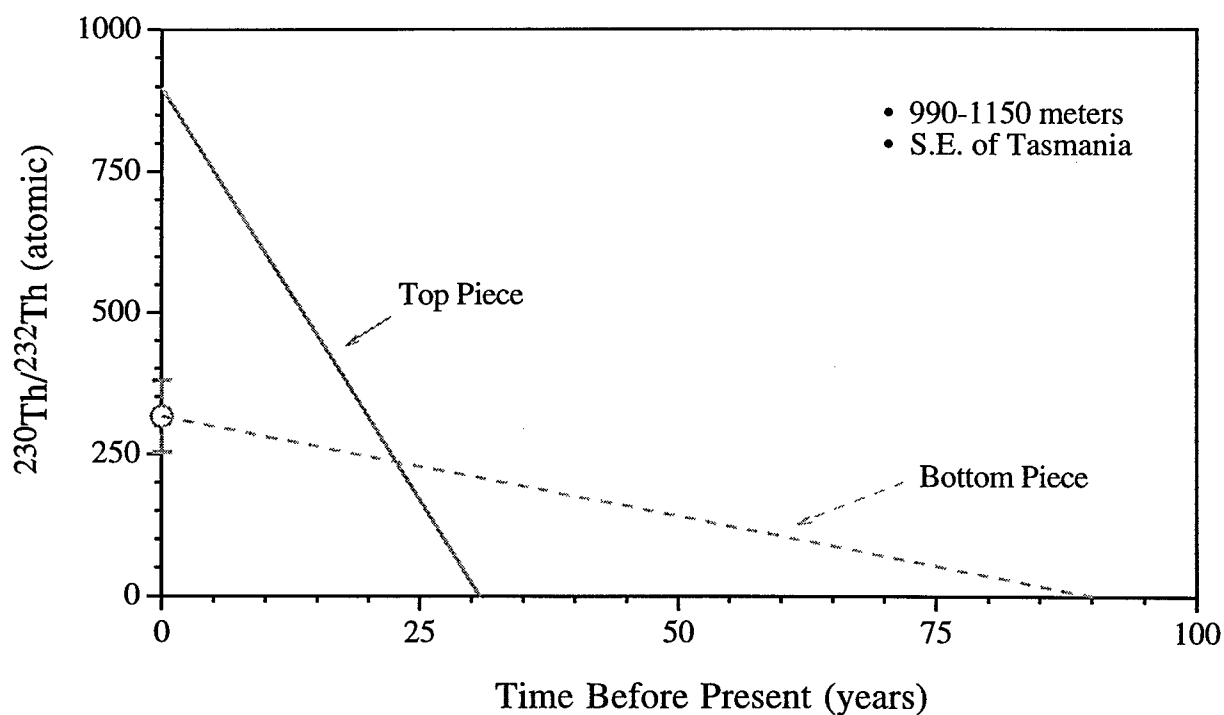


Figure 3.15. Isotope evolution diagram for two septa of sample number 85080. Intersection of top and bottom pieces constrains the lower age limit and intersection with the x-axis constrains the upper age limit.

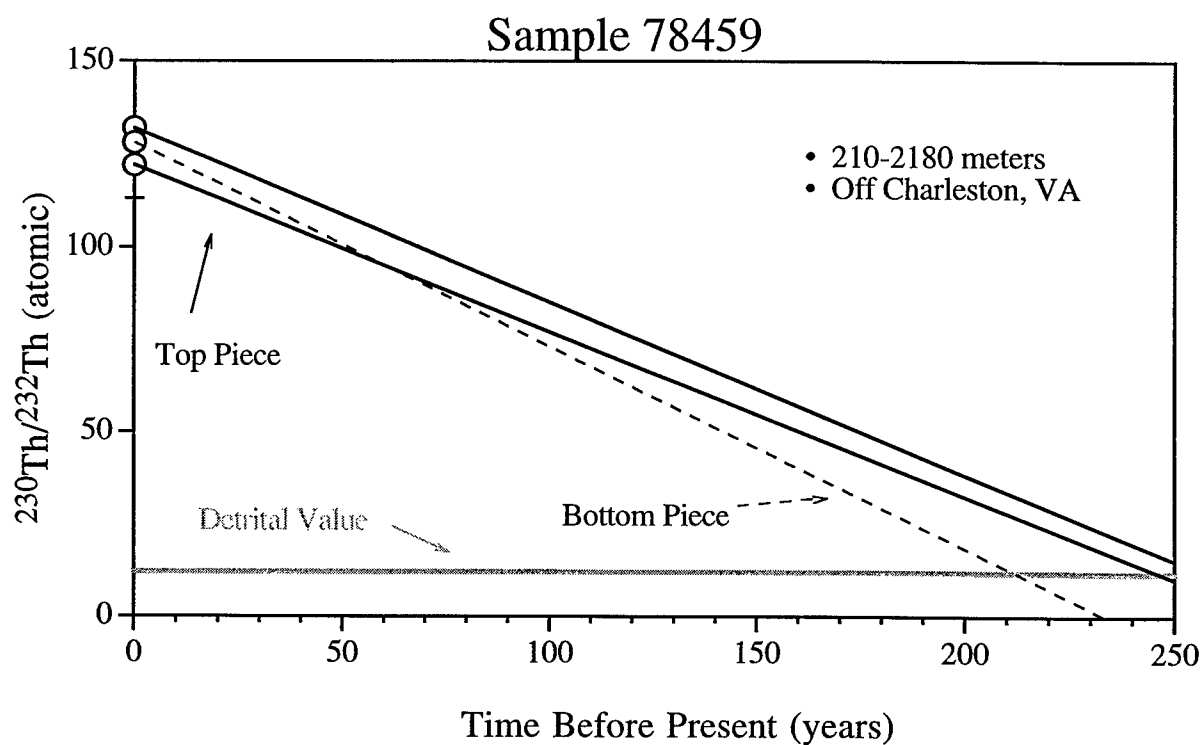
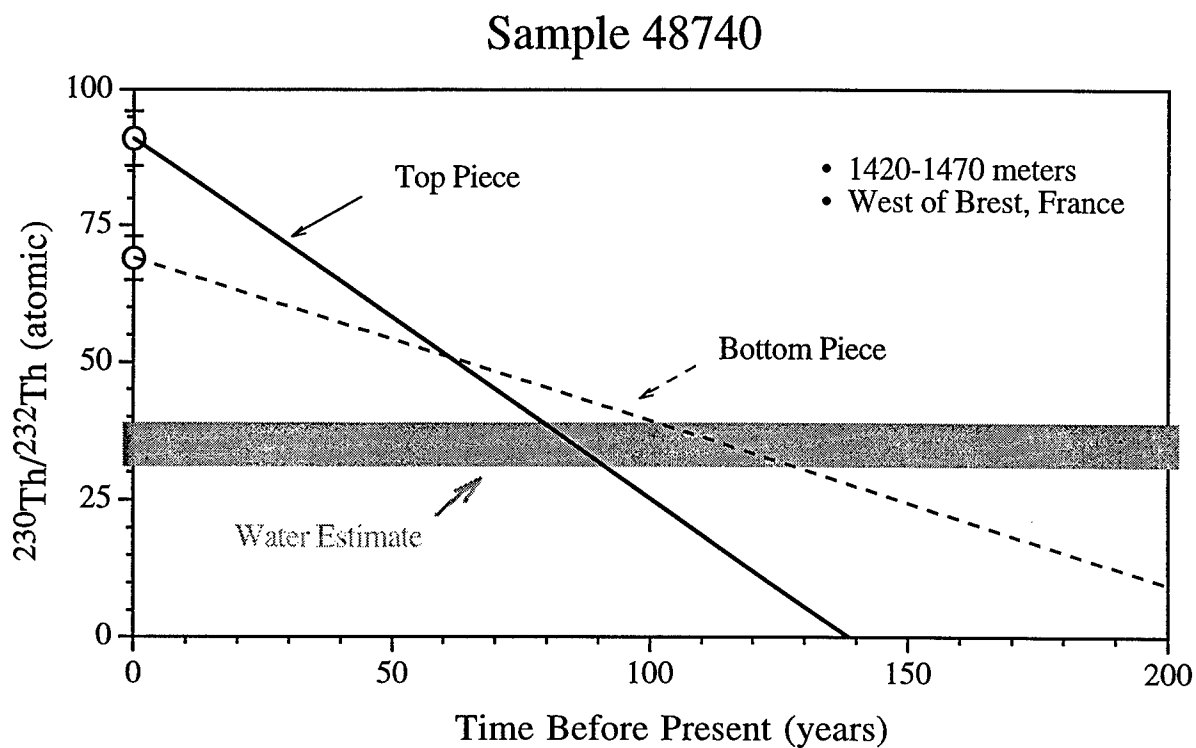
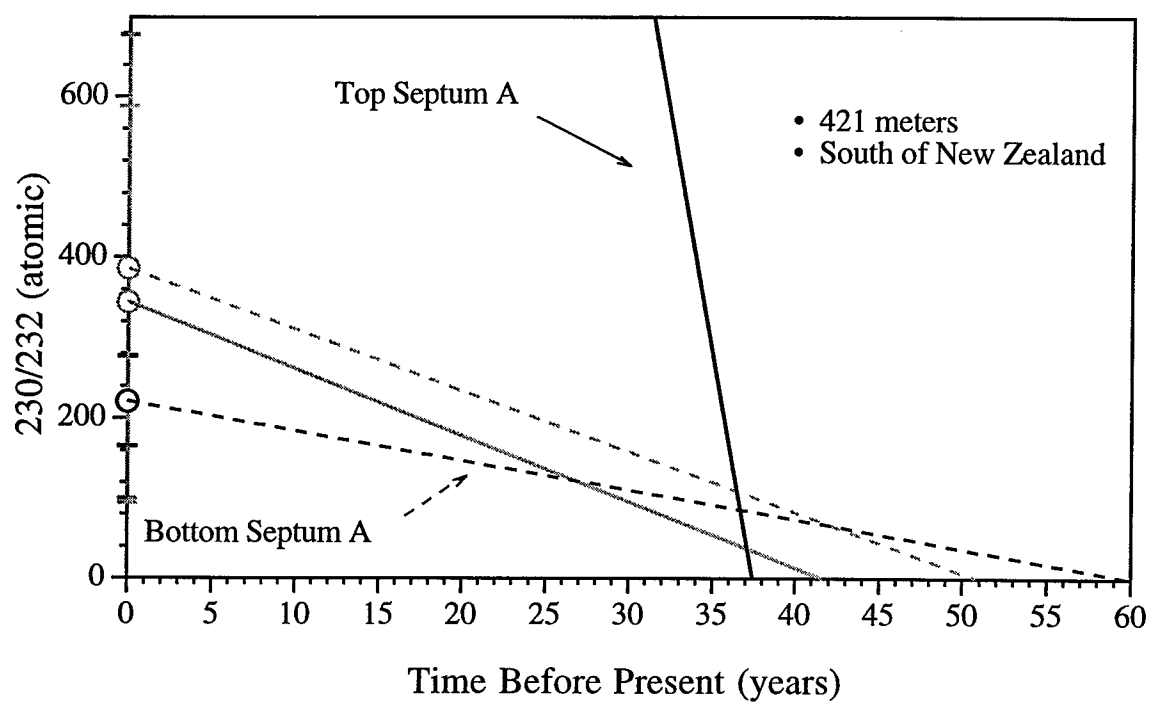


Figure 3.16. Isotope evolution diagram for samples 48740 and 78459. For the upper pannel the $^{230}\text{Th}/^{232}\text{Th}$ ratio of the water helps to constrain the age. The parallel lines of sample 78459 do not provide strong age constraints.

Sample 47413



Sample 84820

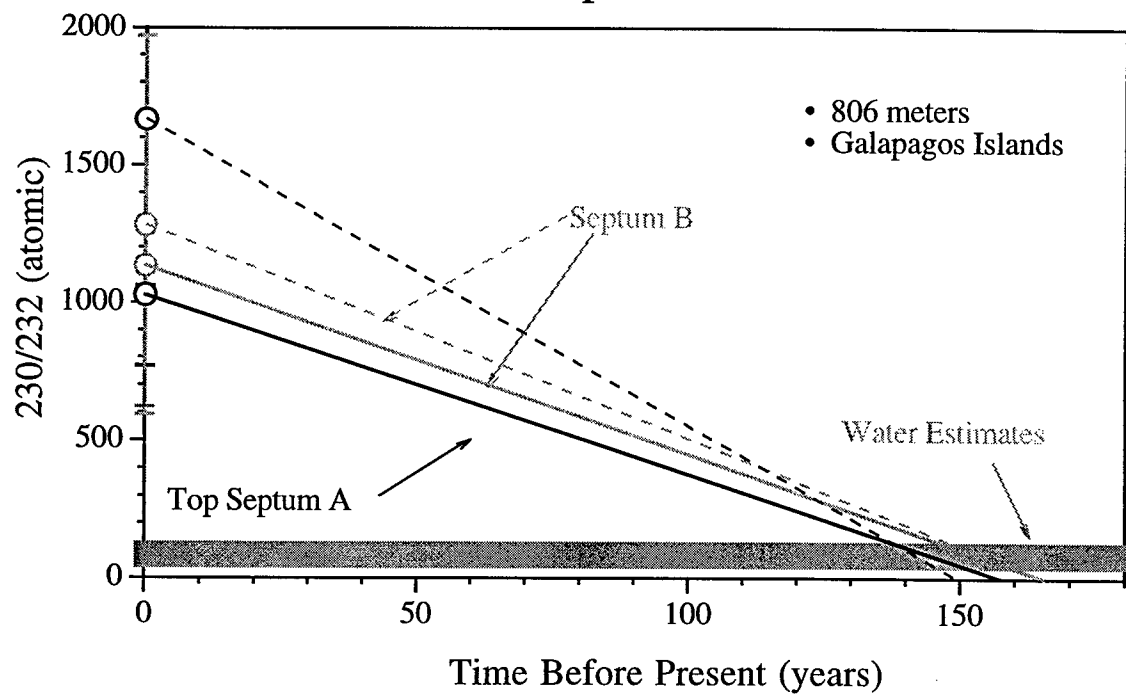


Figure 3.17. Isotope evolution diagrams for samples 47413 and 84820.

ratio. With this range of $^{230}\text{Th}/^{232}\text{Th}$ values, 90-160 ppm, and measurement errors, we calculate the mean age of the top of septum A to be between 15 and 35 years. We calculate an age range of 20-60 years for septum B of this sample using the same initial $^{230}\text{Th}/^{232}\text{Th}$ range. In Table 3.10 these results are used to estimate the band periodicity and growth rate of the septa. We assume the sample was collected alive and subtract the time since collection from our mean age estimates. Periodicity and rates are calculated using twice the mean age to account for the fact that this is an average of the time taken to form the whole length of the coral. Because septum A only uses the top piece, we divided the length and number of bands in half. This sample grew at an average rate of about 0.4-0.6 mm/yr and, if the band pairs are periodic, 0.6-0.8 pairs are laid down per year.

For sample 48740 (Figure 3.16), there are two ways we can try to estimate rates. The intersection of the top and bottom piece, along with the measurement errors, constrain the age to be at least 60 years, while the top piece itself can not be older than 140 years. These ages correspond to a growth rate of 0.1 ± 0.1 mm/yr. However, the coral may have been dead when collected. In this case, we have overestimated the ages and consequently underestimated the growth rate. Using the recent Labrador Sea water column data of Moran et al. [1997], we can try to estimate the initial $^{230}\text{Th}/^{232}\text{Th}$ ratio of this sample. Dissolved and total $^{230}\text{Th}/^{232}\text{Th}$ data from their nearest and most complete station (IOC-93 stn. 2, 54.50°N, 48.46°W) are both higher than the measured ratios in the coral samples. Particulate data has a relatively constant $^{230}\text{Th}/^{232}\text{Th}$ ratio of $35 \pm 5 \times 10^{-6}$ from 500-2000 meters. Using this range, we calculate a top to bottom age difference of 29 ± 25 years. The age is not corrected for collection date because the age difference should remain constant once the coral dies. In addition, the age was not doubled because this age difference between top and bottom is closer to the true lifetime of the coral than a mean age for the whole septum. This type of calculation is only possible when there is a

Sample	Col. Date	Isochron Age (yrs)		Corrected Age ^m (yrs)	Initial 230/232 ^b	Bands # error	Length (mm)	Periodicity		Growth Rate	
		Lower	Upper		Lower	Upper		Band/yr	error	mm/yr	error
47413 A	1/21/64	37	60	20	0	150	41	1.0	0.6	1.0	0.6
47413 B		20	50 ^a								
84820 A	11/23/1986 ⁱ	100	180	132	50	120 ^c	25	0.1	0.0	0.1	0.03
84820 B		70	230	142			25	0.1	0.1	0.1	0.05
85080 A ⁱ	2/25/90	15	35 ^a	21	90	160	33	0.6	0.3	0.4	0.2
85080 B		20	60	36			33	0.8	0.3	0.6	0.2
48740	10/28/73	60	140	79	0	50	19			0.1	0.1
or											
Top-Bottom ^g				29	30	40 ⁱ	19			0.3	0.3
78459	4/16/87	205	255	j	11	13 ^h	28				
or											
Intersection		10	110 ^k	53	70	120	28	0.3	0.3	0.3	0.2

a Estimates based on regressions. The errors are larger because measurements are not well constrained.

b Values are atomic ratios x10⁶.

c Estimate from water data of Bacon and Anderson (1982).

e Age of top piece only. See text.

f Estimate from particulate data of Moran et al. (1997).

g Top minus bottom age difference based on water estimated initial 230/232 ratio. See text.

h Detrital value.

i Because only the top piece is used, half of the bands and half of the length are used.

j The coral was probably dead when collected and the true age can not be constrained using the detrital ²³⁰Th/²³²Th ratio.

k Uses intersection point on development diagram to constrain age

l Probably dead when collected. See text.

m Corrected for age since collection. Assumes corals were collected alive. See text.

Table 3.10: Summary of Modern Growth Rate Data. Values are taken from the isotope evolution diagrams

significant difference between the top and bottom slope and the errors on the measured $^{230}\text{Th}/^{232}\text{Th}$ ratios are small.

For example, the top minus bottom age difference does not work for sample 78459 which was also probably collected dead. Here the replicates of the top piece and the bottom piece are all parallel to each other within error. The detrital value constrains the age to be between 205 and 255 years, but in this range the bottom piece is younger than the top. If we use the intersection point, the age drops to 10-110 years and the initial ratio rises to 70-120 ppm. These values give a growth rate of 0.3 ± 0.2 mm/yr. Sample 84820 from the Galapagos islands also seems to have been collected dead (Figure 3.17). Given its pristine ^{232}Th content, the measured $^{230}\text{Th}/^{232}\text{Th}$ ratios are high because of ^{230}Th ingrowth over time. Using water column data from the Panama Basin, we estimate the initial $^{230}\text{Th}/^{232}\text{Th}$ value to be between 50-120 ppm [Bacon and Anderson, 1982]. Sediment trap data from the nearby STIE site 1110 (5.06°N , 81.02°W) have $^{230}\text{Th}/^{232}\text{Th}$ ratios of $30\text{-}50 \times 10^{-6}$ at 600-1300 meters [Anderson et al., 1983] and bottom water from MANOP site H is only as high as 160 ppm [Moore, 1981]. With these initial constraints, we calculate the age for 84820 septum A to be 100-180 years and that for septum B to be 70-230. The minimum growth rates implied by these maximum ages are around 0.1 mm/yr.

One of our better constrained samples is 47413 from south of New Zealand in 421 meters of water (Figure 3.17). The top of septum A has virtually no ^{232}Th and gives a strong constraint on the age. The bottom of this septum is more enriched in ^{232}Th , but by no means contaminated, and better constrains the initial $^{230}\text{Th}/^{232}\text{Th}$ value. Given the intersection of the top and bottom lines and the errors on the measured ratios, the maximum initial $^{230}\text{Th}/^{232}\text{Th}$ at the time of growth is 150 ppm. The lowest this number can be is zero. Therefore, the age range for this sample is 37-60 years. These values translate into a corrected growth rate of 1.0 ± 0.6 mm/yr. Due to the large measurement

errors the second septum is not as well constrained. We use the same initial value range to estimate an age range of 20-50 years, but the errors on this range are large.

All of the untreated coral generated and water column initial $^{230}\text{Th}/^{232}\text{Th}$ ratios fall in the 80 ± 80 ppm range. This analysis is strong support for our use of this range as a conservative estimate in our fossil coral age and error calculations. Modern corals seem to have an average growth rate of 0.1-1 mm/yr. Banding periodicity varies from 0.1-1 bands/year in our calculations. In addition to the problems with generating precise and accurate ages, the bands themselves are not easy to constrain. Until we have reproducible ways of counting bands for an entire septum, these band periodicities will be a crude estimate, if the bands are periodic at all. Besides the uranium series data, we made an initial attempt to use α -counted ^{210}Pb for dating [Druffel et al., 1990]. Table 3.11 shows the results from breaking off pieces from the top and the bottom of a single septum and measuring their ages. Our initial results show that the growth rate estimates agree well with the ^{230}Th and radiocarbon results (Chapter 4).

V. Conclusions

We have exploited the uranium series decay chain to produce a variety of different types of dates. Sacrificing precision for sample throughput on an ICP-MS allows us to rapidly and inexpensively screen hundreds of deep-sea corals for their ages. Using this method, dozens of paleoceanographically useful samples have been discovered. Better constrained TIMS data provides accurate and precise calendar ages for fossil samples. Corrections for initial ^{230}Th impart an overall error of about 3% to the ages. Improvements in cleaning techniques should be able to shrink this uncertainty. Precise data from modern corals constrain the average growth rate of *D. cristagalli* to be between 0.1 and 1 mm/yr. Band periodicity is not as well established, but falls in the range of 0.1-1 band/year. By collecting samples that we know to be alive when taken from the seafloor, uncertainty in these numbers can be improved.

Sample	weight (mg)	counts		210/209		[²¹⁰ Pb]		Age		Bands	Length mm	Bands/yr		Growth rate	
		209	210	ratio	err	dpm/g	error	years	error					mm/yr	error
Top	208	3338	970	0.292	0.012	0.324	0.013	41	5	60	47	1.5	0.2	1.1	0.1
Bottom	143	3621	1321	0.404	0.014	0.652	0.023								

[Ra-226] 14.51dpm/g

Table 3.11: Growth Rate of sample number 47407 from ²¹⁰Pb Data. Measured ²²⁶Ra content is 14.5 dpm/g

References

- Anderson, R. F., M. Bacon and P. G. Brewer, Removal of ^{230}Th and ^{231}Pa at ocean margins, *Earth and Planetary Science Letters*, 66, 73-90, 1983.
- Bacon, M. P. and R. F. Anderson, Distribution of Thorium isotopes between dissolved and particulate forms in the deep sea, *Journal of Geophysical Research*, 87, 2045-2056, 1982.
- Bard, E., M. Arnold, R. Fairbanks and B. Hamelin, ^{230}Th - ^{234}U and ^{14}C ages obtained by mass spectrometry on corals, *Radiocarbon*, 35, 191-199, 1993.
- Bard, E., B. Hamelin, R. G. Fairbanks and A. Zindler, Calibration of the ^{14}C timescale over 30,000 years using mass spectrometric U-Th ages from Barbados corals, *Nature*, 345, 405-410, 1990.
- Boyle, E. A., Cadmium, zinc, copper, and barium in foraminifera tests, *Earth Planet. Sci. Lett.*, 53, 11-35, 1981.
- Broecker, W. S., D. L. Thurber, J. Goddard, T.-L. Ku, R. K. Matthews and K. J. Mesolella, Milankovitch hypothesis supported by precise dating of coral reefs and deep-sea sediments, *Science*, 159, 297-300, 1968.
- Burnett, W. C. and H. H. Veeh, *Uranium-series studies of marine phosphates and carbonates*, Oxford Science Publications, Uranium-Series Disequilibrium, Applications to Earth, Marine and Environmental Sciences (2nd Edition), M. Ivanovich and R. S. Harmon, Oxford Science Publications, 487-512, 1993.
- Cairns, S. D. and G. D. Stanley Jr., Ahermatypic coral banks: living and fossil counterparts, *Proceedings of the Fourth International Coral Reef Symposium, Manila*, 1, 611-618, 1981.
- Chen, E., U^{238} - U^{234} - Th^{230} - Th^{232} systematics and the precise measurement of time over the past 500,000 years *Earth Planet. Sci. Lett.*, 81, 1986.
- Cheng, H., J. F. Adkins, R. L. Edwards and E. A. Boyle, *^{230}Th dating of deep-sea solitary corals*, AGU, EOS, 1995.
- Cochran, J. K., H. D. Livingston, D. J. Hirschberg and L. Surprenant D., Natural and anthropogenic radionuclide distributions in the northwest Atlantic Ocean, *Earth and Planetary Science Letters*, 84, 135-152, 1987.
- Druffel, E. R. M., L. L. King, R. A. Belastock and K. O. Buesseller, Growth rate of a deep-sea coral using ^{210}Pb and other isotopes, *Geochimica et Cosmochimica Acta*, 54, 1493-1500, 1990.
- Duncan, P. M., On the rapidity of growth and variability of some Madreporaria on an Atlantic cable with remarks upon the the rate of accumulation of foraminiferal deposits, *Annual Magazine of Natural History*, 20, 361-365, 1877.
- Edwards, R. L., W. J. Beck, G. S. Burr, D. J. Donahue, J. M. A. Chappell, A. L. Bloom, E. R. M. Druffel, et al., A large drop in atmospheric $^{14}\text{C}/^{12}\text{C}$ and reduced melting in

- the Younger Dryas, documented with ^{230}Th ages of corals, *Science*, 260, 962-967, 1993.
- Edwards, R. L., J. H. Chen, T.-L. Ku and G. J. Wasserburg, Precise timing of the last interglacial period from mass spectrometric determination of Thorium-230 in corals, *Science*, 236, 1547-1553, 1987.
- Edwards, R. L., J. H. Chen and G. J. Wasserburg, ^{238}U - ^{234}U - ^{230}Th - ^{232}Th systematics and the precise measurement of time over the past 500,000 years, *Earth and Planetary Science Letters*, 81, 175-192, 1986/87.
- Edwards, R. L., F. W. Taylor and G. J. Wasserburg, Dating earthquakes with high-precision thorium-230 ages of very young corals, *Earth and Planetary Science Letters*, 90, 371-381, 1988.
- Faure, G., *Principles of Isotope Geology*, New York, Wiley and Sons, New York, Wiley and Sons, 589, 1986.
- Gallup, C. D., L. R. Edwards and R. G. Johnson, The timing of high sea levels over the past 200,000 years, *Science*, 263, 796-800, 1994.
- Goldstein, S. J., M. T. Murrell, D. Lea, S. Chakraborty and M. Kashgarian, ^{231}Pa and ^{230}Th dating of deep-sea coral, *EOS, Transactions, AGU, 1996 Fall Meeting Supplement*, 77, F291, 1996.
- Grigg, R. W., Growth rings: annual periodicity in two Gorgonian corals, *Ecology*, 55, 876-881, 1974.
- Guo, L., P. Santschi, M. Baskaran and A. Zindler, Distribution of dissolved and particulate ^{230}Th and ^{232}Th in seawater from the Gulf of Mexico and off Cape Hatteras as measured by SIMS, *Earth and Planetary Science Letters*, 133, 117-128, 1995.
- Gvirtzman, G., G. M. Friedman and D. S. Miller, Control and distribution of uranium in coral reefs during diagenesis, *Journal of Sedimentary Petrology*, 43, 985-997, 1973.
- Huh, C.-A. and T. M. Beasley, Profiles of dissolved and particulate thorium isotopes in the water column of coastal Southern California, *Earth and Planetary Science Letters*, 85, 1-10, 1987.
- Ku, T. L., K. G. Knauss and G. G. Mathieu, Uranium in the open ocean: concentration and isotopic composition, *Deep-Sea Research*, 24, 1005-1017, 1977.
- Min, G. R., R. L. Edwards, F. W. Taylor, J. Recy, C. Gallup and J. W. Beck, Annual cycles of U/Ca in coral skeletons and U/Ca thermometry, *Geochimica et Cosmochimica Acta*, 59, 2025-2042, 1995.
- Moore, W. S., The thorium isotope content of ocean water, *Earth and Planetary Science Letters*, 53, 419-426, 1981.
- Moran, S. B., M. A. Charette, J. A. Hoff, R. L. Edwards and W. M. Landing, Distribution of ^{230}Th in the Labrador Sea and its relation to ventilation, *Earth and Planetary Science Letters*, 150, 151-160, 1997.

- Moran, S. B., J. A. Hoff, K. O. Buesseler and R. L. Edwards, High precision ^{230}Th and ^{232}Th in the Norwegian Sea and Denmark by Thermal ionization mass spectrometry, *Geophysical Research Letters*, 22, 2589-2592, 1995.
- Muhs, D. R., G. L. Kennedy and T. K. Rockwell, Uranium-series ages of marine terrace corals from the Pacific coast of North America and implications for last-interglacial sea level history, *Quaternary Research*, 42, 72-87, 1994.
- Nozaki, Y., Y. Horibe and H. Tsubota, The water column distributions of thorium isotopes in the western North Pacific, *Earth and Planetary Science Letters*, 54, 203-216, 1981.
- Nozaki, Y., H.-S. Yang and M. Yamada, Scavenging of Thorium in the ocean, *Journal of Geophysical Research*, 92, 772-778, 1987.
- Pratje, O., Korallenbanke in tiefen und kühlen Wasser, *Zentralbl f Min. Geol.*, 410-415, 1924.
- Roy-Barman, M., J. H. Chen and G. J. Wasserburg, ^{230}Th - ^{232}Th systematics in the central Pacific Ocean: the sources and fates of thorium, *Earth and Planetary Science Letters*, 139, 351-363, 1996.
- Shaw, T., J. and R. Francois, A fast and sensitive ICP-MS assay for the determination of ^{230}Th in marine sediments, *Geochimica et Cosmochimica Acta*, 55, 2075-2078, 1991.
- Shen, G. T. and E. A. Boyle, Determination of lead, cadmium and other trace metals in annually-banded corals, *Chemical Geology*, 67, 47-62, 1988.
- Shen, G. T. and R. B. Dunbar, Environmental controls on uranium in reef corals, *Geochimica et Cosmochimica Acta*, 59, 2009-2024, 1995.
- Stein, M., G. J. Wasserburg, P. Aharon, J. H. Chen, Z. R. Zhu, A. Bloom and J. Chappell, TIMS U-series dating and stable isotopes of the last interglacial event in Papua New Guinea, *Geochimica et Cosmochimica Acta*, 57, 2541-2554, 1993.
- Stein, M., G. J. Wasserburg, K. R. Lajoie and J. H. Chen, U-series ages of solitary corals from the Californian coast by mass spectrometry, *Geochimica et Cosmochimica Acta*, 55, 3709-3722, 1991.
- Stein, R., *Accumulation of organic carbon in marine sediments*, Springer-Verlag, Springer-Verlag, 217, 1991.
- Stirling, C. H., T. M. Esat, M. T. McCulloch and K. Lambeck, High-precision U-series dating of corals from Western Australia and implications for the timing and duration of the last interglacial, *Earth and Planetary Science Letters*, 135, 115-130, 1995.
- Szabo, B. J., K. R. Ludwig, D. R. Muhs and K. R. Simmons, Thorium-230 ages of corals and duration of the last interglacial sea-level high stand on Oahu, Hawaii, *Science*, 266, 93-96, 1994.

- Thompson, G. and H. D. Livingston, Strontium and uranium concentrations in aragonite precipitated by some modern corals, *Earth and Planetary Science Letters*, 8, 439-442, 1970.
- Tiechert, C., Cold and deep-water coral banks, *Bulletin of the American Association of Petroleum Geologists*, 42, 1064-1082, 1958.
- Wedepohl, K. H., *Handbook of Geochemistry*, v. II/5, New York, Springer-Verlag, New York, Springer-Verlag, 1978.

Table A3.1: Smithsonian deep-sea coral samples

Sample #	Age (years)	Age with no ²³² Th	Depth (meters)	Latitude	Longitude	Species I.D.	Comments
16259.1	0	100	1582	37°46.5'N	73°56.5'W	F. alabastrum	Off Virginia. 9/17/87.
16259.2	0	800					
16259.3	0	500					
16259.4	0	500					
16259.5	0	300					
45743.1	5,200	5,200	1050	48°39.7'N	9°53.2'W	L. pertusa	10/26/73. Little Sole Bank
45743.2	3,800	3,800					
45871.1	0	2,200	1080-1089	23°52'N	80°42'W	M. oculata	Straits of Florida. 4/30/69
45871.2	200	3,000					
45871.3	100	2,000					
45871.4	0	7,800					
46306.1	100	2,600	1088-1116	16°58'N	79°28'W	St. diadema	Off SW Jamaica. 7/28/72
46306.2	0	1,900					
46306.3	100	3,000					
46306.4	700	6,600					
46306.5	300	5,300					
46306.6	200	2,700					
46306.7	200	2,300					
46306.8	100	1,300					
46346.1	200	2,900	1281	23°57'N	75°59'W	St. diadema	Exuma Sound.
46346.2	200	2,900					
46346.3	200	2,400					
47373.1	1,400		2010-2100	49°51'S	178°35'E	F. impensum	Antipode Islands. 2/26/68
48378.1	2,800	2,800	1158-1174	47°40.9'N	8°5.7'W	M. oculata	11/1/69. Celtic Sea
48517.1	8,200	8,200	1584	39°13'N	31°35'W	S. variabilis	10/24/71. Azores
48517.2	3,800	3,800					
48523.1	1,900		2550-2770	47°35.5'N	8°47'W	F. angulare	11/18/71. Banc de la chapelle
48698.1	1,700		2440	39°3.5'N	28°25.5'W	C. ambrosia	10/18/71. Azores.
48698.2	1,500						
48698.3	900						
48698.4	700						
48712.1	2,000		2085-2096	37°21'N	25°28.5'W	C. ambrosia	11/7/71. Azores.
48712.10	1,100						
48712.12	300						
48712.13	500						
48712.14	500						
48712.15	1,300						
48712.16	1,100						
48735.1	174,600	174,600	1069-1235	37°57.5'N	25°33'W	D. cristagalli	11/3/71. Azores
48735.2	34,600	34,600					
48738.3	43,600	43,600	665-800	37°48.5'N	25°54'W	D. cristagalli	11/1/71. Azores
48888.1	400		2115	47°32.8'N	8°33.5'W	C. ambrosia	7/16/78. Celtic Sea
48888.2	1,200						
48888.3	700						
48888.4	0						
62588.2	6,300		1853-1858	23°51'N	75°50'W	St. diadema	9/3/81.
62588.3	6,800						
80389.1	1,500		1998-2077	35°11.9'N	7°52.6'W	C. ambrosia	6/5/84. Off Morocco.
80389.2	3,300						
80389.3	37,000	37,000					
80389.4	5,100	5,100					
80389.5	48,800	48,800					
80389.6	13,100	13,100					
80390.1	0	1,400	1998-2077	35°11.9'N	7°52.6'W	F. alabastrum	6/5/84. Off Morocco.
80390.2	2,200						
80390.3	700						

Table A3.1 (Con't)

80391.1	6,700	6,700	1998-2077	35°11.9'N	7°52.6'W	St. nobilis	6/5/84. Off Morocco
80391.2	800						
86562.1	1,200		1517-1611	11°33'S	145°19.3E	St. weberianus	N. Great Barrier Reef. 8/22/88
86562.2	8,400						
86873.1	1,500		1112	25°53'S	5°44'E	St. camp.	Walvis Ridge. Temp. 3.5°. 2/284
91545.1	800		1510-1600	21°18'S	36°18'E	St. nobilis	Mozambique. 10/2/64
91545.2	200						
94022.1	3,100	3,100	1354-1995	38°24'S	178°53'E	C. atlantica	N. New Zealand, E. cape. 5/28/66
94022.2	10,400	10,400					
94046.1	3,600	20,800	1265-1276	28°3.8'S	179°32.4W	C. scobinosa	Colville Ridge
94046.2	700	4,500					
94288.1	0	900	1395	37°34'S	179°22'E	F. apertum	NZOI. N. Island E. Cape
94288.2	100	700					
JFA 48.1	15,200		2475-2820	0°55'N	28°29'W	F. apertum	St. Peter and Paul Rocks. 1988
JFA 48.2	8,500		2475-2821	0°55'N	28°29'W	Cary. sp.	St. Peter and Paul Rocks. 1989
JFA 47.1	1,000		1790-1803	48°9.5'S	148°16'E	Cary. sp.	"Not Sub-antarctic" 2/23/67

Table A3.2: Ages of French deep-sea corals

Sample #	Age (years)	Age with no ²³² Th	Depth (meters)	Latitude	Longitude	Species I.D.	Comments
JFA50.3	400	13,200				D. cristagalli	7/15/1986
JFA50.4	2,700	17,000					
JFA50.6	1,200	15,500					
JFA51.1	19,900		730	46°20.2'S	42°28.2'E	S. varilis	9-8-80, Kara Dag Seamount
JFA51.2	32,000						
JFA52.1	8,300	63,300	2370-2380	23°04'S	40°20'W	F. apertum	5-8-87 Brazil
JFA53.1	337,600		1500	33°12.60'N	29°17.20'W	D. cristagalli	2-1-93 Plato Seamount
JFA53.2	456,200						
JFA53.3	2,100	30,800					
JFA53.4	4,500	75,000					
JFA53.5	4,100	26,700					
JFA54.1	1,000					D. cristagalli	7/22/1986
JFA54.2	1,500						
JFA54.3	100	800					
JFA54.4	300	1,800					
JFA54.5	200	1,100					
JFA55.1	17,000	149,700	730	46°20.2'S	42°28.2'E	M. oculata	9-8-80 Kara Dag Seamount
JFA55.2	18,900	156,700					
JFA55.5	66,000						
JFA55.6	15,200	123,100					
JFA56.1	2,200					S. variblis	7/22/1986
JFA56.2	900						
JFA56.3	100	400					
JFA57.1	2,600					S. variblis	7/15/1986
JFA57.2	6,400						
JFA57.3	700	4,300					
JFA58.1	900	6,300	2370-2380	23°04'S	40°20'W	St. diadem?	5-8-87 Brazil
JFA59.1	14,400		1500	33°12.60'N	29°17.20'W	E. rostrata	2-1-93 Plato Bank
JFA59.2	14,100						
JFA59.3	5,300						
JFA59.4	300	3,400					
JFA60.1	3,600		410-450	38°48.68'S	77°36.14'E	L. pertusa	7-18-86 SE St. Paul
JFA60.2	1,900						
JFA60.3	3,400	18,400					
JFA60.4	3,200	20,800					
JFA60.5	1,400	20,700					
JFA62.1	4,700		1420	33°13.2'N	29°08.2'W	D. cristagalli	1-31-93, Pluto Seamount
JFA62.3	10,500	62,700					
JFA63.1	800		850	22°24.7'S	171°49.0'E	E. rostrata	6-1-89, S. of Vannata
JFA63.2	800						
JFA63.3	300	1,200					
JFA64.1	1,600					E. scillae	quarry of Lazzaro, Calabria
JFA64.2	84,400						
JFA65.1	2,100					S. variblis	7-9-86 NE Amsterdam
JFA65.2	1,000						
JFA66.1	18,400		2370-2380	23°04'S	40°20'W	L. pertusa?	5-8-87 Brazil
JFA66.2	129,200						
JFA67.1	5,000					M. oculata	7/20/1986
JFA67.2	1,200						
JFA68.1	200		745-760	22°18.9'S	43°01.1'E		11-30-73 W. Madagascar
JFA69.1	9,800		730	46°20.2'S	42°28.2'E	D. cristagalli	9-8-80 Kara Dag Seamount
JFA69.2	5,000						
JFA69.3	7,300	56,900					
JFA69.4	7,300	50,700					
JFA69.5	18,300	144,100					
JFA70.1	177,500					D. cristagalli	7/23/1986
JFA70.2	42,300						

Table A3.2 (Con't)

JFA71.3	1,100	56,100	1500-1575	19°01'S	37°47'W	T. feabellum	5-28-87	Brazil
JFA72.1	31,000					C. profunda (?)	3/16/1976	
JFA72.2	29,200							
JFA72.3	1,900	18,200						
JFA72.4	1,300	9,400						
JFA72.5	1,800	9,600						
JFA72.7	1,700	14,200						
JFA73.1	13,100					M. oculata	7/15/1986	
JFA73.2	1,000	5,000						
JFA73.3	500	2,000						
JFA73.4	1,600	8,800						
JFA73.5	0	3,600						
JFA74.1	6,300	74,900	1500	33°12'60N	29°17.20'W	C. atlantica	2-1-93	Plato Seamount
JFA74.3	1,300	12,500						
JFA74.4	49,000							
JFA75.1	2,700		1020	24°00'S	42°14'W		6-2-87	Brazil
JFA75.2	10,000							
JFA76.1	100	500	580-585	12°50.0'S	48°09.1'E		9-11-72	Madagascar NW
JFA77.1	30,400		1000	24°54.4'S	44°26.0'W	L. pertusa (?)	1-25-62	Brazil
JFA77.2	16,300							
JFA78.1	400	2,100	204	63°11.18'N	24°13.79'W	L. pertusa	9-8-92	BIOICE Island
JFA78.2	600	3,700						
JFA78.3	400	4,600						
JFA78.5	400	2,800						
JFA79.1	1,100					S. variblis	7/22/1986	
JFA79.2	1,800							
JFA80.1	11,900		620-635			D. cristagalli	3-16-76	S. of Madagascar
JFA80.2	45,400							
JFA80.4	2,700	26,500						
JFA81.1	0	88,100	2370-2380	23°0.1'S	40°20'W	S. variblis	5-8-87	Brazil
JFA81.3	128,100							
JFA82.1	400	1,300	1300-1475	22°14.06'S	167°29.01'E		9-4-85	Jean Charlot
JFA82.2	1,100							
JFA83.1	8,100	54,400	1330	25°06.36'S	16°01.51'E	Caryophyllic sp.	10-7-86,	New Caledonia
JFA83.2	7,400	44,900						
JFA84.1	300	1,500	1000	24°54.4'S	44°26.0'W	D. cristagalli	1/25/1962	
JFA86.1	3,000	17,400	1500	33°12.60'N	29°17.20'W	S. variblis	2-1-93	Plato Bank
JFA86.2	1,600	13,900						
JFA86.3	3,000	18,500						
JFA87.1	0	1,300	750-785	21°31'S	40°07'W	Caryophyllia sp.	5/10/1987	
JFA87.2	100	1,500						
JFA90.1	1,400		1000	24°54.4'S	44°26.0'W	S. variblis	1/25/1962	
JFA90.2	13,900							
JFA90.3	0	6,700						
JFA90.4	0	600						
JFA90.5	200	3,600						
JFA 95	3,600	17,800						
JFA 96	11,100	96,100						
JFA 97	4,600	26,600						

Table A3.3: U.S. dredge collection samples

Sample #	Age (years)	Age with no ²³² Th	Depth (meters)	Latitude	Longitude	Species I.D.	Comments
JFA 1	3,600	17,300	1684-1829	42 N	29 W	Solenosmilia ?	Lightly Mn Coated
JFA 2	21,600	21,600	1684-1829	42 N	29 W		Heavily Mn Coated
JFA 3	100	1,800	1684-1829	42 N	29 W	Enallopsammia	Heavily Mn Coated
JFA 4	3,100	25,600	1684-1829	42 N	29 W		Very reworked exterior
JFA 6	6,900	94,600	3500	36 N	58 W		Fairly fresh, Gorgonian?
JFA 7	11,800	425,500	3500	36 N	58 W		Flaky Mn crust
JFA 8	16,100	456,300	3500	36 N	58 W		Similar to JFA 7 but longer
JFA 9	4,800	64,900	3500	36 N	58 W		Larger version of JFA 6
JFA 11	52,500	52,500	2800	39 N	66 W		Bottom stem from two fans
JFA 12	46,100	46,100	3300	39 N	65 W		Slabed bottom stem
JFA 18	18,700	18,700	1684-1829	42 N	29 W	Solenosmilia	not Mn coated
JFA 20.1	51,600		1954	38 N	62 W	D. cristalgalli	Mn Coated
JFA 20.2	24,700						
JFA 20.4	21,100						
JFA 20.6	42,500						
JFA 20.7	52,600						
JFA 20.8	69,200						
JFA 20.10	22,700						
JFA 20.11	73,500						
JFA 20.13	49,500						
JFA 20.14	207,600						
JFA 21	67,000	67,000	1940-2100	33 N	62 W	D. cristalgalli	Mn Coated, Muir Seamount
JFA 24.1	24,800		1784	38 N	60 W	D. cristalgalli	Mn coated Manning Sea mount
JFA 24.2	69,900						
JFA 24.3	84,000						
JFA 24.4	77,500						
JFA 24.5	123,700						
JFA 24.6	51,900						
JFA 24.7	48,200						
JFA 24.8	27,500						
JFA 24.9	43,600						
JFA 24.10	37,800						
JFA 24.11	44,500						
JFA 24.12	60,900						
JFA 24.13	107,800						
JFA 24.14	59,600						
JFA 24.15	69,300						
JFA 24.16	42,000						
JFA 24.17	57,500						
JFA 24.18	45,900						
JFA 24.19	20,100						
JFA 24.20	49,700						
JFA 24.21	456,200						
JFA 24.22	260,000						
JFA 24.23	260,000						
JFA 24.24	260,000						
JFA 24.25	260,000						
JFA 24.26	456,200						
JFA 24.27	75,200						
JFA 24.28	87,000						
JFA 24.29	138,800						
JFA 24.30	113,400						
JFA 24.31	93,300						
JFA 24.34	82,100						
JFA 24.36	69,500						
JFA 24.37	59,200						

Table A3.3 (Con't)

JFA 24.39	112,800						
JFA 24.40	23,400						
JFA 24.41	24,700						
JFA 24.43	69,500						
JFA 24.45	19,600						
JFA 24.46	70,700						
JFA 24a	59,800						
JFA 24b	46,700						
JFA 24c	60,800						
JFA 25	32,800	32,800	1279-1298	37 N	59 W	D. cristagalli	Triple head
JFA 30.1	16,400		2150	16°26'N	60°51.5'W		
JFA 32.1	9,000	9,000	2000	16°55'N	61°10'W		
JFA 34.1	1,400		1070	60°2.6'N	29°37.5'W		Col. 9/4/67
JFA 35.1	1,000		990	61°39.5'N	28°0.5'W		Col. 9/10/67
JFA 35.2	1,200						
JFA 35.3	1,100						
JFA 35.5	400						
JFA 35.6	83,100						
JFA 35.7	0						
JFA 36.1	1,100		1125	60°2.5'N	29°40'W		Col. 9/6/67
JFA 36.2	3,100						
JFA 36.3	800						
JFA 36.4	2,900						
JFA 36.5	200						
JFA 36.6	97,800						
JFA 37.2	16,700		1175	59°55'N	29°20'W		Col. 9/8/67
JFA 37.4	1,200						
JFA 37.5	600						
JFA 37.6	8,500	8,500					
JFA 37.7	700						
JFA 37.8	11,900	11,900					
JFA 38.1	0		1435	60°11.5'N	30°3.5'W		Col. 9/7/67
JFA 38.2	2,100						
JFA 40.1	20,000		2200-2500	34°35'N	49°49'W		Col. 8/6/69
JFA 41.3	600	5,600					
JFA 41.5	600	6,300					
JFA 41.6	100	3,700					
JFA 41.7	700	4,700					
JFA 41.8	100	2,400					
JFA 41.9	100	3,800					
JFA 41.10	1,000	5,800					
JFA 41.11	600	4,900					
JFA 41.12	100	600					
JFA 41.13	600	6,900					
JFA 41.14	0	400					
JFA 41.15	200	3,100					
JFA 41.16	200	1,200					
JFA 41.17	4,400	21,400					
JFA 41.19	900	8,000					
JFA 41.20	1,100	12,200					
JFA 41.21	13,900	13900					
JFA 41.22	4,700	4,700					
JFA 41.23	7,100	7,100					
JFA 41.25	8,400	8,400					
JFA 41.26	5,300	5,300					
JFA 41.27	4,000	4,000					
JFA 41.28	6,100	6,100					

Table A3.3 (Con't)

JFA 42.1	19,600	19,600	1375-1400	38°41.4'N	27°33.2'W	Col. 10/9/70
JFA 42.2	600	600				
JFA 42.3	85,800	85,800				
JFA 42.4	54,500	54,500				
JFA 42.5	85,100	85,100				
JFA 42.6	62,600	62,600				
JFA 42.7	17,300	17,300				
JFA 42.8	71,100	71,100				
JFA 42.9	37,200	37,200				
JFA 42.10	1,400	1,400				
JFA 45.1	11,100		640-675	62°21.3'N	25°46.8'W	Col. 7/22/71
JFA 45.2	8,100					
JFA 45.4	4,000					
JFA 45.5	1,800					
JFA 46.1	4,000		2180-2230	8°36.9'S	13°16.1'W	Col. 2/23/81
JFA 46.2	1,000					
JFA 46.3	8,200					
JFA 46.4	2,400					
JFA 46.5	8,400					
JFA 46.6	2,200					
JFA 46.7	2,800					
JFA 46.8	2,400					

Chapter 4: Radiocarbon Methods and Calibration

I. Introduction

Radiocarbon measurements are one of the most powerful chemical tracers of ocean ventilation rate. After creation in the upper atmosphere by collisions between cosmic ray produced neutrons and nitrogen atoms, ^{14}C atoms mix into the lower atmosphere and surface ocean. The decay rate of ^{14}C (5730 year half life) is sufficiently close to the overturning rate of the whole ocean so that radiocarbon is not well mixed in the deep interior basins. This fact makes ^{14}C ideal for studies of large scale ocean circulation rate. GEOSECS measurements show that the oldest oceanic water in the deep North Pacific (2000-3000 meters) has a $\Delta^{14}\text{C}$ of about -250‰ [Ostlund and Stuiver, 1980]. Waters of the Atlantic are much younger and are dominated almost entirely by mixing of northern and southern component waters with very little signal due to *in situ* aging [Broecker et al., 1991]. Using independent tracers of mixing, the mean ventilation age of the deep Western Atlantic has been estimated to be about 100 years [Broecker et al., 1960; Broecker, 1979]. Anthropogenic processes have also made radiocarbon a useful tracer in the modern ocean. Nuclear bomb tests in the 1950s and 1960s produced many radionuclides at rates far above their natural levels. The penetration rate of this bomb produced carbon into the ocean interior can be used to calibrate ocean circulation models [Toggweiler et al., 1989] and constrain the uptake of anthropogenic CO_2 by the oceans [Broecker et al., 1985; Broecker et al., 1995].

For surface water studies, the increase in $\Delta^{14}\text{C}$ of oceanic DIC can be monitored by continuous measurements of seawater over a long time period [Linick, 1980] or by using massive reef building surface corals [Druffel and Linick, 1978; Druffel, 1981]. Long lived corals provide a record of the water $\Delta^{14}\text{C}$ before nuclear testing. Using long records from the Atlantic and the Pacific, estimates of the magnitude of the oceanic Suess effect, the dilution of existing ^{14}C levels by the burning of ^{14}C free fossil fuels, and

measurements of the natural surface ocean to atmosphere radiocarbon difference, or reservoir age, have been made [Druffel and Linick, 1978]. In addition, different areas of the surface ocean are labeled with different amounts of bomb radiocarbon. Therefore, corals from dynamic regions of the surface ocean can monitor circulation switches on seasonal time scales [Druffel, 1987; Druffel and Griffin, 1993; Moore et al., 1997]. These studies are beginning to prove useful for studying the Pacific Ocean's behavior during El Niño events.

Deep-sea corals provide the opportunity to measure $\Delta^{14}\text{C}$ at depth in the past oceans. Chapter II describes the theory of how to calculate past $\Delta^{14}\text{C}$ from deep-sea corals. The coupling of uranium series TIMS dating with radiocarbon data allows us to calculate the initial $\Delta^{14}\text{C}$ of the water in which the coral grew. Given enough deep-sea corals of the same age, the same types of studies of ocean circulation done with the GEOSECS data set could be made for different climatic regimes and the pre-bomb modern oceans. Here I present the laboratory methods and calibration studies we have used to obtain estimates of past ocean ventilation. Chemical and analytical methods are described first. Several checks on the method are also presented. Data from a modern calibration of several different genera of deep-sea coral are discussed in section III. These data also provide a maximum estimate of the amount of respired CO_2 that is fixed into a coral's skeleton. Finally, I present some deep-sea coral data from the Holocene that shows an unexpected circulation switch in the deep Equatorial Atlantic.

II. Methods

Cleaning methods for Accelerator Mass Spectrometry (AMS) analysis of deep-sea corals are designed to remove contaminating carbon sources that accumulated both while the specimen was on the sea floor and while the specimen was stored on land after collection. Black, organic carbon rich crusts that form on fossil corals after death on the sea floor were described previously. All samples used for paired uranium series and

radiocarbon dating had these crusts removed using the precleaning technique outlined in Chapter 3. An approximately 50 mg sub-sample of the precleaned CaCO_3 used for TIMS dating was removed for AMS analysis. As modern corals frequently had deposits of organic matter trapped between septa, the precleaning technique was also used on these samples. This process removes about 10% of the total coral weight. Immediately prior to dissolution, a second acid leach removes an additional 5-75% (see Appendix for % leached from individual samples). This step is designed to reduce adsorbed modern CO_2 that accumulates during sample storage. For the second acid leach, preweighed samples were dipped into 6N HCl for 15-60 seconds and then rinsed in two separate beakers of deionized H_2O . After drying for several minutes in a 60°C oven the samples are cooled and reweighed to determine the percent of sample leached. Samples are then crushed in an agate mortar and pestle to facilitate dissolution in the reaction flasks. All equipment for handling coral samples is cleaned with 10% HCl prior to use.

Dissolution occurs in specially designed finger flasks that contain a side arm for the phosphoric acid reservoir. Crushed samples are transferred to the acid cleaned flask with filter paper and care is taken not to spread fine CaCO_3 on the flask walls. Approximately two milliliters of 85% H_3PO_4 is added to the side arm with a cleaned Pasteur pipette. The flask is connected to a vacuum line using an 18/9 o-ring ball/socket joint and evacuated. Once the pressure has dropped, the sample reaction vessels are closed, removed from the line and tilted to allow the H_3PO_4 to spill out of the side arm and react with the coral sample. After reacting overnight, the samples are extracted on a vacuum line through two dry ice/isopropyl alcohol water traps. The purified sample is expanded into a known volume and measured with an MKS Baratron Type 122A Absolute Pressure Gauge. Two milliliters of CO_2 gas are isolated for AMS analysis and about 4.6% (usually about 0.1-0.3 mL at STP) of the residual is saved for $\delta^{13}\text{C}$ determination. All excess is frozen into a glass tube. The tube is flame sealed and stored. $^{13}\text{C}/^{12}\text{C}$ ratios were determined at the

Woods Hole Oceanographic Institute by Eben Franks on a VG Micromass 602 light isotope ratio mass spectrometer.

Graphitization of the 2 ml CO₂ sample for AMS analysis follows the method of Vogel et al. [Vogel et al., 1987]. This procedure reduces CO₂ to C⁰ in the presence of a Co catalyst at 650°C. Graphite samples are pressed into targets and measured for their ¹⁴C/¹³C ratio at the Lawrence Livermore National Lab Center for Accelerator Mass Spectrometry (CAMS). The corrected fraction modern (F) is reported as described by Donahue et al [Donahue et al., 1990]. The "old" oxalic acid standard is normalized to 1950 and a δ¹³C value of -19‰ and the sample is normalized to a δ¹³C of -25‰. With these adjustments the radiocarbon age is given by [Stuiver and Polach, 1977]

$$\text{Radiocarbon Age} = -\tau \ln F$$

where τ is the Libby mean life of 8033 years. The measured fraction modern, F_m, is converted to the true fraction modern (F) by accounting for the blank introduced during graphite formation:

$$F = F_m(1 + f) - f$$

where f is the fraction modern of a ¹⁴C-free calcite sample that is processed exactly the same way as the coral samples. Our data for these dead calcite blanks is listed in Table 4.1. The long term average value of this blank over the three year period that our samples span is 0.0032±0.0015. This statistic is comparable to the data generated at the Arizona AMS facility on dead NBS graphite [Donahue et al., 1990]. Based on a 2 ml CO₂ sample that has a fraction modern that is two times the standard deviation of this blank, the maximum age we can resolve is >46,000 radiocarbon years. We have also measured several samples twice by forming two graphite targets from the same CO₂ reservoir. As can be seen from Table 4.2, the data always agree within 1σ uncertainty.

There is some question as to how much modern adsorbed CO₂ could be contaminating our samples. Surface corals have been found to have significant modern CO₂ contamination that has bomb radiocarbon Δ¹⁴C values [Burr et al., 1992]. This study

Date	UCID	CAMS	Wt.	CO ₂ Gas (ml)		F _m	error
	#	#	(mg)	Total	AMS		(1 σ)
March 1995	663	19384	52	10.36	1.35	0.0028	0.0002
	664	19385	42	9.76	1.30	0.0027	0.0003
August 1995	1006	22458	82	18.12	1.30	0.0066	0.0006
	1012	22459	61	10.77	1.37	0.0066	0.0004
August 1996	1535A	30195	47	11.35	1.98	0.0025	0.0002
	1535B	30196	47	11.35	2.06	0.0024	0.0002
March 1997	2059	36256	274	61.33	1.93	0.0025	0.0002
	2056	36259	65	13.63	1.93	0.0015	0.0002
May 1997	2205			2.45	1.99	Sample Lost	
	2206	39264		2.08	1.93	0.0040	0.0003
	2207	39265		3.56	1.96	0.0026	0.0001
	2208	39266	65.5	6.94	1.95	0.0024	0.0001
	2209	39267		2.41	1.97	0.0024	0.0003
	2210	39268		1.61	1.53	0.0040	0.0001
	2211	39269		5.59	1.96	0.0031	0.0002
	2212	39270	82.5	9.41	1.95	0.0024	0.0002

Average	0.0032
Std Deviation	0.0015

Table 4.1: Calcite blank data. The variance of the measured fraction modern over this two year time period corresponds to a maximum radiocarbon age of >46,000 years.

Sample	Species	UCID	CAMS #	Fraction Mod.	Error (1 σ)	Difference	Age (^{14}C yrs)	Error (1 σ)	Difference
JFA 2	D. cristagalli ?	658A	19376	0.2213	0.0015	0.0018	12,120	60	60
		658B	19377	0.2195	0.0014		12,180	50	
JFA 20.10 Top	D. cristagalli	1529A	30183	0.1717	0.0010	0.0013	14,160	50	70
		1529B	30184	0.1730	0.0011		14,090	60	
JFA 20.10 Bot.	D. cristagalli	1530A	30185	0.1756	0.0012	0.0005	13,970	60	30
		1530B	30186	0.1751	0.0013		14,000	60	
JFA 24.19 Top	D. cristagalli	1531A	30187	0.1658	0.0012	0.0026	14,440	60	120
		1531B	30188	0.1631	0.0014		14,560	70	
JFA 24.19 Bot.	D. cristagalli	1532A	30189	0.1738	0.0012	0.0003	14,060	60	10
		1532B	30190	0.1735	0.0012		14,070	60	
JFA 24.8 Top	D. cristagalli	1533A	30191	0.1652	0.0012	0.0021	14,460	60	110
		1533B	30192	0.1631	0.0012		14,570	60	
JFA 24.8 Bot.	D. cristagalli	1534A	30193	0.1795	0.0015	0.0022	13,800	70	100
		1534B	30194	0.1773	0.0010		13,900	50	
JFA 62.1 Bot.	D. cristagalli	2053A	36254	0.0248	0.0008	0.0008	29,690	280	270
		2053B	36255	0.0240	0.0008		29,960	290	

Table 4.2: Duplicate AMS runs of the same CO₂ sample. All data agrees within a one sigma uncertainty.

has shown that it is necessary to leach away up to 50% of surface coral samples before an uncontaminated signal is obtained. However, the morphology of these samples is very porous and there is a large surface area to volume ratio. As the deep-sea samples have fewer exposed surfaces, they are not as susceptible to adsorbed modern CO₂ contamination. To test the deep-sea corals' sensitivity to adsorbed CO₂, we measured the fraction modern in successive leaches of JFA 20c, a *Desmophyllum cristagalli* that has been TIMS dated to be 65,250±250 years old (F=0.0003). However, the initial $\delta^{234}\text{U}$ of this sample is several permil higher than modern seawater indicating that it may be slightly diagenetically altered. At the time, it was the only sample that we were reasonably sure was radiocarbon dead. We believe adsorbed CO₂ is a bigger contamination problem than endolithic activity in our samples because we take care to sample around any burrow structures or obvious reworking.

Three separate leaching experiments were performed. Two pieces of JFA 20c were not precleaned or leached in any way. A third piece of the sample was precleaned according to the normal procedure but not leached in HCl prior to reaction in the sample apparatus. All three samples were reacted in excess 85% H₃PO₄ and aliquots of CO₂ were drawn off so that smaller fractions were captured first and larger ones towards the end. Results are listed in the Appendix and displayed in Figure 4.1. Only about 45% of the precleaned piece reacted after several days in the presence of excess 85% H₃PO₄. A milky white solution was left in the flask along with a single large chunk of sample. Uncleaned pieces of JFA 20c were reacted in twice the acid volume of the cleaned piece and reacted fully by the end of the experiment (six days total). From Figure 4.1 it is clear that the precleaning technique removes contaminating carbon phases. Both of the uncleaned samples have higher fraction modern values than the cleaned piece. There is also evidence that adsorbed modern CO₂ affects the first fraction (4-5%) leached from the samples. For the precleaned piece, the next three leaches all have the same fraction modern value within 1 σ error. The final leaches for all samples are higher than the

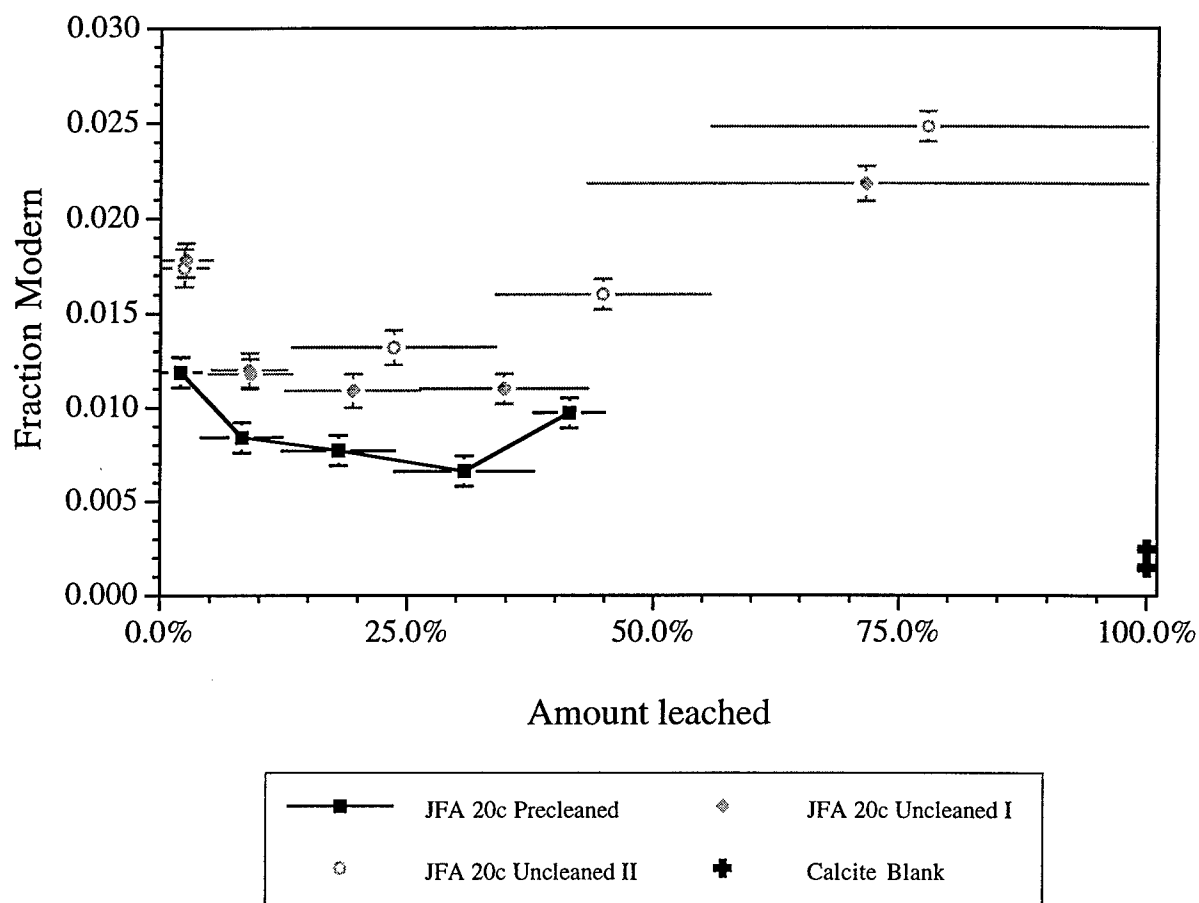


Figure 4.1 Leaching experiment with cleaned and uncleaned corals. Precleaning clearly removes radiocarbon contamination. High values of the last fraction from each sample are probably due to leakage through the o-ring seal of atmospheric CO_2 . The precleaned sample was not acid leached before dissolution and may show a small effect of adsorbed modern CO_2 .

previous ones. Because these samples sat for several days in the reaction vessel in order to complete the acidification, we believe these elevated values are due to leakage of atmospheric CO₂ through the flask's o-ring seal. These results show we can remove the bulk of the contamination with precleaning and leaching of a small amount of coral immediately prior to dissolution.

The lowest fraction modern value in the precleaned coral is 0.0066 ± 0.0008 . This is slightly above the calcite blank's value for this graphite formation run (Figure 4.1). It is, however, within the range of the long term average of calcite blanks (Table 4.1) and is the same value measured on this sample in March 1995 (Sample JFA 20c, Table A4.1). This slightly elevated value may mean that this deep-sea coral is compromised at the 0.003-0.004 fraction modern level. While this is a very small correction for any of the samples discussed in this thesis, we were concerned enough to investigate further. When we plot the same F data versus the sample volume, rather than percent reacted, there is evidence for a blank (Figure 4.2). The decreasing fraction modern trend with increasing sample size trend in Figure 4.2 is indicative of a constant amount of blank being diluted by larger and larger samples. This is only true for the precleaned sample, but the clear contamination on the uncleaned samples makes them suspect for blank studies. We checked the leaching procedure for blank problems by carrying out the same successive leaches experiment as above on acid leached calcite blanks that were both crushed and uncrushed. The data in Figure 4.3 and the Appendix show that all of these samples fall in the range of observed calcite blanks for totally dissolved samples run over several years. Since the very first fraction of the crushed sample has one of the lowest fraction modern values, the acid leaching step prior to dissolution seems to have removed any adsorbed modern CO₂ on calcite. At sample sizes below 2 mL there might be a blank influence, but this is smaller than the volumes in Figure 4.2. We conclude that the trend in the precleaned data of Figure 4.2 is not due to a blank effect and that the original explanation is correct.

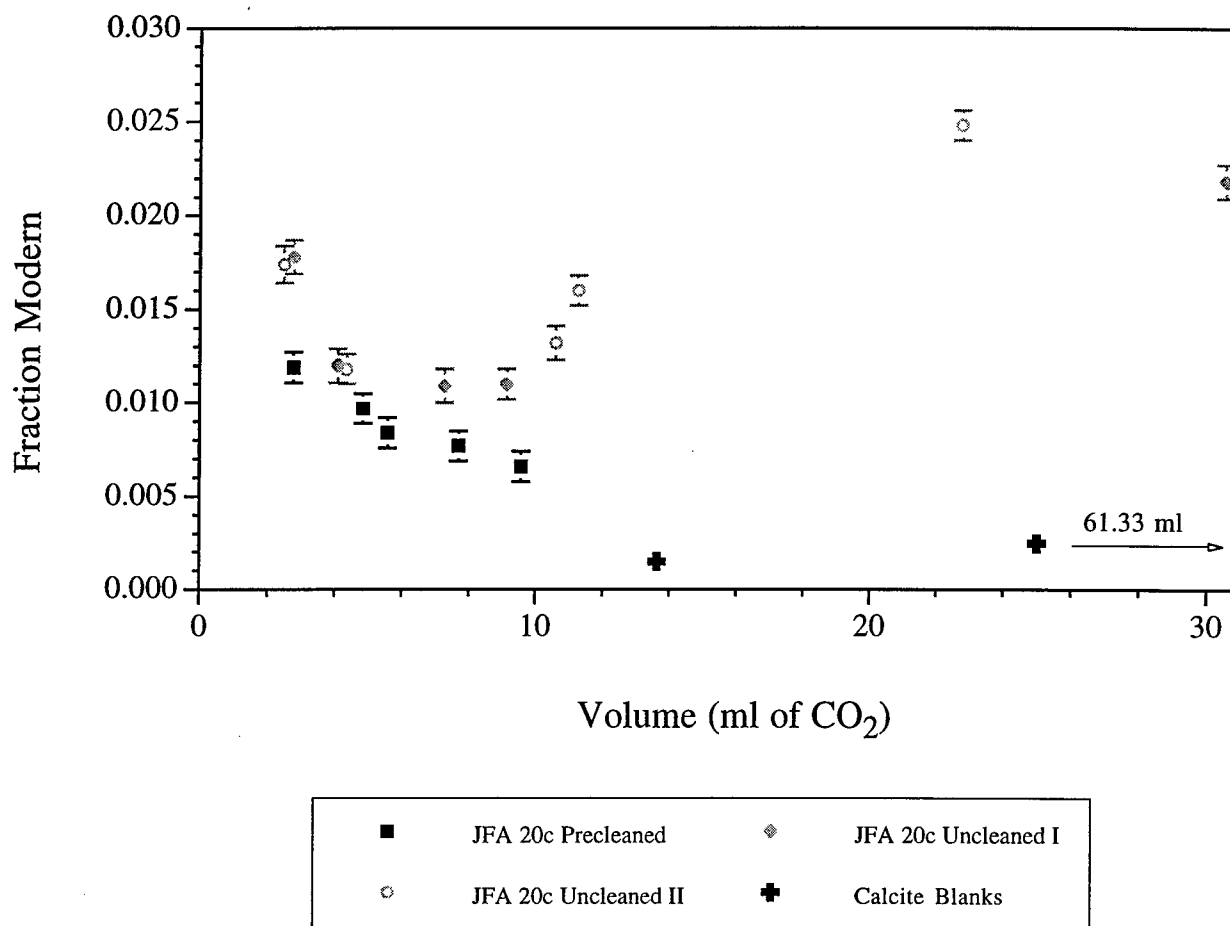


Figure 4.2. Leaching experiment data with cleaned and uncleaned corals. This is the same data as in Figure 4.1 but plotted against the volume of sample. For the precleaned sample, there is a trend consistent with a blank problem. However, the data in Figure 4.3 from dead calcite samples shows that there is no trend of F with sample size above 2 mL. The trend here is a coincidence of the first sample being modern CO₂ contaminated and the second sample being affected by sample apparatus leakage over several days.

All Calcite Blank Data

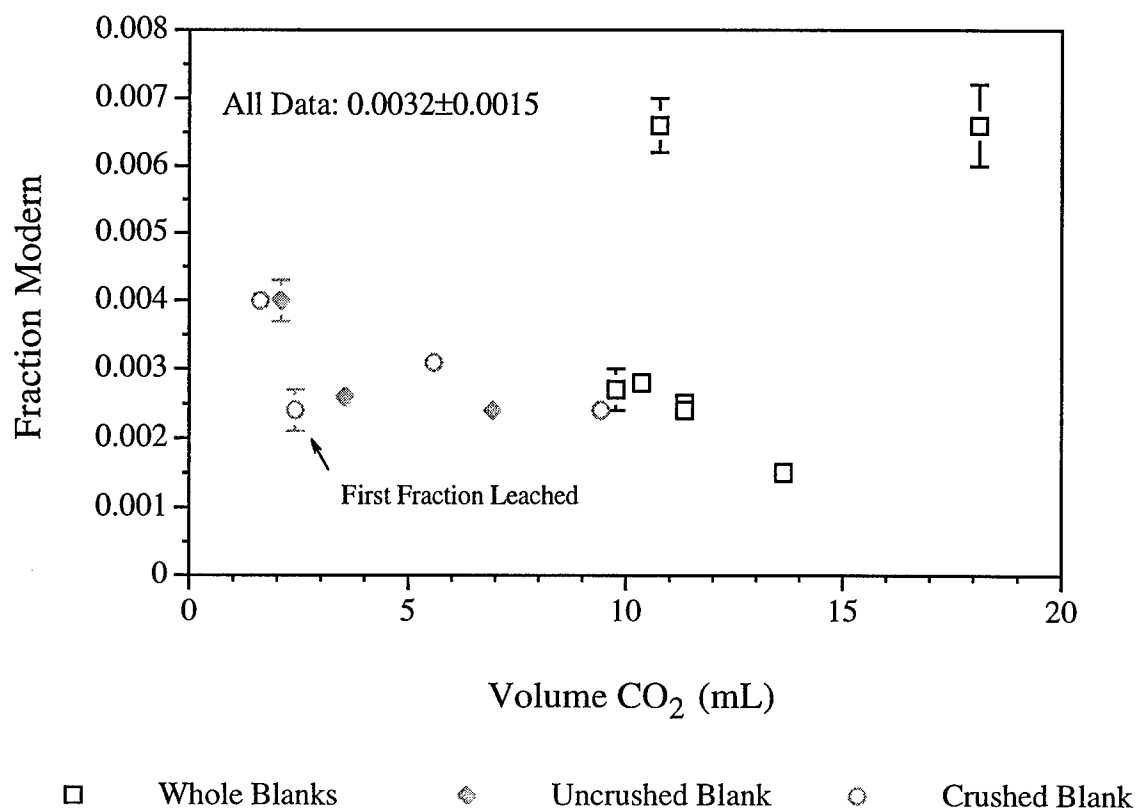


Figure 4.3. All Calcites run in thesis versus volume of sample. Whole blanks that were 100% dissolved are black squares. Gray data are from the calcite leaching experiment.

As a final check of the coral processing procedure, we tried to measure the difference in radiocarbon age between the top and bottom of a single Holocene coral. This type of sampling is crucial to the deglacial circulation switch we document in Chapter 6. In that chapter, top and bottom ^{14}C ages from a deglacial *D. cristagalli* show an age "inversion". Here we test that a coral from a quiescent time in deep ocean circulation has only a "normal" ^{14}C pattern due to growth from bottom to top. Sample JFA 62.1 is a 25 mm long *D. cristagalli* from 1420 meters deep on the Pluto Seamount in the North Atlantic that was ICP-MS age screened to be about 4,000 years old. Fraction modern data from four successive leaches of precleaned samples from the top and the bottom of JFA 62.1 are shown in Figure 4.4. All fractions from the same sample have the same fraction modern values within 1σ error. For both samples, the initial leaches are higher than the second fractions. However after the second fraction, the bottom sample shows a slight decrease in age with amount leached while the top sample shows the opposite. We interpret these data as indicative of a slight amount of modern CO_2 adsorption in the first 10% of CO_2 released. Our leaching procedure for ventilation age samples removes at least this much immediately prior to dissolution. The weighted mean age difference between the top and bottom is 55 ± 50 radiocarbon years. Given the 25 mm height of this sample, we calculate an approximate growth rate of about 0.5 mm/yr. This value is in good agreement with the TIMS uranium series data for *D. cristagalli* from Chapter 3 (0.1-1 mm/yr).

The sample preparation methods and leaching experiments described here indicate that it is extremely important to remove the black crusts of fossil corals prior to AMS ^{14}C dating. Untreated samples have higher F values than precleaned samples from the same coral. *Desmophyllum cristagalli* does not seem to be as adversely affected by modern CO_2 adsorption during storage as surface corals. While there is some contamination, only about 10-15% of a sample needs to be acid leached before it is again pristine. The problem is greatest for older samples (>25,000 years) that are less than about 8 ml total

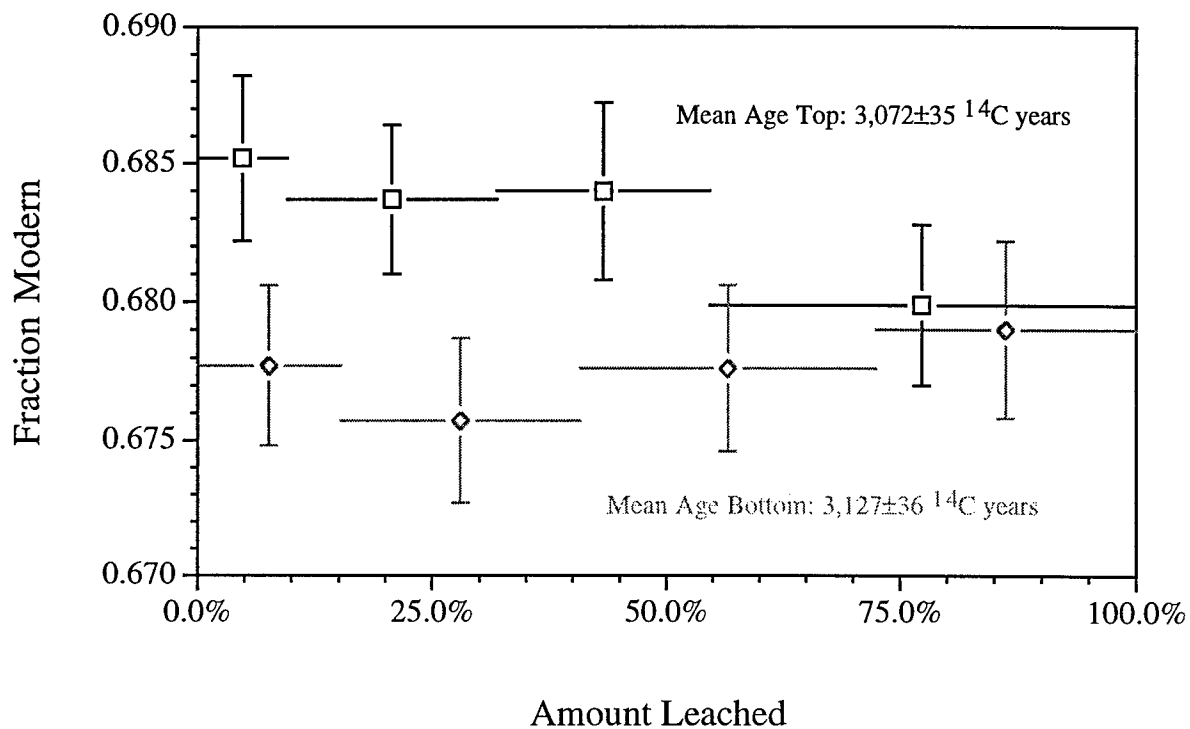


Figure 4.4. Leaching experiment on a Holocene *D. cristagalli*. The top and bottom of sample number JFA 62.1 from 1420 meters depth on the Pluto Seamount were leached separately. Within error, there is no effect from modern adsorbed CO_2 . A weighted average of the samples shows that the top is 55 ± 50 years younger than the bottom as expected from the growth pattern of *D. cristagalli*.

CO₂. Sample number JFA 20c should be ¹⁴C dead according to the TIMS age from Chapter III. However, on two separate occasions we have measured a fraction modern slightly above the calcite background. This sample may have been diagenetically altered, as its $\delta^{234}\text{U}$ value is slightly higher than modern seawater. At this point we have no definitive reason for this age discrepancy.

III. Modern Ocean Calibration and Holocene Data

Even with the best, most artifact free AMS technique, we still need to know if the deep-sea corals themselves can record the $\Delta^{14}\text{C}$ of the water in which they grew. We selected 12 samples from our collection that had either intact organic matter or fresh looking septa for a modern ocean calibration. The $\Delta^{14}\text{C}$ of each of these samples was measured using the above techniques and compared to seawater values from nearby GEOSECS stations [Ostlund and Stuiver, 1980; Stuiver and Ostlund, 1980; Stuiver and Ostlund, 1983] (Figure 4.5 and Table 4.3). All data falls either on or below a 1:1 line. The several samples that do not agree with the 1:1 water estimates are older than the water DIC. On the belief that some samples may not have been alive when picked from the sea floor, we TIMS uranium series dated several specimens to correct for radiocarbon decay since death. The data in Figure 4.6 and Table 4.3 show that all samples that were TIMS dated fall back on the 1:1 line. Six different genera of scleractinian deep-sea coral all show very good agreement between water $\Delta^{14}\text{C}$ and coral $\Delta^{14}\text{C}$. Deep-sea corals are an excellent archive of water radiocarbon values.

The observation that deep-sea corals never have a ¹⁴C age younger than the water in which they grow is an important constraint on the amount of respired CO₂ that they incorporate into their skeletons. These organisms are essentially filter feeders, eating the available detritus that washes over them. Several of the specimens in Figure 4.6 grew when this food source was contaminated by bomb radiocarbon. The elevated level of

Modern Coral $\Delta^{14}\text{C}$ Calibration

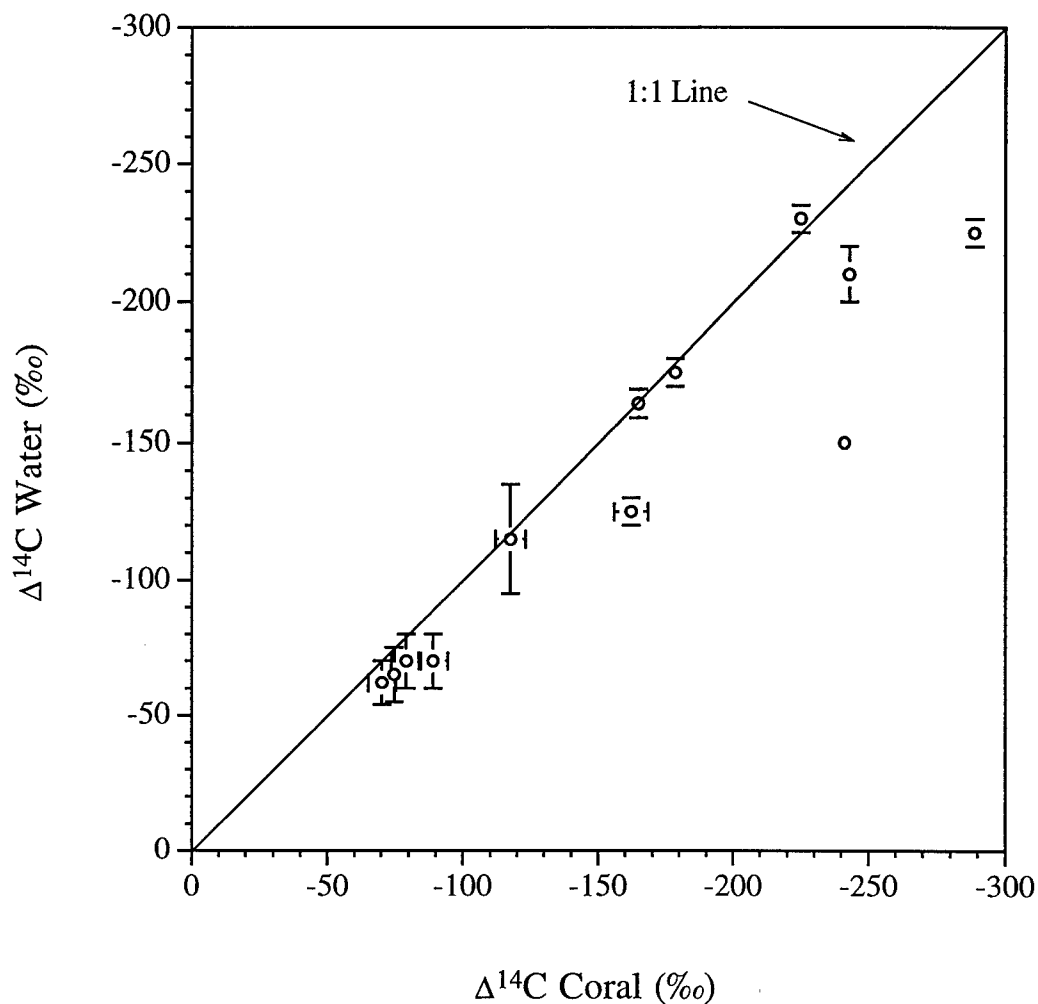


Figure 4.5. Modern calibration of $\Delta^{14}\text{C}$ in deep-sea corals. Water estimates were taken from nearby GEOSECS stations and generally have larger errors than the coral measurements. Eight different species are represented in this data. All coral points fall on or below the 1:1 correspondence line indicating corals are the same age as or older than the water in which they grew.

Modern Samples													
ID	UCID	CAMS #	Depth (meters)	Lat	Long	Species	Cal Age (years)	14C Age err	$\Delta^{14}C$ (‰)	err	Water $\Delta^{14}C$	err	Atm. Vent Age (years)
BI-103-3	1013	22454	1355	18°N	157°W	E. rostrata	686	8	-225	5	-230	12	2064
91545.2	1003	22446	1510-1600	21°18'S	36°18'E	St. nobilis	407	22	-134	6	-125	10	1023
86873.1	1018	22460	1112	25°53'S	5°44'E	St. campaniformis	336	71	-125	10	-120	8	944
JFA 47.1	1021	22463	1790-1803	48°10'S	148°16'E		848	14	-156	6	-150	20	1292
47373	1022	22464	2010-2100	49°51'S	178°35'E	F. impensum			-162	5	-164	8	
48518	1023	22465	1420-1470	48°41'N	10°54'W	S. variabilis			-77	6	-70	10	
48740.1	1020	22462	1420-1470	48°41'N	10°54'W	D. cristagalli	100	40	-75	7	-70	10	
83522	1004	22447	1760	21°31'S	81°31'W	Caryophyllia sp.			-241	4	-210	10	
93177.3	999	22442	4100	34°43'N	123°4'W	F. marenzelleri			-222	4	-230	10	
47413	654	19372	421	50°38'S	167°38'E	D. cristagalli	50	20	-65	5	-62	8	
85080	655	19373	990-1150	43°47'S	150°29'E	D. cristagalli	30	10	-114	6	-115	20	
78459	656	19374	2110-2180	38°45'N	72°39'W	D. cristagalli	60	50	-69	7	-65	10	
Holocene Samples													
ID	UCID	CAMS #	Depth (meters)	Lat	Long	Species	Cal Age (years)	14C Age err	$\Delta^{14}C$ (‰)	err	Water $\Delta^{14}C$	err	Atm. Vent Age (years)
JFA 45.4	1011	22453	640-675	62°21'N	25°47'W		2598	30	-45	8	-50	10	402
JFA 48.2	1017	22457	2475-2820	0°55'N	28°29'W	F. apertum	5810	55	21	9	-105	10	440
JFA 46.3	1009	22451	2180-2230	8°36.9'S	13°16.1'W		6347	52	-7	9	-110	10	753
86562.2	1016	22456	1517-1611	11°33'S	145°19.3'E	St. weberianus	7486	64	-96	10	-170	20	1494
JFA 46.5	1019	22461	2180-2230	8°36.9'S	13°16.1'W		7384	56	-39	11	-110	10	841

Table 4.3: Deep-Sea coral ^{14}C and ventilation age data. Coral $\Delta^{14}C$ values are calculated from calendar ages and radiocarbon data. Water $\Delta^{14}C$ values are estimated from the nearest GEOSECS station. Atmospheric ventilation ages are calculated as described in Chapter 2.

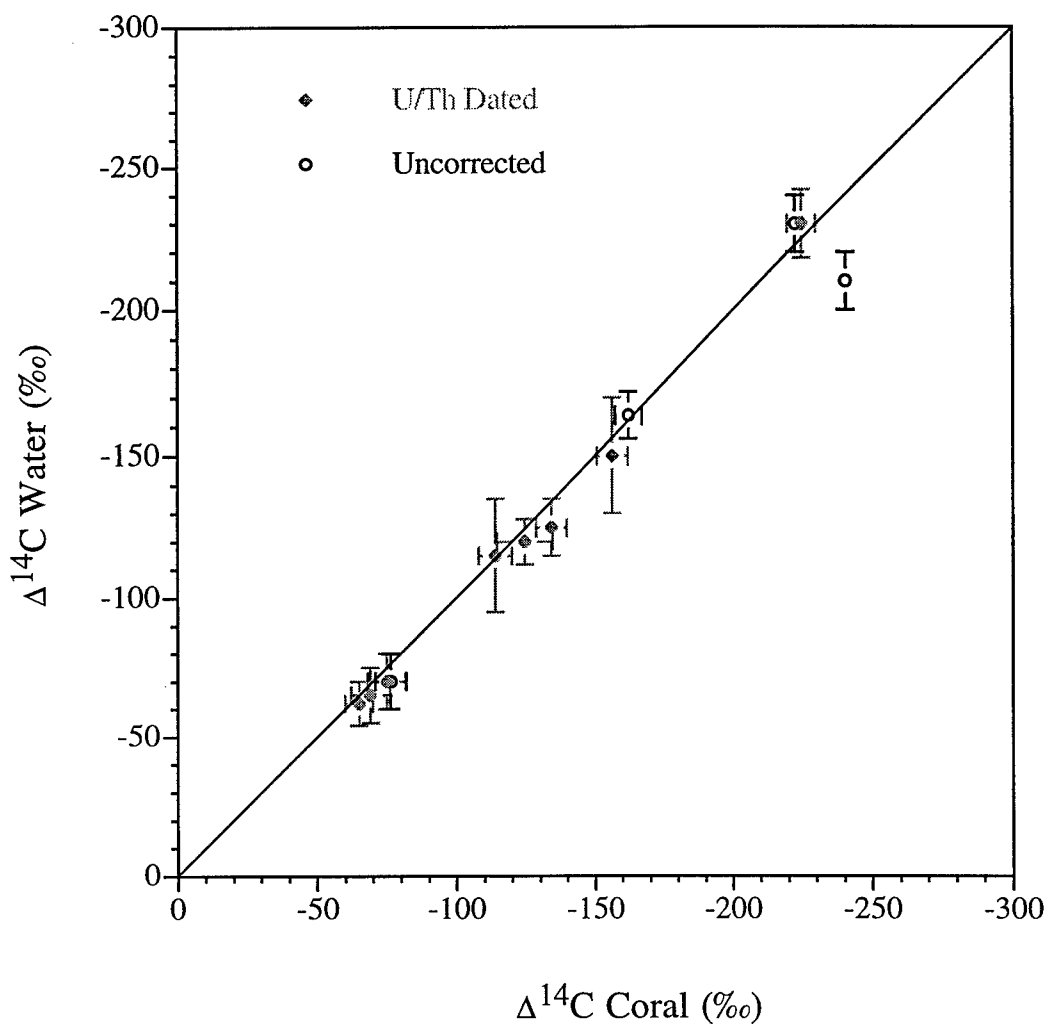


Figure 4.6. Uranium series age corrected modern calibration of $\Delta^{14}\text{C}$ in deep-sea corals. These are the same samples as in Figure 4.5 except that points in gray have been corrected for decay since death of the coral. In one case this is an 850 year correction. Here all corrected data fall on the 1:1 within the uncertainties.

$\Delta^{14}\text{C}$ in this organic matter relative to the surrounding DIC provides a test of how much organically derived CO_2 is fixed into the skeletal aragonite. We can write the equation:

$$(\text{Fraction Respired } \text{CO}_2)(\Delta^{14}\text{C of Food}) + (1 - \text{Fraction Respired } \text{CO}_2)(\Delta^{14}\text{C of DIC}) = \text{Coral } \Delta^{14}\text{C}$$

While all of our data falls on a 1:1 line between DIC $\Delta^{14}\text{C}$ and coral $\Delta^{14}\text{C}$, there is uncertainty within the AMS error bars to calculate the maximum amount of bomb CO_2 that could be in our data and still fall on the line. Sample number 93177.3 is a *Fungiacyathus marenzelleri* that was picked alive from 4100 meters in the sub-tropical north-east Pacific (very close to Station M, 34°50'N, 123°00'W) on October 20, 1992. Within error this sample ($\Delta^{14}\text{C} = -222\text{‰}$) agrees with the bottom water DIC $\Delta^{14}\text{C}$ value (4050 m, sample taken 50 meters above bottom). However, the absolute value is about 8‰ too young. By adopting a water to coral difference of 10‰ and using a water $\Delta^{14}\text{C}$ value of -230‰, we can rewrite the above equation:

$$\Delta^{14}\text{C of Food} = 10 / (\text{Fraction Respired } \text{CO}_2 - 230)$$

This function is plotted in Figure 4.7 for a range of respired CO_2 from 0-25%. Using data on the $\Delta^{14}\text{C}$ of suspended and sinking particulate organic carbon (POC) from almost exactly the coral's location [Druffel et al., 1996], we can constrain the maximum respired CO_2 our data allows there to be in the skeleton. The oldest food source, suspended POC, gives a maximum value of about 8% which is in good agreement with estimates for surface corals based on stable isotope studies [McConnaughey et al., 1997]. Within the errors of our AMS measurements and the estimates of bottom water $\Delta^{14}\text{C}$ of DIC, the skeletons of deep-sea corals are drawn entirely from ambient inorganic carbon. There is room in the data for a maximum of 8% of the skeleton to be of a respired origin. This result has important implications for the mechanism of coral calcification which will be discussed further in Chapter 5.

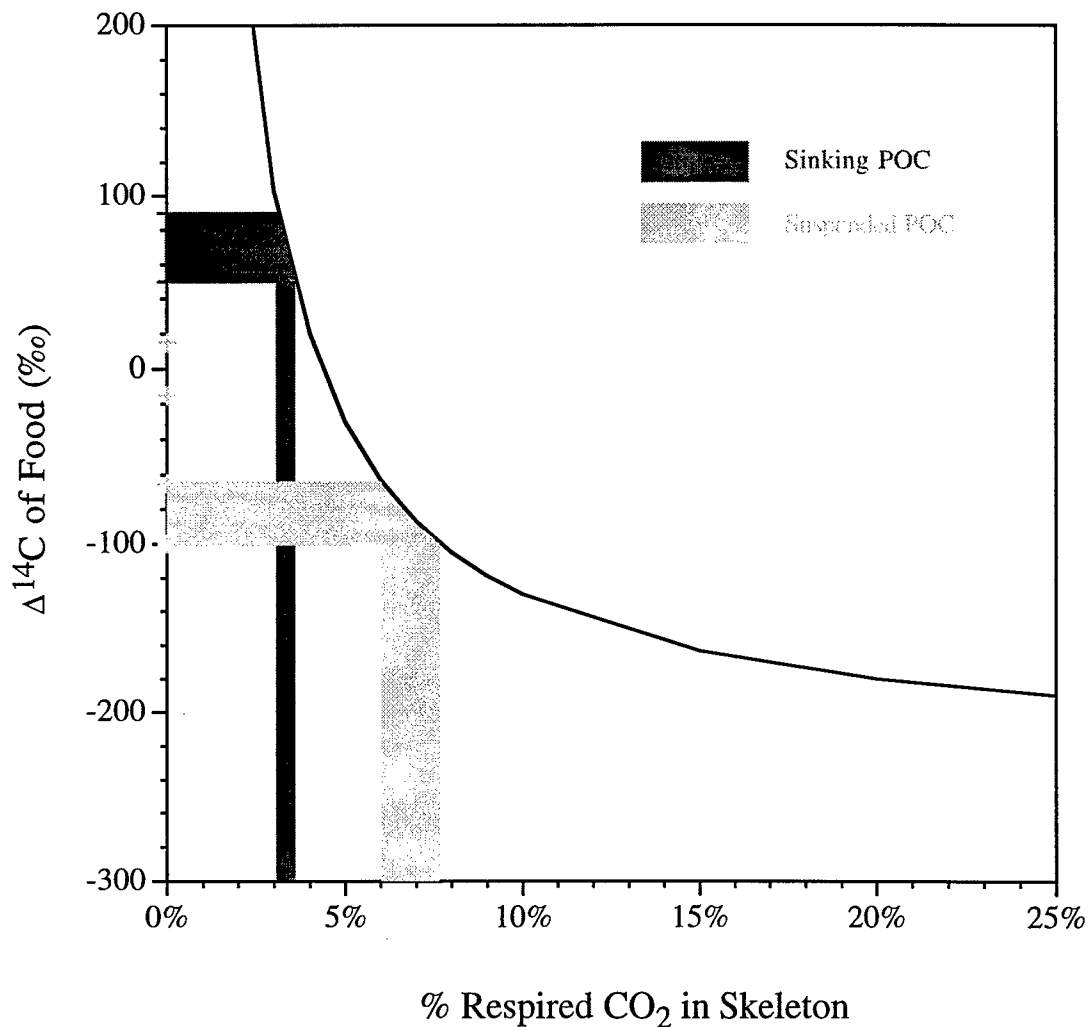


Figure 4.7. Calculation of the amount of respired CO_2 that can be in the skeleton of sample number 93177.3. This coral is a *F. marenzelleri* from 4100 meters depth in the North East Pacific Ocean. Using a water $\Delta^{14}\text{C}$ value of -230‰ and a maximum $\Delta^{14}\text{C}$ elevation of 10‰ in the coral sample (see Table 4.3), we calculate the black line. Estimates of the $\Delta^{14}\text{C}$ of the food source (Druffel et al., 1996) constrain the respired CO_2 to make up less than 8% of the aragonitic skeleton.

Five of the samples we selected for paired TIMS uranium series and AMS radiocarbon dating are of Holocene age. We converted the calculated $\Delta^{14}\text{C}$ values for these samples to ventilation ages using the ^{14}C projection method outlined in Chapter 2 [Adkins and Boyle, 1997]. The ventilation ages were then converted back into $\Delta^{14}\text{C}$ values to obtain the radiocarbon value of the water in which the coral grew relative to the past atmosphere. This procedure allows us to plot the Holocene data, with their calendar ages in black, on the same figure as the modern calibration data (Figure 4.8). Two of the corals fall directly on the 1:1 line. 7,500 years ago in the Coral Sea south of New Guinea at about 1,550 meters, the $\Delta^{14}\text{C}$ was the same as it is there today. About 2,600 years ago the high latitude North Atlantic near the Reykjanes Ridge (650 meters deep) was 400 radiocarbon years old (Figure 4.9). This -50‰ value is the same as the pre-bomb modern difference between the atmosphere and the surface ocean in the North Atlantic [Druffel and Linick, 1978; Bard, 1988]. This reservoir age is an important value for the dating of deep-sea cores by AMS dates on planktonic foraminifera and may change with different climate regimes [Bard et al., 1994; Austin et al., 1995; Gronvold et al., 1995; Birks et al., 1996]. We have many other samples from this area and depth range which span the Holocene and deglaciation. These samples can provide important constraints on the North Atlantic reservoir age through time.

Three of the Holocene samples in Figure 4.8 do not fall on the modern correlation line between coral and seawater $\Delta^{14}\text{C}$. Though they span about 1600 years of time, the three samples all were found in the south equatorial Atlantic (from 2,200 and 2,600 meters depth) on the Mid-Ocean Ridge (Figure 4.9). All of these specimens show younger waters in the past than are found there today. These equatorial waters decreased in ventilation age from near the modern value of about 850 radiocarbon years to about 450 radiocarbon years over a span of 1600 calendar years. By about 5,800 years ago the waters at 2600 meters depth had the same radiocarbon age as the modern reservoir age. This extremely rapid ventilation of the deep equatorial Atlantic can be better

Holocene Ventilation Data

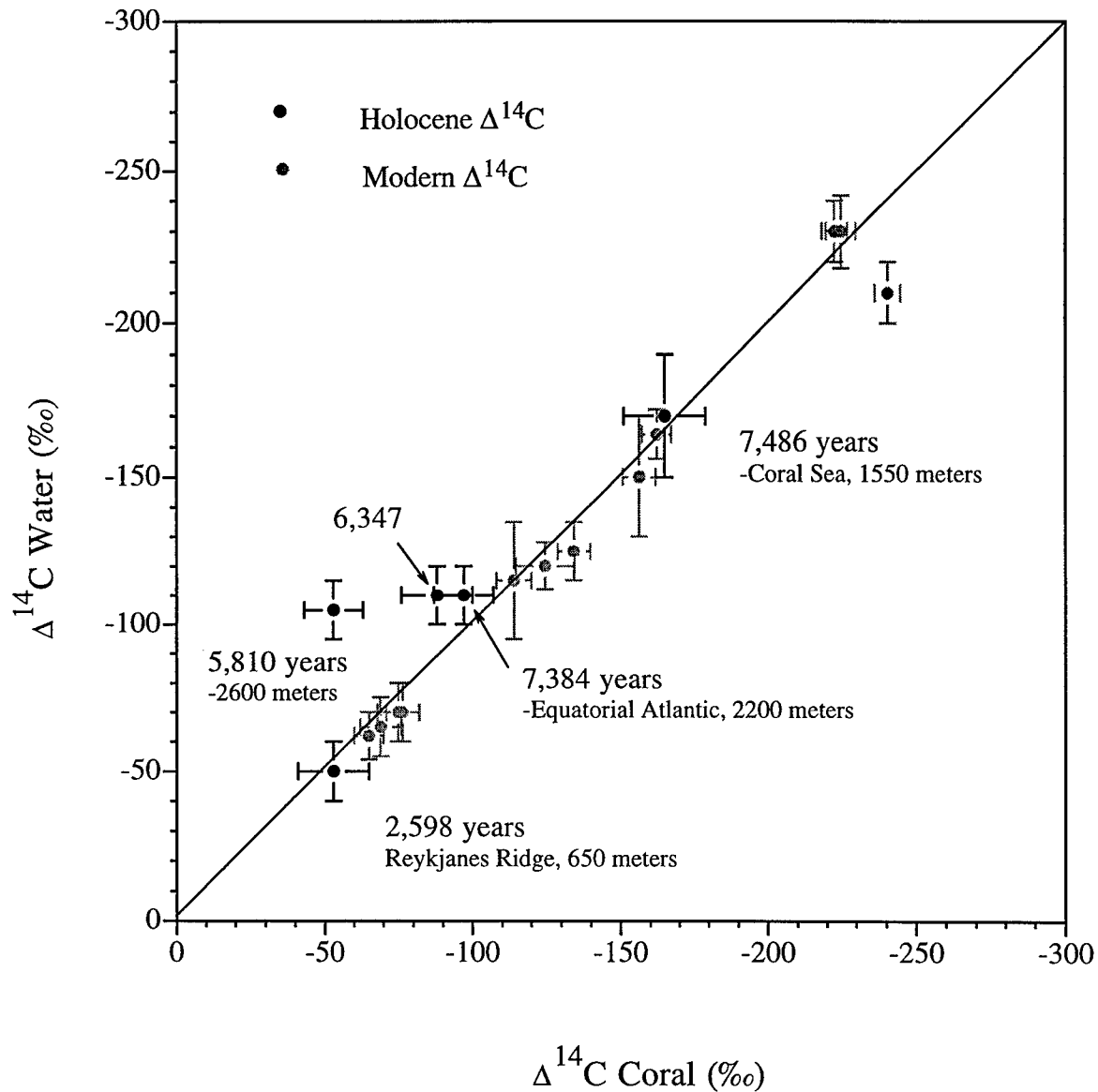


Figure 4.8. Holocene ventilation ages from deep-sea corals. Five Holocene corals are shown in black. Gray circles are the corrected data from Figure 4.7. The Equatorial Atlantic corals show a pronounced minimum in ventilation age at 2600 meters depth and 5,810 years ago. This point has a $\Delta^{14}\text{C}$ value close to the modern reservoir age.

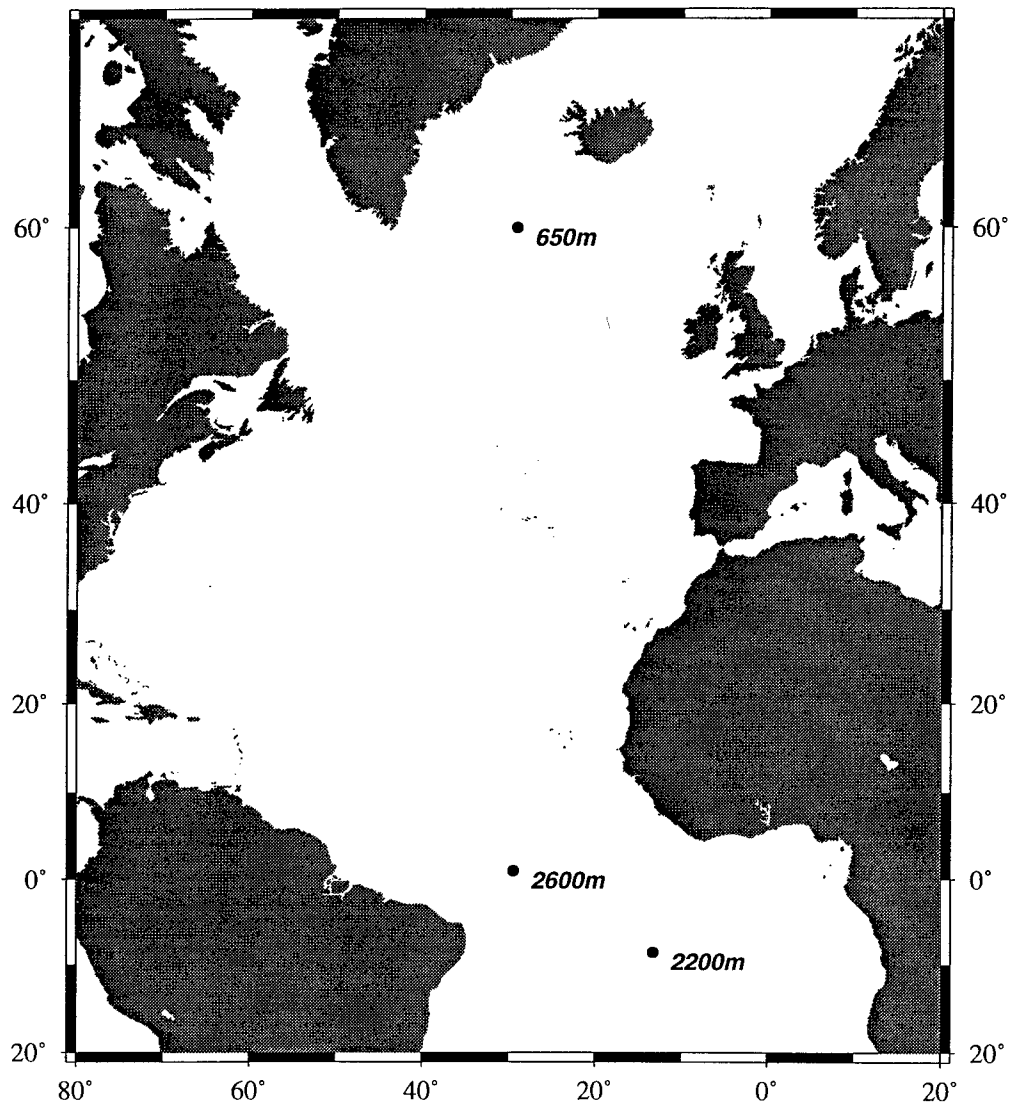


Figure 4.9. Locations of Atlantic Holocene corals measured as part of this thesis.

characterized with more coral from this area as well as high resolution sediment records of the Holocene.

Based on the studies described in this chapter, we believe deep-sea corals are an excellent archive of past ocean $\Delta^{14}\text{C}$. To obtain a pristine signal, it is extremely important to remove the black crusts from fossil samples. In addition, an acid leach that removes over 10% of the sample immediately prior to total dissolution is necessary to eliminate modern adsorbed CO_2 from the coral. With these methods, there is a 1:1 correspondence between the $\Delta^{14}\text{C}$ of the coral skeleton and the $\Delta^{14}\text{C}$ of the ambient DIC. While our data suggests that all of the skeletal CaCO_3 is from inorganic sources, at most 8% of the skeleton can be from respired CO_2 . Finally, we have documented a ventilation age change in the Holocene Equatorial Atlantic that has not been previously observed. Given the magnitude of the circulation change, other high resolution Holocene data sets should see an event at around the same time.

References

- Adkins, J. F. and E. A. Boyle, Changing atmospheric $\Delta^{14}\text{C}$ and the record of deep water paleoventilation ages, *Paleoceanography*, 12, 337-344, 1997.
- Austin, W. E. N., E. Bard, J. B. Hunt, D. Kroon and J. D. Peacock, The ^{14}C age of the Icelandic Vedde Ash: implications for Younger Dryas marine reservoir age corrections, *Radiocarbon*, 37, 53-62, 1995.
- Bard, E., Correction of accelerator mass spectrometry ^{14}C ages measured in planktonic foraminifera: paleoceanographic implications, *Paleoceanography*, 3, 635-645, 1988.
- Bard, E., M. Arnold, J. Mangerud, M. Paterne, L. Labeyrie, J. Duprat, M.-A. Melieres, et al., The North Atlantic atmosphere-sea surface ^{14}C gradient during the Younger Dryas climatic event, *Earth and Planetary Science Letters*, 126, 275-287, 1994.
- Birks, H., H., S. Gulliksen, H. Hafliðason, J. Mangerud and G. Possnert, New radiocarbon dates for the Vedde Ash and the Saksunarvatn Ash from Western Norway, *Quaternary Research*, 45, 119-127, 1996.
- Broecker, W. S., A revised estimate for the radiocarbon age of North Atlantic Deep Water, *Journal of Geophysical Research*, 84, 3218-3226, 1979.
- Broecker, W. S., S. Blanton, M. Smethie Jr. and G. Ostlund, Radiocarbon decay and oxygen utilization in the deep Atlantic Ocean, *Global Biogeochemical Cycles*, 5, 87-117, 1991.
- Broecker, W. S., R. Gerard, M. Ewing and B. C. Heezen, Natural radiocarbon in the Atlantic Ocean, *Journal of Geophysical Research*, 65, 2903-2931, 1960.
- Broecker, W. S., T.-H. Peng, G. Ostlund and M. Stuiver, The distribution of bomb radiocarbon in the Ocean, *Journal of Geophysical Research*, 90, 6953-6970, 1985.
- Broecker, W. S., S. Sutherland and W. Smethie, Oceanic radiocarbon: Separation of the natural and bomb components, *Global Biogeochemical Cycles*, 9, 263-288, 1995.
- Burr, G. S., R. L. Edwards, D. J. Donahue, E. R. M. Druffel and F. W. Taylor, Mass spectrometric ^{14}C and U-Th measurements in coral, *Radiocarbon*, 34, 611-618, 1992.
- Donahue, D. J., A. J. T. Jull and L. J. Toolin, Radiocarbon measurements at the University of Arizona AMS facility, *Nuclear Instruments and Methods*, B52, 224-228, 1990.
- Donahue, D. J., T. W. Linick and A. J. T. Jull, Isotope ratio and background corrections for accelerator mass spectrometry radio carbon measurements, *Radiocarbon*, 32, 135-142, 1990.
- Druffel, E. M. and T. Linick W., Radiocarbon in annual coral rings of Florida, *Geophysical Research Letters*, 5, 913-916, 1978.
- Druffel, E. R., Radiocarbon in annual coral rings from the eastern tropical Pacific Ocean, *Geophys. Res. Lett.*, 8, 59-62, 1981.

- Druffel, E. R., Bomb radiocarbon in the Pacific: annual and seasonal timescale variations, *J. Mar. Res.*, 45, 667-698, 1987.
- Druffel, E. R. M., J. E. Bauer, P. M. Williams, S. Griffin and D. Wolgast, Seasonal variability of particulate organic radiocarbon in the northeast Pacific Ocean, *Journal of Geophysical Research*, 101, 20,543-20,552, 1996.
- Druffel, E. R. M. and S. Griffin, Large variations of surface ocean radiocarbon: evidence of circulation changes in the southwestern Pacific, *Journal of Geophysical Research*, 98, 20,249-20,259, 1993.
- Gronvold, K., N. Oskarsson, S. J. Johnsen, H. B. Clausen, C. U. Hammer, G. Bond and E. Bard, Ash layers from Iceland in the Greenland GRIP ice core correlated with oceanic and land sediments, *Earth and Planetary Science Letters*, 135, 149-155, 1995.
- Linick, T. W., Bomb-produced carbon-14 in the surface water of the Pacific Ocean, *Radiocarbon*, 22, 599-606, 1980.
- McConnaughey, T. A., J. Burdett, J. F. Whelan and C. K. Paull, Carbon isotopes in biological carbonates: Respiration and photosynthesis, *Geochimica et Cosmochimica Acta*, 61, 611-622, 1997.
- Moore, M. D., D. P. Schrag and M. Kashgarian, Coral radiocarbon constraints on the source of the Indonesian throughflow, *Journal of Geophysical Research*, 102, 12,359-12,365, 1997.
- Ostlund, H. G. and M. Stuiver, GEOSECS Pacific radiocarbon, *Radiocarbon*, 22, 25-53, 1980.
- Stuiver, M. and H. G. Ostlund, GEOSECS Atlantic radiocarbon, *Radiocarbon*, 22, 1-24, 1980.
- Stuiver, M. and H. G. Ostlund, GEOSECS Indian Ocean and Mediterranean radiocarbon, *Radiocarbon*, 25, 1-29, 1983.
- Stuiver, M. and H. A. Polach, Reporting of ^{14}C data, *Radiocarbon*, 19, 355-363, 1977.
- Toggweiler, J. R., K. Dixon and K. Bryan, Simulations of radiocarbon in a coarse-resolution world ocean model 2. Distributions of bomb-produced carbon 14, *Journal of Geophysical Research*, 94, 8243-8264, 1989.
- Vogel, J. S., D. E. Nelson and J. R. Southon, ^{14}C background levels in an accelerator mass spectrometry system, *Radiocarbon*, 29, 323-333, 1987.

Sample	Species	UCID #	CAMS #	Start wt. (mg)	CO ₂ Gas (ml) Total	AMS	Percent leached	Fraction Modern	error	¹⁴ C Age (years)	error
47413	D. cristagalli	654	19372	27	5.60	2.11		0.9297	0.0051	590	50
85080	D. cristagalli	655	19373	57	10.68	1.41		0.8825	0.0056	1000	60
78459	D. cristagalli	656	19374	37	7.79	1.03	11%	0.9251	0.0046	630	50
JFA 24c	D. cristagalli	657	19375	38	7.09	1.67		0.1731	0.0012	14090	60
JFA 2	D. cristagalli ?	658A	19376	86	8.59	2.09	51%	0.2213	0.0015	12120	60
		658B	19377	35	6.00	1.45		0.2195	0.0014	12180	60
JFA 17	Solenosmillia. sp.	659	19378	21	3.67	1.38		0.2284	0.0016	11860	60
JFA 20a	D. cristagalli	660	19379	24	3.71	1.43		0.0025	0.0009	48040	2930
JFA 20b	D. cristagalli	661	19380	29	6.00	2.00		0.0035	0.0010	45390	2350
JFA 20c	D. cristagalli	662	19381	54	7.60	1.00	6%	0.0056	0.0010	41640	1390
Calcite		663	19384	52	10.36	1.35		0.0028	0.0002	47230	620
Calcite		664	19385	42	9.76	1.30		0.0027	0.0003	47560	890

Table A4.1

Sample	Species	UCID #	CAMS #	Start wt. (mg)	CO ₂ Gas (ml) Total AMS	Percent leached	Fraction Modern	error	$\Delta^{14}\text{C}$ (‰)	error	¹⁴ C Age (years)	error
93177.3	Fung. mar.	999	22442	58	9.58	19%	0.7773	0.0044	-226.9	4.4	2,020	50
JFA 48.1	F. apertum	1000	22443	71	11.27	7%	0.2389	0.0024	-762.4	2.4	11,500	80
JFA 20.4	D. cristagalli	1001	22444	62	8.47	6%	0.1755	0.0024	-825.4	2.4	13,980	110
JFA 20.2	D. cristagalli	1002	22445	65	9.65	12%	0.1781	0.0021	-822.8	2.1	13,860	100
91545.2	St. nobilis	1003	22446	60	8.28	15%	0.8241	0.0048	-180.4	4.8	1,550	50
83522	Carry sp.	1004	22447	88	17.25	10%	0.7594	0.0043	-244.8	4.3	2,210	50
JFA 20.10	D. cristagalli	1005	22448	60	10.78	17%	0.1742	0.0024	-826.7	2.4	14,040	120
JFA 24.40	D. cristagalli	1007	22449	54	5.29	44%	0.1954	0.0022	-805.7	2.2	13,120	100
JFA 24.41	D. cristagalli	1008	22450	58	2.05	55%	0.1622	0.0022	-838.7	2.2	14,610	110
JFA 46.3		1009	22451	53	7.73	25%	0.4605	0.0032	-542.0	3.2	6,230	60
JFA 24.45	D. cristagalli	1010	22452	49	4.61	47%	0.1718	0.0022	-829.2	2.2	14,150	110
JFA 45.4		1011	22453	54	2.26	24%	0.6969	0.0052	-306.8	5.2	2,900	70
PV-237	E. rostrata	1013	22454	56	7.18	34%	0.7133	0.0045	-290.5	4.5	2,710	60
JFA 30.1		1014	22455	59	1.75	44%	0.2108	0.0022	-790.4	2.2	12,510	90
86562.2	St. weberianus	1016	22456	64	8.83	25%	0.3653	0.0028	-636.7	2.8	8,090	70
JFA 48.2	Carry. Sp.	1017	22457	47	6.05	34%	0.5054	0.0028	-497.3	2.8	5,480	50
Calcite		1006	22458	82	18.12		0.0066	0.0006	-993.4	0.6	40,310	710
Calcite		1012	22459	61	10.77	20%	0.0066	0.0004	-993.4	0.4	40,300	470
86873.1	St. campaniformis	1018	22460	63	4.51	46%	0.8404	0.0063	-164.2	6.3	1,400	60
JFA 46.5		1019	22461	62	9.59	19%	0.3926	0.0034	-609.5	3.4	7,510	70
48740.1	D. cristagalli	1020	22462	54	5.59	41%	0.9137	0.0053	-91.3	5.3	730	50
JFA 47.1	Carry. Sp.	1021	22463	60	1.96	23%	0.7612	0.0049	-242.9	4.9	2,190	60
47373	F. impensum	1022	22464	59	3.35	76%	0.8377	0.0049	-166.8	4.9	1,420	50
48518	S. variabilis	1023	22465	51	5.27	43%	0.9235	0.0055	-81.5	5.5	640	50
JFA 24.1	D. cristagalli	1024	22466	50	4.19	34%	0.0136	0.0022	-986.5	2.2	34,550	1,320
JFA 24.8	D. cristagalli	1025	22467	49	5.1	35%	0.1844	0.0023	-816.6	2.3	13,580	100
JFA 24.19	D. cristagalli	1026	22468	59	6.85	36%	0.1690	0.0022	-831.9	2.2	14,280	110

Table A4.2

Sample	Species	UCID #	CAMS #	Start wt. (mg)	CO ₂ Gas (ml) Total	AMS	Percent leached	Fraction Modern	error	¹⁴ C Age (years)	error
JFA 20.10 Top	D. cristagalli	1529A	30183	48.7	37.8	2.03	8%	0.1717	0.0010	14160	50
		1529B	30184			1.97		0.1730	0.0011	14090	60
JFA 20.10 Bot.	D. cristagalli	1530A	30185	25.7	21.4	1.81	7%	0.1756	0.0012	13970	60
		1530B	30186			1.94		0.1751	0.0013	14000	60
JFA 24.19 Top	D. cristagalli	1531A	30187	70.5	46.5	1.98	10%	0.1658	0.0012	14440	60
		1531B	30188			1.98		0.1631	0.0014	14560	70
JFA 24.19 Bot.	D. cristagalli	1532A	30189	83.8	46.2	1.99	8%	0.1738	0.0012	14060	60
		1532B	30190			2.01		0.1735	0.0012	14070	60
JFA 24.8 Top	D. cristagalli	1533A	30191	102.1	53.6	1.70	7%	0.1652	0.0012	14460	60
		1533B	30192			2.14		0.1631	0.0012	14570	60
JFA 24.8 Bot.	D. cristagalli	1534A	30193	66.3	45.6	2.05	10%	0.1795	0.0015	13800	70
		1534B	30194			2.02		0.1773	0.0010	13900	50
Calcite		1535A	30195		47.1	1.98		0.0025	0.0002	48290	610
		1535B	30196			2.06		0.0024	0.0002	48520	590

Table A4.3

Sample (JFA 20c)	Species	UCID #	CAMS #	Start wt. (mg)	CO ₂ Gas (ml)		Percent leached	Fraction Modern	error	¹⁴ C Age (years)	error
Coral Standard		2060	36239	268.9	62.38	1.94		0.9455	0.0035	450	30
TOP#1	D. cristagalli	2039	36240		2.77	1.87	N.A.	0.0119	0.0008	35610	570
TOP#2	D. cristagalli	2040	36241		5.58	1.95	"	0.0084	0.0008	38400	800
TOP#3	D. cristagalli	2041	36242		7.70	1.92	"	0.0077	0.0008	39130	890
TOP#4	D. cristagalli	2042	36243		9.56	1.93	"	0.0066	0.0008	40330	1010
TOP#5	D. cristagalli	2043	36244	301.1	4.85	1.92	"	0.0097	0.0008	37270	710
BOT I#1	D. cristagalli	2044	36245		2.78	1.62	"	0.0178	0.0009	32380	430
BOT I#2	D. cristagalli	2045	36246		4.09	1.90	"	0.0120	0.0009	35540	590
BOT I#3	D. cristagalli	2046	36247		7.28	1.93	"	0.0109	0.0009	36270	640
BOT I#4	D. cristagalli	2047	36248		9.13	1.93	"	0.0110	0.0008	36200	620
BOT I#5	D. cristagalli	2048	36249	231.8	30.55	1.94	"	0.0218	0.0009	30720	320
BOT II#1	D. cristagalli	2049	36250		2.48	1.68	"	0.0174	0.0010	32540	460
BOT II#2	D. cristagalli	2050	36251		4.36	1.94	"	0.0118	0.0008	35670	570
BOT II#3	D. cristagalli	2051	36252		10.59	1.92	"	0.0132	0.0009	34740	540
BOT II#4	D. cristagalli	2052	36253		11.26	1.93	"	0.0160	0.0008	33220	420
BOT II#5	D. cristagalli	2053A	36254	226.6	22.75	1.91	"	0.0248	0.0008	29690	280
		2053B	36255			1.93	"	0.0240	0.0008	29960	290
Calcite		2059	36256	273.8	61.33	1.93		0.0025	0.0002	48130	730
JFA 24.19 Mid.	D. cristagalli	2054	36257	51.2	8.49	1.95	26%	0.1651	0.0010	14470	50
JFA 24.8 Mid.	D. cristagalli	2055	36258	88.8	16.32	1.89	17%	0.1658	0.0010	14440	50
Calcite-leached		2056	36259	65	13.63	1.93	9%	0.0015	0.0002	52050	1130

Table A4.4

Sample (JFA 62.1)	Species	UCID #	CAMS #	Start wt. (mg)	CO ₂ Gas (ml) Total	AMS	Percent leached	Fraction Modern	error	¹⁴ C Age error (years)
Top #1	D. cristagalli	2197	39255		1.95	1.87		0.6852	0.0030	3040 40
Top #2		2198	39256		4.56	1.98		0.6837	0.0027	3050 40
Top #3		2199	39257		4.65	1.97		0.6840	0.0032	3050 40
Top #4		2200	39258	87.8	9.26	1.95	5%	0.6799	0.0029	3100 40
Bot. #1		2201	39259		1.66	1.57		0.6777	0.0029	3130 40
Bot. #2		2202	39260		2.8	1.88		0.6757	0.0030	3150 40
Bot. #3		2203	39261		3.44	1.96		0.6776	0.0030	3130 40
Bot. #4		2204	39262	48.5	3.02	1.95	7%	0.6790	0.0032	3110 40
Calcite #1	uncrushed	2205			2.45	1.99		Lost during graphitization		
Calcite #2		2206	39264		2.08	1.93		0.0040	0.0003	44430 650
Calcite #3		2207	39265		3.56	1.96		0.0026	0.0001	47930 390
Calcite #4		2208	39266	65.5	6.94	1.95	3%	0.0024	0.0001	48530 350
Calcite #1	crushed	2209	39267		2.41	1.97		0.0024	0.0003	48530 870
Calcite #2		2210	39268		1.61	1.53		0.0040	0.0001	44360 190
Calcite #3		2211	39269		5.59	1.96		0.0031	0.0002	46290 470
Calcite #4		2212	39270	82.5	9.41	1.95	2%	0.0024	0.0002	48390 720

Table A4.5

Chapter 5: Stable Isotopes in Deep-Sea Corals

I. Introduction

The pioneering work of Weber and Woodhead found a strong linear correlation between bulk coral $\delta^{18}\text{O}$ and *in situ* water temperature [Weber and Woodhead, 1972]. Different coral species showed offsets in the absolute $\delta^{18}\text{O}$ value, but all surface corals had nearly the same slope of $\delta^{18}\text{O}$ vs. temperature (Figure 5.1). At the same time as this Weber and Woodhead study, radioactive bands were found in corals from Eniwetok Atoll that precisely matched the timing of nuclear bomb tests at this remote Pacific site [Knutson et al., 1972; Buddemeier et al., 1974]. By counting density bands, both between bomb tests, and from the date of collection to the last bomb test, these authors proved that coral density bands were annual. Subsequent studies of natural radionuclides confirmed the annual periodicity of density band pairs from other tropical locations [Moore and Krishnaswami, 1972; Moore et al., 1973; Dodge and Thomson, 1974]. Fairbanks and Dodge and Emiliani et al. used the banding chronometer to show that $\delta^{18}\text{O}$, and to a lesser degree $\delta^{13}\text{C}$, values also had an annual periodicity [Emiliani et al., 1978; Fairbanks and Dodge, 1979]. Numerous studies have used this fundamental work to reconstruct the temperature and water $\delta^{18}\text{O}$ history of surface waters over the past several decades [Dunbar and Wellington, 1981; Cole et al., 1993]. One recent study has even proposed that the $\delta^{13}\text{C}$ signal itself can be used as a precise chronometer in areas with periodic mass spawning events [Gagan et al., 1994].

Given the success of the early surface coral stable isotope work, it is no wonder that most of the first deep-sea coral studies were concentrated on $\delta^{18}\text{O}$ and $\delta^{13}\text{C}$ variations. Following on their earlier work, Weber used ahermatypic corals to extend the paleo-temperature equation (Figure 5.1)[Weber, 1973]. This new data agreed remarkably well with the surface coral calibration. However, several other papers showed a strong linear correlation between $\delta^{18}\text{O}$ and $\delta^{13}\text{C}$ across a wide range of values within a single

Temperature Dependence of $\delta^{18}\text{O}$ in Aragonite

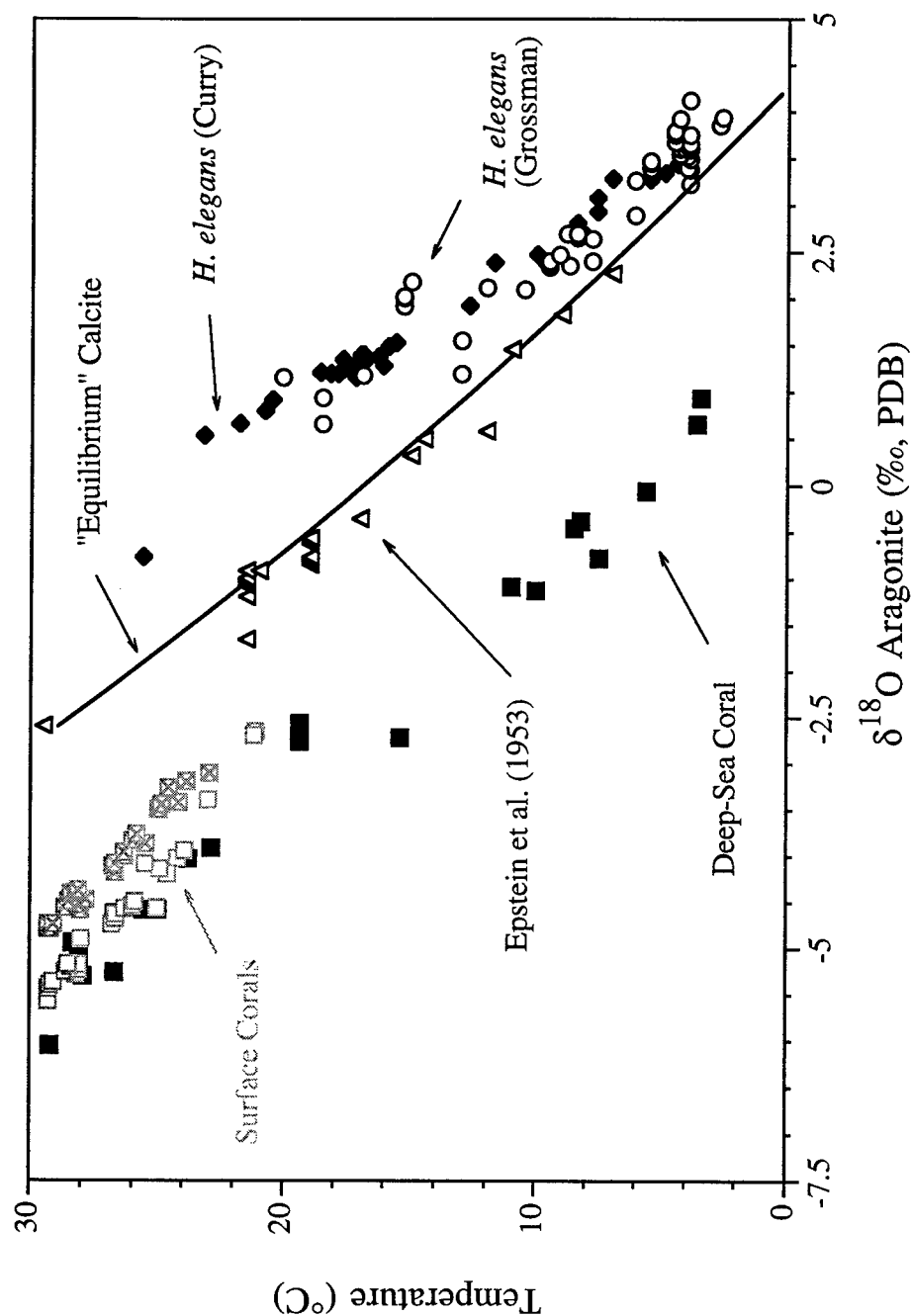


Figure 5.1. Aragonite $\delta^{18}\text{O}$ versus temperature relationships from the literature. The calcite line is from O'Neil et al. (1969). Triangles are from the mollusc data of Epstein et al (1953). All coral data are from Weber and Woodhead (1972) and Weber (1973). The aragonitic benthic foram *Hoglundina elegans* data is from Grossman and Ku (1986) and unpublished data from Dr. Bill Curry (WHOI).

individual [Land et al., 1977; Emiliani et al., 1978; Mikkelsen et al., 1982]. This discrepancy is probably due to the larger sample size used by Weber and Woodhead. In their methods papers it is not clearly stated what size was used for coral samples, but they seem to be between 5-80 mg [Weber and Raup, 1966; Weber and Woodhead, 1970]. More recent work uses 100-4000 times less material. McConnaughey found the same linear correlation for the ahermatypic coral *Tubastrea* as seen previously in other species [McConnaughey, 1989]. He also pointed out that the linear correlation was due to mixing between an end-member at seawater equilibrium and an isotopically light end-member. McConnaughey proposed that this light end-member is due to a kinetic fractionation during CO₂ hydrolysis that is slower than the precipitation rate. In this scenario, corals can trap the kinetic fractionation in their skeleton before the calcifying pool can come to complete isotopic equilibrium. In a companion paper, he demonstrated that large offsets from equilibrium could be obtained in a purely inorganic system which tried to mimic the geometry of the coral's calcifying pool [McConnaughey, 1989]. For lack of a better understanding of their causes, these offsets from isotopic equilibrium have become known as "vital effects". A recent survey of stable isotopes in calcifying organisms by McConnaughey concluded that surface corals have under 10% metabolic CO₂ in their skeletons [McConnaughey et al., 1997] and that the majority of their vital effect was due to other processes. This result is in agreement with our radiocarbon data in Chapter 4.

Recently Jodie Smith and Mike Risk at McMaster University in Canada have rekindled interest in the stable isotope composition of deep-sea corals. Using samples from Orphan Knoll that grew at the end of the Younger Dryas, these authors claim to have found an abrupt change in circulation at 1600 meters depth [Smith et al., 1997]. This same group has used a suite of modern corals, and a novel method for overcoming the stable isotope vital effects, to estimate the average water temperature any single coral sample [Smith et al., 1997]. By establishing a consistent, but arbitrary, choice of the $\delta^{13}\text{C}$

for each individual, these authors get an excellent calibration of their " $\delta^{18}\text{O}$ intercept" value versus temperature. The drawback to this method is that it does not provide high resolution time series of temperature. It does provide a good estimate of deep temperature at a well constrained time in the past from a single coral.

In this Chapter, we present our work on the stable isotope distribution of deep-sea corals with an emphasis on *Desmophyllum cristagalli*. Several tests of our methods are presented first. Next, we confirm the strong linear $\delta^{13}\text{C}$ vs. $\delta^{18}\text{O}$ relationship seen by all other authors and demonstrate that it is consistent across genera. Akin to the seminal work of McConnaughey, we try to map out the vital effect in an attempt to find a way to sample around it. These micro-sampling studies are described for both modern and fossil corals.

II. Methods Tests

All of the data presented in this chapter were collected on the Finnigan MAT-252 light gas mass spectrometer in the lab of Dr. Bill Curry (WHOI). This machine is fitted with an automatic carbonate sample introduction system, "Kiel Device", which uses a preset reaction time of 10 minutes. Two separate reaction lines (A and B) are run simultaneously to save time during sample handling. All data are reported as per mil values and are corrected to the PDB scale by comparison with the NBS-19 carbonate standard [Craig, 1957]. Two other standards are also run with every sample batch to extend the ‰ range of the calibration. Standard Atlantis II has the heaviest $\delta^{18}\text{O}$ of the three standards (Table 5.1) and is itself a deep-sea coral which was mechanically crushed in a hand mill to homogenize the sample.

Several of our early studies on the stable isotope composition of deep-sea corals used large chunks of uncrushed sample that did not completely dissolve during the Kiel Device reaction time. The resulting incomplete transfer of reacted CO_2 gas could lead to isotopic fractionation which is not accounted for by the standards. We investigated this problem

Standard	$\delta^{13}\text{C}$		$\delta^{18}\text{O}$		Number of
Name	‰	Std. Dev	‰	Std. Dev	Runs
<i>AtlantisII</i>					
A line	0.86	0.07	3.46	0.08	447
B line	0.84	0.09	3.48	0.07	438
<i>B1</i>					
A line	0.63	0.08	0.12	0.07	1358
B line	0.63	0.09	0.13	0.06	1319
<i>Carrera</i>					
A line	2.06	0.04	-1.95	0.09	438
B line	2.06	0.02	-1.94	0.06	434
<i>NBS19</i>					
A line	1.95	0.02	-2.20	0.08	1047
B line	1.95	0.03	-2.20	0.06	1026

Table 5.1: WHOI Standard Data Since 1993. Atlantis II is a hand milled deep-sea coral. B1 is a sample of the Pee Dee Belemnite limestone formation. Carrera is a marble from the quarry in Italy.

in two ways. Because we know the pressure of gas that is trapped by the Kiel Device and the original weight of the sample, we can compare the extent of reaction with the sample's isotopic value. Figures 5.2 and 5.3 show the empirical calibration of the pressure sensors for both the A and B lines. NBS-19 samples used in this calibration were known to have reacted completely and the non-linear behavior of the sensors is typical for these gauges. Measured pressures for each sample are converted to equivalent CaCO_3 weights and compared to total weights to calculate the percentage reacted. Plots of $\delta^{18}\text{O}$ and $\delta^{13}\text{C}$ vs. reaction extent for one of our runs where many samples did not fully react are shown in Figure 5.4. There is no trend of either isotopic value with reaction extent.

Another test of possible fractionations due to incomplete reaction and/or sample size uses the isotopically homogenous Carrera marble. We generated a variety of size fractions of this CaCO_3 by hand crushing a single large piece with an agate mortar and pestle under an Argon atmosphere. Plots of $\delta^{18}\text{O}$ vs. $\delta^{13}\text{C}$ for the different size fractions are shown in Figure 5.5. There is one flier with a very light $\delta^{13}\text{C}$ and a slightly depleted $\delta^{18}\text{O}$. We have no concrete explanation for this point but note that it is from the smallest size fraction and therefore most susceptible to dust contamination. The enlarged view of the data shows that the one point that did not react completely has a slightly depleted $\delta^{13}\text{C}$ value. This 0.25‰ depletion is very small relative to the signal observed in coral samples that did not react completely. Statistics for the Carrera marble (Table 5.2) agree well with other labs' absolute values (Barry Grant, personal communication) and show a $\delta^{18}\text{O}$ standard deviation of 0.03‰ and a $\delta^{13}\text{C}$ standard deviation of 0.07‰ (including the partially reacted sample).

Some of our samples were pre-cleaned, as described in Chapter 3, before stable isotope analysis. The septal grid study described below resulted in samples that were more or less contaminated with remnant polyp organic matter and the resin used to hold the sample to the glass slide. Both of these phases were easily removed with the

Pressure Calibration A-Line

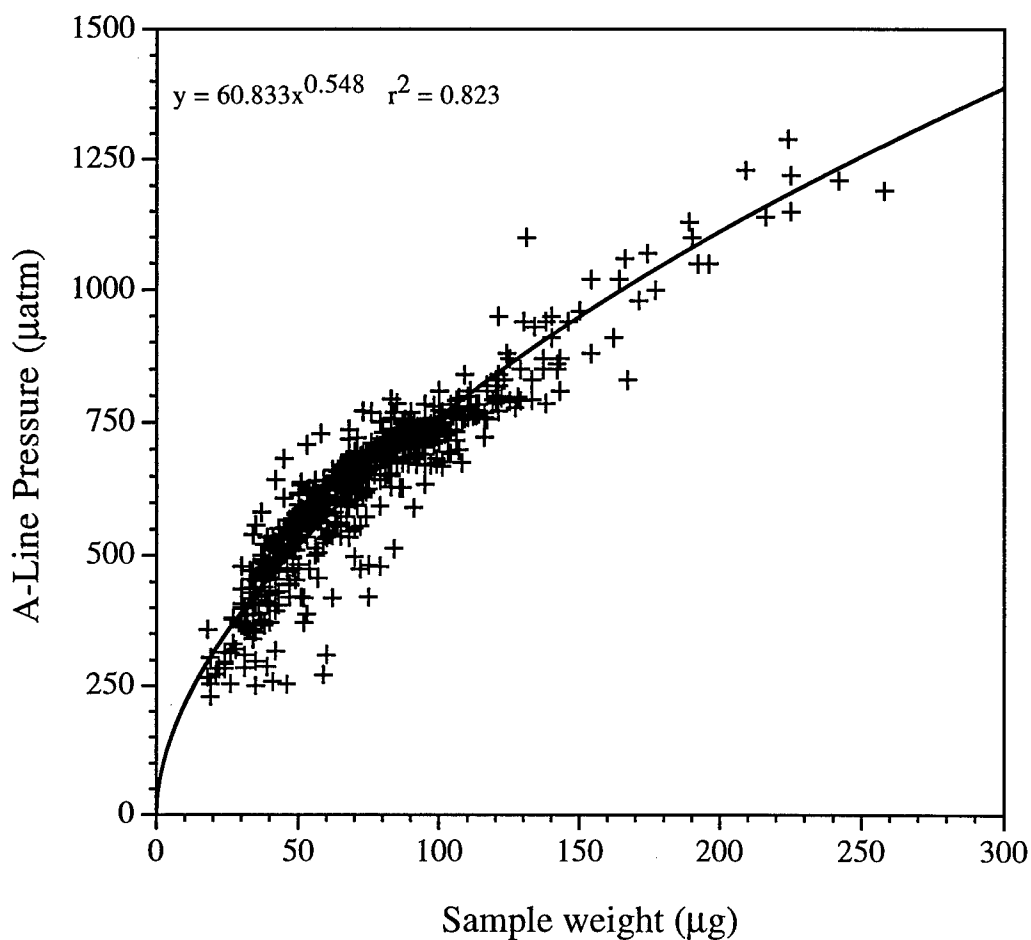


Figure 5.2. Pressure sensor calibration of the WHOI Finnigan MAT-252 light gas stable isotope mass spectrometer A-line. All points are from NBS-19 which was known to react completely in the Kiel Device. The curve fit was used to calculate expected pressures for the % reaction study.

Pressure Calibration B-Line

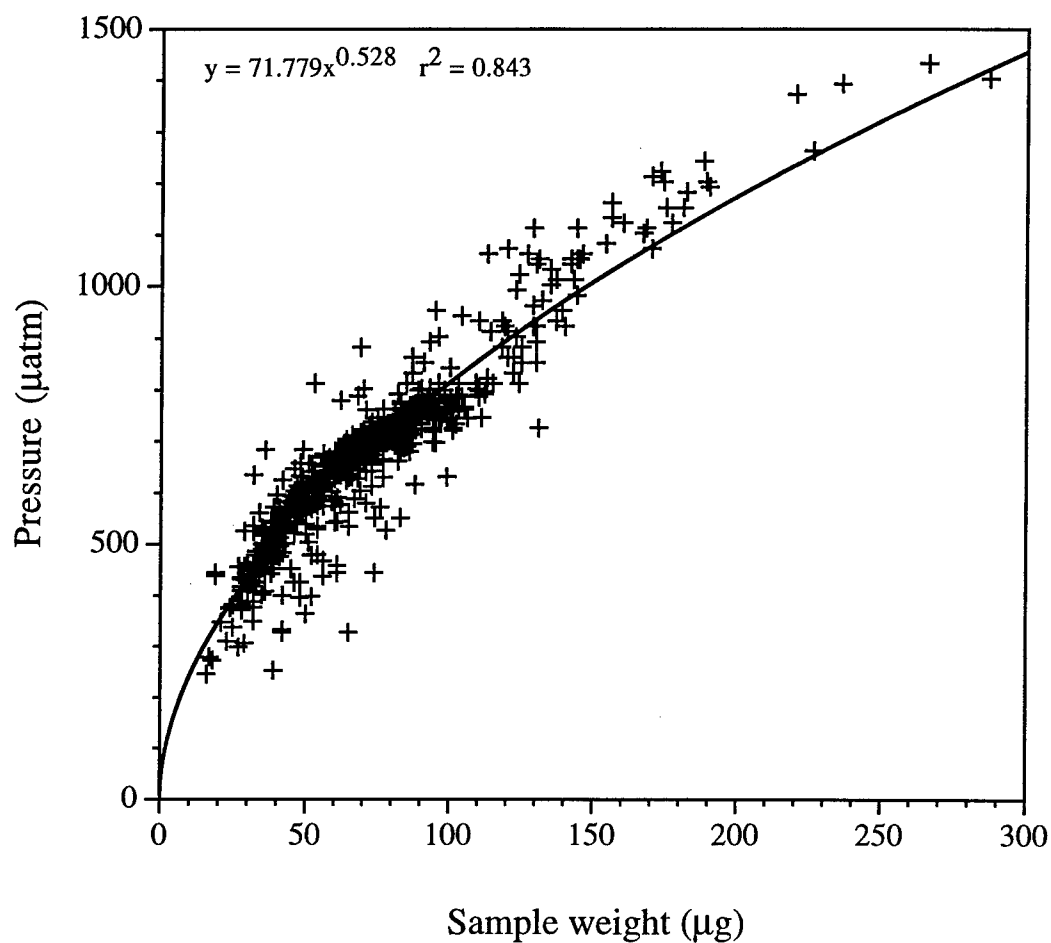


Figure 5.3. Pressure sensor calibration of the WHOI Finnigan MAT-252 light gas stable isotope mass spectrometer B-line. All points are from NBS-19 which was known to react completely in the Kiel Device. The curve fit was used to calculate expected pressures for the % reaction study.

% Reaction's Effect on Isotopic Value

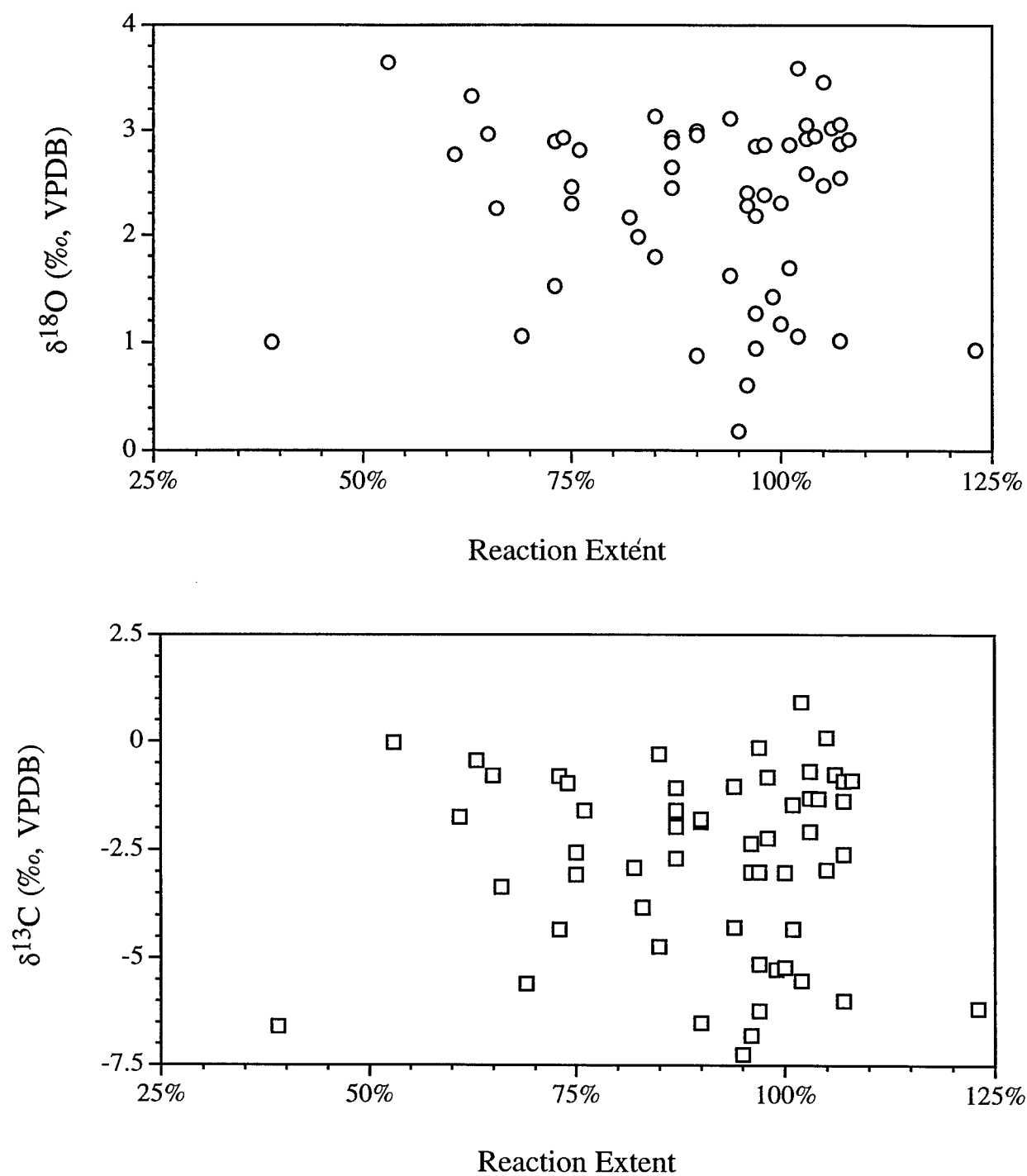


Figure 5.4. Relationship between reaction extent and isotopic value for *D. cristagalli* samples. Neither $\delta^{13}\text{C}$ nor $\delta^{18}\text{O}$ show any relationship with reaction percentage.

Carrera Marble Size Fractions

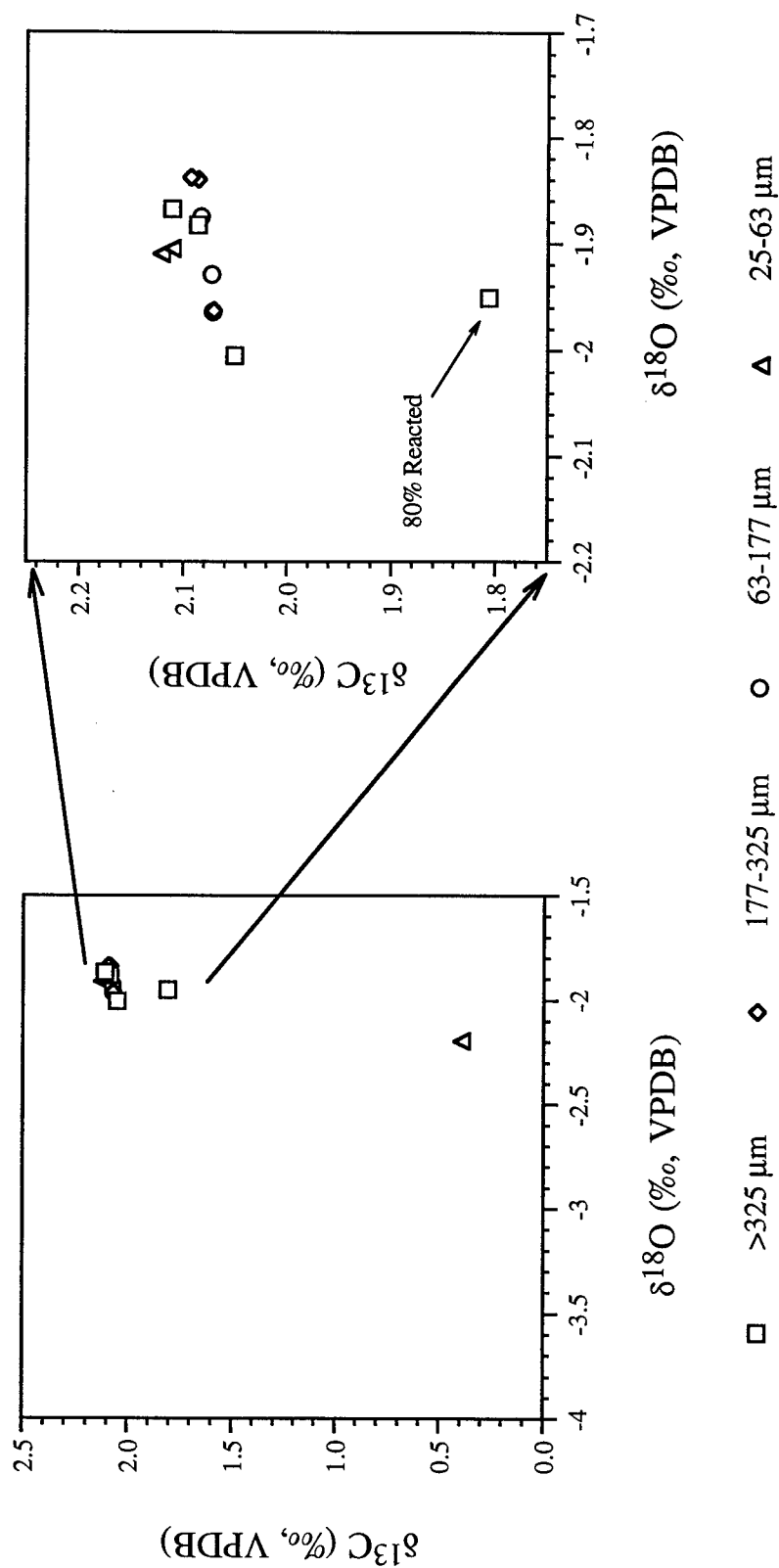


Figure 5.5. Size fraction study of Carrera Marble. This isotopically homogenous standard should give the same value for all size fractions. Outside of one flier, this is generally true. One sample that did not react completely is slightly depleted in $\delta^{13}\text{C}$. Sample statistics are listed in Table 5.2.

Size (μm)	Number	$\delta^{18}\text{O}$ (‰)		$\delta^{13}\text{C}$ (‰)	
		Average	error	Average	error
300	4	-1.927	0.063	2.014	0.141
177-325	3	-1.880	0.072	2.083	0.011
63-177	3	-1.923	0.045	2.076	0.006
25-63	2	-1.908	0.004	2.116	0.007
All	12	-1.911	0.053	2.064	0.084

Table 5.2: Isotopic values of Carrera marble size fractions. Errors are one standard deviation.

chemical pre-cleaning step. To eliminate the possibility of artifacts introduced by this procedure, we analyzed *D. cristagalli* sample number 84820 from 806 meters deep near the Galapagos Islands both with and without pre-cleaning. The data in Figure 5.6 show that there is no systematic bias introduced by the chemical treatment. All data fall along the same linear trend. In addition, there are several samples that did not completely react and all of which fall on the linear trend (Table A5.3). These methods studies suggest that there is no isotopic bias introduced by either incomplete reaction in the Kiel Device or chemical pre-cleaning. All samples from the micro-sampling studies discussed below reacted completely in the Kiel Device.

III. Septal vs. Innerseptal Studies

The single most striking feature of all deep-sea coral stable isotope data is the strong linear correlation between $\delta^{18}\text{O}$ and $\delta^{13}\text{C}$. In the deep North Atlantic *D. cristagalli* sample pictured in Figure 5.7, values range between about 0 and -7‰ in $\delta^{13}\text{C}$ and about 0 and 3‰ in $\delta^{18}\text{O}$. Ranges this large can not be found anywhere in the deep ocean, let alone at one location over the lifetime of a deep-sea coral. Therefore, this linear trend and large range of stable isotope values must be due to a biologically induced "vital effect". We can gain some insight into how to sample these animals for paleo-time series, as well as the nature of this vital effect, by comparing the isotopic values of different skeletal components. Two *D. cristagalli* specimens were sampled with a thin diamond blade attached to a Dremel tool. First, a single large septum was removed from the individual by cutting each sample as if slicing a piece of pie. Individual septa were then divided into the thin septal aragonite and the thicker, connective innerseptal aragonite. As it is difficult to precisely separate the two components, we tried to ensure that septal samples had no innerseptal material, but not visa-versa. We then gently crushed each sample in an argon atmosphere with an agate mortar and pestle to create a range of size fractions. Data from an Atlantic and a Pacific *D. cristagalli* show that generally the

Pre-Cleaning's Effect on Isotope Values

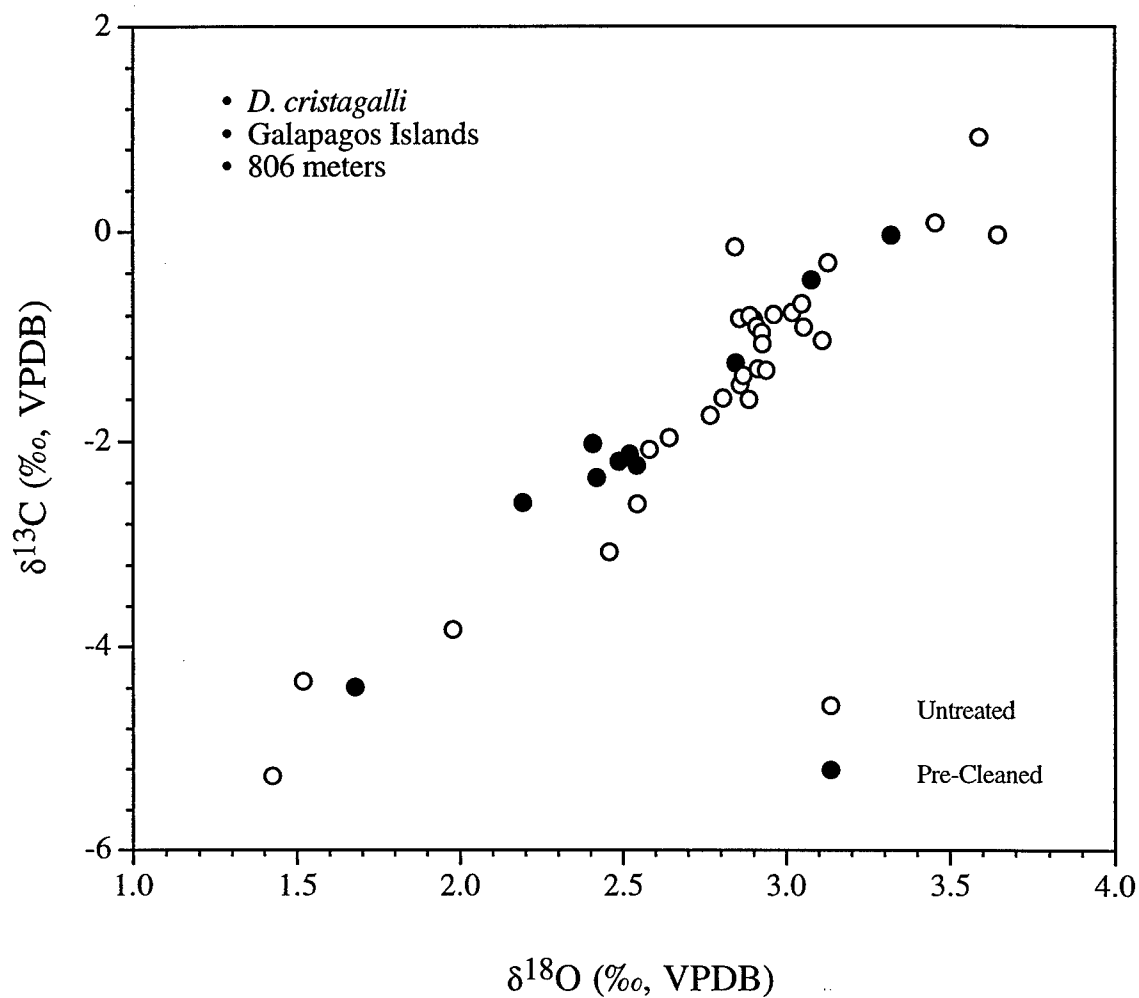


Figure 5.6. Isotopic effect of chemical pre-cleaning. A crushed *D. cristagalli* sample was treated with the oxidative pre-cleaning described in Chapter 3. There is no apparent effect of this procedure on the stable isotope value.

Sample #78459 Stable Isotopes

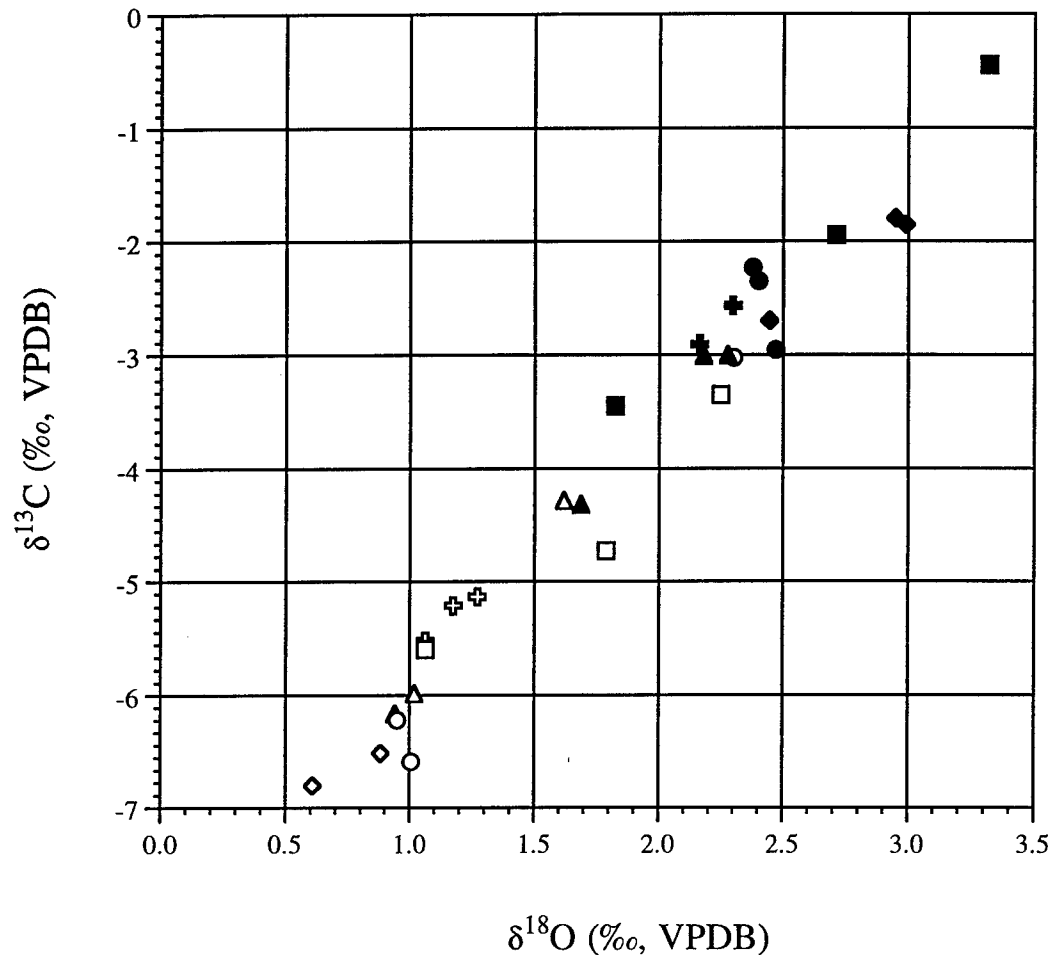


Figure 5.7. Stable isotope data from a single septum of *D. cristagalli* from 2110-2180 meters water depth near the Hudson Canyon. Filled symbols are from the thinner septal portion of the skeleton. Open symbols are from the thicker connective aragonite on the innerspetum of the skeleton. Symbol shapes correspond to size fractions of samples: squares are >600 μm , diamonds are 600-425 μm , circles are 425-250 μm , triangles are 250-63 μm and plus signs are <63 μm .

septal portion of the skeleton is heavier in $\delta^{18}\text{O}$ and $\delta^{13}\text{C}$ (Figures 5.7 and 5.8). While there are exceptions in the data, the thin septum seems to have less of a vital effect influence. In addition, the larger size fractions, above 250 μm (squares, diamonds and circles in Figures 5.6 and 5.7) seem to have the more extreme isotopic values. Smaller size fractions tend to cluster together and have less of a septal vs. innerseptal difference. Because there are a larger number of total coral grains in these samples, they are a better representation of the whole sample average. Large size fractions, on the other hand, are usually single pieces and are more likely to be influenced by extreme isotopic values.

A *Lophelia* sample from the Muir Seamount in the North Atlantic was also analyzed for its stable isotope pattern (Figure 5.9). As this genus has a completely different morphology than *D. cristagalli*, we could not easily separate its different skeletal components. This sample was also gently crushed to create a range of size fractions. Again, only the smallest size fraction has a relatively homogeneous composition indicating that large spatial gradients in $\delta^{18}\text{O}$ and $\delta^{13}\text{C}$ also exist in this sample. A very striking result is that all three samples seem to have nearly the same slope of $\delta^{18}\text{O}$ vs. $\delta^{13}\text{C}$ (Figure 5.10, Table 5.3). Regardless of genus or location, these samples all seem to be responding to roughly the same factors influencing their stable isotope composition. They seem to be the result of mixing between a heavy, more equilibrium like, end-member and an extremely vital effect influenced light end-member.

We can assess how close the heavy end-member is to seawater equilibrium by estimating the growth environment of each sample. Table 5.4 lists all of the samples for which we have environmental information and the calculated aragonite $\delta^{18}\text{O}$ and $\delta^{13}\text{C}$ equilibrium values. Water column data are estimated from nearby stations in Prof. Joseph Reid's hydrographic database [Joe Reid, personal communication]. Water $\delta^{18}\text{O}$ values are estimated from the salinity data and the GEOSECS global $\delta^{18}\text{O}$ /salinity relationship [Broecker, 1986]. The $\delta^{13}\text{C}$ of total dissolved inorganic carbon is calculated from the $[\text{PO}_4]$ data. The foraminiferal core top $\delta^{13}\text{C}$ calibration of Duplessy et al.

Sample #84820 Stable Isotopes

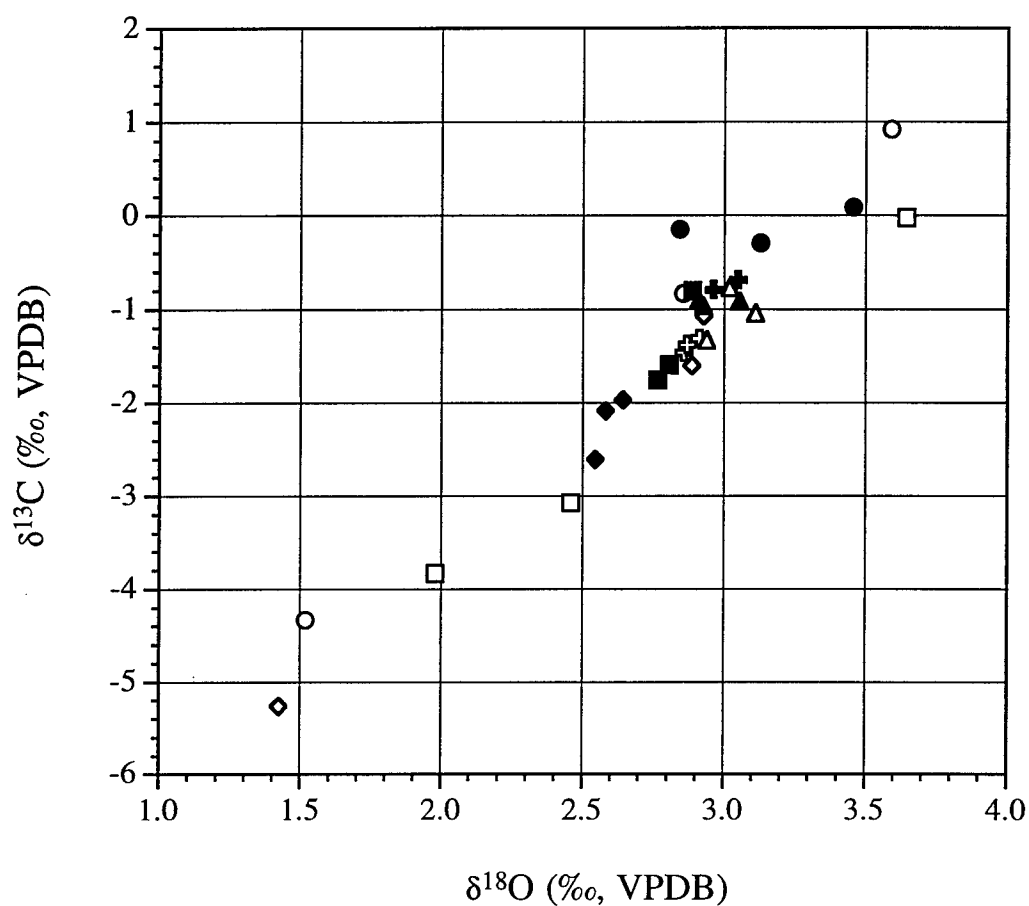


Figure 5.8. Stable isotope data from a single septum of *D. cristagalli* from 806 meters water depth off the Galapagos Islands. Filled symbols are from the thinner septal portion of the skeleton. Open symbols are from the thicker connective aragonite on the innerspetum of the skeleton. Symbol shapes correspond to size fractions of samples: squares are $>600\mu\text{m}$, diamonds are $600-425\mu\text{m}$, circles are $425-250\mu\text{m}$, triangles are $250-63\mu\text{m}$ and plus signs are $<63\mu\text{m}$.

Lophelia from Muir Seamount

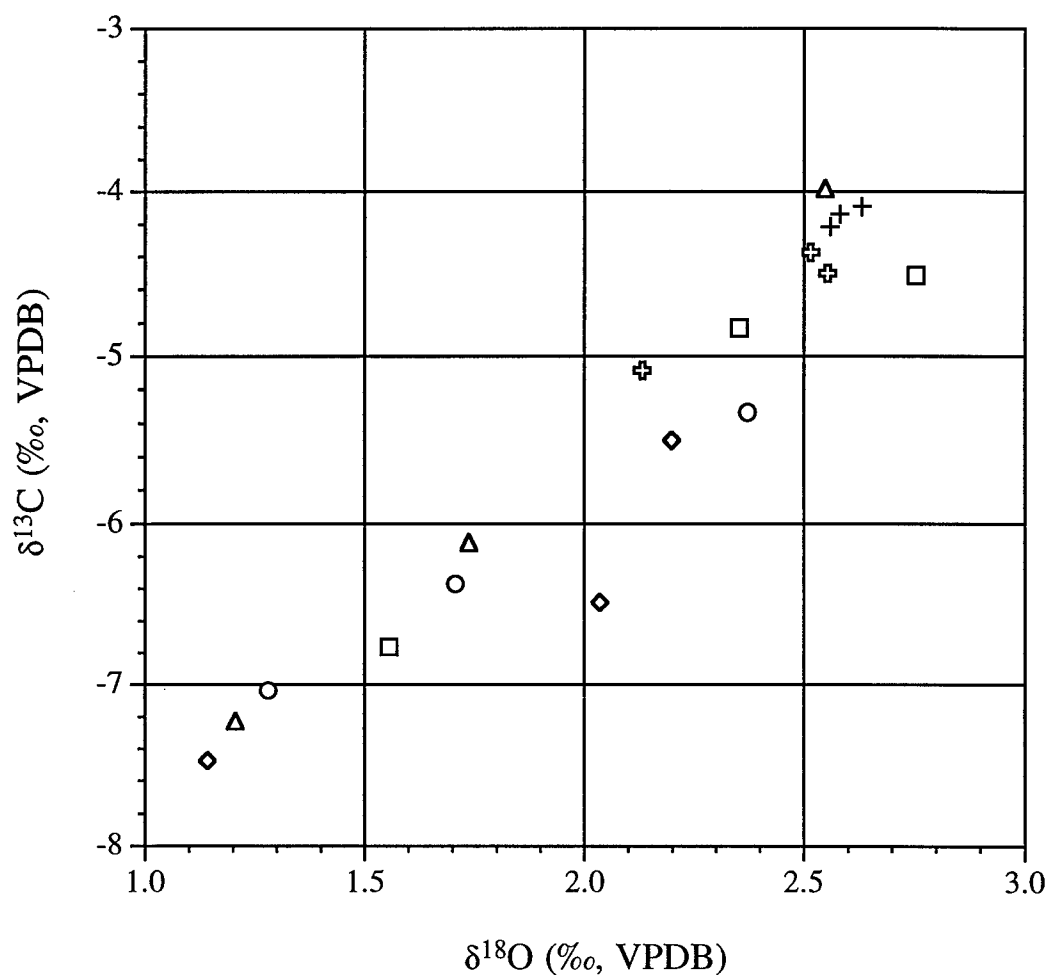


Figure 5.9. Stable isotope values of a *Lophelia* from 1940-2100 meters depth on the Muir Seamount. Symbols refer to different size classes run on the mass spectrometer; squares are $>500\ \mu\text{m}$, diamonds are $425\text{--}500\ \mu\text{m}$, circles are $300\text{--}425\ \mu\text{m}$, triangles are $180\text{--}300\ \mu\text{m}$, open plus signs are $63\text{--}180\ \mu\text{m}$ and crosses are $<63\ \mu\text{m}$.

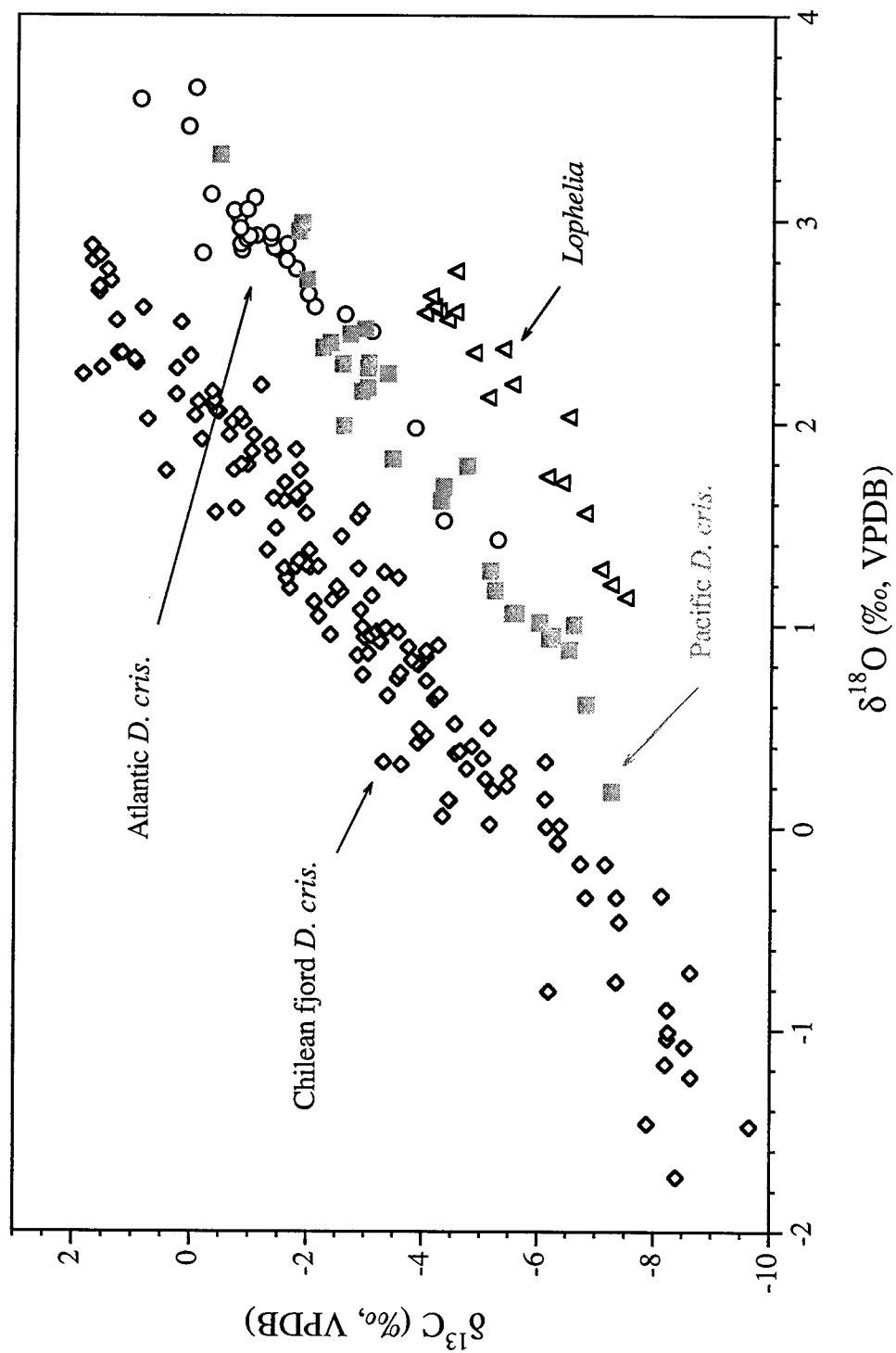


Figure 5.10. All non-micro-sampled stable isotope deep-sea coral data in this thesis. Slopes are consistent between samples and across genera.

Sample Number	Species	Slope	Standard error	Intercept (‰)	Standard error	Regression r^2
78459	<i>D. cristagalli</i>	2.26	0.08	-8.13	0.16	0.97
84820	<i>D. cristagalli</i>	2.59	0.16	-8.74	0.44	0.91
All-260	<i>Lophelia</i>	2.16	0.16	-9.98	0.35	0.92
Chilean	<i>D. cristagalli</i>	2.59	0.05	-5.62	0.08	0.94
47407-G	<i>D. cristagalli</i>	2.12	0.08	-5.88	0.22	0.94
47407-2A	<i>D. cristagalli</i>	2.63	0.12	-8.15	0.37	0.97

Table 5.3: Regression statistics for deep-sea coral stable isotopes.

Sample Number	47407	78459	84820	A260-49
Depth (m)	549	2110-2180	806	1940-2100
Latitude	54.49°N	38.45°N	0.14°N	33.36°N
Longitude	129.48°W	72.39°W	91.36°W	62.26°W
Species	<i>D. cristagalli</i>	<i>D. cristagalli</i>	<i>D. cristagalli</i>	<i>Lophelia sp.</i>
Temp ^a (°C)	5.5±1.0	3.2±0.3	5.6±0.2	3.6±0.2
Salinity ^a	34.2±0.1	34.96±0.02	34.56±0.02	34.97±0.02
[PO ₄] ^a (μM)	1.8±0.2	1.2±0.1	2.8±0.2	1.2±0.1
δ ¹⁸ O _{water} ^b (‰)	0.3±0.2	0.3±.1	0.1±0.1	0.3±0.1
δ ¹³ C _{DIC} ^c (‰)	0.6±0.4	1.0±0.25	-0.2±0.1	1.0±0.25
δ ¹⁸ O _{aragonite} ^d (‰)	3.7±0.7	4.5±0.4	3.9±0.2	4.4±0.2
δ ¹³ C _{aragonite} ^e (‰)	3.3±0.6	3.7±0.5	2.5±0.5	3.7±0.5

^a Estimated from Joe Reid Database (Personal Communication)

^b Interpolated from data in Broecker (1986)

^c Calculated from [PO₄] regression and δ¹³C of core tops in Duplessy et al. (1984)

^d From Grossman and Ku (1986) equation (1)

^e From Romanek et al. (1992)

Table 5.4: Equilibrium calculations for stable isotopes.

[Duplessy et al., 1984] and estimated bottom water $[PO_4]$ for these sites (from Prof. Reid's database and independent checks from other hydrographic data) are used to create a linear regression between $\delta^{13}C_{DIC}$ and phosphate concentration [E.A. Boyle, personal communication]. The equation of this line is, $\delta^{13}C_{DIC}=1.863-0.716*[PO_4]$. We use the aragonite $\delta^{18}O$ equilibrium equation of Grossman and Ku that incorporates all of their samples (equation 1) and the water column data to calculate the expected equilibrium value for our coral sample [Grossman and Ku, 1986]. Taking the $\delta^{13}C_{DIC}$ value to be roughly equal to the $\delta^{13}C$ of HCO_3 , we use the 2.7‰ fractionation factor between HCO_3 and aragonite determined by Romanek et al. to calculate the expected coral $\delta^{13}C$ value [Romanek et al., 1992].

The $\delta^{13}C$ calculation needs to be further investigated. Grossman and Ku find a temperature dependence of the $\delta^{13}C_{DIC}$ to aragonite fractionation using biogenic $CaCO_3$ where Romanek et al., in a purely inorganic system, do not. While presumably the inorganic study is a better measure of equilibrium without a vital effect influence, Romanek et al. can not directly measure the $\delta^{13}C$ of HCO_3 in their solutions. Their calculation uses the old $CO_{2(g)}$ to $CO_{2(aq)}$ fractionation factor of Vogel et al. [Vogel et al., 1970] which has been redetermined by Zhang et al. [Zhang et al., 1995]. Further consideration of the pH dependence of this fractionation will also change the calculated equilibrium $\delta^{13}C$ of our coral samples.

Coral stable isotope data are plotted with calculated equilibrium values in Figures 5.11-5.13. Both of the *D. cristagalli* samples extrapolate to near intersection with equilibrium. Within error sample 84820 from the Pacific intersects equilibrium, while sample 78459 from the Atlantic is depleted by about 0.8‰ in $\delta^{13}C$ for a given $\delta^{18}O$. If we assume that there is a calcifying pool from which skeletal material is made [McConnaughey, 1989; ter Kuile and Erez, 1989; Elderfield et al., 1996], then the *D. cristagalli* pool appears to have a small amount of light, possibly respired, CO_2 incorporated into it. Using a $\delta^{13}C$ respired end-member of -25‰, the 0.8‰ offset from

Sample #78459 with Equilibrium

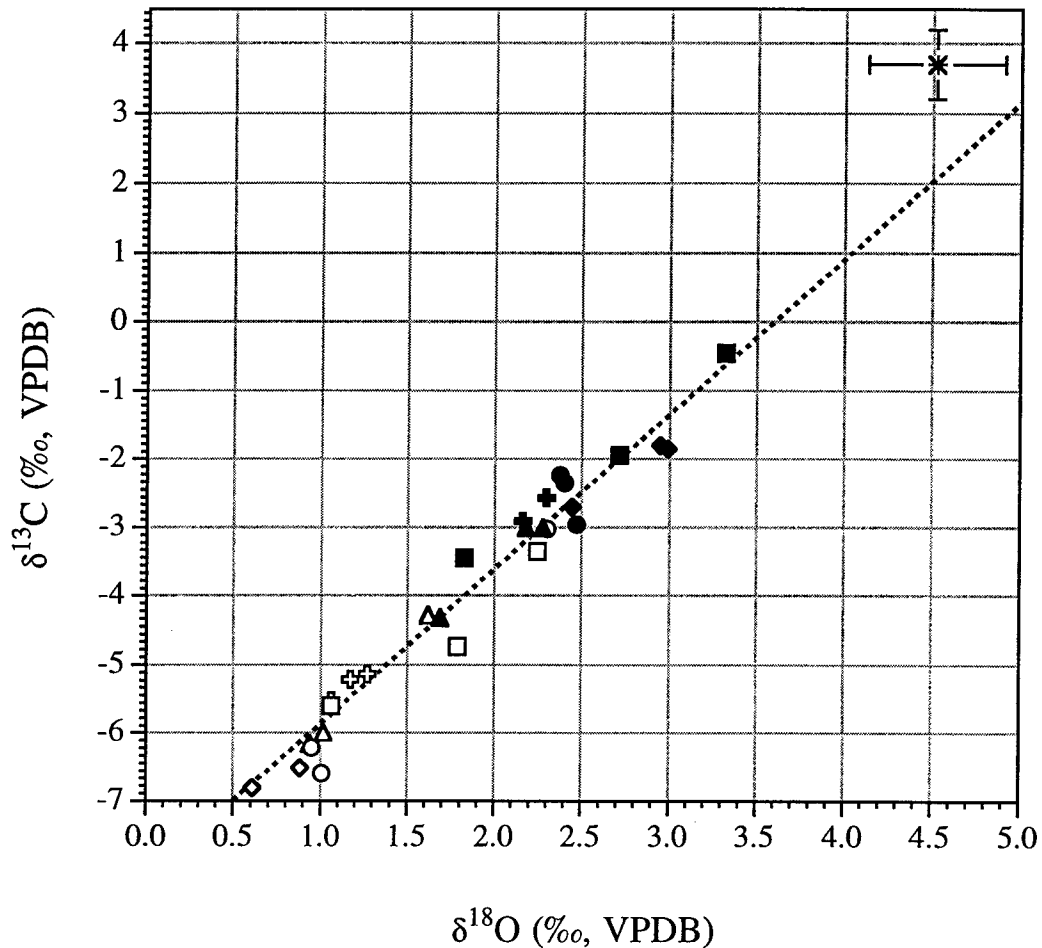


Figure 5.11. Stable isotope data from a single septum of *D. cristagalli* from 2110-2180 meters water depth near the Hudson Canyon. Filled symbols are from the thinner septal portion of the skeleton. Open symbols are from the thicker connective aragonite on the innerspetum of the skeleton. Symbol shapes correspond to size fractions of samples: squares are >600 μm , diamonds are 600-425 μm , circles are 425-250 μm , triangles are 250-63 μm and plus signs are <63 μm . Equilibrium with ambient seawater is plotted as a star in the upper right corner and calculated as described in the text.

Sample #84820 with Equilibrium

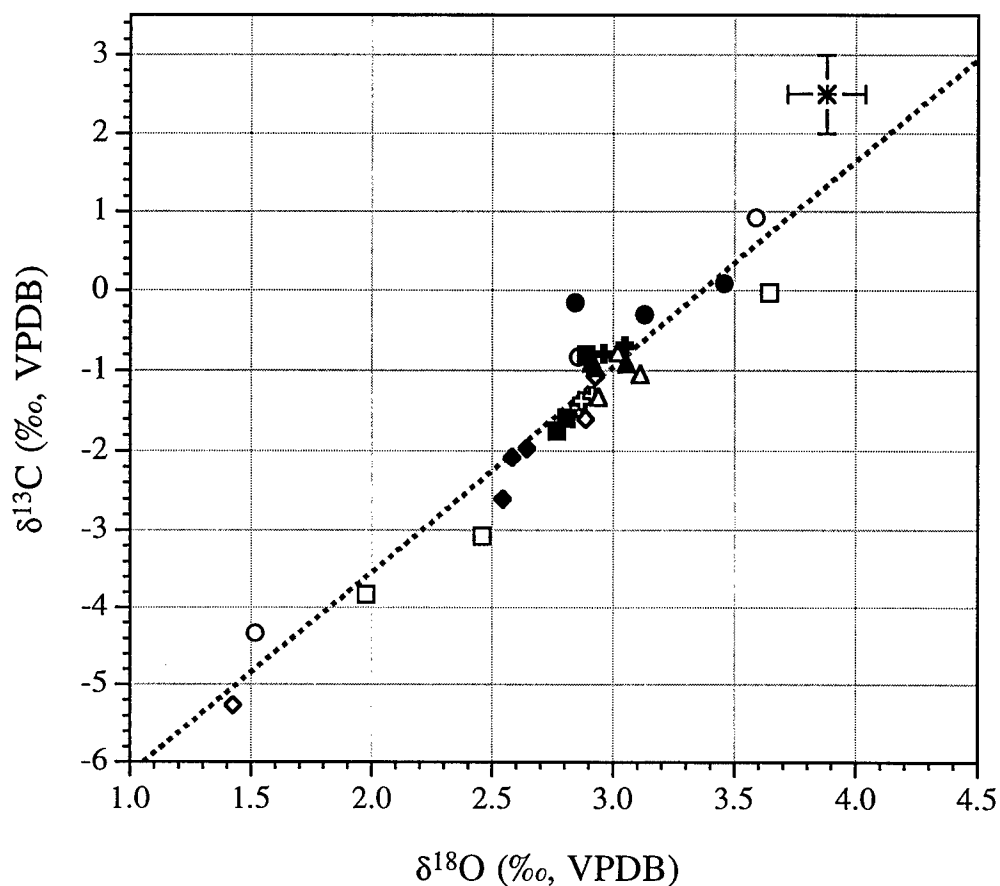


Figure 5.12. Stable isotope data from a single septum of *D. cristagalli* from 806 meters water depth off the Galapagos Islands. Filled symbols are from the thinner septal portion of the skeleton. Open symbols are from the thicker connective aragonite on the innerspetum of the skeleton. Symbol shapes correspond to size fractions of samples: squares are $>600\mu\text{m}$, diamonds are $600\text{--}425\mu\text{m}$, circles are $425\text{--}250\mu\text{m}$, triangles are $250\text{--}63\mu\text{m}$ and plus signs are $<63\mu\text{m}$. Equilibrium with ambient seawater is plotted as a star in the upper right corner and calculated as described in the text.

Lophelia Compared to Equilibrium

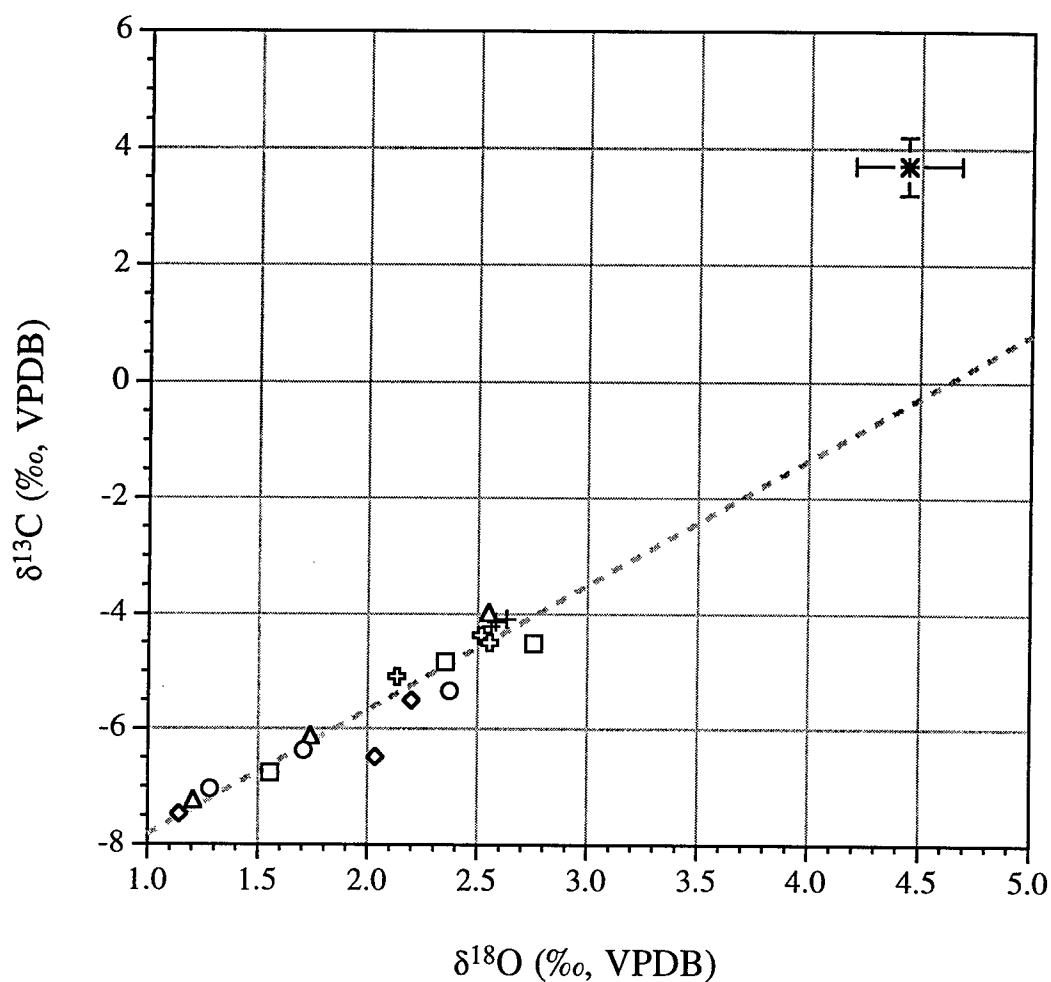


Figure 5.13. Stable isotope values of a *Lophelia* from 1940-2100 meters depth on the Muir Seamount. Symbols refer to different size classes run on the mass spectrometer; squares are >500 μm , diamonds are 425-500 μm , circles are 300-425 μm , triangles are 180-300 μm , open plus signs are 63-180 μm and crosses are <63 μm . Equilibrium with ambient seawater is plotted as a star in the upper right and calculated as described in the text.

equilibrium implies that 4% of the total carbon in the skeleton has a depleted origin. This value is in good agreement with the ^{14}C estimate of less than 8% found in Chapter IV. Equilibrium $\delta^{13}\text{C}$ values in the figures are from the Romanek et al. equation. However, if we use the Grossman and Ku equation, then both of these samples directly intersect equilibrium. This disagreement with the inorganic study possibly represents a slight vital effect in the biological aragonite used by these authors, but may reflect some of the other factors in the Romanek study mentioned above. The *Lophelia* data in Figure 5.13 show a much larger offset from equilibrium regardless of the equation used. We have no radiocarbon data from this genus to compare with the stable isotope offset.

IV. Mapping Out the Vital Effect

Rather than trying to find the exact mechanism of stable isotope fractionation in deep-sea corals, we investigated the spatial pattern of this offset from equilibrium. This is essentially the approach taken by the surface coral community to generate time series of $\delta^{18}\text{O}$ change [McConnaughey, 1989]. In their case, samples are taken from the fastest extending axis of a sample where there is the largest, but relatively consistent, offset from equilibrium. McConnaughey developed this sampling technique by making a spatial map of stable isotope values on a slabbed coral section that contained several annual growth bands. Mimicking this type of study, we sampled a large single *D. cristagalli* septum from a Chilean fjord as described above. The septum was then attached to a glass slide with epoxy and mounted to the X:Y:Z stage of a computer controlled micro-sampler. K. C. Lohman at the University of Michigan designed the sampler to read images from a photograph and then follow a pre-determined path along the sample with a rotating mill tool. In this experiment, we used the sampler in "discrete" mode, without a digitized photograph, and a thin diamond blade mounted like a saw mill as the cutting tool. A grid pattern of seven columns and eleven rows was cut through the coral and into the epoxy below (Figure 5.14). Sample chunks were approximately 2 mm square and varied in

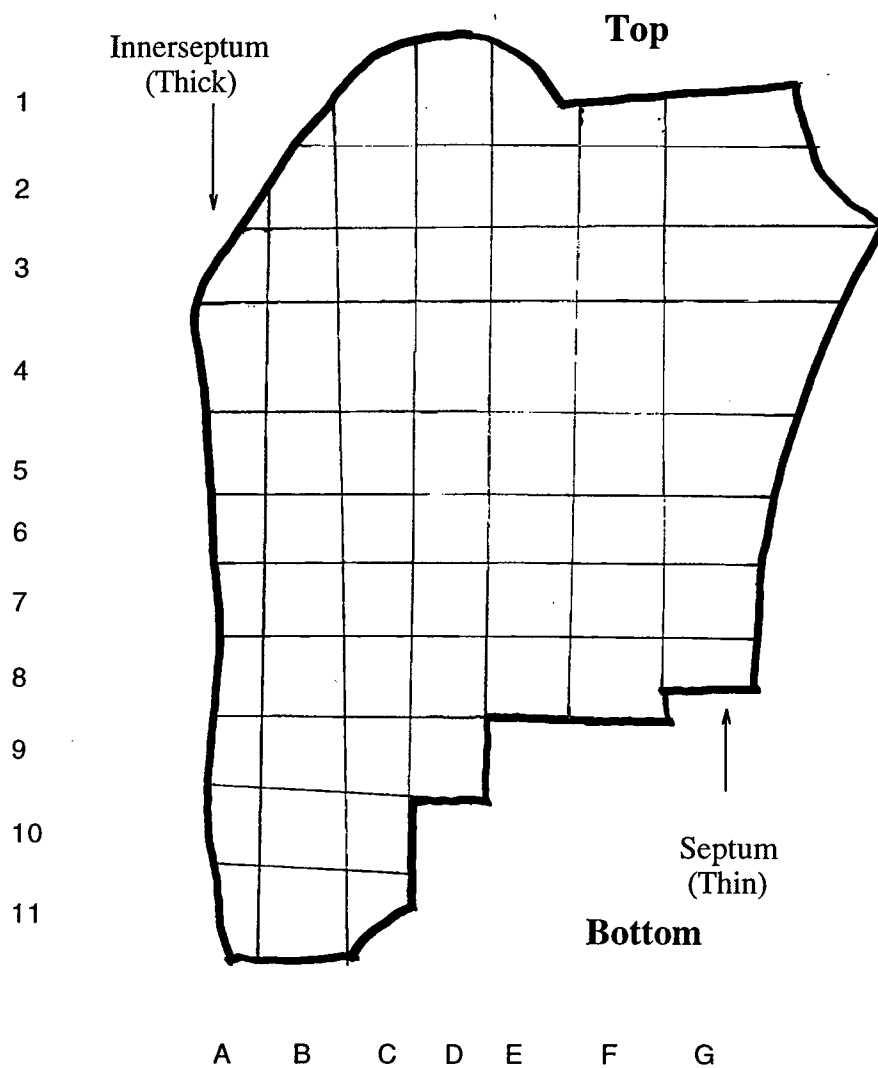


Figure 5.14. Sampling pattern used in the single septum grid study. Grid squares are 2 mm on each side and were cut with a thin diamond abrasive wheel. The sample is a *D. cristagalli* from 650 meters depth in a Chilean fjord.

thickness depending on their location on the coral. Thickest samples came from the innerseptal, or outer rim, aragonite while samples from near the polyp cavity were much thinner.

After sampling, all coral was pre-cleaned, using the chemical methods described in Chapter 3, and the remaining layers of epoxy were easily peeled off under the microscope. Many samples were large enough so that we could lightly crush them and make triplicate measurements on the fragments. The entire data set is shown in Figure 5.15. As there is no water column data for this fjord, we can not make reliable equilibrium estimates but the slope of $\delta^{18}\text{O}$ vs. $\delta^{13}\text{C}$ is the same as for other *D. cristagalli* specimens. We conclude that the non-open ocean location of this sample is probably not biasing the study's relevance to more "useful" corals. Because there are multiple measurements from many grid points, we can construct a grid of the average $\delta^{18}\text{O}$ value and the variance of $\delta^{18}\text{O}$ within each grid cell (Figure 5.16 and 5.17). These figures need to be interpreted with the caveat that they are highly averaged. Eleven of the fifty-eight total cells had one or zero data points (see Appendix) and values had to be kriged in between data gaps to use the plotting program. Therefore only the large scale trend in the data can be faithfully interpreted. Heaviest values of $\delta^{18}\text{O}$ are found near the top and septal edges of the coral. These are the thinnest and most recently precipitated portions of the sample. The grid point standard deviation data show that these areas are also the most homogenous in their isotopic value. On average, $\delta^{18}\text{O}$ decreases in absolute value and becomes more scattered the further away from the thin edges.

With the micro-sampling technology developed by K. C. Lohman [Dettman and Lohmann, 1993] and its implementation at WHOI for mollusc shells by Dr. Chris Weidman [Weidman et al., 1994], we can investigate the spatial variation of stable isotopes in *D. cristagalli* at the tens of microns level. Septa from sample number 47407 were cut, mounted to glass slides and imaged as described in Chapter 1. We made slides from both a "top view" and a "side view" perspective. Images from these slides (Figures

Chilean Single Septum Isotopes

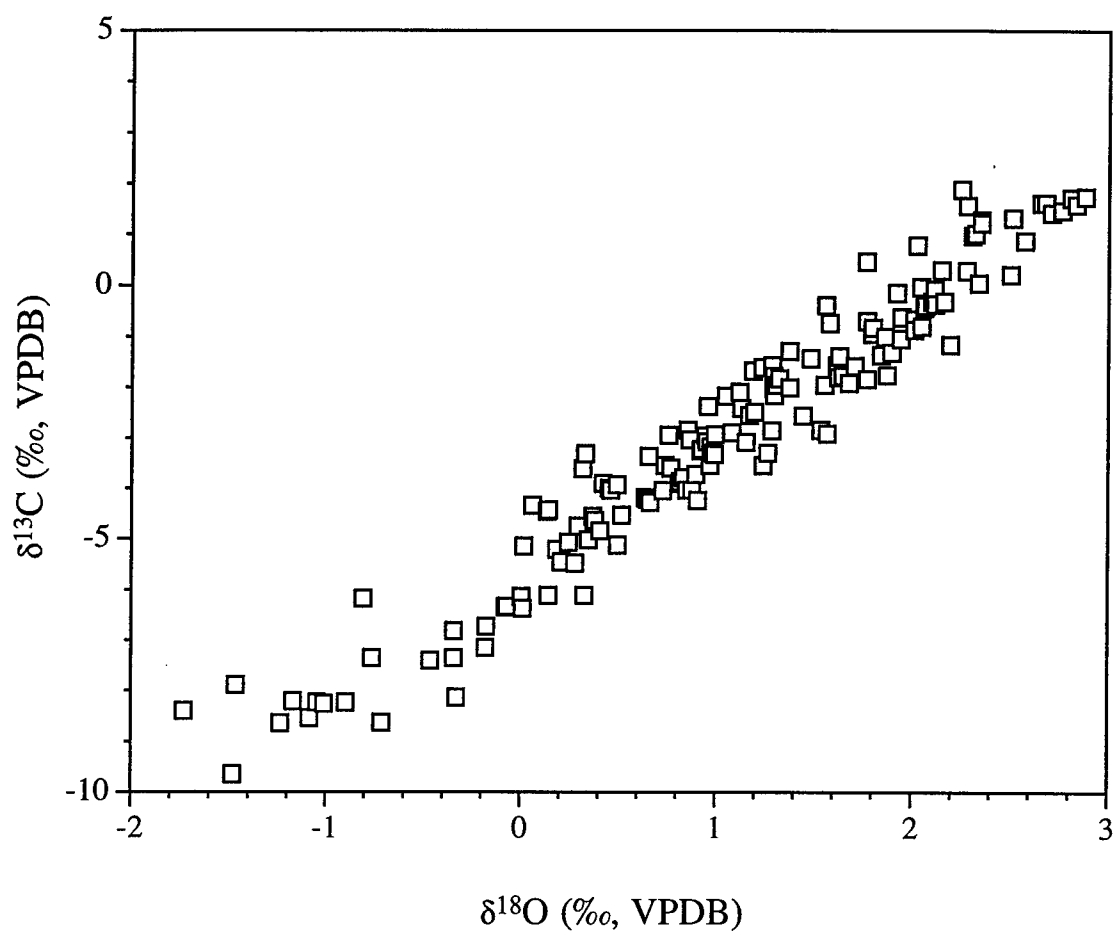


Figure 5.15. All stable isotope data from the single septum grid study. This slope in the range of that found for all other samples.

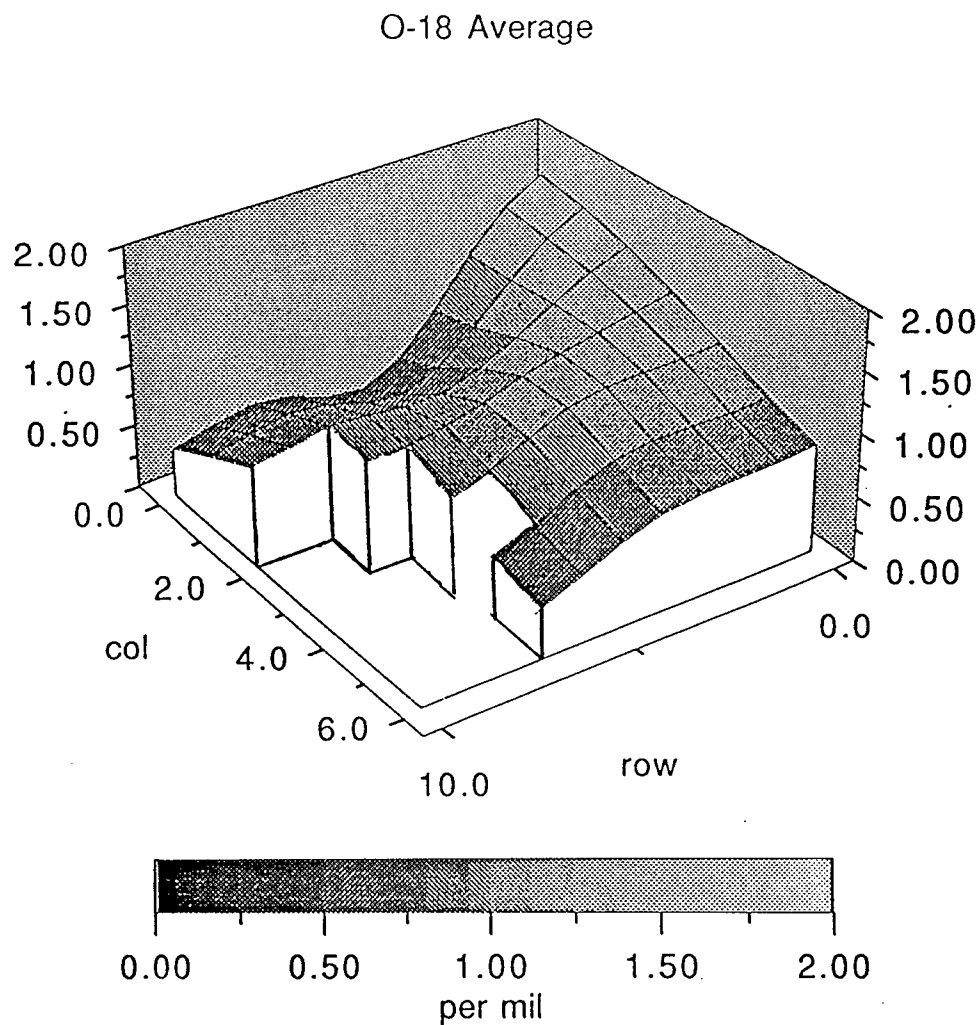


Figure 5.16. Average of $\delta^{18}\text{O}$ replicates in each grid cell from the single septum *D. cristagalli* study. Row one and column A were left out because of large sample gaps. Other gaps were filled in by kriging the data before plotting.

O-18 Standard Deviation

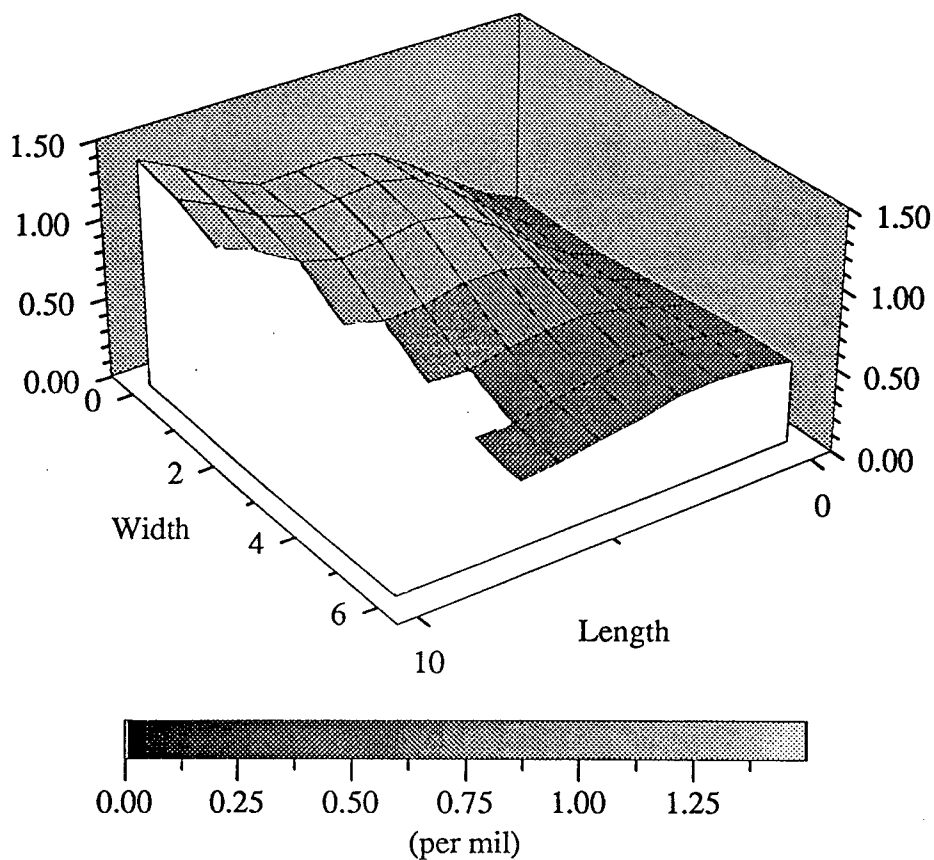


Figure 5.17. Standard deviation of $\delta^{18}\text{O}$ replicates in each grid cell from the single septum *D. cristagalli* study. Row one and column A were left out because of large sample gaps. Other gaps were filled in by kriging the data before plotting.

5.18, 5.19 and 5.21) were digitized and used to drive the computer controlled sampling pattern. Our strategy was to sample normal to the banding pattern with the miniature cutting tool. This three sided aluminum tool mills out CaCO_3 dust as it moves along an edge of the sample. Initially we ease the tool into the resin to the side of the sample and then slowly work our way to the edge of the coral. Once the tool is cutting only coral, we collect each pass until there is enough material for a stable isotope sample. Depending on the length of each pass, this technique can give us a sampling resolution of under 50 microns. In this manner, we collect all of the aragonite along a single path.

We generated two data sets from the top view sample; an innerseptal transect (Figure 5.18) and a septal transect (Figure 5.19). Both transects show a remarkable consistency between the banding pattern and the $\delta^{18}\text{O}$ value. Heaviest values are associated with dark coral bands and light values are associated with light bands. In these figures, light bands are optically dense while dark bands are areas where more light from the enlarger could pass through the sample. The very light central band, corresponding to the first aragonite precipitated, consistently shows the furthest offset from isotopic equilibrium. In Figure 5.18 there is an area where the large S1 septum and a secondary (S2) septum "interfere". This is also an area of less structured $\delta^{18}\text{O}$. Data from the septal transect (Figure 5.19) are about 0.5‰ heavier at their peak than the dark bands in the innerseptal transect. This difference between skeletal components is the same type of distinction we noted in the size fraction studies described above. When plotted as $\delta^{18}\text{O}$ vs. $\delta^{13}\text{C}$ (Figure 5.20), we can see that the heaviest values on the septal portion are at $\delta^{18}\text{O}$ equilibrium. Because this sample comes from a relatively shallow depth in the polar frontal zone of the Pacific sector of the Southern Ocean, the error bars on the equilibrium estimate are large. The dark bands on the thin part of the S1 septa represent aragonite that was precipitated at equilibrium with ambient seawater. Because we can trace these bands from the bottom of the coral to the top (Chapter 1), they represent a potential sampling strategy for obtaining high resolution time series of past deep water mass behavior.

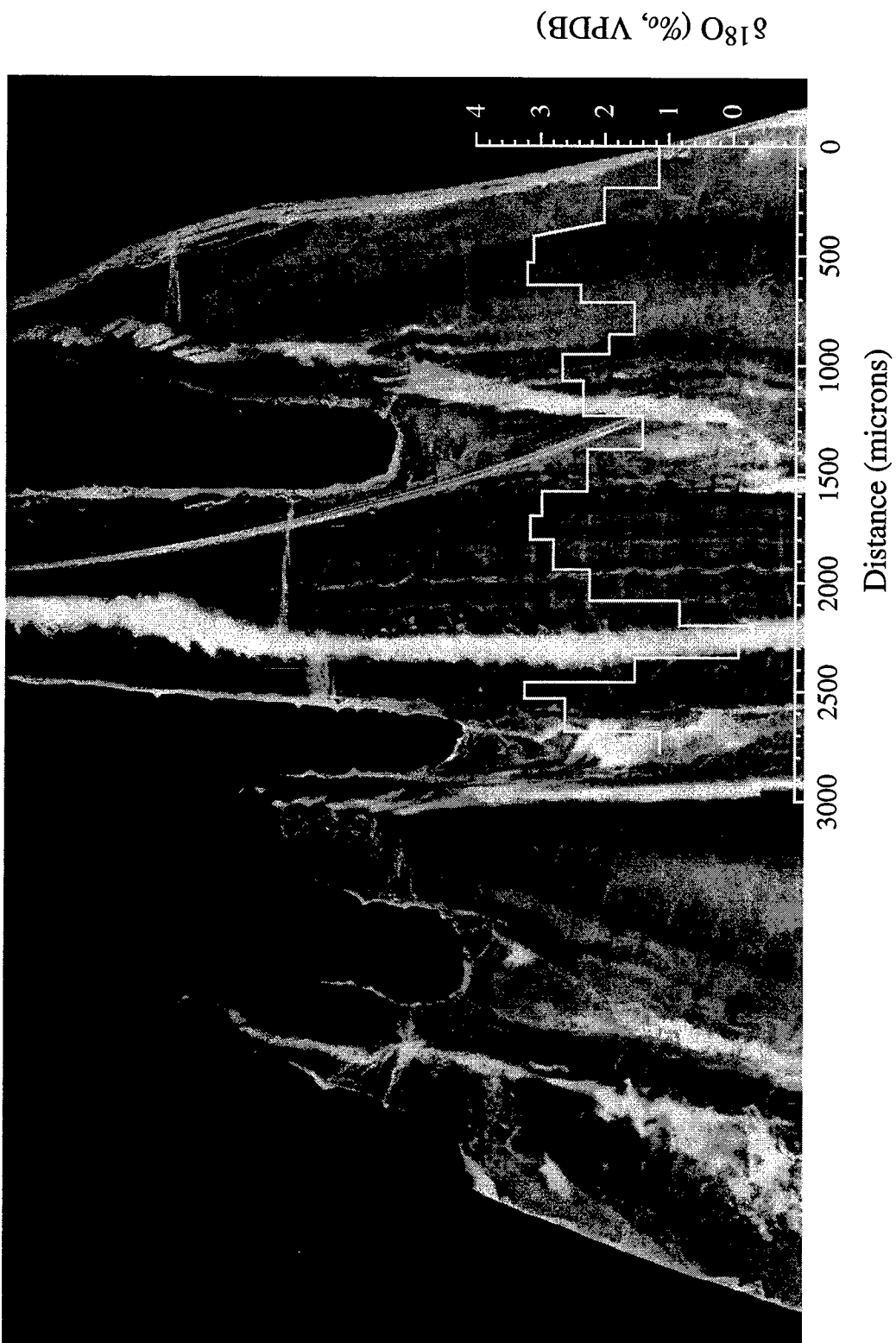


Figure 5.18. Banding and $\delta^{18}\text{O}$ in *D. cristagalli* sample 47407G. Sample is about 230 μm thick and mounted to a glass slide. Dark bands correspond to heavy isotope values and light bands to light values.

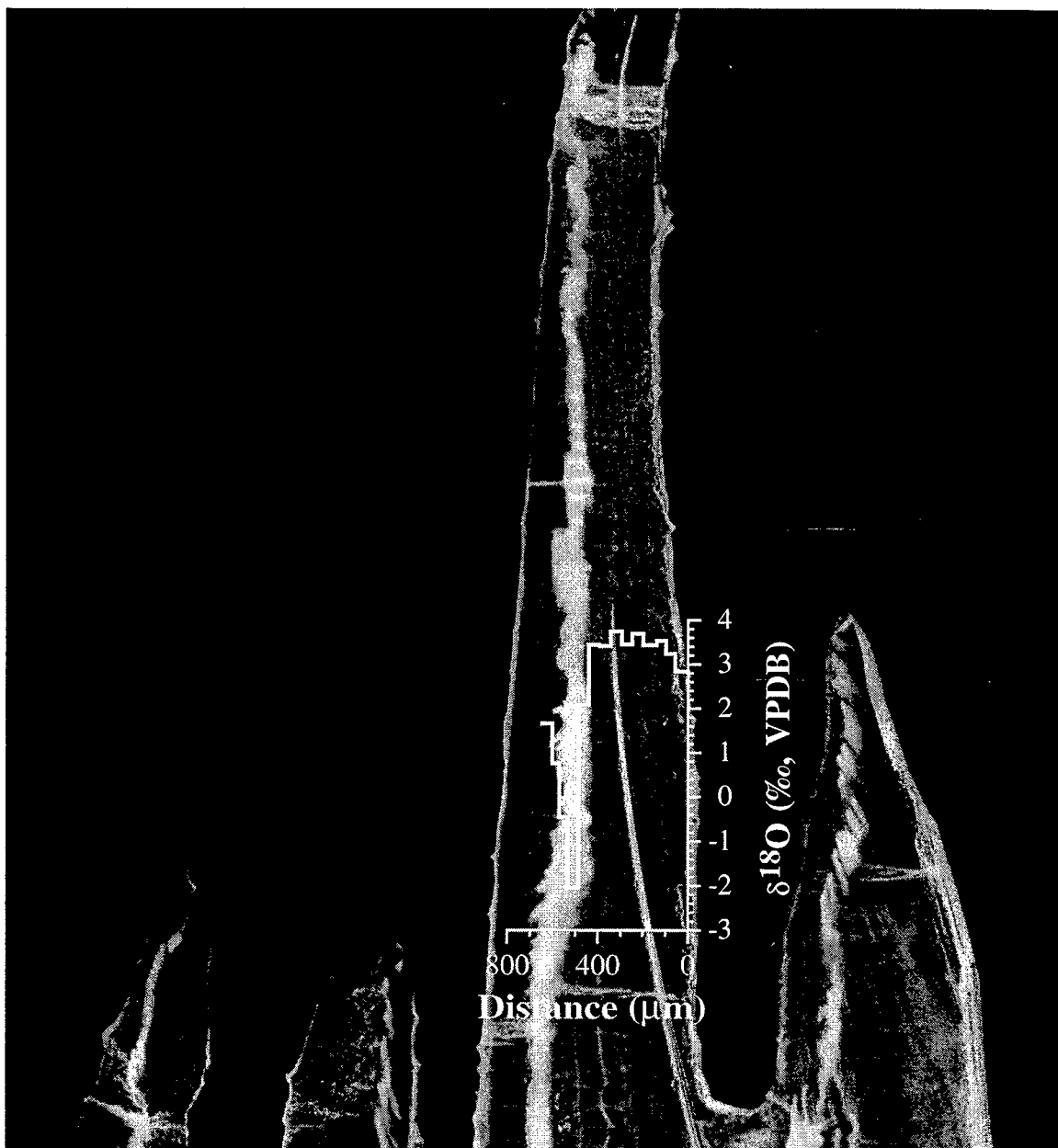


Figure 5.19. Banding with $\delta^{18}\text{O}$ on sample 47407G septal. This *D. cristagalli* sample is 230 μm thick and mounted on a glass slide. The dark band is at $\delta^{18}\text{O}$ equilibrium with the ambient seawater.

47407 Micro-Sampling Isotopes

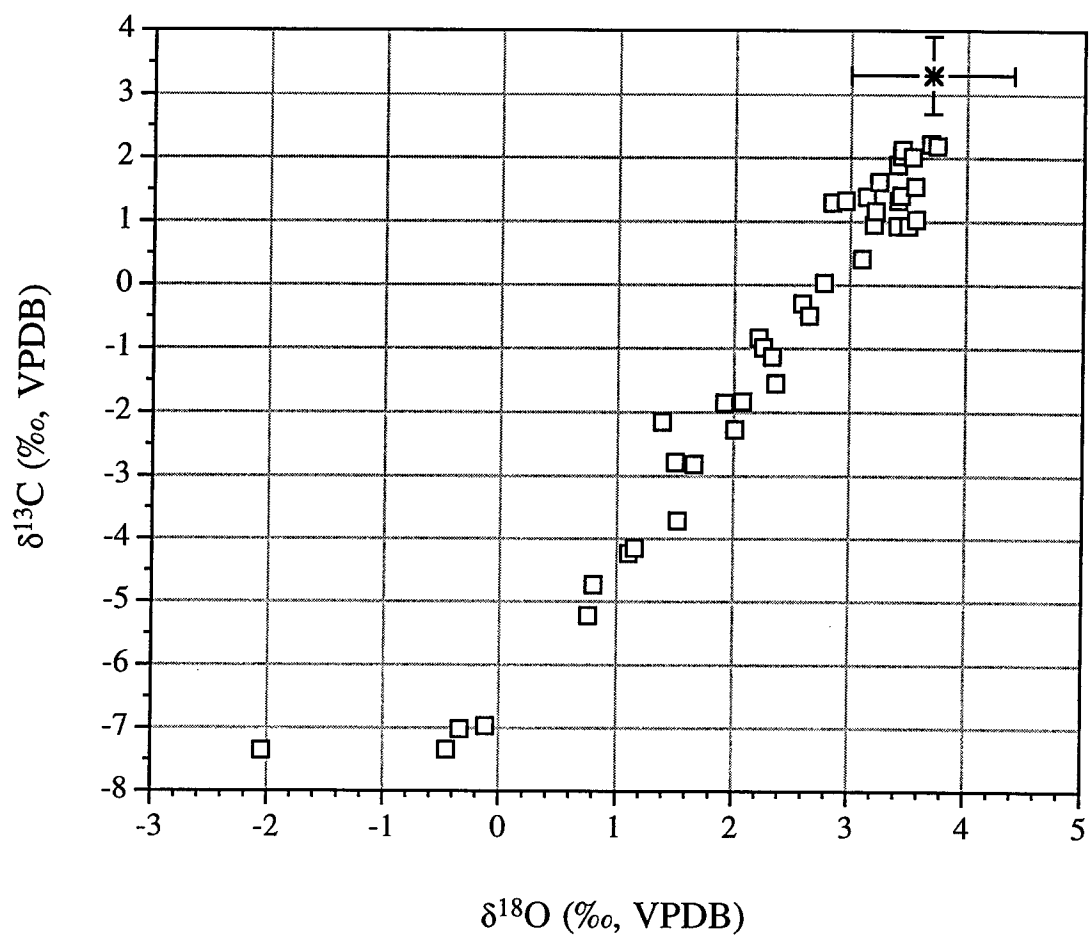


Figure 5.20. All stable isotope data from micro-sampling of *D. cristagalli* sample 47407. The heaviest samples are at $\delta^{18}\text{O}$ equilibrium.



Figure 5.21. Front View of sample 47407-2A. White dots are the control points programed into the micro-sampler. White lines connect the dots of the first and last path in the direction the sampler moved. The sampler moved parallel to the banding in order to generate an overall transect normal to the banding. These points were used to digitally sample the image for the gray scale along $\delta^{18}\text{O}$ sampling paths. The combined gray scale and $\delta^{18}\text{O}$ plots are shown in Figure 5.22.

We also micro-sampled this same specimen, but not the same septum, normal to the top view discussed above. This side view sample is pictured in Figure 5.21 with the digitized points, used to guide the micro-sampler, shown as white dots. The sampler moved from dot to dot as shown by the two white lines. Sampling lines were cut normal to the banding pattern so that an isotope sample contained as much coral of the same density as possible. As can be seen from the figure, there are gradients in gray across any one sample line and certainly along adjacent lines. For this reason and the angle of the growth lines, we did not plot the $\delta^{18}\text{O}$ values directly on top of the photograph. Instead, we sampled the image digitally, using the NIH Image program, along the same lines cut for isotopic analysis. These values were averaged and are compared to the $\delta^{18}\text{O}$ data in Figure 5.22. Again there is a clear association between the banding pattern and the isotopic value. The gray scale data was sampled at higher resolution because of both the image pixel density and the fact that we had to combine several cutting tool passes to obtain enough aragonite to run on the mass spectrometer. We seem to have captured a full banding/isotope cycle and the heaviest values are again at equilibrium for $\delta^{18}\text{O}$. If we can establish that these bands are periodic, and at what frequency, the $\delta^{18}\text{O}$ data may be a powerful stratigraphic tool.

The following chapter describes our investigation a *D. cristagalli* sample, JFA 24.8, that grew 15.4 ka ago during a rapid transition in deep circulation structure. In addition to the Cd/Ca and radiocarbon data presented in Chapter 6, we tried to establish the stable isotope variability during this coral's lifetime. Using the method described above, we sampled a septum from JFA 24.8 in the side view sense to expose the full bottom to top growth history. By sampling across the septum, normal to the banding, in three separate places (Figure 5.23), we hoped to capture at least one isotope sample that was not altered by the extensive *D. cristagalli* vital effect. Figure 5.24 shows that, like the modern data, this coral has the lightest isotopic values associated with the light central band. Along each sample line, values decrease nearly monotonically from the edge towards the central

Isotopes and Banding in Sample 47407-2A

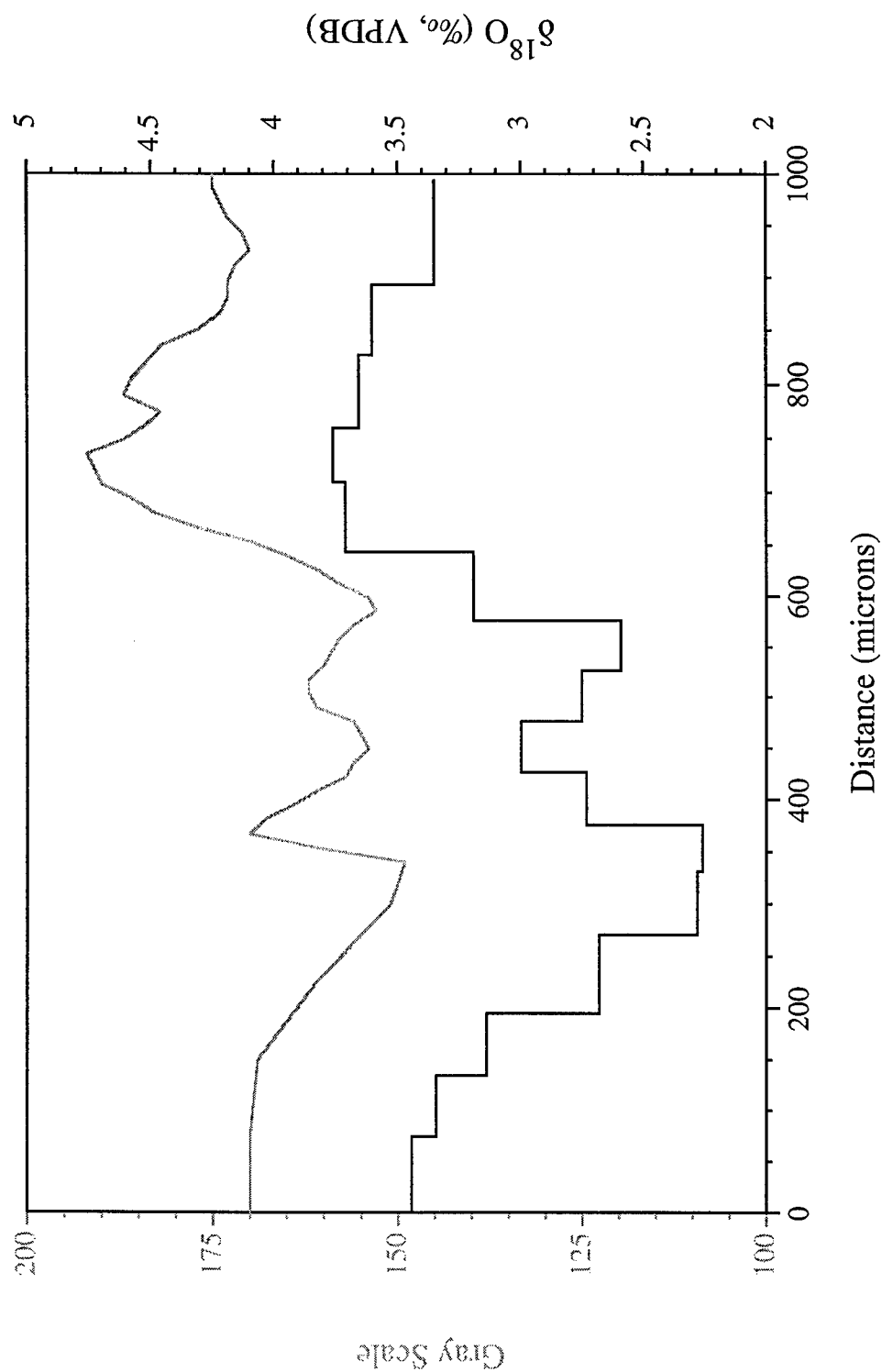


Figure 5.22. Gray scale (0-255, raw data from "normal" gamma-corrected flatbed scanner) and $\delta^{18}\text{O}$ values in the "side view" of sample 47407-2A. Stable isotopes are sampled at lower resolution than the gray scale data.

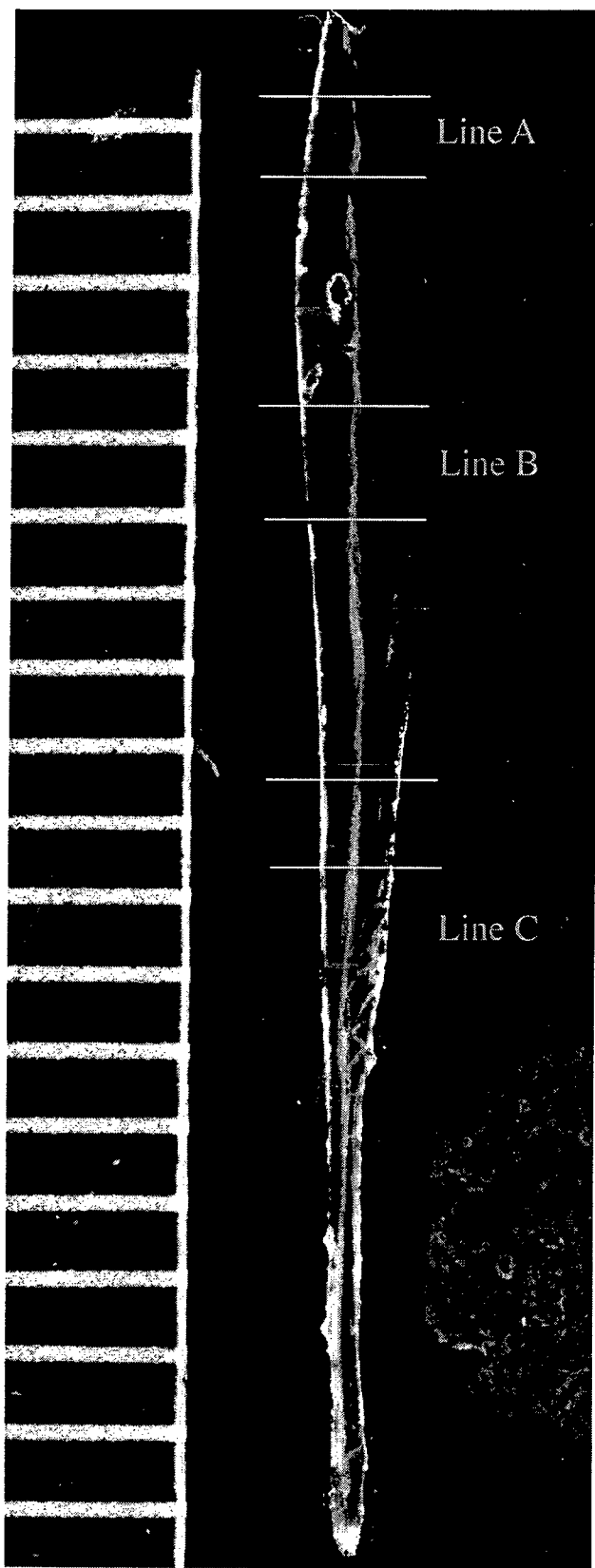


Figure 5.23. Sampling bands for stable isotopes on sample JFA 24.8. Line C contains the oldest material and Line A the youngest. Stable isotope data are shown in Figure 5.24

Stable Isotopes in JFA 24.8

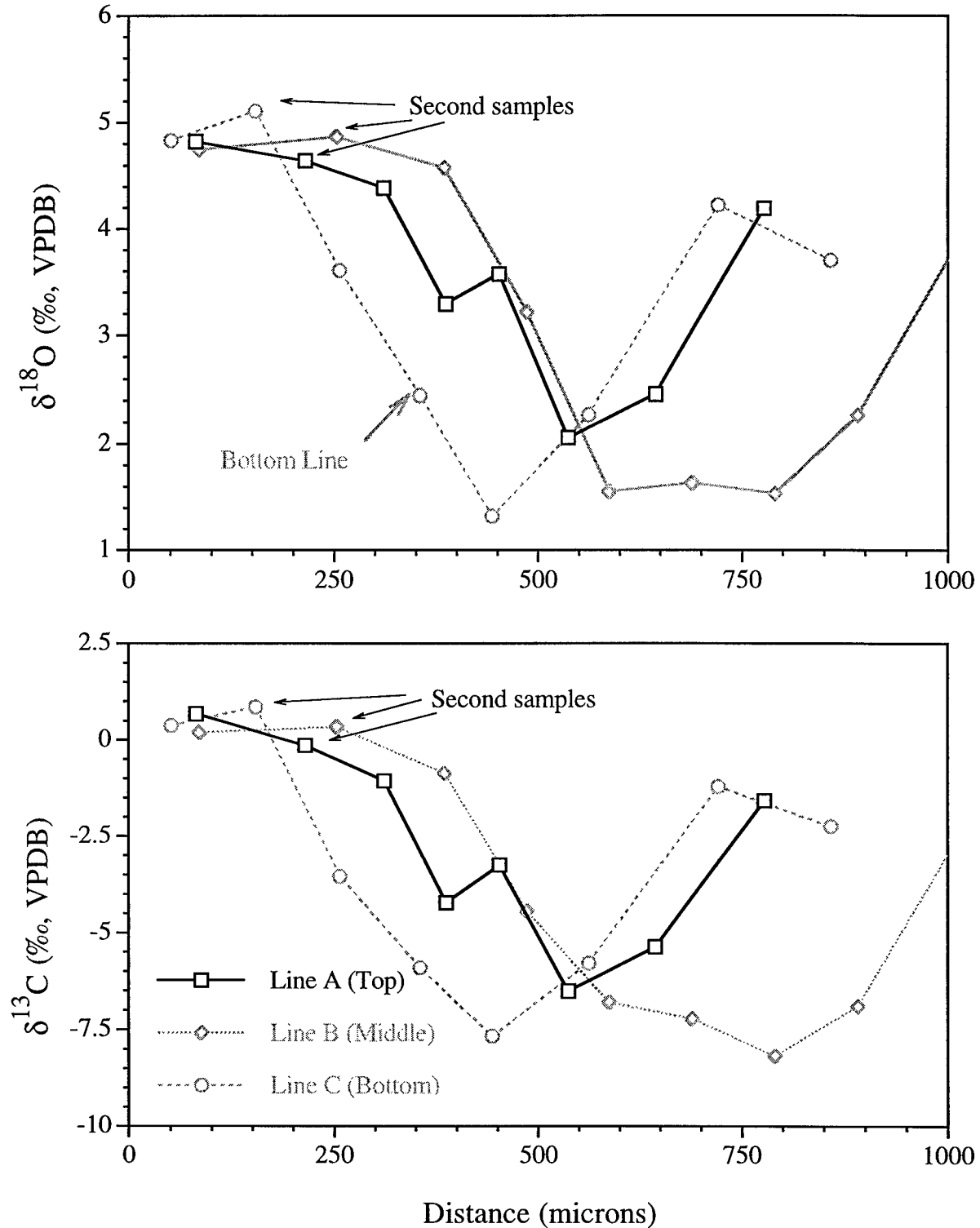


Figure 5.24. Three stable isotope transects on sample JFA 24.8. This 15.4 ka coral from 1784 meters deep in the North Atlantic is shown, in Chapter 6, to grow through a deep circulation transition. Samples are taken across three lines with Line C, the bottom, the oldest and Line A, the top, the youngest.

band. In agreement with our "stacked chevrons" model of *D. cristagalli* growth (Chapter 1), the first isotopic values of all three lines are the same. These are most likely contemporaneous samples. However, just inside the left hand edge, the aragonite at the bottom should be older than the aragonite at the top. Comparison of the second samples (from the left) in each transect shows a decrease in both $\delta^{18}\text{O}$ and $\delta^{13}\text{C}$ from bottom to top. Given the sampling resolution, there is no way to be sure that these second samples are unaffected by the coral's vital effect. We can not even say if they are all affected to the same degree. However, the $\delta^{13}\text{C}$ decrease is consistent with the water mass aging implied by the Cd/Ca and ^{14}C data in Chapter 6. $\delta^{18}\text{O}$ values indicate that the water bathing the coral became progressively warmer or fresher. On this small sample we do not have the spatial resolution to find true maxima in $\delta^{18}\text{O}$ and $\delta^{13}\text{C}$ that we can confidently attribute to a pure seawater influence.

Conclusions

Individual samples of *D. cristagalli* all show a strong linear relationship between $\delta^{18}\text{O}$ and $\delta^{13}\text{C}$. The slope of this trend is consistent between samples and across genera. In agreement with previous studies, this vital effect seems to have a small contribution, less than 8%, from isotopically light metabolic CO_2 . Some of the data implies no effect at all. In light of this constraint, some other mechanism for consistent $\delta^{13}\text{C}$ and $\delta^{18}\text{O}$ fractionations needs to be discovered. Micro-sampling of *D. cristagalli* shows that the optically dense initial aragonite is furthest out of equilibrium for $\delta^{18}\text{O}$ and $\delta^{13}\text{C}$. Optically less dense bands from the thin septum seem to capture equilibrium values for $\delta^{18}\text{O}$. A top to bottom transect of these bands is a possible means to generate paleo-time series of $\delta^{18}\text{O}$.

References

- Broecker, W. S., Oxygen isotope constraints on surface ocean temperature, *Quaternary Research*, 26, 121-134, 1986.
- Buddemeier, R. W., J. E. Maragos and D. W. Knutson, Radiographic studies of reef coral exoskeletons: rates and patterns of coral growth., *Journal of Experimental Marine Biology and Ecology*, 14, 179-200, 1974.
- Cole, J., E., R. Fairbanks G. and G. Shen T., Recent variability in the Southern Oscillation: isotopic records from a Tarawa Atoll coral, *Science*, 260, 1790-1793, 1993.
- Craig, H., Isotopic standards for carbon and oxygen and correction factors for mass-spectrometric analysis of carbon dioxide, *Geochimica et Cosmochimica Acta*, 12, 133-149, 1957.
- Dettman, D. L. and K. C. Lohmann, *Seasonal change in Paleogene surface water $\delta^{18}O$: fresh-water bivalves of western North America*, Climate Change in Continental Isotopic Records, 153-163, 1993.
- Dodge, R. and J. Thomson, The natural radiochemical and growth records in contemporary hermatypic corals from the Atlantic and Caribbean., *Earth and Planetary Science Letters*, 23, 313-322, 1974.
- Dunbar, R. B. and G. M. Wellington, Stable isotopes in a branching coral monitor seasonal temperature variation., *Nature*, 298, 453-455, 1981.
- Duplessy, J.-C., N. J. Shackleton, R. K. Matthews, W. Prell, W. F. Ruddiman, M. Caralp and C. H. Hendy, ^{13}C record of benthic foraminifera in the last interglacial ocean: implications for the carbon cycle and the global deep water circulation, *Quaternary Research*, 21, 225-243, 1984.
- Elderfield, H., C. J. Bertram and J. Erez, A biomineralization model for the incorporation of trace elements into foraminiferal calcium carbonate., *Earth and Planetary Science Letters*, 142, 409-423, 1996.
- Emiliani, C., J. H. Hudson, E. Shinn and R. Y. George, Oxygen and carbon isotopic growth record in a reef coral from the Florida Keys and a deep-sea coral from Blake Plateau, *Science*, 202, 627-629, 1978.
- Fairbanks, R. G. and R. E. Dodge, Annual periodicity of the $^{18}O/^{16}O$ and $^{13}C/^{12}C$ ratios in the coral *Montastrea annularis*., *Geochimica et Cosmochimica Acta*, 43, 1009-1020, 1979.
- Gagan, M. K., A. R. Chivas and P. J. Isdale, High-resolution isotopic records from coral using ocean temperature and mass-spawning chronometers., *Earth and Planetary Science Letters*, 121, 549-558, 1994.
- Grossman, E. L. and T.-L. Ku, Oxygen and carbon isotope fractionation in biogenic aragonite: temperature effects., *Chemical Geology*, 59, 59-74, 1986.

- Knutson, D. W., R. W. Buddemeier and S. V. Smith, Coral chronometers: seasonal growth bands in reef corals, *Science*, 177, 270-272, 1972.
- Land, L. S., J. C. Lang and D. J. Barnes, On the stable carbon and oxygen isotopic composition of some shallow water, ahermatypic, scleractinian coral skeletons, *Geochimica et Cosmochimica Acta*, 41, 169-172, 1977.
- McConnaughey, T., ^{13}C and ^{18}O isotopic disequilibrium in biological carbonates: I. Patterns, *Geochimica et Cosmochimica Acta*, 53, 151-162, 1989.
- McConnaughey, T., C^{13} and O^{18} isotopic disequilibrium in biological carbonates: II. In vitro simulation of kinetic isotope effects., *Geochimica et Cosmochimica Acta*, 53, 163-171, 1989.
- McConnaughey, T. A., J. Burdett, J. F. Whelan and C. K. Paull, Carbon isotopes in biological carbonates: Respiration and photosynthesis, *Geochimica et Cosmochimica Acta*, 61, 611-622, 1997.
- Mikkelsen, N., E. Erlenzenkeuser, J. S. Killingley and W. H. Berger, Norwegian corals: Radiocarbon and stable isotopes in *Lophelia pertusa*, *Boreas*, 11, 163-171, 1982.
- Moore, W. S. and S. Krishnaswami, Coral growth rates using ^{228}Ra and ^{210}Pb ., *Earth and Planetary Science Letters*, 15, 187-190, 1972.
- Moore, W. S., S. Krishnaswami and S. G. Bhat, Radiometric determinations of coral growth rates., *Bulletin of Marine Science*, 23, 157-176, 1973.
- Romanek, C. S., E. L. Grossman and J. W. Morse, Carbon isotopic fractionation in synthetic aragonite and calcite: effects of temperature and precipitation rate., *Geochimica et Cosmochimica Acta*, 56, 419-430, 1992.
- Smith, J. E., M. Risk J., H. P. Schwarcz and T. A. McConnaughey, Rapid climate change in the North Atlantic during the Younger Dryas recorded by deep-sea corals, *Nature*, 386, 818-820, 1997.
- Smith, J. E., H. P. Schwarcz, M. J. Risk, T. McConnaughey and N. Keller, Deep-sea corals as paleotemperature indicators: overcoming 'vital effects'. *Geochimica et Cosmochimica Acta*, Submitted, 1997.
- ter Kuile, B. and J. Erez, Mechanism for the uptake of inorganic carbon by two species of symbiont-bearing foraminifera., *Mar. Biol.*, 103, 241-251, 1989.
- Vogel, J. C., P. M. Grootes and W. G. Mook, Isotope fractionation between gaseous and dissolved carbon dioxide., *Z. Phys.*, 230, 225-238, 1970.
- Weber, J. N., Deep-sea ahermatypic scleractinian corals: isotopic composition of the skeleton, *Deep-Sea Research*, 20, 901-909, 1973.
- Weber, J. N. and D. M. Raup, Fractionation of the stable isotopes of carbon and oxygen in marine calcareous organisms-the Echinoidea. Part I. Variation of ^{13}C and ^{18}O content within individuals., *Geochimica et Cosmochimica Acta*, 30, 681-703, 1966.

- Weber, J. N. and P. M. J. Woodhead, Carbon and oxygen isotope fractionation in the skeletal carbonate of reef-building corals, *Chemical Geology*, 6, 93-117, 1970.
- Weber, J. N. and P. M. J. Woodhead, Temperature dependence of oxygen-18 concentration in reef coral carbonates., *Journal of Geophysical Research*, 77, 463-473, 1972.
- Weidman, C. R., G. A. Jones and K. C. Lohmann, The long lived mollusc *Arctica islandica*: a new paleoceanographic tool for the reconstruction of bottom temperatures for the continental shelves of the northern North Atlantic Ocean., *Journal of Geophysical Research*, 99, 18,305-18,314, 1994.
- Zhang, J., P. D. Quay and D. O. Wilber, Carbon isotope fractionation during gas-water exchange and dissolution of CO₂., *Geochimica et Cosmochimica Acta*, 59, 107-114, 1995.

Table A5.1: *D. Cristagalli* Sample #78459

WHOI Spec. #	Size (μm)	Position	Line	wt. (μg)	Pressure (μatm)		% Reaction	$\delta^{18}\text{O}$		$\delta^{13}\text{C}$	
					measured	calculated		per mil	error	per mil	error
18244	>600	septal	A	835	1529	2433	63%	3.321	0.017	-0.449	0.008
18247	>600	septal	B	404	1453	1703	85%	2.712	0.017	-1.948	0.008
18246	>600	septal	A	438	1439	1708	84%	1.824	0.017	-3.449	0.008
18249	425-600	septal	B	260	1173	1350	87%	2.444	0.011	-2.701	0.007
18248	425-600	septal	A	160	889	983	90%	2.991	0.018	-1.855	0.009
18251	425-600	septal	B	272	1243	1382	90%	2.948	0.021	-1.800	0.010
18250	250-425	septal	A	88	694	708	98%	2.376	0.010	-2.232	0.009
18253	250-425	septal	B	54	617	589	105%	2.470	0.021	-2.958	0.013
18252	250-425	septal	A	94	703	734	96%	2.401	0.004	-2.353	0.010
18255	63-250	septal	B	137	933	963	97%	2.180	0.008	-3.007	0.004
18254	63-250	septal	A	81	685	677	101%	1.687	0.004	-4.320	0.012
18257	63-250	septal	B	81	701	729	96%	2.277	0.008	-3.005	0.006
18256	<63	septal	A	22	247	331	75%	2.297	0.026	-2.569	0.014
18259	<63	septal	B	10	119	242	49%	Bellows not balanced			
18258	>600	inseptal	A	726	1479	2253	66%	2.249	0.012	-3.354	0.008
18261	>600	inseptal	B	408	1463	1712	85%	1.789	0.015	-4.729	0.011
18260	>600	inseptal	A	641	1459	2104	69%	1.063	0.003	-5.598	0.007
18263	425-600	inseptal	B	280	1333	1404	95%	0.181	0.014	-7.254	0.021
18262	425-600	inseptal	A	175	929	1033	90%	0.882	0.010	-6.515	0.008
18265	425-600	inseptal	B	249	1263	1319	96%	0.609	0.013	-6.804	0.024
18266	250-425	inseptal	A	34	407	421	97%	0.950	0.043	-6.221	0.011
18269	250-425	inseptal	B	52	578	577	100%	2.301	0.017	-3.025	0.011
18268	250-425	inseptal	A	69	243	620	39%	1.006	0.066	-6.591	0.046
18271	63-250	inseptal	B	53	715	583	123%	0.939	0.009	-6.162	0.003
18270	63-250	inseptal	A	36	406	434	94%	1.619	0.030	-4.283	0.021
18273	63-250	inseptal	B	144	1053	988	107%	1.018	0.011	-5.987	0.010
18272	<63	inseptal	A	173	1029	1026	100%	1.174	0.017	-5.213	0.003
18275	<63	inseptal	B	95	766	793	97%	1.271	0.014	-5.135	0.014
18274	<63	inseptal	A	72	647	635	102%	1.062	0.013	-5.524	0.017
18277	<63	septal	B	18	270	330	82%	2.162	0.029	-2.908	0.014

Table A5.2: *D. Cristagalli* Sample #84820

WHOI Spec. #	Size (μm)	Position	Line	wt. (μg)	Pressure (μatm)		% Reaction	$\delta^{18}\text{O}$		$\delta^{13}\text{C}$	
					measured	calculated		per mil	error	per mil	error
18290	>600	septal	A	272	1119	1315	76%	2.806	0.014	-1.592	0.005
18291	>600	septal	B	447	1483	1797	61%	2.767	0.014	-1.750	0.010
18292	>600	septal	A	334	1259	1472	73%	2.888	0.013	-0.805	0.007
18293	425-600	septal	B	120	784	898	87%	2.642	0.005	-1.968	0.011
18294	425-600	septal	A	79	697	668	107%	2.543	0.021	-2.606	0.006
18295	425-600	septal	B	68	671	665	103%	2.581	0.017	-2.082	0.010
18296	250-425	septal	A	68	638	615	105%	3.456	0.020	0.086	0.004
18297	250-425	septal	B	24	377	384	85%	3.129	0.039	-0.300	0.011
18298	250-425	septal	A	43	485	478	97%	2.844	0.052	-0.151	0.013
18299	63-250	septal	B	53	624	583	107%	3.054	0.011	-0.915	0.015
18300	63-250	septal	A	58	607	564	108%	2.910	0.012	-0.906	0.007
18301	63-250	septal	B	23	328	375	74%	2.926	0.021	-0.962	0.018
18302	<63	septal	A	21	267	323	65%	2.962	0.071	-0.793	0.021
18311	<63	septal	B	76	711	705	103%	3.048	0.013	-0.689	0.011
18304	<63	septal	A	41	15	466	3%	Bellows not balanced			
18313	>600	inseptal	B	539	1523	1983	53%	3.645	0.011	-0.027	0.010
18305	>600	inseptal	A	228	1059	1194	83%	1.978	0.010	-3.829	0.005
18315	>600	inseptal	B	337	1443	1548	75%	2.457	0.016	-3.075	0.020
18306	425-600	inseptal	A	140	787	914	87%	2.928	0.005	-1.073	0.012
18317	425-600	inseptal	B	133	953	948	99%	1.424	0.018	-5.264	0.013
18308	425-600	inseptal	A	169	909	1013	87%	2.886	0.014	-1.601	0.009
18321	250-425	inseptal	B	57	616	606	102%	3.589	0.014	0.917	0.011
19309	250-425	inseptal	A	28	318	378	73%	1.518	0.047	-4.335	0.011
18323	250-425	inseptal	B	38	503	489	98%	2.857	0.012	-0.830	0.013
18310	63-250	inseptal	A	53	573	536	106%	3.019	0.027	-0.773	0.011
18325	63-250	inseptal	B	34	464	461	94%	3.111	0.047	-1.042	0.020
18312	63-250	inseptal	A	52	562	531	104%	2.939	0.048	-1.325	0.010
18327	<63	inseptal	B	87	749	758	101%	2.858	0.011	-1.461	0.004
18314	<63	inseptal	A	56	593	553	107%	2.869	0.016	-1.377	0.013
18328	<63	inseptal	B	84	749	744	103%	2.913	0.015	-1.314	0.019

Table A5.3: *D. Cristagalli* Sample #84820 (pre-cleaned)

WHOI Spec. #	Size (μm)	Line	wt. (μg)	Pressure (μatm)		% Reaction	$\delta^{18}\text{O}$		$\delta^{13}\text{C}$	
				measured	calculated		per mil	error	per mil	error
18276	>600	A	353	1319	1517	87%	3.077	0.010	-0.463	0.009
18279	>600	B	344	1483	1565	95%	2.845	0.008	-1.252	0.009
18278	>600	A	199	1119	1108	101%	2.542	0.007	-2.236	0.009
18281	425-600	B	133	923	948	97%	2.418	0.014	-2.355	0.014
18280	425-600	A	123	796	851	94%	1.677	0.014	-4.393	0.010
18283	425-600	B	203	1103	1185	93%	3.321	0.007	-0.036	0.004
18316	250-425	A	51	537	525	102%	2.192	0.017	-2.592	0.006
18329	250-425	B	54	617	589	105%	2.407	0.018	-2.025	0.004
18318	250-425	A	79	684	668	102%	2.902	0.011	-0.843	0.005
18330	63-250	B	36	491	476	103%	2.520	0.016	-2.126	0.005
18320	63-250	A	22	252	331	76%	Bellows not balanced		-2.026	0.014
18331	63-250	B	46	588	541	109%	2.487	0.020	-2.197	0.006

Table A5.4: Carrera Marble Data

WHOI	Size	Line	wt.	Pressure (μatm)		%	$\delta^{18}\text{O}$		$\delta^{13}\text{C}$	
Spec. #	(μm)		(μg)	measured	calculated	Reaction	per mil	error	per mil	error
20076	>325	A	80	694	672	103%	-1.883	0.023	2.086	0.008
20077	>325	B	103	666	828	80%	-1.951	0.006	1.806	0.008
20078	>325	A	58	545	564	97%	-1.868	0.014	2.111	0.013
20079	>325	B	49	537	560	96%	-2.005	0.016	2.051	0.016
20080	177-325	A	99	709	756	94%	-1.840	0.018	2.086	0.015
20081	177-325	B	45	530	535	99%	-1.963	0.018	2.071	0.024
20082	177-325	A	52	508	531	96%	-1.838	0.022	2.093	0.006
20083	63-177	B	56	608	600	101%	-1.964	0.013	2.072	0.008
20084	63-177	A	78	698	663	105%	-1.875	0.020	2.083	0.001
20085	63-177	B	81	741	729	102%	-1.929	0.007	2.073	0.011
20086	25-63	A	41	549	466	118%	-1.910	0.007	2.121	0.014
20087	25-63	B	83	727	739	98%	-2.195	0.020	0.390	0.006
20088	25-63	A	65	590	600	98%	-1.905	0.019	2.111	0.009

Table A5.5: Muir Seamount *Lophelia* Data

WHOI Spec. #	Size (μm)	Description	Line	wt. (μg)	Pressure (μatm)		% Reaction	$\delta^{18}\text{O}$		$\delta^{13}\text{C}$	
					measured	calculated		per mil	error	per mil	error
20089	>500	1piece	B	313	1423	1420	100%	2.353	0.013	-4.831	0.018
20090	>500	1piece	A	499	1509	1834	82%	1.556	0.009	-6.761	0.013
20091	>500	1piece	B	203	316	1120	28%	2.754	0.025	-4.512	0.017
20092	425-500	1piece	A	117	263	828	32%	2.035	0.031	-6.485	0.015
20093	425-500	1piece	B	86	758	700	108%	1.141	0.017	-7.475	0.011
20094	425-500	1piece	A	92	740	726	102%	2.198	0.003	-5.501	0.016
20095	300-425	1piece	B	101	801	764	105%	2.372	0.011	-5.335	0.005
20098	300-425	1piece	A	47	561	502	112%	1.706	0.023	-6.369	0.012
20099	300-425	1piece	B	87	771	704	110%	1.281	0.014	-7.037	0.022
20100	180-300	1piece	A	32	400	407	98%	1.205	0.018	-7.227	0.016
20101	180-300	2pieces	B	44	556	484	115%	2.548	0.032	-3.980	0.006
20102	180-300	2pieces	A	86	704	700	101%	1.737	0.014	-6.114	0.019
20103	63-180	many	B	38	513	447	115%	2.515	0.019	-4.374	0.020
20104	63-180	many	A	61	620	579	107%	2.553	0.030	-4.501	0.019
20105	63-180	many	B	81	720	677	106%	2.132	0.009	-5.085	0.012
20106	<63	many	A	78	672	663	101%	2.559	0.015	-4.216	0.003
20107	<63	many	B	50	565	520	109%	2.631	0.017	-4.090	0.007
20108	<63	many	A	79	681	668	102%	2.581	0.014	-4.139	0.007

Table A5.6: Chilean Coral from Reina Adeliada Archipelago

WHOI Spec. #	Sample Number	Line	Grid Position	wt. (μ g)	$\delta^{18}\text{O}$		$\delta^{13}\text{C}$	
					per mil	error	per mil	error
21764	JFA-AJ1A	A	A2	56	2.147	0.009	0.292	0.012
21765	JFA-AJ2A	B	A3	87	2.111	0.022	-0.086	0.010
21766	JFA-AJ2B	A	A3	80	2.061	0.011	-0.436	0.009
21767	JFA-AJ2C	B	A3	28	0.185	0.034	-5.206	0.014
21768	JFA-AJ3A	A	A4	36	0.655	0.061	-3.375	0.021
21769	JFA-AJ3B	B	A4	64	1.283	0.014	-2.854	0.014
21770	JFA-AJ3C	A	A4	55	-0.343	0.016	-7.351	0.019
24856	JFA-AJ4a	A	A5	70	0.326	0.015	-6.116	0.012
24857	JFA-AJ4b	B	A5	31	1.291	0.025	-2.020	0.008
24858	JFA-AJ4c	A	A5	44	0.421	0.019	-3.901	0.012
24859	JFA-AJ5a	B	A7	34	1.120	0.019	-2.091	0.011
24860	JFA-AJ5b	A	A7	72	0.945	0.016	-2.966	0.017
24861	JFA-AJ5c	B	A7	29	0.638	0.025	-4.188	0.020
21771	JFA-AJ6A	B	A8	46	0.379	0.012	-4.627	0.008
21772	JFA-AJ6B	A	A8	62	-1.084	0.012	-8.534	0.020
21773	JFA-AJ6C	B	A8	35	-0.762	0.016	-7.350	0.014
21774	JFA-AJ7A	A	A9	76	0.856	0.017	-2.850	0.012
21775	JFA-AJ8A	B	A10	32	1.128	0.038	-2.410	0.010
21776	JFA-AJ8B	A	A10	60	-1.466	0.022	-7.886	0.026
21777	JFA-AJ8C	B	A10	70	-1.044	0.026	-8.237	0.020
24862	JFA-AJ9a	A	A11	49	-1.730	0.039	-8.395	0.012
24863	JFA-AJ9b	B	A11	46	-0.078	0.007	-6.342	0.017
24864	JFA-AJ9c	A	A11	40	1.051	0.031	-2.170	0.014
21778	JFA-AJ10A	A	B1	40	2.024	0.049	0.782	0.018
24865	JFA-AJ11a	B	B2	33	1.894	0.025	-1.318	0.019
24866	JFA-AJ11b	A	B2	46	2.276	0.025	0.284	0.012
24867	JFA-AJ11c	B	B2	36	2.009	0.040	-0.669	0.026
21779	JFA-AJ12A	B	B3	132	1.873	0.019	-1.765	0.005
21780	JFA-AJ12B	A	B3	66	0.969	0.017	-3.549	0.015
21781	JFA-AJ12C	B	B3	65	1.772	0.018	-0.706	0.009
24868	JFA-AJ13a	A	B4	99	1.239	0.007	-3.549	0.005
24869	JFA-AJ13b	B	B4	28	1.770	0.049	-1.831	0.018
24870	JFA-AJ13c	A	B4	47	Bellows not balanced			
21782	JFA-AJ14A	A	B5	71	-0.464	0.010	-7.399	0.014
21783	JFA-AJ14B	B	B5	67	-0.714	0.024	-8.629	0.016
21786	JFA-AJ14C	A	B5	85	-0.179	0.018	-7.153	0.011
24871	JFA-AJ15a	B	B6	37	-0.178	0.024	-6.721	0.011
24872	JFA-AJ15b	A	B6	40	1.236	0.027	-1.610	0.017
24873	JFA-AJ15c	B	B6	33	Bellows not balanced			
21787	JFA-AJ16A	B	B7	75	-1.011	0.007	-8.253	0.020
21788	JFA-AJ16B	A	B7	56	-0.899	0.014	-8.228	0.014
21789	JFA-AJ16C	B	B7	53	0.876	0.020	-4.038	0.013
24924	JFA-AJ17a	A	B8	70	1.863	0.018	-1.008	0.006
24925	JFA-AJ17b	B	B8	50	2.011	0.009	-0.862	0.008
24926	JFA-AJ17c	A	B8	35	2.305	0.021	0.975	0.004
21790	JFA-AJ18A	A	B9	143	2.161	0.014	-0.323	0.009
21791	JFA-AJ18B	B	B9	109	1.708	0.022	-1.576	0.005
21792	JFA-AJ18C	A	B9	33	-1.480	0.014	-9.652	0.033
24927	JFA-AJ19a	B	B10	47	0.142	0.015	-6.112	0.009
24928	JFA-AJ19b	A	B10	44	2.352	0.046	1.219	0.011
24929	JFA-AJ19c	B	B10	46	1.645	0.014	-1.775	0.005
21793	JFA-AJ20A	B	B11	79	2.832	0.017	1.589	0.009
21794	JFA-AJ20B	A	B11	71	-1.235	0.010	-8.644	0.027
21795	JFA-AJ20C	B	B11	42	0.494	0.008	-5.118	0.015

Table A5.6 (Con't)

WHOI Spec. #	Sample Number	Line	Grid Position	wt. (μ g)	$\delta^{18}\text{O}$		$\delta^{13}\text{C}$	
					per mil	error	per mil	error
21796	JFA-AJ21A	A	C1	33	2.193	0.031	-1.161	0.006
21797	JFA-AJ21B	B	C1	31	2.337	0.030	0.045	0.023
21798	JFA-AJ22A	A	C2	26	1.443	0.041	-2.561	0.020
21799	JFA-AJ22B	B	C2	70	0.010	0.019	-6.365	0.013
21800	JFA-AJ22C	A	C2	27	1.264	0.036	-3.310	0.015
24930	JFA-AJ23a	A	C3	69	-1.171	0.006	-8.206	0.022
24931	JFA-AJ23b	B	C3	45	0.293	0.008	-4.744	0.010
24932	JFA-AJ23c	A	C3	72	-0.332	0.011	-8.131	0.018
21801	JFA-AJ24A	B	C4	31	2.116	0.029	-0.370	0.014
21802	JFA-AJ24B	A	C4	33	Bellows not balanced			
21803	JFA-AJ24C	B	C4	45	2.066	0.028	-0.397	0.011
24933	JFA-AJ25a	B	C5	63	Bellows not balanced			
24934	JFA-AJ25b	A	C5	51	1.631	0.023	-1.385	0.009
24935	JFA-AJ25c	B	C5	34	2.575	0.024	0.867	0.009
21804	JFA-AJ26A	A	C6	32	2.708	0.033	1.415	0.009
21805	JFA-AJ26B	B	C6	113	1.844	0.008	-1.370	0.012
21716	JFA-AJ26C	A	C6	50	2.655	0.022	1.604	0.014
21717	JFA-AJ27A	B	C8	67	1.678	0.011	-1.912	0.012
21718	JFA-AJ28A	A	C9	63	2.512	0.016	1.310	0.009
24874	JFA-AJ29a	A	C10	44	0.459	0.025	-4.033	0.018
24875	JFA-AJ29b	B	C10	54	1.943	0.015	-1.043	0.005
21719	JFA-AJ30A	B	C11	57	1.150	0.008	-3.090	0.009
21720	JFA-AK1A	A	D1	34	2.323	0.033	1.008	0.013
21721	JFA-AK2A	B	D2	53	0.816	0.005	-3.863	0.014
21722	JFA-AK2B	A	D2	70	0.957	0.012	-2.378	0.010
21723	JFA-AK2C	B	D2	41	0.972	0.013	-3.179	0.009
24936	JFA-AK3a	A	D3	35	2.248	0.052	1.874	0.019
24937	JFA-AK3b	B	D3	54	2.043	0.020	-0.036	0.003
24938	JFA-AK3c	A	D3	43	2.278	0.066	1.558	0.012
21724	JFA-AK4A	A	D4	55	1.767	0.034	0.462	0.014
21725	JFA-AK4B	B	D4	32	2.680	0.025	1.604	0.037
21726	JFA-AK4C	A	D4	49	1.561	0.026	-0.391	0.011
24939	JFA-AK5a	B	D5	59	2.878	0.014	1.733	0.006
24940	JFA-AK5b	A	D5	71	2.807	0.018	1.713	0.018
24941	JFA-AK5c	B	D5	34	2.760	0.016	1.464	0.015
21727	JFA-AK6A	B	D6	50	0.905	0.023	-4.242	0.011
24942	JFA-AK7a	A	D8	348	2.045	0.017	-0.799	0.002
21728	JFA-AK8A	A	D9	55	0.140	0.014	-4.433	0.012
21729	JFA-AK8B	B	D9	24	0.896	0.032	-3.731	0.014
21730	JFA-AK8C	A	D9	129	-0.808	0.008	-6.181	0.015
24943	JFA-AK9a	B	E1	66	1.797	0.010	-0.942	0.008
24946	JFA-AK9b	A	E1	36	1.581	0.057	-0.743	0.008
24947	JFA-AK9c	B	E1	76	0.923	0.014	-3.255	0.016
21731	JFA-AK10A	B	E2	66	1.800	0.019	-0.832	0.009
21732	JFA-AK10B	A	E2	44	0.315	0.037	-3.614	0.008
21733	JFA-AK10C	B	E2	69	1.323	0.025	-1.829	0.003
24948	JFA-AK11a	A	E3	38	2.350	0.026	1.283	0.017
24949	JFA-AK11b	B	E3	46	1.945	0.025	-0.621	0.007
24950	JFA-AK11c	A	E3	85	0.768	0.013	-3.597	0.012
21734	JFA-AK12A	A	E4	131	2.100	0.018	-0.320	0.013
21735	JFA-AK12B	B	E4	66	1.168	0.023	-2.556	0.014
21738	JFA-AK12C	A	E4	88	2.503	0.017	0.210	0.006
21739	JFA-AK13A	B	E7	53	0.992	0.021	-3.335	0.013
21740	JFA-AK14A	A	E8	63	-0.343	0.026	-6.818	0.020
21741	JFA-AK14B	B	E8	90	0.005	0.017	-6.139	0.020
21742	JFA-AK14C	A	E8	98	0.275	0.024	-5.478	0.006

Table A5.6 (Con't)

WHOI Spec. #	Sample Number	Line	Grid Position	wt. (μ g)	$\delta^{18}\text{O}$		$\delta^{13}\text{C}$	
					per mil	error	per mil	error
24951	JFA-AK15a	B	F1	54	1.080	0.022	-2.897	0.011
24952	JFA-AK15b	A	F1	38	0.327	0.044	-3.316	0.023
24953	JFA-AK15c	B	F1	27	0.833	0.031	-3.788	0.022
21743	JFA-AK16A	B	F2	79	1.292	0.026	-1.768	0.013
21744	JFA-AK16B	A	F2	54	1.295	0.015	-2.159	0.008
21745	JFA-AK16C	B	F2	36	1.373	0.021	-2.006	0.008
24954	JFA-AK17a	A	F3	73	1.285	0.016	-1.571	0.012
24955	JFA-AK17b	B	F3	70	Bellows not balanced			
24956	JFA-AK17c	A	F3	25	1.187	0.049	-1.669	0.013
21746	JFA-AK18A	A	F4	49	1.923	0.021	-0.147	0.011
21747	JFA-AK18B	B	F4	121	1.618	0.021	-1.566	0.014
21748	JFA-AK18C	A	F4	120	1.624	0.018	-1.798	0.011
24957	JFA-AK19a	B	F5	95	1.556	0.018	-1.946	0.004
24958	JFA-AK19b	A	F5	40	1.482	0.019	-1.430	0.021
24959	JFA-AK19c	B	F5	43	Bellows not balanced			
21749	JFA-AK20A	B	F6	29	0.405	0.022	-4.840	0.018
21750	JFA-AK20B	A	F6	49	0.449	0.030	-3.997	0.013
21751	JFA-AK20C	B	F6	58	0.848	0.016	-4.038	0.021
24960	JFA-AK21a	A	F7	77	0.925	0.009	-3.232	0.014
24961	JFA-AK21b	B	F7	91	0.018	0.006	-5.148	0.008
24962	JFA-AK21c	A	F7	76	0.369	0.012	-4.554	0.010
21752	JFA-AK22A	A	G1	122	0.491	0.019	-3.931	0.010
21753	JFA-AK22B	B	G1	96	1.304	0.019	-1.950	0.036
21754	JFA-AK22C	A	G1	38	1.375	0.062	-1.283	0.013
24963	JFA-AK23a	B	G2	56	1.194	0.022	-2.483	0.010
24964	JFA-AK23b	A	G2	54	0.136	0.025	-4.451	0.016
24965	JFA-AK23c	B	G2	74	0.951	0.021	-3.080	0.019
21755	JFA-AK24A	B	G3	111	0.809	0.007	-3.907	0.006
21756	JFA-AK24B	A	G3	101	0.662	0.005	-4.271	0.013
21757	JFA-AK24C	B	G3	84	0.727	0.014	-4.045	0.010
25145	JFA-AM1a	A	G4	44	0.865	0.013	-3.035	0.011
25146	JFA-AM1b	B	G4	39	0.345	0.036	-5.022	0.018
25147	JFA-AM1c	A	G4	48	0.995	0.011	-2.934	0.012
25148	JFA-AM2a	B	G5	113	0.984	0.012	-3.304	0.009
25149	JFA-AM2b	A	G5	36	0.758	0.068	-2.945	0.018
25150	JFA-AM2c	B	G5	30	-0.072	0.043	-6.334	0.018
25151	JFA-AM3a	A	G6	158	0.208	0.015	-5.448	0.012
25152	JFA-AM3b	B	G6	19	1.535	0.023	-2.842	0.010
25153	JFA-AM3c	A	G6	43	0.739	0.024	-3.543	0.022
25154	JFA-AM4a	B	G7	98	0.516	0.026	-4.535	0.005
25155	JFA-AM4b	A	G7	17	Bellows not balanced			
25156	JFA-AM4c	B	G7	43	1.568	0.058	-2.916	0.013
25157	JFA-AM5a	A	G8	39	0.058	0.055	-4.336	0.014
25158	JFA-AM5b	B	G8	22	0.647	0.022	-4.216	0.020
25159	JFA-AM5c	A	G8	63	0.242	0.007	-5.072	0.007

Table A5.7: Sample 47407G Innerseptal Micro-sampling

WHOI Spec. #	Sample Number	Line	Distance (μm)	wt. (μg)	$\delta^{18}\text{O}$		$\delta^{13}\text{C}$	
					per mil	error	per mil	error
33520	1.6	A	0	54	1.153	0.024	-4.146	0.021
			189					
33522	1.7	A	189	61	2.007	0.029	-2.271	0.027
			348					
33528	1.9	A	410	41	3.099	0.058	0.413	0.015
			531					
33526	1.10	A	531	56	3.201	0.047	0.953	0.013
			634					
33529	1.11	B	634	56	2.363	0.018	-1.544	0.009
			711					
33530	1.12	A	711	113	1.525	0.024	-3.706	0.013
			858					
33531	1.13	B	858	42	1.92	0.031	-1.85	0.018
			948					
33532	1.14	A	948	97	2.649	0.036	-0.486	0.008
			1071					
33533	1.15	B	1071	76	2.326	0.036	-1.131	0.03
			1233					
33534	1.16	A	1233	60	1.385	0.013	-2.148	0.017
			1386					
33535	1.17	B	1386	78	2.253	0.012	-0.984	0.015
			1580					
33536	1.18	A	1580	60	2.959	0.071	1.334	0.028
			1690					
33537	1.19	B	1690	72	3.139	0.011	1.395	0.008
			1801					
33538	1.20	A	1801	77	2.776	0.053	0.036	0.006
			1940					
33539	2.4	B	1940	71	2.21	0.02	-0.834	0.01
			2081					
33542	2.5	A	2081	67	0.802	0.032	-4.736	0.015
			2196					
33543	2.6	B	2196	25	-0.337	0.017	-7.023	0.026
			2256					
33544	2.7	A	2256	45	-0.118	0.037	-6.963	0.009
			2345					
33545	2.8	B	2345	64	1.499	0.014	-2.778	0.01
			2456					
33546	2.9	A	2456	44	3.214	0.092	1.167	0.025
			2531					
33548	2.10	A	2531	51	2.59	0.03	-0.285	0.02
			2684					
33547	2.11	B	2684	26	1.103	0.03	-4.235	0.017
			2780					

Table A5.8: 47407G Septal Micro-sampling

WHOI Spec. #	Sample Number	Line	Distance (μm)	wt. (μg)	$\delta^{18}\text{O}$		$\delta^{13}\text{C}$	
					per mil	error	per mil	error
35541	septum 1	A	0	43	2.839	0.027	1.307	0.014
			56					
35542	septum 2	B	56	38	3.242	0.024	1.634	0.016
			98					
35543	septum 3	A	98	53	3.533	0.03	2.017	0.017
			140					
35544	septum 4	B	140	39	3.44	0.043	2.041	0.026
			198					
35545	septum 5	A	198	44	3.688	0.081	2.224	0.027
			247					
35546	septum 6	B	247	25	3.444	0.033	2.129	0.008
			296					
35547	septum 7	A	296	42	3.742	0.081	2.193	0.028
			344					
35548	septum 8	B	344	45	3.403	0.03	1.895	0.019
			393					
35549	septum 9	A	393	34	3.432	0.043	1.417	0.007
			440					
35550	septum 10	B	440	48	2.072	0.014	-1.831	0.004
			487					
35551	septum 11	A	487	42	-2.049	0.05	-7.354	0.011
			533					
35552	septum 12	B	533	50	-0.454	0.019	-7.344	0.011
			570					
35553	septum 13	A	570	33	0.755	0.027	-5.218	0.023
			602					
35554	septum 14	B	602	34	1.663	0.045	-2.808	0.025
			644					
35555	septum 15b	A		34	3.408	0.048	1.331	0.032
35556	septum 15c	B		42	3.567	0.025	1.039	0.007
35557	septum 15a	A		36	3.552	0.03	1.559	0.014
35558	septum 15e	B		40	3.499	0.028	0.937	0.009
35560	septum 15f	B		22	3.404	0.013	0.941	0.01

Table A5.9: Sample 47407-2A Micro-Sampling

WHOI Spec. #	Sample Number	Line	Distance (μm)	wt. (μg)	$\delta^{18}\text{O}$		$\delta^{13}\text{C}$	
					per mil	error	per mil	error
41173	1	A	0	25	3.444	0.051	0.760	0.013
			75					
41175	3	A	75	21	3.344	0.056	0.490	0.014
			135					
41176	4	B	135	40	3.139	0.012	-0.133	0.005
			195					
41177	5	A	195	53	2.681	0.012	-0.907	0.010
			271					
41178	6	B	271	50	2.280	0.009	-1.923	0.009
			331					
41179	7	A	331	41	2.260	0.027	-2.164	0.012
			376					
41180	8	B	376	51	2.732	0.023	-1.115	0.011
			426					
41181	9	A	426	29	2.999	0.036	-0.418	0.009
			476					
41182	10	B	476	44	2.752	0.009	-1.087	0.010
			526					
41183	11	A	526	30	2.593	0.019	-1.405	0.005
			576					
41184	12	B	576	53	3.192	0.009	0.053	0.006
			643					
41189	13	A	643	43	3.714	0.020	1.396	0.007
			709					
41190	14	B	709	49	3.764	0.009	1.756	0.019
			760					
41191	15	A	760	43	3.659	0.022	1.693	0.010
			827					
41192	16	B	827	37	3.603	0.006	1.607	0.011
			893					
41193	17	A	893	33	3.349	0.010	1.135	0.006
			994					

Table A5.10: Sample JFA 24.8 Septum 1 Micro-Sampling

WHOI Spec. #	Sample Number	Line	Distance (μm)	wt. (μg)	$\delta^{18}\text{O}$		$\delta^{13}\text{C}$	
					per mil	error	per mil	error
42109	Line A1	A	0	30	4.824	0.042	0.682	0.006
			161					
42111	Line A2	B	161	26	4.644	0.020	-0.140	0.011
			268					
42112	Line A3	A	268	31	4.387	0.022	-1.052	0.004
			354					
42113	Line A4	B	354	29	3.294	0.034	-4.226	0.008
			419					
42114	Line A5	A	419	36	3.573	0.025	-3.255	0.007
			484					
42115	Line A6	B	484	30	2.056	0.037	-6.510	0.026
			590					
42116	Line A7	A	590	28	2.458	0.040	-5.360	0.011
			697					
42117	Line A8	B	697	27	4.189	0.042	-1.572	0.009
			856					
42118	Line B1	A	0	25	4.748	0.023	0.202	0.005
			171					
42119	Line B2	B	171	35	4.868	0.026	0.341	0.014
			335					
42120	Line B3	A	335	23	4.576	0.038	-0.865	0.010
			435					
42121	Line B4	B	435	29	3.217	0.009	-4.445	0.018
			537					
42122	Line B5	A	537	25	1.555	0.020	-6.803	0.022
			638					
42123	Line B6	B	638	24	1.633	0.020	-7.223	0.008
			740					
42124	Line B7	A	740	30	1.534	0.030	-8.183	0.013
			841					
42125	Line B8	B	841	32	2.262	0.024	-6.902	0.020
			942					
42126	Line B9	A	942	29	3.965	0.032	-2.271	0.010
			1095					
42127	Line C1	B	0	23	4.836	0.010	0.382	0.016
			102					
42128	Line C2	A	102	27	5.110	0.035	0.853	0.006
			205					
42129	Line C3	B	205	21	3.608	0.028	-3.546	0.019
			308					
42132	Line C4	A	308	31	2.448	0.014	-5.903	0.012
			401					
42133	Line C5	B	401	28	1.323	0.012	-7.671	0.028
			485					
42134	Line C6	A	485	42	2.268	0.016	-5.783	0.013
			638					
42135	Line C7	B	638	53	4.219	0.015	-1.205	0.012
			803					
42136	Line C8	A	803	31	3.703	0.037	-2.240	0.011
			914					

Chapter 6: Deglacial Deep-Sea Corals and Cd/Ca Data

The bulk of this chapter is a paper that has been submitted to *Science* on the rate of deep circulation and deep water transitions during the deglaciation. As a key part of the evidence in this paper is based on Cd/Ca data in *D. cristagalli*, I have added a section after the paper that presents the Cd/Ca methods and calibration that are only briefly referred to in the *Science* paper.

Deep-Sea Coral Evidence for Rapid Change in Ventilation of the Deep North Atlantic at 15.4 ka

Jess F. Adkins^{1,4}, Hai Cheng², Edward A. Boyle¹, Ellen R. M. Druffel³ and R. Lawrence Edwards²

¹ Dept. of Earth, Atmosphere and Planetary Sciences, MIT, Cambridge, MA 02139

² Dept. of Geology and Geophysics, U. of Minnesota, Minneapolis, MN 55455

³ Dept. of Earth System Science, U. of California at Irvine, Irvine, CA 92697-3100

⁴ Also at MIT/WHOI Joint Program in Oceanography

Deep-sea corals offer the ability to monitor deep ocean circulation changes on sub-decadal time scales and to assign precise and accurate calendar ages to these changes (1). Coupled radiocarbon and ^{230}Th dates from uranium rich benthic coral species reveal large variations in the North Atlantic upper deep water ventilation rate during the early last deglaciation. Several corals of the same age, 15.4 ka, and nearly the same depth, 1800 meters, in the Western North Atlantic show up to a 670 year aging of the deep waters during their 30-160 year life spans. One individual analyzed for Cd/Ca over its growth history shows an increase in the nutrient content of these waters consistent with the radiocarbon evidence. There is a sharp transition from young, lower nutrient waters to older more poorly ventilated waters in under 160 years. As there is ample evidence from other atmospheric and surface ocean indicators for a major climate transition at this time, the coral data show for the first time that the deep ocean can change on decadal-centennial time scales comparable to the surface ocean and the atmosphere. Coupled ^{14}C and Cd/Ca coral data also allow us to calculate radiocarbon deficiencies (corrected for water mass mixing) of ~500 years for the deepest waters of the Atlantic at 40°N prior to 15.4 ka, compared to less than 100 years in the modern Atlantic.

Records from Greenland ice cores have revealed extremely rapid high amplitude shifts in the glacial polar climate. Glacial cold, from 18-40 ka, is periodically punctuated by rapid returns to milder conditions, called interstadials, that can last for hundreds of years. In addition, temperature, ice accumulation, methane concentration and major ion content all show large changes on decadal to sub-decadal time scales at the end of the Younger Dryas cooling event (11.5 ka) during the last deglaciation (2, 3, 4, 5, 6, 7, 8, 9). Analogous changes in sea surface properties, corresponding to both the Younger Dryas and the interstadials, have been found in high and low latitude North Atlantic, Cariaco Basin and Santa Barbara Basin sediment cores. The global extent of

these surface ocean and atmosphere correlations show that these reservoirs change coherently and abruptly during major climate transitions.

Currently, the role of the deep ocean in these events is still largely unconstrained. As the largest reservoir of heat and mass by far in the climate system, the deep ocean could play an important role in the mechanisms of rapid climate change. Shifts in deep circulation patterns, as recorded by the stable carbon isotope composition of benthic foraminifera, have been shown to correspond to interstadials of longer duration (10, 11). However, the time resolution of sediments is limited by bioturbation of the upper few centimeters. We present data from a new archive of ocean history, deep-sea corals which are not limited by bioturbation, that show a very rapid deep deglacial circulation change. The circulation switch happens at a comparable rate to contemporaneous changes in the surface and atmosphere and is coincident with the first major warming of the deglaciation.

Today the deep North Atlantic ocean is partially ventilated by North Atlantic Deep Water (NADW), a low nutrient water mass that is formed in the Nordic and the Labrador Seas. NADW reaches to bottom depths in the modern Western Atlantic as far south as about 40°N and then continues spreading southward as a thick lens of salty, nutrient depleted water (12). However, at the Last Glacial Maximum (LGM), foraminiferal data show that the large scale circulation in the Atlantic was quite different from today's (13, 14, 15, 16). Nutrient rich bottom waters of a southern origin have been found to spread to 60°N (17, 18) and NADW shoaled to form its glacial analog, Glacial North Atlantic Intermediate/Deep Water (GNAI/DW). Recent work has mapped a sharp nutrient gradient, representative of the GNAI/DW and southern source water mass boundary, at 2000 meters depth and 60° N in the LGM North Atlantic (19). Because our samples come from the same depth range, this result is an important constraint on our interpretation of the deep-sea coral data. While these sediment studies have greatly improved our knowledge of past circulation patterns, they can not tell us the ventilation

age of past deep circulation nor the rate at which the deep circulation changes.

Constraining this ventilation age is crucial to calculating climatically important variables such as deep ocean heat and salt transport. We show how coupled ^{230}Th and ^{14}C dates along with Cd/Ca measurements from a single deep sea coral can both monitor changes in deep water characteristics at sub-decadal resolution and tell us the radiocarbon decay in these waters since leaving the surface.

Similar to surface reef building corals, some of these deep, aragonitic, solitary species have paired light and dark density bands. This banding structure and growth rates of about 0.2-1mm/yr provide the potential for annual to decadal records of deep ocean change uncorrupted by bioturbation (20). Several cosmopolitan genera that inhabit all major ocean basins have been identified. While reported depth habitats of deep sea coral range from 60-6000 meters, the bulk of the specimens are found between 500-2000 meters (21), making deep-sea corals ideal for studies of intermediate and upper deep water masses during the past glacial period and deglaciation. Corals have been dredged from the ocean floor since the days of the Challenger expedition (1872-1876), so thousands of samples exist in the world's collections. Because these collections rarely have ages associated with the samples, we developed an age screening method to sort through our over 300 samples for interesting specimens. We have used the deep-sea scleractinian *Desmophyllum cristagalli*, one of several ubiquitous species, from the deglacial North Atlantic to constrain the rate of deglacial deep ocean climate change.

We measured paired Thermal Ionization Mass Spectrometry (TIMS) uranium series dates (20, 22) and Accelerator Mass Spectrometry (AMS) radiocarbon dates (23) on six corals. Four of our samples are *D. cristagalli*, and all of them are from near 40°N and about 1800 meters deep in the Atlantic (Table 6.1). From the paired TIMS and AMS dates, we calculate the initial coral $^{14}\text{C}/^{12}\text{C}$ ratio, denoted $\Delta^{14}\text{C}$ (24), which is also the $\Delta^{14}\text{C}$ value of the water in which the coral grew. In the modern ocean, we know the initial $\Delta^{14}\text{C}$ value, for deep water masses and can therefore calculate a radiocarbon

Sample	Depth (m)	Lat	Long	Species	²³⁸ U (ppb)	²³² Th (ppt)	²³⁴ U (measured)	²³⁰ Th/ ²³⁸ U (activity)	Age (years)	Initial $\delta^{234}\text{U}$	¹⁴ C Age (¹⁴ C years)	$\Delta^{14}\text{C}$ (‰)	Vent. (Age, years)
JFA 24.8	1784	38 N	60 W	<i>D. cristagalli</i>	3460±3	1813±51	150.5±1.4	0.15467±0.00081	15,413±171	157.2±1.5	13,570±100	192±26	440±210
JFA 24.19	1784	38 N	60 W	<i>D. cristagalli</i>	3623±3	1175±44	149.4±1.9	0.15356±0.00056	15,400±109	156.1±2.0	14,270±100	90±19	1,260±150
JFA 20.10	1954	38 N	62 W	<i>D. cristagalli</i>	3943±3	2754±64	148.8±1.2	0.15518±0.00105	15,413±226	155.4±1.3	14,020±110	126±31	1,010±280
JFA 24C	1784	38 N	60 W	<i>D. cristagalli</i>	3858±1	3255±36	144.8±1.3	0.15497±0.00059	15,358±395	151.2±1.4	14,090±60	123±24	1,180±250
JFA 2	1684-1829	42 N	29 W	?	3752±2	1723±26	144.8±1.5	0.13787±0.00068	13,694±222	150.5±1.6	12,120±60	157±20	90±200
JFA 17	1684-1829	42 N	29 W	<i>Solenosmilia sp.</i>	3851±1	877±22	147.1±1.3	0.12976±0.00057	12,912±119	152.6±1.3	11,860±60	90±12	510±110

Table 6.1: Ventilation age data for deep-sea corals in Science paper.

deficiency from a deep $\Delta^{14}\text{C}$ value measured downstream. However, in the past ocean the initial $\Delta^{14}\text{C}$ of surface waters at deep water formation zones is variable. This initial water $\Delta^{14}\text{C}$ value is largely determined by the atmospheric $\Delta^{14}\text{C}$ history, which is itself a function of the production rate of ^{14}C in the upper atmosphere and the exchange rates of ^{14}C between active carbon reservoirs. In order to avoid this problem of variable initial $\Delta^{14}\text{C}$, we used a " ^{14}C projection age" calculation to remove the effects of changing atmospheric radiocarbon contents on the measured deep $\Delta^{14}\text{C}$ for each of our samples (25). This procedure extrapolates back from the deep value along a closed system ^{14}C decay path to the intersection with the known atmospheric $\Delta^{14}\text{C}$ record. The difference between the age of the intersection and the coral's calendar age is the " ^{14}C projection age". The more conventional ventilation age, measured relative to the sea surface, is calculated by subtracting the surface ocean "reservoir age" from the ^{14}C projection age of the sample.

Our coral data is plotted in Figure 6.1A. While the data from the four corals at 15.4 ka form the bulk of our discussion, we first describe the significance of the two younger data points. The modern North Atlantic reservoir age of 400 years has been subtracted from the ^{14}C age projections to obtain the ventilation age value relative to the tropical surface ocean for all of our data. Several authors have asserted that during the Younger Dryas this surface to atmosphere age difference was 600-800 years, significantly older than the modern value of 400 years (26, 27, 28, 29). However, for our data point from 13.7 ka, subtracting much more than 400 years from the projection age would imply a negative ventilation age. Therefore, during the Bølling/Allerød warm period, the reservoir age must be close to the modern value, with an upper limit of 700 years. While our data is not from the same climatic period as the previous work, it is an important constraint on how much the reservoir age can change through time.

The rate of sea level rise from TIMS dated surface corals (22, 30) is also seen in Figure 6.1A. These meltwater pulses, commonly believed to originate in the Northern

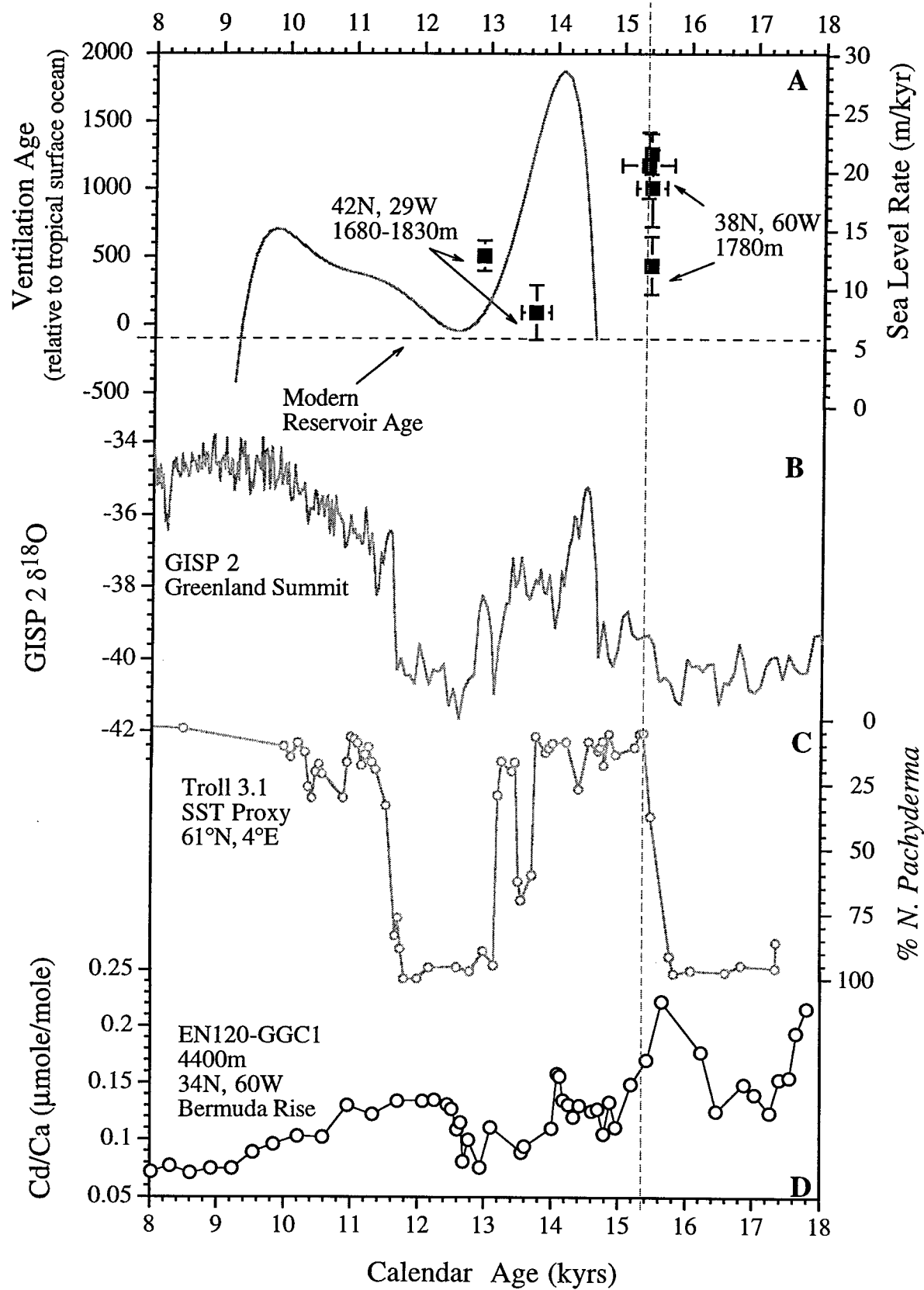


Figure 6.1

Hemisphere, are the major forcing of thermohaline circulation during this deglacial time period. The "Salt-Oscillator" hypothesis asserts that large inputs of fresh water to the North Atlantic will reduce or halt NADW formation and cause abyssal circulation to stagnate (31, 32). Our deep-sea coral data show that ventilation at 1,680-1,830 meters was relatively rapid during melt water pulse 1a (about 14.0 ka) and somewhat more sluggish during the period of reduced melting. One interpretation of the data point is that during rapid ice sheet melting into the North Atlantic, NADW shoaled and left its well ventilated radiocarbon signature on the 13.7 ka coral. By 12.9 ka, once melting was reduced, NADW sank to deeper depths and left the coral site to be bathed by an older water mass. This scenario agrees with the glacial nutrient data discussed earlier. At the LGM, nutrient rich older bottom waters spread much further northward and, conversely, intermediate/upper deep waters were more nutrient depleted. As our coral data are from between 1680 and 1830 meters depth, they are more representative of the upper deep waters than the abyssal circulation that is expected to stagnate in the "Salt-Oscillator" hypothesis. Alternatively it is important to note that the data point at 13.7 ka does not correspond exactly with the peak of deglacial melting. In the coral sea level data set there is 24 meters of sea level rise during the one thousand year interval surrounding 13.7 ka. However, 20 meters of this rise occurs from 14.2-13.7 ka and only 4 meters in the following 500 years. The relatively rapid ventilation measured in the deep-sea coral at 13.7 may be reflecting a system that has already reacted to the meltwater peak and is recording a ventilation age and circulation pattern similar to today's.

All four of the corals at 15.4 ka have the same ^{230}Th age but they have very different radiocarbon ages. The calculated ventilation ages vary by a factor of two. Separate AMS ^{14}C dates for the tops and bottoms of three of these corals show an age reversal in each sample (Table 6.2). All three corals have tops, the biologically younger part of the coral, older than their bottoms, the biologically older portion. We interpret this as a change in the ventilation age of the water during the corals' lifetimes. From ^{230}Th and ^{210}Pb dates

Sample	Position	UCID #	CAMS #	Age	Radiocarbon age (^{14}C Years B.P.) $\pm 1\sigma$	Age Diff.	$\pm 1\sigma$	Length (cm)	Lifetime (years)
JFA 20.10	Top	1529	30183-84	14,120	40	140	60	3.0	30-150
	Bottom	1530	30185-86	13,980	40				
JFA 24.19	Top	1531	30187-88	14,500	50	440	60	2.8	30-140
	Middle	2054	36257	14,500	50				
	Bottom	1532	30189-90	14,060	40				
JFA 24.8	Top	1533	30191-92	14,520	40	670	60	3.2	30-160
	Middle	2055	36258	14,470	50				
	Bottom	1534	30193-94	13,850	40				

Table 6.2: Top/Bottom age differences for deep-sea corals in *Science* paper.

on modern *D. cristagalli*, we expect that these corals lived for no longer than about 160 years (20). The largest age difference, 670 years younger at the top of JFA 24.8 than at the bottom, implies a $\Delta^{14}\text{C}$ difference of about 80‰. This is nearly the full range of pre-bomb $\Delta^{14}\text{C}$ values in the entire water column of the modern Atlantic (33, 34). To check for the large water mass switch implied by these data, we also measured the Cd/Ca ratios in JFA 24.8. A near factor of two change in coral Cd/Ca (Fig. 6.2) strongly supports the ^{14}C evidence for a large change in circulation in under 160 years at this site (35).

We know from other climate data (Fig. 6.1) that 15.4 ka was a period of major climate reorganization as North Atlantic SST rose dramatically. Bølling-Allerød warming begins in the Greenland ice cores at virtually the same time (Fig. 6.1). Benthic Cd/Ca values at the Bermuda Rise also show a large increase around 15.6 ka (Fig. 6.1). In addition, benthic $\delta^{13}\text{C}$ data (36) from many North Atlantic sediment cores show a large decrease in the $\delta^{13}\text{C}$ of the bottom waters (nutrient enrichment) at this same time (18). We find that the deep ocean can change during rapid climate events at a comparable rate to the atmosphere and the surface ocean. Whether the deep ocean is merely responding to or actively modulating these rapid climate changes is not yet determined.

Based on a modern calibration of the sensitivity of Cd/Ca in *D. cristagalli* to the water [Cd], these corals have a distribution coefficient of about 1.6 (37). Data from benthic foraminifera with a D of 2.9 show a Holocene Cd/Ca value in NADW of 0.07 $\mu\text{mole/mole}$ (Fig. 6.1). This corresponds to a *D. cristagalli* ratio of 0.04 $\mu\text{mole/mole}$ ($1.6/2.9 \times 0.07$). Assuming the top of JFA 24.8 as representative of pure southern source water (0.19 $\mu\text{mole/mole}$), then the bottom of JFA 24.8 (0.11 $\mu\text{mole/mole}$) grew in a 50/50 mixture of northern and southern water masses. This ratio is only slightly dependent on the *D. cristagalli* distribution coefficient because NADW has a very low initial nutrient content. We are justified in this two end-member approach because there is known to be a sharp gradient between northern and southern source water masses at 2000 meters and 60° N during the LGM (19). Apparently the bottom of this coral grew in the transitional

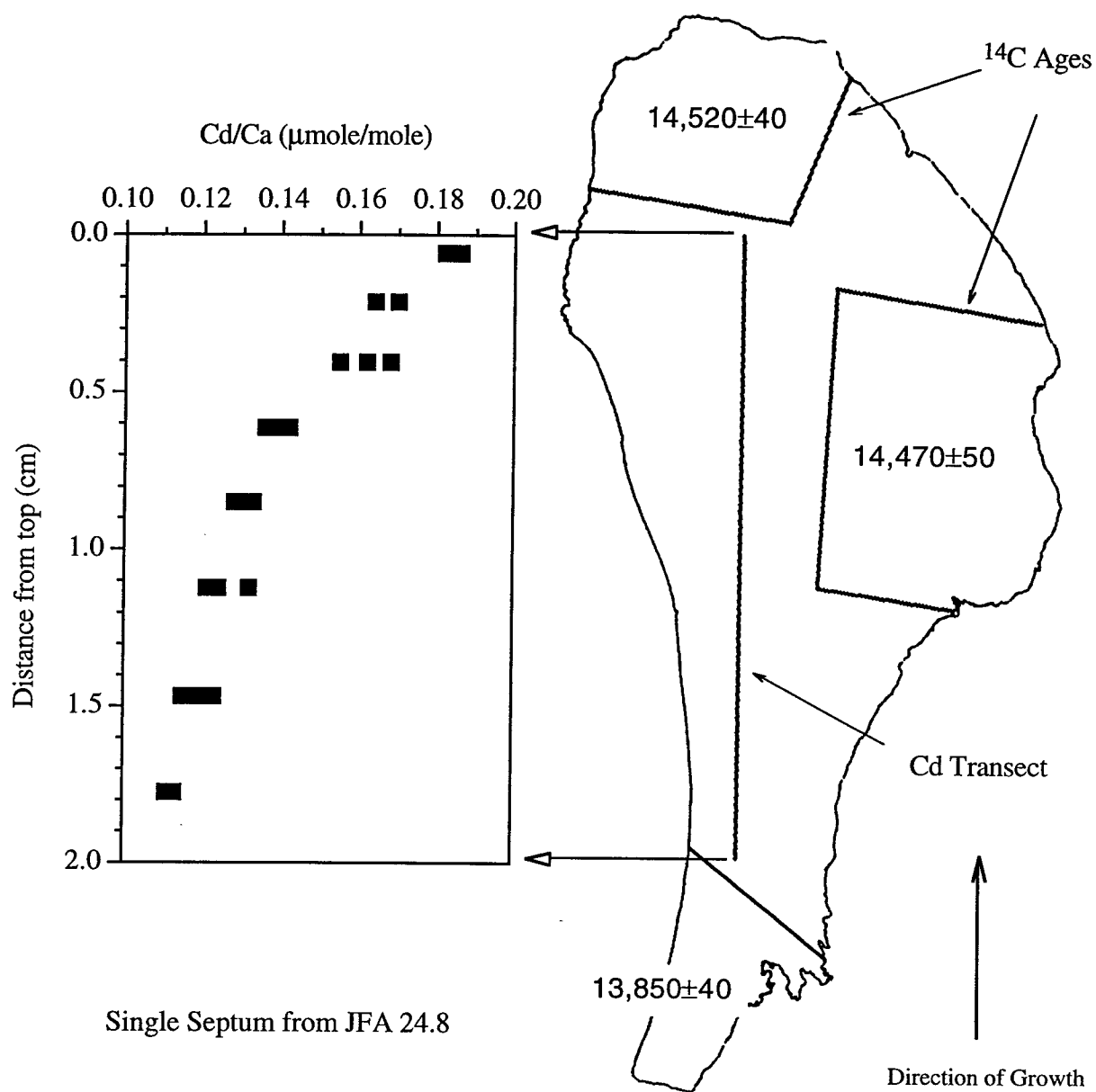


Figure 6.2

zone of this glacial North Atlantic nutrient gradient. During the coral's lifetime this nutricline shoaled and left the sample bathed in pure southern source (old) waters. Cd/Ca in core EN120-GGC1 (Fig. 6.1 D) shows the abyssal Atlantic was in the process of becoming better ventilated at the same time the 1800 meter corals show more poorly ventilated waters. Presumably the nutricline at 2000 meters shoals because GNAI/DW becomes more dense than the underlying southern source water. This inverse behavior of upper deep and abyssal nutrient concentrations is consistent with the studies mentioned earlier (19). However, this is not a firm conclusion because the uncertainty between the two time scales can not constrain the phasing of the events in the corals and the sediment.

The data shown in Figure 6.1 display an interesting conundrum in the deglacial climate. Why do the deep ocean and the sea surface temperature lead the largest atmospheric temperature increase by about 800 years? The abundance of *N. pachyderma* is essentially a threshold proxy. Generally in the high latitude North Atlantic, low % *pachy.* means the polar front is north of the core site, and vice-versa. Perhaps the polar front moved past the site of Troll 3.1 early in the deglaciation but not far enough into the Nordic Seas to alter the atmospheric temperature above Greenland. It is also possible that the radiocarbon age of high latitude surface waters early in the deglaciation was older than the modern value of 400 years. This change would move the age of the % *pachy.* shift, based on planktonic radiocarbon data, towards the ice core $\delta^{18}\text{O}$ transition. In this case, there is an event at 15.4 ka in the deep-sea corals and in nutrient proxies in benthic foraminifera but it is not found in the Nordic Sea or ice core indicators. This scenario implies that there can be a deep ocean circulation change with no expression in the high latitude surface ocean or atmosphere.

The coupled ^{14}C and Cd/Ca data allow us to deconvolve the radiocarbon data and calculate a radiocarbon deficiency of this southern source water mass. The 670 year radiocarbon difference from top to bottom in JFA 24.8 is equal to the radiocarbon age of

the southern water mass (S.O.) minus a 50/50 mixture of this water mass and the radiocarbon age of the northern water mass (N.A.):

$$S.O. - (50\%(S.O.) + 50\%(N.A.)) = 670$$

If we assume the N.A. value is similar to the pre-bomb North Atlantic, 540 years (38), then the southern source water mass had a radiocarbon age of 1880 years at 40° N. This age is the sum of the initial radiocarbon age the water had when it left its formation zone and the transit time to the coral's location. Again assuming a modern initial age for southern source waters, about 1400 years (38), the high nutrient water mass bathing JFA 24.8 aged for about 480 years before reaching 40° N. This result is in stark contrast to the modern Atlantic Ocean where, for radiocarbon data, the effects of mixing largely mask effects due to water mass aging. The deep Atlantic circulation appears to have been more sluggish than today.

In under 160 years at 15.4 ka the glacial nutrient gradient between northern and southern source waters masses in the North Atlantic shoaled by several hundred meters. At the same time, surface ocean and atmospheric climate show a rapid transition to the warming of the Bølling-Allerød period. The deep ocean's reservoir of heat and mass is in communication with surface reservoirs on short time scales during rapid climate changes. With coupled radiocarbon and Cd/Ca data from deep-sea corals, we can directly calculate the radiocarbon age of past deep ocean waters. Coupling these age measurements with estimates of water temperature, could allow for the direct calculation of past deep ocean heat transport. It is important to note that the assumption of modern initial radiocarbon ages for the northern and southern water masses may be incorrect. Future work on shallow deglacial deep-sea corals from high latitudes will better constrain these initial values. Regardless of the preliminary nature of this ventilation age calculation, we have found evidence for rapid changes in deep circulation at comparable rates to the surface ocean and atmosphere.

FIGURE CAPTIONS

Figure 6.1. Deep-sea coral ventilation ages and related climate data. Coral ventilation ages relative to the tropical surface ocean are plotted as black squares in panel A.

Vertical error bars are a combination of analytical errors in the TIMS and AMS measurements as well as uncertainties in the estimates of past atmospheric $\Delta^{14}\text{C}$ (25).

The black line is the first derivative of a sixth order polynomial fit to the coral sea-level data (22, 30). No attempt was made to account for the different depth habitats of particular coral species. The other panels are from previously published data. (B)

Oxygen isotopic data from the GISP 2 core at 2 meter resolution is a proxy for atmospheric temperature at the Greenland Summit (4, 5). (C) The relative abundance of the cold dwelling planktonic foraminifera *N. pachyderma* in core Troll 3.1 (39) is a proxy for sea surface temperature. Because the end of the Younger Dryas (YD) cooling occurs during a ^{14}C age plateau, the age model from the original reference has been altered (S. Lehman, personal communication) to match the ice core age for the termination of the YD, 11,640 years (6), while the other control points are left the same (39). (D) Cd/Ca ratios from benthic foraminifera in core EN120-GGC1 at the Bermuda Rise are a proxy for deep ventilation (14, 40). Higher values represent a larger content of nutrient rich waters, of a southern origin in the Atlantic, and lower values correspond to a higher content of nutrient poor waters, of a northern origin in the Atlantic. The coral data from 15.4 ka correspond to rapid events in all the other tracers, from the atmosphere to the deep ocean.

Figure 6.2. Cd/Ca data and radiocarbon ages from *D. cristagalli* sample JFA 24.8.

This sample from 1784 meters depth at 40° N in the western basin of the Atlantic was ^{238}U - ^{230}Th dated to be $15,410 \pm 170$ years old. Radiocarbon data from three samples of a single septum show a 670 ± 60 year continuous rise in ^{14}C age, over and above the growth trend, towards younger ages at the top of a sample. Cd/Ca data were sampled at about

2.3 mm average resolution along the line connecting the top and bottom ^{14}C samples. These data also show a continuous trend to older more poorly ventilated waters during the coral's lifetime. Our growth rate study using ^{230}Th dating in five modern *D. cristagalli* constrains the extension rate to be no less than about 0.2 mm/yr, and therefore the life span of this sample to be no more than about 160 years (20). This evidence for a rapid change in deep ocean circulation corresponds to the first major deglacial event seen in many climate records (see Fig. 1).

Table 6.1. AMS radiocarbon and TIMS uranium series dates for the six deep-sea corals in Figure 1A. Calendar ages were calculated as described in (20). The measured $^{230}\text{Th}/^{238}\text{U}$ ratio was corrected for initial ^{230}Th . Initial ^{230}Th was estimated from the sample's ^{232}Th value and a measured $^{230}\text{Th}/^{232}\text{Th}$ atomic ratio of $85 \pm 80 \times 10^{-6}$ from a suite of modern corals. Calendar age errors are a combination of the uncertainty in this initial $^{230}\text{Th}/^{232}\text{Th}$ ratio and analytical uncertainty in the measured $^{230}\text{Th}/^{238}\text{U}$ ratio. AMS radiocarbon dates were measured at the Lawrence Livermore National Lab Center for Accelerator Mass Spectrometry (CAMS) using standard procedures. Ventilation ages were calculated with the " ^{14}C projection age" method described in (25). In three of the corals there is a slight elevation in initial $\delta^{234}\text{U}$, indicating a small degree of exchange with a high $\delta^{234}\text{U}$ reservoir. We infer that the effect of this exchange on ^{230}Th age is small, from the observation that there is no significant correlation between ^{230}Th age and $\delta^{234}\text{U}$ in different fragments of the same coral (20).

Table 6.2. Radiocarbon dates from the Top/Bottom study of three 15.4 ka *D. cristagalli*. All three corals show an age "reversal" corresponding to the water mass shift discussed in the text. Samples have different top-bottom ages because they grew at slightly different times during the deep circulation event. Lengths are measured from the top and bottom most portions of the sample, not the mid-point of the chunk used for AMS dating. Lifetimes are calculated from the growth rate estimates of 0.2-1.0 mm/yr (20).

REFERENCES

1. J. Smith E., M. Risk J., H. P. Schwarcz, T. A. McConnaughey, *Nature* **386**, 818-820 (1997).
2. W. Dansgaard, et al., *Nature* **364**, 218-220 (1993).
3. GRIP, *Nature* **364**, 203-207 (1993).
4. P. M. Grootes, M. Stuiver, J. W. C. White, S. Johnsen, J. Jouzel, *Nature* **366**, 552-554 (1993).
5. M. Stuiver, P. M. Grootes, T. F. Braziunas, *Quaternary Research* **44**, 341-354 (1995).
6. R. B. Alley, et al., *Nature* **362**, 527-529 (1993).
7. E. J. Brook, T. Sowers, J. Orchardo, *Science* **273**, 1087-1091 (1996).
8. J. Chappellaz, et al., *Nature* **366**, 443-445 (1993).
9. P. A. Mayewski, et al., *Science* **261**, 195-197 (1993).
10. L. Keigwin D., G. Jones A., *Journal of Geophysical Reserch* **99**, 12,397-12,410 (1994).
11. W. Curry B., D. Oppo W., *Paleoceanography* **12**, 1-14 (1997).
12. A. E. Bainbridge, *GEOSECS Atlantic Ocean Expedition, Vol. 2, Sections and Profiles*. (U.S. Government Printing Office, Washington D.C., 1980).
13. E. A. Boyle, L. D. Keigwin, *Science* **218**, 784-787 (1982).
14. E. A. Boyle, L. D. Keigwin, *Nature* **330**, 35-40 (1987).
15. D. Oppo, R. G. Fairbanks, *Earth and Planetary Science Letters* **86**, 1-15 (1987).
16. D. W. Oppo, R. G. Fairbanks, *Paleoceanography* **5**, 277-288 (1990).
17. J. C. Duplessy, et al., *Paleoceanography* **3**, 343-360 (1988).
18. M. Sarnthein, et al., *Paleoceanography* **9**, 209-268 (1994).
19. D. W. Oppo, S. J. Lehman, *Science* **259**, 1148-1152 (1993).
20. H. Cheng, J. F. Adkins, R. L. Edwards, E. A. Boyle, *Geochimica et Cosmochimica Acta* **submitted**, (1997).
21. S. D. Cairns, G. D. Stanley Jr., *Proceedings of the Fourth International Coral Reef Symposium, Manila* **1**, 611-618 (1981).
22. R. L. Edwards, et al., *Science* **260**, 962-967 (1993).
23. Samples were cleaned of exterior organic carbon and coatings of manganese/iron oxides with successive leaches in a 50/50 mixture of 30% peroxide and 1N NaOH. A

final short leach in a 50/50 mixture of peroxide and 1% perchloric acid was used to remove all remaining organic stains. These pre-cleaning steps removed 15-25% of the original coral weight. Immediately prior to final dissolution and graphitization, corals were soaked in 10% HCl to remove an additional 7-30% of aragonite. This procedure overcomes contamination problems from modern carbon due to storage and handling and organic carbon from polyp and crust material. Samples were carefully chosen to avoid secondary calcification from endolithic activity.

24. The $^{14}\text{C}/^{12}\text{C}$ ratio is expressed with Δ notation, where $\Delta^{14}\text{C}$ (per mil) is the per mil deviation from the $^{14}\text{C}/^{12}\text{C}$ ratio in 19th-century wood. We report $\Delta^{14}\text{C}$ values as prescribed by Stuiver and Polach (*Radiocarbon*, **19**, 355 (1977)) for geochemical samples.
25. J. F. Adkins, E. A. Boyle, *Paleoceanography* **12**, 337-344 (1997).
26. E. Bard, et al., *Earth and Planetary Science Letters* **126**, 275-287 (1994).
27. W. E. N. Austin, E. Bard, J. B. Hunt, D. Kroon, J. D. Peacock, *Radiocarbon* **37**, 53-62 (1995).
28. K. Gronvold, et al., *Earth and Planetary Science Letters* **135**, 149-155 (1995).
29. H. Birks H., S. Gulliksen, H. Hafliðason, J. Mangerud, G. Possnert, *Quaternary Research* **45**, 119-127 (1996).
30. E. Bard, M. Arnold, R. Fairbanks, B. Hamelin, *Radiocarbon* **35**, 191-199 (1993).
31. W. S. Broecker, G. Bond, M. Klas, G. Bonani, W. Wolfli, *Paleoceanography* **5**, 469-477 (1990).
32. G. E. Birchfield, W. S. Broecker, *Paleoceanography* **5**, 835-843 (1990).
33. M. Stuiver, H. G. Ostlund, *Radiocarbon* **22**, 1-24 (1980).
34. W. S. Broecker, R. Gerard, M. Ewing, B. C. Heezen, *Journal of Geophysical Research* **65**, 2903-2931 (1960).
35. We measured the spatial variation in Cd/Ca ratios from within a single modern *D. cristagalli* to check for vital effects. These biologically induced non-thermodynamic deviations from equilibrium for a particular tracer have been found to dominate the stable carbon and oxygen isotope signatures of deep-sea corals (1). A coral from 550 meters in the South Pacific had an average Cd/Ca value of 0.172 umole/mole with a one standard deviation of 0.016 umole/mole. There was no within coral spatial pattern to this variation. While *D. cristagalli* may contain vital effects for Cd/Ca, this 10% standard deviation is smaller than the signal in JFA 24.8 and does not have the top to bottom coherence we find in the 15.4 ka sample. For these reasons we believe sample JFA 24.8 has faithfully captured a change in the [Cd] of the past water masses.
36. The carbon isotopic ratio is defined as follows:

$$\delta^{13}\text{C} = [(^{13}\text{C}/^{12}\text{C})_{\text{sample}} / (^{13}\text{C}/^{12}\text{C})_{\text{standard}} - 1] 1000$$
 relative to the Pee Dee Belemnite standard [see H. Craig, *Geochim. Cosmochim. Acta* **3**, 53 (1953)].

37. The coral Cd distribution coefficient is the ratio of Cd/Ca in the coral to Cd/Ca in the water. Similar to a core top calibration in foraminifera, we measured Cd/Ca ratios in a suite of modern *D. cristagalli* that span a range of 0.5-3.2 μM $[\text{PO}_4]$. Six of these coral fall on a line with a slope of 1.6 coral/water Cd/Ca ratio. This value implies a $[\text{PO}_4]$ of 3.6 μM for the top of sample JFA 24.8. However, there are three other samples from this calibration that have significantly higher Cd/Ca ratios in the coral than predicted by their water [Cd]. Based on this study, we believe the distribution coefficient for *D. cristagalli* is 1.6 or higher and that the 3.6 μM $[\text{PO}_4]$ estimate for JFA 24.8 is a maximum value.
38. W. S. Broecker, S. Blanton, M. Smethie Jr., G. Ostlund, *Global Biogeochemical Cycles* **5**, 87-117 (1991).
39. S. J. Lehmann, L. D. Keigwin, *Nature* **356**, 757-762 (1992).
40. L. D. Keigwin, G. A. Jones, S. J. Lehman, E. A. Boyle, *J. Geophys. Res.* **96**, 16811-16826 (1991).

II. Cd/Ca Analytical Methods

Samples for Cd/Ca analysis are obtained by either breaking off pieces from the thin portions of the septa or using the laser supplied with our VG Micro Probe. For the modern calibration study I broke samples off the most easily accessible thinnest portion of the S1 septum. These samples were gently crushed in an agate mortar and pestle and several pieces were weighed into clean 0.5 mL centrifuge tubes for cleaning. Care was taken to ensure that samples from all individuals came from the same type of septal material. To obtain samples from more precisely known spatial locations on the coral, I use the Continuum Minilite Nd:YAG UV laser (266 nm, 2 millijoules) housed in our VG UV Laser Lab. A 200-250 μm thick sample slab, mounted on a glass slide as described in previous chapters, is placed on the computer controlled X:Y:Z stage. Because I use the laser solely as a cutting tool and not an ICP-MS sample introduction mechanism, I remove the Argon containing sample cell from the stage. Lines are cut through the coral by firing the laser at 10 Hz on maximum power with no aperture. Several passes over the same line are required to cut all the way to the glass slide. The system is guided using the reflected light video camera system attached to the UV Micro Probe and a photographic enlargement of the sample. After cutting, laser paths are easily imaged by scanning with a 400 dpi flatbed, 256 level Lacie Silverscanner II using Adobe Photoshop. Sample chunks are removed with a razor blade and small tweezers and weighed into clean 0.5 mL centrifuge tubes for cleaning. This process usually breaks the sample into several pieces as it "peels back" off the slide so crushing in the agate mortar and pestle is not required.

Once sampled, corals are subjected to a rigorous cleaning procedure to remove trace metal contaminants. We modified the techniques for foraminifera [Boyle, 1981; Boyle and Keigwin, 1985/6] and surface corals [Shen and Boyle, 1988] to suit the particular cleaning requirements of deep-sea corals. The extended pre-cleaning step to remove black Mn/Fe oxides and the full trace metal cleaning are described in Chapter 3, section II. Because the cadmium samples are much smaller, the main difference between the

Thorium and Cd/Ca cleaning is the amount of reagents used. Dilute acid rinses use 100 μl of 0.1% HNO_3 and the oxidizing and reducing steps use the same solutions as described in Chapter 3 but only 250 μl of each. Recently the foraminiferal cleaning technique has been modified to eliminate a CdS phase. This diagenetic contamination produced in sediments can be easily removed by switching the order of the oxidative and the reductive cleaning steps [Boyle and Rosenthal, 1996]. I carried out a series of tests to check the efficiency of our deep-sea coral Cd/Ca cleaning technique, which preserves the original order of oxidative and then reducing steps, against this new method.

The tests and results are listed in Table 6.3. A large sample of *D. cristagalli* from the Smithsonian Institution was crushed and sieved for the 250-710 μm size fraction. About 1 mg of coral pieces were selected at random from the crushed sample pool and subjected to one of the ten steps listed in Table 6.3. The average and standard deviation of three replicates of this sample and a surface coral sample from Dr. Glen Shen at the University of Washington are also shown in the table. Due to the extremely low concentration of Cd in surface corals, this sample, without preconcentration steps, should represent a sample processing blank in my procedure. It is clear that the runs without a pre-cleaning step (#s 2 and 3) and the run with fine fractions (#8) were either not fully cleaned, variably cleaned or both. The no pre-cleaning run also had the highest blank Cd/Ca ratio. All other runs were very consistent with the possible exception of run number 5 which left out the perchloric step in the pre-cleaning routine. Switching the order of the oxidizing and reducing steps had no effect on the Cd/Ca values. Results from the small total weight were quite variable. However, I believe this is due to poor technique on my part during the beginning stages of measuring Cd/Ca ratios. As I performed more runs over the course of the thesis, I was able to decrease the overall sample size and still get consistent results. I continue to run the U. of Washington surface coral blank with many of my samples as a check on contamination during the cleaning process. Results of all blanks run during this thesis are listed in Table 6.4.

Run #	Cleaning Description	Smithsonian Standard			U. of Washington Blank		
		Average	$\pm 1\sigma$	n	Ave.	Stdev	n
1	Normal	0.047	0.004	3	0.004	N.A.	1
2	No pre-clean	0.060	0.020	3	0.004	0.001	3
3	No pre-clean, reverse Ox. and Red. Steps	0.045	0.014	3	0.017	0.018	3
4	Pre-clean, reverse Ox. and Red. Steps	0.042	0.009	3	0.006	N.A.	1
5	No perchloric leach	0.052	0.012	3	0.005	0.002	2
6	Large total wt. (~3 mg)	0.050	0.004	3	0.000	0.002	3
7	Small total wt. (~0.3 mg)	0.044	0.023	3	0.001	N.A.	1
8	Fine Fraction, normal cleaning	0.093	N.A.	1	0.003	0.003	3
9	1N NaOH in Oxidative cleaning	0.049	0.010	3	0.005	0.005	2
10	Normal	0.044	0.013	2	0.001	N.A.	1

Table 6.3: Results of the Cd/Ca cleaning tests. Only one replicate of the Smithsonian standard fine fraction survived the cleaning.

Run	Date	Cd/Ca
AF	November 15, 1994	0.004
		0.004
		0.017
		0.006
		0.005
		0.000
		0.001
		0.003
		0.005
		0.001
AY	June 18, 1997	-0.025
		-0.020
		-0.003
		0.005
		-0.011
AZ	July 5, 1997	0.006
		0.001
		0.005
BA	July 27, 1997	-0.001
		0.003
		0.005

Table 6.4: All surface coral blanks run during the thesis.

Cd/Ca ratios were measured on dissolved coral solutions by atomic adsorption spectrophotometry. Most samples were dissolved in 150 μ l of trace metal clean 1% HNO₃ acid. Cd concentrations were measured on an a Hitachi Z-8100 Polarized Zeeman AAS. Samples were compared to a four point matrix matched standard curve. The Cd sensitivity's dependence on sample [Ca] was determined empirically once, and then applied to all further runs. Because I used the same amount of acid to dissolve all samples regardless of post-cleaning size, this correction could vary from 0-13% and is a possible source of uncertainty in the Cd/Ca ratio. Calcium concentrations were determined on a 20 μ l aliquot of the original coral solution by diluting with 5 mL of a La/HCl matrix solution and measuring on a Perkin-Elmer 403 Flame AAS. Replicates of the single point standard over the course of a Ca run were typically better than 0.5%, while the Cd standards were always linear to better than an r^2 of 0.999. Consistency standards with two different Cd/Ca ratios, in sample like proportions and concentrations, were run with every batch of corals. Over the course of three years, the measured Cd/Ca ratio for each standard varied by less than 4% (Table 6.5).

When I intercalibrated my matrix matched Cd standards with those of Ed Boyle and Yair Rosenthal, mine were 13% too dilute. This problem was discovered by running Ed Boyle's consistency standard against my standards and getting a Cd/Ca value that was too high. The [Ca] data agreed but the [Cd] was off. In an effort to track down the problem I also compared the cadmium standards from which each matrix matched set was made up. These data agreed at the 1% level. Therefore, the deviation must have occurred during the dilution and Ca addition necessary to make up working, matrix matched standards. The offset has been constant through time. Intercomparison with Yair Rosenthal occurred in October of 1994 while intercomparison with Ed Boyle occurred in October of 1997. I have no absolute reason for why my matrix matched standards are off. One possibility is that cation exchange resin beads used to clean up the Ca matrix solution

	Consistency Standard 1			Consistency Standard 2		
	[Ca] (mM)	[Cd] (nM)	Cd/Ca (μ mole/mole)	[Ca] (mM)	[Cd] (nM)	Cd/Ca (μ mole/mole)
Run AE	22.21	1.644	0.074	22.41	3.647	0.163
	22.31	1.606	0.072	21.92	3.481	0.159
	22.21	1.741	0.078	22.16	3.446	0.156
Run AF	21.87	1.558	0.071	21.98	3.335	0.152
	21.96	1.604	0.073	21.84	3.303	0.151
	21.93	1.566	0.071	21.79	3.367	0.155
Run AZ	21.71	1.656	0.076	22.27	3.185	0.143
	22.84	1.614	0.071	20.95	3.200	0.153
	22.35	1.576	0.070	21.13	3.185	0.151
Run BA	21.74	1.632	0.075	21.69	3.215	0.148
	21.66	1.620	0.075	21.79	3.233	0.148
	21.76	1.636	0.075	21.62	3.210	0.148
Run BB	21.67	1.617	0.075	21.17	3.140	0.148
	21.44	1.620	0.076	21.34	3.129	0.147
	21.39	1.572	0.073	21.27	3.049	0.143
Totals						
Average	21.94	1.617	0.074	21.69	3.275	0.151
Stdev	0.39	0.045	0.002	0.44	0.157	0.005
RSD	1.76%	2.78%	3.08%	2.02%	4.79%	3.56%

Table 6.5: All Cd/Ca consistency standards run with the GFAA during the thesis. Based on this data we report an analytical error of under 4% on our Cd/Ca values.

escaped filtering and got into the standard bottles. I have adjusted all Cd/Ca data reported here for this offset.

III. Cd Vital Effects and Modern Calibration

Before trying a modern calibration of Cd/Ca ratios in *D. cristagalli*, I was worried that the same type of vital effects observed for $\delta^{18}\text{O}$ and $\delta^{13}\text{C}$ (see chapter 5) could be affecting Cd/Ca values as well. Because the micro-sampler used in the stable isotope studies generates fine grained dust which I can not reliably clean for Cd/Ca analysis, I had to develop another method for sampling chunks of aragonite from known spatial locations on a septum. This need was the impetus to use the laser sampling described above. With the photographic image of a 200-250 μm thick slab of coral and the laser's video system, I can reliably move around the sample and cut out chunks from known locations. Septa from *D. cristagalli* sample number 47407 were slabbed for both a "top view" and a "side view" transect of Cd/Ca values (Figures 6.3 and 6.4 respectively). Black lines represent the laser cutting paths and numbers in white boxes are the Cd/Ca values for each point. All data, including two replicates are listed in Table 6.6. There is no large scale spatial pattern to the Cd/Ca data. In addition, there is no difference between samples with white bands and those without. As central bands are the portion of the septum most affected in the stable isotope data, this is strong evidence that Cd/Ca is behaving differently than $\delta^{18}\text{O}$ and $\delta^{13}\text{C}$. The data show a relative standard deviation of about 10% which is larger than the analytical error (estimated to be about 3-4% from consistency standards). I can not rule out a vital effect at this level of uncertainty (the overall range is about 0.05 $\mu\text{mole/mole}$), but there is no regular spatial pattern to the data.

Given that there is a small to negligible vital effect for Cd/Ca ratios, I tried to calibrate this tracer in *D. cristagalli*. Similar to a core top calibration for benthic foraminifera, I compared measured Cd/Ca values in a suite of modern corals with estimates of the water $[\text{PO}_4]$. Using the global $[\text{PO}_4]$ to $[\text{Cd}]$ relationship, I converted

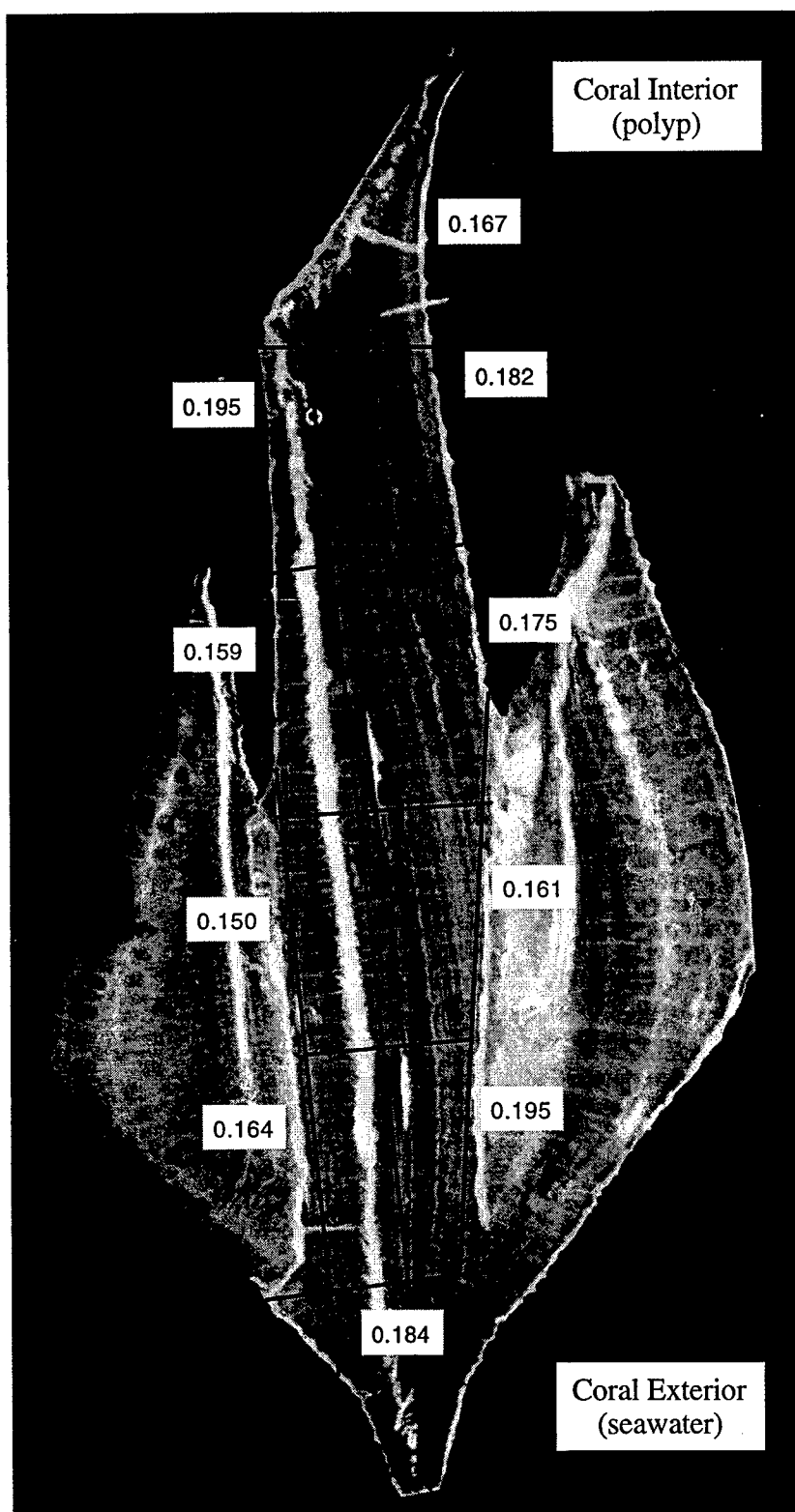


Figure 6.3. Top view of sample 47407-H with Cd/Ca data. There is no spatial pattern to the ratios and there is no difference between samples with and without the center white band.

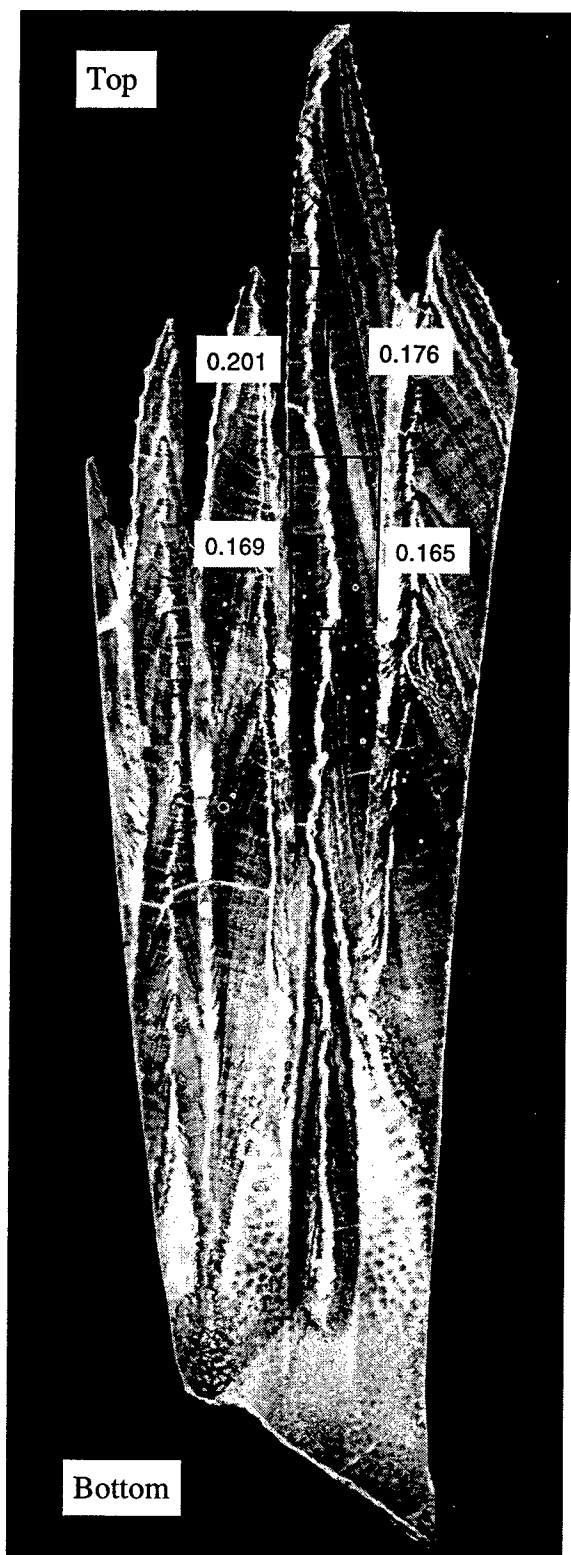


Figure 6.4. Front view of sample 47407-2A with Cd/Ca data. There is no spatial pattern to the data and there is no difference between samples with and without the center white band.

Sample Number	Cd/Ca (μ mole/mole)		
AY 1	0.176	Dark Band	
AY 2	0.201	Ave	0.176
AY 3	0.165	Stdev	0.012
AY 4	0.169	RSD	6.84%
AY 5	0.167	Light Band	
AY 6	0.182	Ave	0.170
AY 7	0.195	Stdev	0.019
AY 8	0.159	RSD	11.40%
AY 9	0.175	Total	
AY 10	0.150	Ave	0.172
AY 11	0.161	Stdev	0.016
AY 12	0.164	RSD	9.32%
AY 13	0.195		
AY 14	0.184		
AY 15	0.167	replicate of AY 4	
AY 16	0.144	replicate of AY 10	

Table 6.6: Cd/Ca data from laser sampling
D. cristagalli number 47407.

the [PO₄] estimates into Cd/Ca ratios for each sample. This global relationship is known to have a "kink" in the linear trend between these two species [Boyle, 1988; Frew and Hunter, 1992; Boyle, 1994]. To account for this kink in my water Cd/Ca estimations, I used a line of [PO₄] (in μM) vs [Cd] (in nM) that has a slope of 0.4 and intercept of -0.25 for phosphate concentrations above 1.3 μM. Below this value, I used a line with a slope of 0.2 and an intercept of zero. The [PO₄] estimates, the resulting Cd/Ca values and the measured coral Cd/Ca ratios are listed in Table 6.7. Six of the nine corals measured show a strong linear correlation between coral Cd/Ca and water Cd/Ca. If we define an empirical partition coefficient, D_p , as:

$$D_p = \frac{Cd / Ca_{coral}}{Cd / Ca_{water}}$$

then these six corals correspond to a D_p of 1.6 (Figure 6.5). Surface corals and the aragonitic benthic foraminifera *Hoglundina* both have a D_p of one [Shen et al., 1987; Boyle et al., 1995]. Calcitic foraminifera have a depth dependent D_p that varies between 1 and 2.9 [Boyle, 1992]. Our value of about 1.6 for *D. cristagalli* is consistent with these other calcifying organisms. In addition, the precision of our replicates from the same sample confirm the conclusion that there are not large vital effects in this species.

However, three of our corals fall far off the linear trend (Figure 6.5). All three of these samples have very high Cd/Ca values and varying degrees of precision. It is possible that these samples were contaminated during collection and/or storage. One of the high individuals, sample number 47407, is the same coral used in the vital effect study. By grinding away the exterior surfaces and sampling the interior aragonite of a single septum on 47407, we measured a Cd/Ca value of 0.172 μmole/mole. While more precise than the data from Table 6.7, the average value is still too high relative to its assumed [PO₄]. We are unable to explain why some corals fall on a consistent line and why others are too high. While we can not say for sure what the value of the distribution coefficient for *D. cristagalli* is, we can say that any individual specimen seems to have a

Sample Number	Depth (m)	Latitude	Longitude	Cd/Ca ($\mu\text{mole/mole}$)	[PO ₄] (μM)	err	Water [Cd] (nM)	Water Cd/Ca ($\mu\text{mole/mole}$)
47407	549	54.49S	129.48W	0.493 0.384 0.855	1.8	0.2	0.470	0.046
83583	488-440	32.54N	127.47W	0.131 0.130 0.141	2.8	0.3	0.870	0.084
78459	2110-2180	38.45N	72.39W	0.037 0.045 0.038	1.2	0.02	0.230	0.022
84820	806	0.14N	91.36W	1.093 1.119 0.943	2.8	0.2	0.870	0.084
78595	1097	Gulf of California		0.151 0.146 0.150	3.2		1.030	0.100
48740	1420-1470	48.40N	10.54W	0.278 0.319 0.298	1.16	0.1	0.214	0.021
85080	990-1150	43.47S	150.29E	0.089 0.083	2.15	0.1	0.610	0.059
47413	421	50.38S	167.38E	0.078 0.089 0.090	1.66	0.03	0.414	0.040
36544	636	51.52S	73.41W	0.059 0.064 0.065	1.75		0.450	0.044

Table 6.7: Modern Cd/Ca calibration data. [PO₄] estimates are taken from nearby hydrographic data (see text). Conversion to water [Cd] uses the global Cd:PO₄ relationship including the "kink" at about 1.2 μM [PO₄].

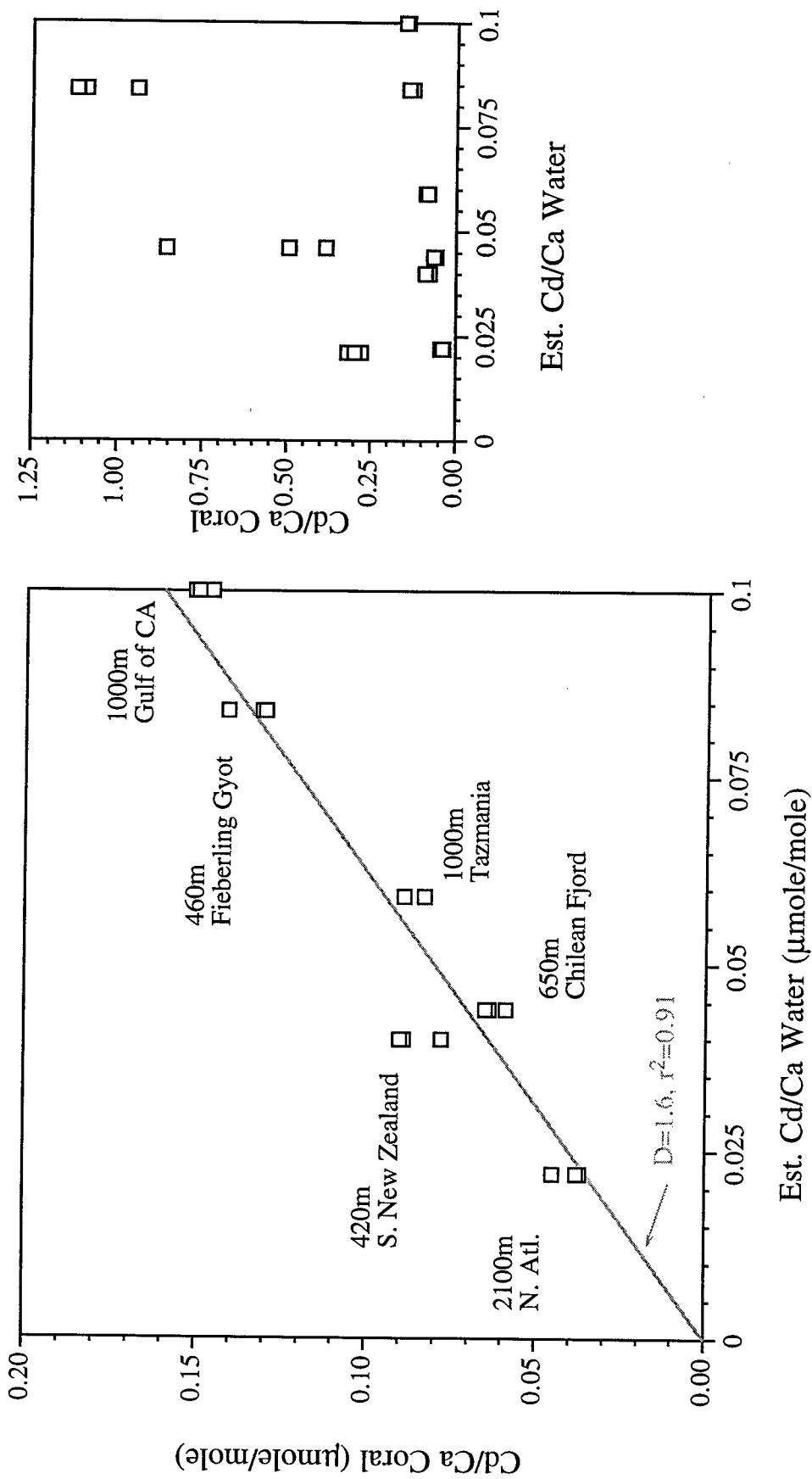


Figure 6.5. Modern calibration of Cd/Ca in *D. cristagalli*. Six of the nine samples fall along a well defined line. We can not explain why the three other samples are elevated in their Cd/Ca ratio (see right hand panel).

constant D_p . In the future I would like to use corals that fall on the $D_p=1.6$ line for a vital effect study to test the conclusion of a small to negligible vital effect in *D. cristagalli*.

The *Science* paper that constitutes the first part of this chapter uses Cd/Ca ratios in a 15.4 ka old coral to estimate the deep water composition at 1800 meters and 40°N in the Atlantic. Due to space limitations in that paper, we could not show all of the information about this sample and the others for which we have ^{14}C data. I reproduce here (Figure 6.6) the banding and laser cutting pattern used in the Cd/Ca time series of Figure 6.2 and the data itself (Table 6.8). In an effort to obtain material from only one septum and not the attached secondary septa, I first cut the long vertical lines seen in Figure 6.6. Based on the sample size requirements for three replicates of each point, I divided the sample into eight pieces. The overall length of the septum is 1.83 cm which corresponds to an average sampling interval of 2.3 mm. Cd/Ca data show a very consistent change from low values at the bottom to higher values at the top that we interpret as a change in the water [Cd] during the lifetime of this coral. The range of Cd/Ca data is both larger than the range in the vital effect experiment and is spatially consistent. For these reasons, we believe the Cd/Ca data in JFA 24.8 represents an accurate measure of the evolution of the proportion of nutrient rich to nutrient poor deep waters at our site.

In an early effort to check the top/bottom radiocarbon results from the 15.4 ka corals, Ed Boyle ran Cd/Ca data from different samples from the same septum as the ^{14}C data (Table 6.9). His data also shows a large Cd/Ca change in sample JFA 24.8 of about 0.1 $\mu\text{mole/mole}$. However, the absolute values are different than the top and bottom of the transect shown in Figure 6.6. This difference is most likely due to the different sampling locations of the two studies on the same septum that grew through a water mass transition. The other two corals do not show the Cd/Ca increase expected from the ^{14}C data. Without transects from bottom to top, it is difficult to fully interpret this difference. During this time of rapid deep water transition, it is possible that the Cd and ^{14}C data could become decoupled from one another by changes in the initial radiocarbon age of

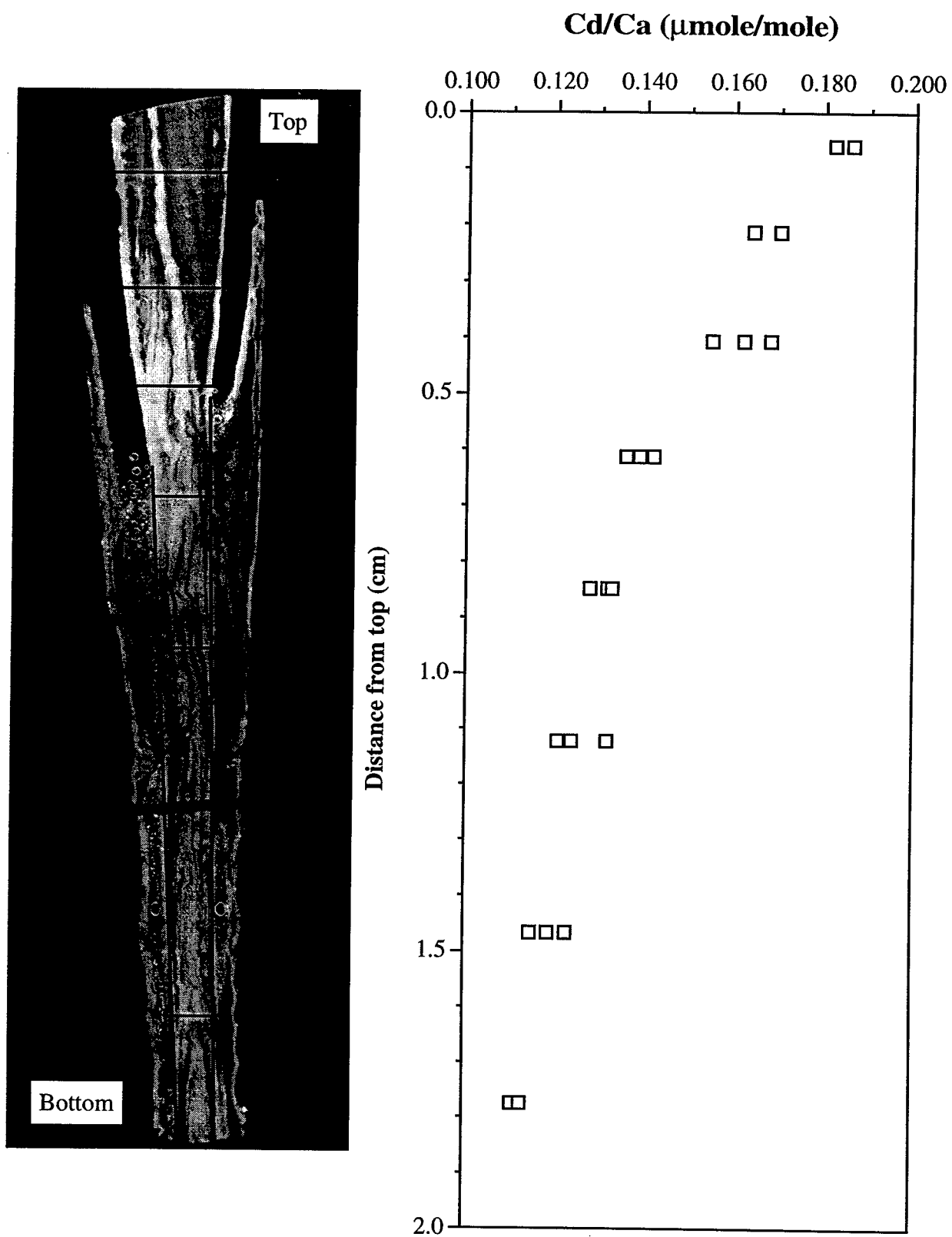


Figure 6.6. Cd/Ca sample blocks from *D. cristagllai* JFA 24.8. I have tried to line up the Cd/Ca data length axis with the scale of the sample image. The two secondary septa were avoided for Cd/Ca analysis.

Sample Number	Distance (cm)		Cd/Ca (μ mole/mole)
	From Top	Average	
BA 2	0.118	0.059	0.210
BA 17		0.059	0.206
BA 11	0.310	0.214	0.192
BA 23		0.214	0.185
BA 7	0.502	0.406	0.183
BA 13		0.406	0.190
BA 30		0.406	0.175
BA 9	0.724	0.613	0.157
BA 27		0.613	0.161
BA 15		0.613	0.154
BA 1	0.975	0.849	0.151
BA 19		0.849	0.145
BA 28		0.849	0.149
BA 8	1.270	1.123	0.149
BA 14		1.123	0.137
BA 22		1.123	0.140
BA 3	1.664	1.467	0.130
BA 20		1.467	0.135
BA 24		1.467	0.140
BA 4	1.886	1.775	0.128
BA 16		1.775	0.126

Table 6.8: JFA 24.8.3 *D. cristagalli* Cd/Ca data.

Sample	Position	Boyle Cd/Ca (μ mole/mole)	
JFA 20.10	Top	0.207	0.202
	Bottom	0.256	0.250
JFA 24.8	Top	0.248	
	Bottom	0.145	
JFA 24.19	Top	0.087	0.093
	Bottom	0.097	0.101

Table 6.9: Cd/Ca data from 15.4 ka corals run by Ed Boyle. These are from the same septa as the ^{14}C data but not the exact same sample.

source waters to this site, or by some other process. In addition, the inverse change in Cd/Ca in sample JFA 20.10 may represent a different deep water ventilation history at this slightly deeper site. Alternatively, there is still much to understand about Cd/Ca as a deep water tracer in *D. cristagalli*. The data in Table 6.9 were not sampled along a single transect and may represent our imperfect understanding of growth patterns in this coral. The data in Figure 6.6 show that when sampled in a consistent manner along known growth trends, *D. cristagalli* can be a powerful archive of rapid changes in deep ocean ventilation.

IV. Conclusions

Cd/Ca ratios from the deep-sea coral *D. cristagalli* can be used to reconstruct past water mass variations at high temporal resolution. A modern calibration shows that Cd has a partition coefficient in *D. cristagalli* of 1.6 or greater. Vital effects observed for $\delta^{18}\text{O}$ and $\delta^{13}\text{C}$ are not nearly as prominent in the Cd/Ca data. While there is a 10% range in Cd/Ca across a single modern septum, circulation signals that are larger than this potential vital effect can be reliably measured. At 15.4 ka and 1800 meters depth in the North Atlantic there was an abrupt shift in the pattern of deep water circulation. In under 160 years, older more nutrient rich waters from a southern source replaced a 50/50 mixture of these waters and GNAI/DW. Combining the quasi-conservative mixing tracer Cd/Ca and the ^{14}C data results in a transit time of 500 years for the deep southern source waters that fill the North Atlantic prior to 15.4 ka.

References

- Boyle, E. A., Cadmium, zinc, copper, and barium in foraminifera tests, *Earth Planet. Sci. Lett.*, 53, 11-35, 1981.
- Boyle, E. A., Cadmium: chemical tracer of deep water paleoceanography, *Paleoceanography*, 3, 471-489, 1988.
- Boyle, E. A., Cadmium and $\delta^{13}\text{C}$ paleochemical ocean distributions during the stage 2 glacial maximum, *Annual Review of Earth and Planetary Sciences*, 20, 245-287, 1992.
- Boyle, E. A., *A comparison of carbon isotopes and cadmium in the modern and glacial maximum ocean: can we account for the discrepancies?*, Springer-Verlag, NATO ASI Series, R. Zhan et al., Springer-Verlag, I 17, 167-193, 1994.
- Boyle, E. A. and L. D. Keigwin, Comparison of Atlantic and Pacific paleochemical records for the last 250,000 years: changes in deep ocean circulation and chemical inventories, *Earth Planet. Sci. Lett.*, 76, 135-150, 1985/6.
- Boyle, E. A., L. Labeyrie and J.-C. Duplessy, Calcitic foraminiferal data confirmed by cadmium in aragonitic *Hoeglundina*: Application to the last glacial maximum in the northern Indian Ocean., *Paleoceanography*, 10, 881-900, 1995.
- Boyle, E. A. and Y. Rosenthal, *Chemical hydrography of the South Atlantic during the Last Glacial Maximum: Cd vs. $\delta^{13}\text{C}$* , Berlin, Springer-Verlag, The South Atlantic: Past and present circulation, B. Wefer Siedler and Webb, Berlin, Springer-Verlag, 423-443, 1996.
- Frew, R. D. and K. A. Hunter, Influence of Southern Ocean waters on the cadmium-phosphate properties of the global ocean, *Nature*, 360, 144-146, 1992.
- Shen, G. T. and E. A. Boyle, Determination of lead, cadmium and other trace metals in annually-banded corals, *Chemical Geology*, 67, 47-62, 1988.
- Shen, G. T., E. A. Boyle and D. W. Lea, Cadmium in corals as a tracer of historical upwelling and industrial fallout, *Nature*, 328, 794-796, 1987.

Appendix: Preliminary Laser probe ICP-MS measurements in *D. cristagalli*

Ba/Ca and Sr/Ca ratios were also measured in a septum from the deglacial *D. cristagalli* sample JFA 24.8. A separate septum from the ones used for ^{14}C , Cd/Ca and stable isotope analysis was mounted to a glass slide and polished to around 230 μm thick in the same manner as the other samples. The spatial distributions of Ba/Ca and Sr/Ca were investigated using a VG laser probe attached to the ICP-MS. Six samples were ablated from dark bands between the top and the bottom to see if Ba and Sr also show a circulation signal. The data are listed in Table A6.1. Care was taken to ensure that all data came from laser ablations that sampled only aragonite and not the glass slide below. In addition, a pre-ablation period was used to burn away the surface of each hole to reduce contamination from sample handling. Each point represents the average of four closely spaced "holes" and the reported errors are the standard deviations of these averages.

Both Ba/Ca and Sr/Ca ratios increase from the bottom to the top on this sample. This Ba/Ca increase agrees with the interpretation from ^{14}C and Cd/Ca data, which implies that this coral was increasingly bathed by more nutrient rich waters of a southern origin during its lifetime. However, the concurrent large increase in the Sr/Ca ratio implies that the Ba/Ca signal may, instead, be due to a "vital effect". The Ba/Sr ratio is relatively constant for all of the dark band samples and is about 10 times above the expected modern ratio. Two samples from the central, optically dense, white band on this septum were also measured for their Ba and Sr content. These points show an elevated Ba/Ca ratio for an equivalent Sr/Ca value and are further evidence for a biological influence on these ratios (Figure A6.1). No attempt was made to standardize the ablation process. The elevated Ba/Sr ratios show that there is probably a large fractionation of these two elements during sampling.

Location	Ba/Ca ($\mu\text{mole/mole}$)	error	Sr/Ca (mmole/mole)	error	Ba/Sr (mmole/mole)	error
Top	113	7	23.4	0.9	4.85	0.36
	105	4	22.1	0.5	4.75	0.20
	103	6	21.9	0.9	4.68	0.35
	103	5	21.5	0.8	4.79	0.31
	96	7	20.5	1.4	4.71	0.47
Bottom	93	8	18.4	1.1	5.06	0.51
white	141	8	23.4	1.3	6.02	0.49
white	120	29	19.6	2.7	6.13	1.69

Table A6.1. Laser probe ICP-MS data from JFA 24.8 Septum #1b.

Data were taken sequentially from top to bottom on the coral so that the length series should also represent a time series. All points come from dark bands except the two data points at the bottom of the table which were ablated from the optically dense central white band.

Distance (cm)	Ba/Ca ($\times 10^{-6}$)	Sr/Ca ($\times 10^{-3}$)	Ba/Sr ($\times 10^{-3}$)
0.059	15.67	10.48	1.50
0.059	17.86	10.16	1.76
0.214	17.17	11.22	1.53
0.214	18.24	10.14	1.80
0.406	19.73	9.50	2.08
0.406	17.38	10.78	1.61
0.406	19.00	10.55	1.80
0.613	19.17	9.54	2.01
0.613	19.72	10.83	1.82
0.613	20.25	10.20	1.99
0.849	20.73	11.21	1.85
0.849	20.52	11.21	1.83
0.849	21.62	11.31	1.91
1.123	19.24	10.02	1.92
1.123	20.41	10.27	1.99
1.123	18.45	11.09	1.66
1.467	22.59	11.95	1.89
1.467	21.97	11.38	1.93
1.467	21.27	11.03	1.93
1.775	20.46	11.89	1.72
1.775	21.17	11.45	1.85

Table A6.2. Wet chemistry data for septum JFA 24.8 #3.

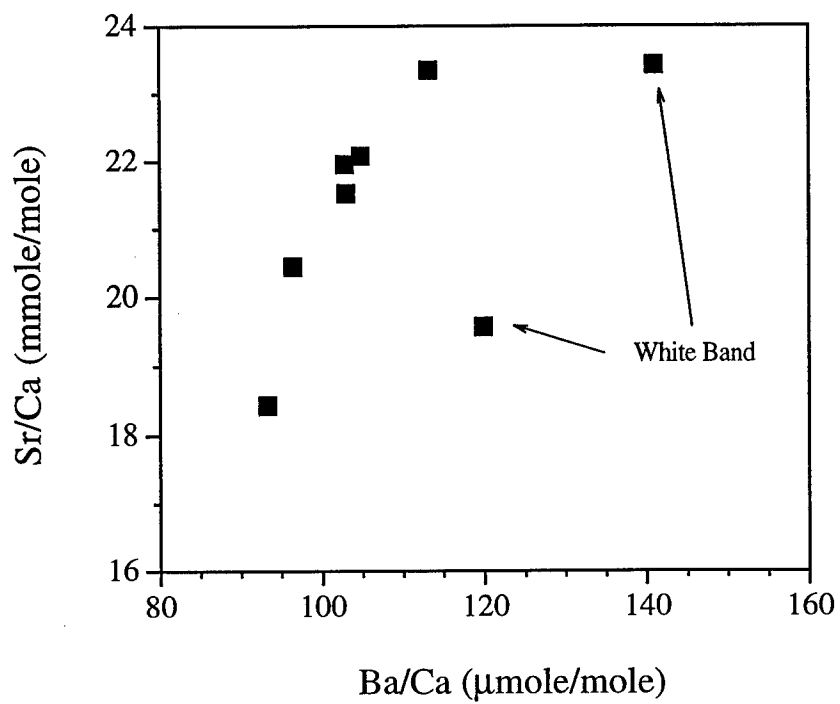


Figure A6.1. Results from laser ICP-MS sampling of JFA 24.8 Septum #1b. For an equivalent Sr/Ca ratio the white band is enriched in Ba/Ca.

Ba/Ca and Sr/Ca data measured by isotope dilution on the ICP-MS from the same solutions used in the Cd/Ca determinations show a different trend than the laser probe data (Table A6.2). Here the trend is for decreasing Ba/Ca ratios from bottom to top on the septum. While the data come from separate septa, they are from the same coral and should show the same circulation history. Clearly the Ba/Ca signal is being influenced by a biological artifact. As this artifact can vary between septa, we can not use the wet chemistry isotope dilution data to check the veracity of the probe data. There are probably standardization problems with the laser probe method because the Ba/Sr ratio, which may have less of a vital effect than the Ca ratios, is about a factor of 4 different between the two methods. This preliminary work is promising for finding patterns of Ba and Sr distribution on individual septa but more work is needed before quantitative Ba/Ca and Sr/Ca ratios can be measured with laser ablation ICP-MS on deep-sea corals.

Biographical Note

Jess Adkins was born in New York City on February 7, 1968. He grew up in the suburban town of Chappaqua, NY and attended the local public schools. In September of 1986, he entered Haverford College where he studied Chemistry and Philosophy. After graduating in May of 1990, Jess took a job as a technician in the laboratory of Dr. David Lea at the University of California at Santa Barbara. After this initial exposure to the Earth Sciences, he entered the MIT/WHOI Joint Program in Oceanography in August of 1992. During his thesis work, Jess received a NASA Global Change Fellowship to study deep-sea corals. In 1997, he received a NOAA Postdoctoral Fellowship in Global Change and a Lamont Fellowship to continue studying the history of the earth's climate.

DOCUMENT LIBRARY

Distribution List for Technical Report Exchange – February 1996

University of California, San Diego
SIO Library 0175C
9500 Gilman Drive
La Jolla, CA 92093-0175

Hancock Library of Biology & Oceanography
Alan Hancock Laboratory
University of Southern California
University Park
Los Angeles, CA 90089-0371

Gifts & Exchanges
Library
Bedford Institute of Oceanography
P.O. Box 1006
Dartmouth, NS, B2Y 4A2, CANADA

NOAA/EDIS Miami Library Center
4301 Rickenbacker Causeway
Miami, FL 33149

Research Library
U.S. Army Corps of Engineers
Waterways Experiment Station
3909 Halls Ferry Road
Vicksburg, MS 39180-6199

Institute of Geophysics
University of Hawaii
Library Room 252
2525 Correa Road
Honolulu, HI 96822

Marine Resources Information Center
Building E38-320
MIT
Cambridge, MA 02139

Library
Lamont-Doherty Geological Observatory
Columbia University
Palisades, NY 10964

Library
Serials Department
Oregon State University
Corvallis, OR 97331

Pell Marine Science Library
University of Rhode Island
Narragansett Bay Campus
Narragansett, RI 02882

Working Collection
Texas A&M University
Dept. of Oceanography
College Station, TX 77843

Fisheries-Oceanography Library
151 Oceanography Teaching Bldg.
University of Washington
Seattle, WA 98195

Library
R.S.M.A.S.
University of Miami
4600 Rickenbacker Causeway
Miami, FL 33149

Maury Oceanographic Library
Naval Oceanographic Office
Building 1003 South
1002 Balch Blvd.
Stennis Space Center, MS, 39522-5001

Library
Institute of Ocean Sciences
P.O. Box 6000
Sidney, B.C. V8L 4B2
CANADA

National Oceanographic Library
Southampton Oceanography Centre
European Way
Southampton SO14 3ZH
UK

The Librarian
CSIRO Marine Laboratories
G.P.O. Box 1538
Hobart, Tasmania
AUSTRALIA 7001

Library
Proudman Oceanographic Laboratory
Bidston Observatory
Birkenhead
Merseyside L43 7 RA
UNITED KINGDOM

IFREMER
Centre de Brest
Service Documentation - Publications
BP 70 29280 PLOUZANE
FRANCE

REPORT DOCUMENTATION PAGE	1. REPORT NO. MIT/WHOI 98-07	2.	3. Recipient's Accession No.
4. Title and Subtitle Deep-Sea Corals: A New Oceanic Archive		5. Report Date February 1998	
7. Author(s) Jess F. Adkins		6.	
9. Performing Organization Name and Address MIT/WHOI Joint Program in Oceanography/Applied Ocean Science & Engineering		8. Performing Organization Rept. No.	
12. Sponsoring Organization Name and Address Massachusetts Institute of Technology		10. Project/Task/Work Unit No. MIT/WHOI 98-07	
		11. Contract(C) or Grant(G) No. (C) (G)	
15. Supplementary Notes This thesis should be cited as: Jess F. Adkins, 1998. Deep-Sea Corals: A New Oceanic Archive. Ph.D. Thesis. MIT/WHOI, 98-07.		13. Type of Report & Period Covered Ph.D. Thesis	
		14.	
16. Abstract (Limit: 200 words) <p>Deep-sea corals are an extraordinary new archive of deep ocean behavior. The species <i>Desmophyllum cristagalli</i> is a solitary coral composed of uranium rich, density banded aragonite that I have calibrated for several paleoclimate tracers. Using a newly developed ICP-MS age screening method, large numbers of samples can be processed relatively quickly and inexpensively to uncover interesting fossil corals for further analysis.</p> <p>Deep-Sea corals can be used to calculate the past $\Delta^{14}\text{C}$ of a water mass. Combining uranium series and radiocarbon dates allows for the direct measurement of past water $\Delta^{14}\text{C}$. Along with Cd/Ca data from the same sample, to account for water mass mixing, this $\Delta^{14}\text{C}$ value is a direct measurement of the past ventilation age. Samples from 1800 meters depth in the North Atlantic at 15.4 ka show a large deep water circulation switch that occurred in under 160 years. This deep event is coincident with the first sea surface warming of the deglaciation in the North Atlantic. This data shows that deep circulation can change on comparable timescales to the rapid events previously observed for the atmosphere and the surface ocean.</p>			
17. Document Analysis a. Descriptors <p>Paleoceanography Geochemistry</p> <p>b. Identifiers/Open-Ended Terms</p> <p>c. COSATI Field/Group</p>			
18. Availability Statement Approved for publication; distribution unlimited.		19. Security Class (This Report) UNCLASSIFIED	21. No. of Pages 234
		20. Security Class (This Page)	22. Price